Physical Properties of Single-Sheet DNA Origami Nanotiles

Ashley Connor Stammers

Submitted in accordance with the requirements for the degree of Doctor of Philosophy

The University of
Leeds

School of Electrical and Electronic Engineering
&
School of Physics and Astronomy

September 2018

The candidate confirms that the work submitted is his own and that the appropriate credit has been given where reference has been made to the work of others

This copy has been supplied on the understanding that it is copyright material and no quotation from this may be published without proper acknowledgment

The right of Ashley Connor Stammers to be identified as Author of this work has been asserted by him in accordance with the Copyright, Designs and Patents act 1988

© 2018 The University of Leeds and Ashley Connor Stammers

Acknowledgements

I would firstly like to express my sincerest thanks and gratitude to my supervisors Neil Thomson and Christoph Walti. Your assistance and guidance as well as belief in me and my work have helped immensely over the years. I would also like to thank Jamie Goodchild and Simon Connell who have, among other things, been of great help in the lab. My thanks also go to the MNP group and CDT for molecular-scale engineering, whose friendships over the years have made the experience far more enjoyable.

I would also like to thank my family, whose support and belief over the years has been of great help. Finally, I would like to thank Emily Stell, who has always been there for me, ensuring that I always get my work done.

Abstract

Central to DNA origami is the need to have oligomeric DNA bind adjacent DNA helices, whose spacing is dependent on the spatial offset between the helices. In square-based origami, this spacing must be an odd-number of half-turns, requiring a non-integer number as B-form DNA has a helical pitch of 10.50 bp. The inability to have non-integer spacings creates a phasing mismatch, leading to curvature of origami. This work explores how cationic concentration and species affect this curvature.

Asymmetric single-sheet DNA origami with varying crossover spacings, said to be overwound, planar and underwound, were imaged under bulk aqueous solution with AFM, where the adsorption orientation served as a metric to infer the magnitude and direction of curvature. The combination of these three designs demonstrated how the effective Mg^{2+} concentration affects both DNA helicity as well as the electrostatic repulsion between the tightly packed helices. Low Mg^{2+} concentrations caused helix destabilisation; leading to flatter origami, whilst elevated Mg^{2+} concentrations appeared to shield electrostatic repulsions, causing a decrease in curvature. These results highlight the importance of Mg^{2+} concentration and its effect on origami curvature.

Exposure to UV radiation induced unwinding of DNA through the formation of photoproducts, causing the overwound origami to experience a decrease in adsorption bias whereas the planar and underwound origami experienced an increase in bias. These results aid the idea that the direction of curvature is independent of crossover spacing. The combination of tiles in varying Mg^{2+} and those exposed to UV radiation served as a baseline to determine the effects that Ba^{2+} has on the DNA helix. Ba^{2+} appeared to induce over-winding of the DNA helix, whilst remaining in an overall destabilised state, compared to that of Mg^{2+}. This caused the underwound origami to exhibit more curvature compared to those of the overwound and planar origami.

Contents

List of Abbreviations

A	Adenine
AFM	Atomic force microscop(e/y)
AGE	Agarose gel electrophoresis
AM	amplitude modulation
bp	base pair
bppt	base pair per turn
C	Cytosine
CPD	Cyclobutane pyrimidine dimer
Cryo-EM	Electro cryomicroscopy
DNA	Deoxyribonucleic acid
dsDNA	Double-stranded DNA
DX	Double crossover
EDTA	Ethylenediaminetetraacetic acid
EM	Electron microscop(e/y)
FM	Frequency modulation
G	Guanine
HC	Honeycomb
IC	Intermittent contact
Mg-ace	Magnesium acetate
ML-O	Multi-layer origami
NC	Non-contact
nt	Nucleotide
QNM	Quantitative nanomechanical mapping
RNA	Ribonucleic acid
RNAP	RNA polymerase
ROS	Reactive oxygen species
SL-O	Single-layer origami

SPd^{3+}	Spermidine
SQ	Square
ssDNA	Single-stranded DNA
SPM	Scanning probe microscopy
STM	Scanning tunnelling microscopy
SX	Single-crossover
T	Thymine
TAE	Tris-Acetate EDTA
U	Uracil
UV(A/B/C)	Ultra violet A/B/C

List of figures

List of tables

1 Introduction

The applications of DNA nanotechnology are far reaching, having been implemented into a wide range of research areas. One area of particular interest is structural DNA nanotechnology, where the specific Watson-Crick base pairing and predictability of DNA secondary structure has been used to create DNA-based nanostructures. The field was started by Nadrian Seeman, who was able to rationally design immobile junctions [1], [2]. Seemans original vision was to create structures for immobilising proteins into periodic motifs, for the purpose of performing X-ray crystallography on proteins [1]. The difficulty in determining the structure of proteins still remains a problem today due to their instability in ex vivo environments as well as complex structure. Seeman then went on to develop robust structural motifs, known as DX tiles, through a process of reciprocal strand exchange. This led to the creation of programmable 2D arrays, demonstrating how DNA could be used to create new nanomaterials. The field of DNA nanotechnology was changed forever in 2006 when Rothemund demonstrated his DNA origami method, whereby a long ssDNA strand is folded into shape with shorter ssDNA strands complementing the folding pattern [3]. Rothemund was able to demonstrate the versatility of his technique by creating arbitrary 2D shapes, functionalised origami surfaces and even the ability to join origami tiles together. Since then, the number of applications has grown significantly, infiltrating a wide range of research areas. This includes solution-based applications such as drug delivery methods, platforms for DNA walkers and dynamic structures [4]. An important application that is of particular interest, are the surface-supported applications such as functionalised arrays for sensing applications, whose efficacy is dependent on the ability to access functional groups attached to origami, which single-sheet are positioned to solve.

One of the challenges for structural DNA nanotechnology is to be able to create macroscale arrays with full addressability. In the early days of Seeman, this was achieved through sticky-end interactions between DX motifs. Although sticky-ends offer the specificity required, errors in binding still occur due to the prevalence on non-specific

interactions. Origami alleviated this to an extent by increasing the size of the tile subunit, but has yet to create fully-addressable microscale arrays. Creating anisotropic arrays from DNA origami is similar to the design and creation of a jigsaw puzzle. A jigsaw puzzle contains hundreds of pieces, each with a unique position and part of the image. The position of a jigsaw piece is determined by how it interlinks with its surrounding pieces. The known completed design of the puzzle itself, and the partial-design on the piece itself, can be used to help locate its position. For DNA origami to create a jigsaw puzzle, careful selection of the sticky ends is required to ensure error-free binding. Unlike jigsaw puzzles, the internal design of origami can't be used as an aid for correct placement, and is strictly dependent on DNA binding along the edges of the tiles. Additionally, the tiles are unable to re-orientate themselves once adsorbed onto the surface, such that they could be upside down. Tikhomirov et al. recently demonstrated the creation of micron-scale origami through a multistage process, leading to an 8x8 "jigsaw" puzzle [5]. This used a combination of sticky-end and blunt-ends to program the interactions between pieces, but only resulted in a ~2% yield of the final design. An alternative method to create arrays has been to employ blunt-end stacking between helices of origami, whilst keeping the tiles mobile [6], [7].

1.1 Project aims

The aim of this project was to understand how the internal crossover spacing affects curvature of single-sheet origami through analysis of adsorption orientation of asymmetric DNA origami tiles. This was extended into methods for controlling curvature of origami, to understand how changes in the helical properties of DNA affects the mismatch inherent to square-based single-sheet origami. This was achieved by having three origami designs of the same shape and size with differing crossover compositions and investigating how helix stabilisation as well as buffer conditions affect the crossover mismatch.

The importance of controlling the solution structure of origami, and understanding what factors affect it as well as what the effects are, will allow for better design of both isotropic

and anisotropic DNA-based arrays. This is also important for dynamic origami, whose structure is dependent on solution conditions, which can also act as a means to control conformations.

1.2 **Synopsis**

Using high resolution and high throughput imaging by atomic force microscopy (AFM) this thesis details the effect that buffer conditions have on the structure and stability of the DNA helix, and what effect this has on the solution curvature of origami tiles by measuring their adsorption orientation under aqueous conditions.

Chapter 1 introduces the work contained in this thesis, introducing the general field of DNA-based technologies along with the core aims of the work. An overview of each chapter is given outlining the main points. Chapter 2 introduces the chemical nature and structure of nucleic acids with focus on the variety of factors that affect DNA stability. The various forms of DNA are given along with alternative structural elements that are observed. A summary of DNA in biology is given due to its prominence as the carrier of genetic information. Chapter 3 begins with an overview of DNA nanotechnology and how rational design have led to the development of novel materials and devices. A history on the developmental process and tools are given, highlighting the specific rules which govern DNA origami. Applications of DNA origami are given demonstrating its potential as a disruptive technology in a variety of areas.

The main tool used for analysing DNA origami structure was AFM, whose operation is discussed in chapter 4. This chapter explores the basic modes of AFM for imaging under aqueous conditions, which are suited for DNA-based studies. An overview of literature concerning the study of DNA materials is given, detailing drawbacks that are present with AFM and how the scope of this work hopes to aid some of the misunderstandings. Chapter 5 contains the general methods use in this thesis, detailing the folding recipes and sample preparation methods used for imaging origami under aqueous conditions. Details on the analysis methods can be found in the appendix, along with example AFM images.

The three origami tiles are deemed to be underwound, planar or overwound, based on the composition of crossovers contained within. Chapter 6 explores the notion of what is meant by under/over-wound origami, based on the terminology of supercoiled DNA, noting that curvature of origami arises due to the DNA double helices between cross-overs maintaining a B-form structure. With the aid of computer-generated models, the orientation and magnitude of the curvature for the three origami tiles were assessed under a range of Mg^{2+} concentrations. The results from AFM experiments indicated that the underwound and overwound tiles showed the same bias to the mica surface, suggesting that the curvature of the tiles were in the same direction. This was in contradiction to CanDo models; a finite element modelling software tool, which is used widely to attempt predictions of origami curvature, mechanics and structure. By contrast, OxDNA models (provided by Prof. J. Doye of the University of Oxford and Dr. John S. Schrek of Columbia University, NYC) agreed with the AFM data, indicating that CanDo has limitations in predicting origami shape and curvature. Further proof on the binding orientation of the origami tiles was demonstrated by depositing the tiles under various Mg^{2+} concentrations, which also was corroborated with OxDNA models. These results gave a baseline on how the stability of the DNA helix affects curvature of origami, questioning how the relative Mg^{2+} concentration with respect to DNA concentration affects the inherent stability of the DNA molecule.

Chapter 7 details how UV exposure forms cyclobutane pyrimidine dimers (CPDs) along the DNA helix, distorting the helix and altering the degree of twist of the underlying crossovers. Literature on CPD formation notes that it causes unwinding of the DNA helix. UV exposure caused the overwound origami to bind with a decreased bias, whilst the planar and underwound tiles experienced an increase in bias to surface binding. This demonstrated how the formation of a CPD causes a distortion in the helix, affecting the inherent crossover mismatch. It further supports the designation of supercoiling between the three origami. It also demonstrates that the direction of curvature is always into the same plane, regardless of crossover composition. This chapter also details the effect

that Ba^{2+} ions have on the structure of the DNA helix, and how this affects the origami of the curvature. It was noted that regardless of crossover composition or Ba^{2+} concentration, the origami showed the same magnitude and orientation of curvature. This was investigated further by imaging the origami in a mixture of both Ba^{2+} and Mg^{2+} ions, revealing that the two ions have different binding modes to the DNA helix. It was noted that at lower ionic strengths than "standard" Mg^{2+}, a mixture of Ba^{2+} and Mg^{2+} caused the underwound origami to become more curved.

Chapter 8 details high resolution imaging of origami tiles under aqueous conditions, detailing the appearance of an internal diamond lattice that arises from the electrostatic repulsions between the tightly packed helices. High-resolution imaging also revealed the presence of a major axis, which is comprised of crossover spacings which do not contain a nicked strand. This leads to the exploration of how the arrangement of crossovers inside the origami affect CanDo models, acting as a potential method for controlling structure of origami. This chapter also looks at how altering the spacing between crossovers affects the formation of the internal diamond lattice, noting that the sides of the diamonds corresponds to the underlying crossover spacing.

Chapter 9 discusses the main conclusions and outcomes of the research, with emphasise on how the phase mismatch causes origami to curve into the same plane unlike what has been previously reported in literature. The implications of underwinding induced by UV radiation acts a method to explain the observed binding of origami under varying Mg^{2+} concentrations, whose combined results serve as a baseline for the Ba^{2+} work. Future work is discussed, in both the context of this work and how it can be used to aid work of those in the field.

The appendix contains the list of DNA sequences used for folding the origami, such that others can reproduce the work. A selection of example AFM images are given. The images are by no means exhaustive, but act to serve as an example. Due to the nature of the analysis and the origami design involved, AFM images are indistinguishable unless

analysis is carried out. An overview on the analysis methods as well as relevance on the size of the areas scanned is presented.

2 Introduction to nucleic acids

2.1 Structure of nucleic acids

2.1.1 DNA and RNA

Nucleic acids consist of three structural elements; a sugar ring, a phosphate group and a base, which together form a monomer unit known as a nucleotide. There are two naturally occurring nucleic acids; RNA and DNA, along with artificially produced nucleic acids whose composition and function can vary greatly. The sugar found in RNA is ribose, in the form of β-D-Ribose, and in DNA is 2'-deoxyribose, which lacks the oxygen atom on the 2' carbon (Figure 1). The five primary bases found in nucleic acids are adenine (A), thymine (T), cytosine (C), guanine (G) and uracil (U) (figure 1). Both RNA and DNA contain A, C and G whilst U is found only in RNA and T found only in DNA. These are grouped as being either purines (A, G) or pyrimidines (T, C, U). Nucleosides

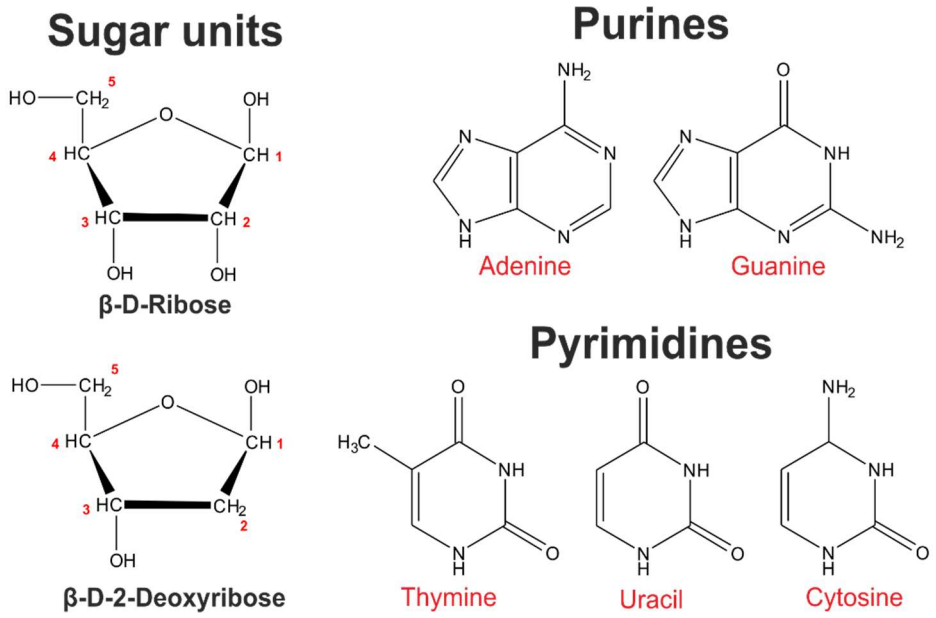

Figure 1: Sugar units and nucleic acid bases that occur in DNA and RNA. The DNA sugar ring lacks the OH group on the carbon 2' atom. Uracil lacks the methyl group present in Thymine.

contain one base and one sugar and are formed when the N9 of the purines or the N1 of the pyrimidines bond to the 1' carbon of the sugar. A nucleotide consists of a nucleoside with either 1, 2 or 3 phosphate groups (labelled as α, β, and γ respectively) attached to the 5' carbon of the sugar. The naming of nucleotides is given as the

nucleoside followed by the number of phosphate groups, e.g. adenosine diphosphate (ADP). A more general form uses N in place of a specific nucleoside along with M, D or T to represent mono-, di- or tri-phosphates. Monomer units can then be joined together via the formation of a phosphodiester bond between the α-phosphate group on the 5' carbon of one nucleotide and the 3' carbon of another nucleotide, forming nucleic acid chains (Figure 2B). This leads to a directionality of the nucleic acid chain, whereby one end is terminated by the phosphate group on the 5' carbon (5'-end) and the other terminated by the hydroxyl group on the 3' carbon (3'-end). This binding between the different carbon group is what adds direction as well as chirality to the ssDNA molecule. This chain of nucleotides is more commonly referred to as single-stranded, which can be either DNA or RNA.

2.1.2 **DNA double helix**

The complementary pairing of two ssDNA molecules forms double-stranded DNA (dsDNA), whose structure was first proposed by Watson and Crick following the X-ray fibre diffraction work conducted by Franklin [8], [9]. In the structure proposed by Watson and Crick, the DNA adopts a right-handed helix with the sugar-phosphate groups on the exterior of the strand, known as the sugar-phosphate backbone, and the bases orientated perpendicularly to the backbone whilst being situated on the interior of the strand [8]. This organisation of the bases means that the interior of the helix is hydrophobic whereas the backbone is hydrophilic.

The two ssDNA strands naturally bind together in an antiparallel fashion such that one runs in the 5' to 3' direction with the other running 3' to 5'. The bases in each strand are complementary to each other such that A binds T and G binds C (Figure 2A). This binding of bases is highly specific and mediated by hydrogen bonds; with two hydrogens between A and T and three hydrogen bonds between G and C. This binding is known as Watson-Crick base pairing, with alternative binding possible under special circumstances. The additional hydrogen bond between G and C results in a higher energy required to disrupt the bond, meaning that DNA strands with a higher GC content

require more energy to denature [10]. This highly specific binding also means that in any DNA strand there is an equal amount of G bases as there are C bases, and T bases as

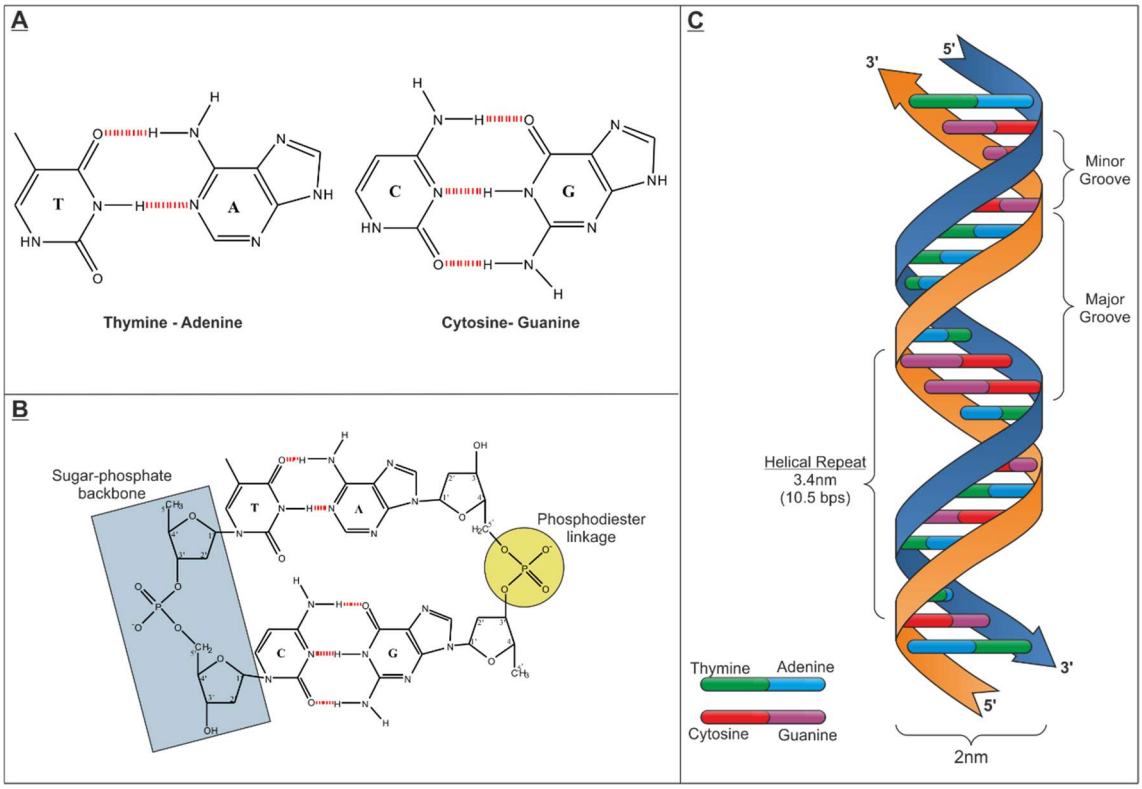

Figure 2: Watson crick strucuture of B-form DNA. A) Watson-Crick base pairing showing hydrogen bonds between A:T and G:C. B) Phosphodiester linkage between adjacent sugar rings of B-form DNA. C) Shematic of the B-form strucutre of DNA, highlighting the helical repeat as well as helical diameter.

there are A bases, which is known as Chargaff's rule [11]. The helical structure of DNA also contains two grooves; the major and the minor groove, as seen in figure 2C, due to the bases not pairing across the centre of the helical axis. The grooves play an important role for the binding of proteins, enzymes and drugs [12].

2.2 Stabilising factors

2.2.1 Base stacking

The hydrogen bonding between the bases of the two anti-parallel ssDNA strands is not enough to form a stable right-handed helix. Bonding between the bases leads to an aromatic geometry, allowing π-π interactions between adjacent base pairs, which are both attractive and noncovalent [13]. Rotations in the sugar-phosphate backbone allow base-pairs to lie in the same plane, increasing the strength of π-π interactions and hence DNA stability. The exact strength of the stacking interaction is dependent on the DNA

sequence, as well as salt concentration, which gives DNA the ability to adopt alternative forms [14].

2.2.2 **Charge neutralisation**

The sugar-phosphate backbone of the DNA contributes to destabilisation of the DNA helix due to mutual electrostatic repulsions of the negatively charged phosphate groups [15]. In vivo this negative charge is shielded through interactions with cations. The most notable cation that is responsible for charge neutralisation is Mg^{2+}, which bonds to two adjacent negative charges along one ssDNA [16]. It is believed that Mg^{2+} binds indirectly through hydration layers, due to the specific formation of water molecules that surround both the DNA as well as the Mg^{2+} ion itself [17]. This stabilisation of the DNA helix has been observed by investigating the effect of salt concentration on the melting temperature of dsDNA molecules [18].

As well as Mg^{2+}, other cations, including monovalent ones such as Na^{+} can be used to stabilise the DNA helix. Due to its decreased charge, as well differing binding mode, a higher concentration of Na^{+} is needed to stabilise the B-form of DNA [19]. It is also possible to promote DNA condensation with the use of molecules that have a higher net-charge, such as Hexaminecobalt(III) chloride ($[Co(NH_3)_6]Cl_3$) [20]. Other metals such as the group (II) and transition metals have also shown to stabilise the DNA helix, but these result in slight deformations of the helix due to the presence of differing binding modes [21]–[23]. This is of particular importance when studying the effects of heavy metals, which are toxic to organisms. Hg^{2+} for example is able to bind and stabilise two opposing thymine's, which would not otherwise be able to form under normal conditions [24].

2.2.3 **Temperature**

Another important aspect that affects the stability of the double-helix is the temperature of the solution. As the anti-parallel strands of the DNA molecule are held together through hydrogen bonds, these can be readily broken with an increase in temperature. DNA melting simply refers to double-helix denaturation, separating into single strands and can also be caused by a decrease in salt concentration as well as a change in pH. The

melting temperature of the DNA strand is also dependent on the sequence composition, as GC bonds contain three hydrogens, whilst AT bonds contain only two [10].

2.2.4 **pH**

pH can also cause destabilisation of the DNA helix [25], [26]. The optimal pH range of DNA is around 6 - 8. At moderate alkali levels, the OH^- ions can cause deprotonation of the bases, affecting both the base-stacking as well as hydrogen bonding. This can lead to a reduction in the melting temperature of the DNA. At higher pH levels, hydrolysis of the phosphodiester bond can occur, causing the DNA to fragment. In more acidic conditions the H^+ ions can cause deprivation of the purines, resulting in melting due to a loss of 50% of the bases. At extremely low pH levels the phosphodiester bond becomes cleaved, resulting in nucleosides and nucleotides [27].

2.3 **RNA**

The presence of the hydroxyl group on the ribose sugar means that RNA does not adopt the B-form helical structure that is prevalent to DNA. RNA forms an A-form double helix, often forming inter-strand binding where sequence complementarity allows, forming complex secondary structures. The ability to form complex structures, similar to what is seen for proteins, means that RNA displays some enzymatic activity, as seen in enzymes known as ribozymes, present in the ribosome [28]. This enzymatic activity that is seen with RNA leads some to believe that it pre-dates DNA as a carrier of genetic information [29].

2.4 **Alternative DNA forms**

There are several forms of DNA that occur in vivo, with the most common being B-form; the form discovered by Watson and Crick. The exact size and shape of the DNA helix is dependent on the environment in which the DNA resides. In general, it is accepted that B-form DNA has an average diameter of 2 nm and a helical pitch of 10.50 bp with a base pair separation of 0.31 - 0.34 nm, resulting in an average rise of 3.6 nm per helical turn. The other common in vivo forms of DNA include A-form and Z-form [30]. DNA adopts A-form in low humidity environments, resulting in a number of structural changes. Although A-form adopts the same right-handedness as seen with B-form, the helix is wider and less coiled than B-form. A-form typically occurs when the DNA is dehydrated, but can also result from certain molecular machinery stripping the DNA of its counter ions [31]. The final most common form of DNA found in vivo is Z-form. Unlike A-form and B-form DNA, Z-form adopts a left-handed twist. Z-form occurs when the DNA sequence contains pyrimidine repeats and at higher salt concentrations [32], [33]. As mentioned above, DNA bases bind together co-operatively through hydrogen bonds in the form of Watson-Crick base pairing. There is however another form of base binding called Hoogsteen base

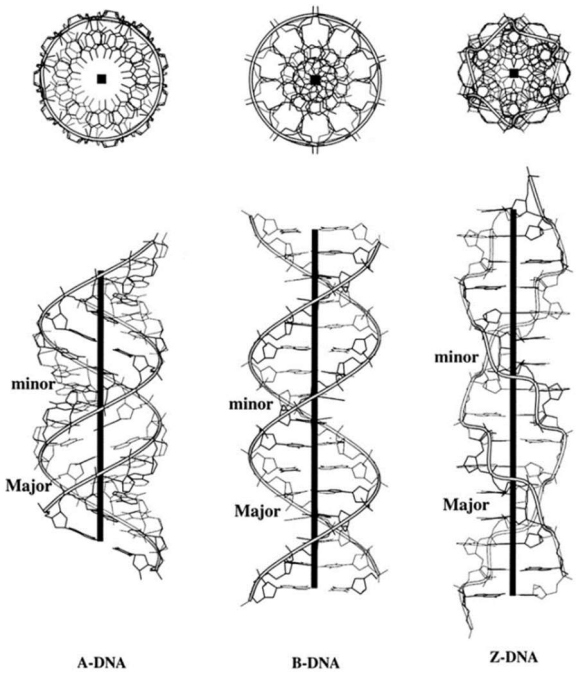

Figure 3: Conformations of A, B and Z-form DNA. B and A-DNA adopt a right-hand helix, whilst Z-form is left-handed. Z-DNA also has a smaller diameter. (Image recreated from x3dna.org).

pairing [34]. In Hoogsteen base pairs, the purine bases are rotated about the glycosidic bond (the linkage between the base and the C1 carbon on the sugar-ring). This also causes the GC base-pair to bind with two hydrogen bonds and leads to variations in the chemical properties of DNA as well as its physical shape.

2.5 DNA secondary structure

The linear sequence of bases is the primary structure of DNA and contains no information on the physical structure of the DNA molecule. The B, A and Z-forms of are all examples of possible secondary structure of DNA that occur from inter-chain base-pairing. Similar to RNA, DNA can also form intra-chain base pairs, which can result in various secondary structures [35], [36]. A summary of these secondary structures is shown in figure 4. Hairpin loops and cruciforms arise when one, or both, of the ssDNA strands contains an inverted self-complementary sequence. This leads to intra-chain base pairing and the extrusion of a loop from the DNA helix. Hairpin loops are a common method for the functionalisation of DNA origami as they allow extrusion of DNA strands from the origami surface. They also occur in vivo, playing an important role in DNA replication [3], [37], [38]. A similar structure to this is the slipped structure. Slipped structures can occur when there are sequence repeats in one of the ssDNA strands [39]. This can cause misalignment between the two strands, resulting in the formation of a loop that is, like hairpins, extruded from the DNA helix. DNA can also form triple and even quadruple helical structures. Triple-helical structures occur when the DNA contains a mirrored stretches of homopurine:homopyrimidine bases. This allows for a single strand polynucleotide sequence to bind to the major groove of the underlying DNA to form a triple strand. The two most common tetraplexes are G-quadruplexes and I-motifs [36], [40], [41]. G-quadruplexes are formed by long stretches of G bases, following Hoogsten base pairing rather than abiding to Watson-Crick base paring. I-motifs are formed from stretches of C-rich DNA, forming unusual cytosine-cytosine bonds. I-motifs have been shown to be more stable in acidic conditions [42]. The DNA helix can also

contain sequence of both B and Z-form DNA, which occur when there are variations in the DNA sequence.

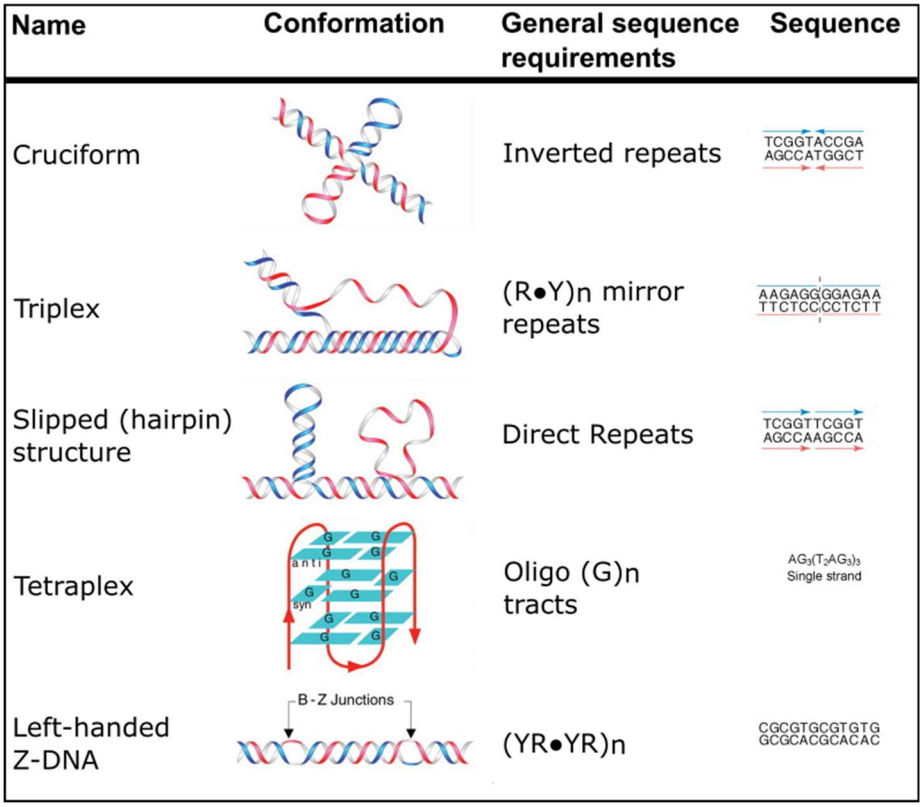

Figure 4: Examples of Non-B DNA structures. Each example gives a schematic of the of geometry of each type of secondary strand, along with the necessary conditions which cause it [159]**.**

2.6 **Supercoiling**

Supercoiling is the difference in topology of a DNA molecule compared to its relaxed counterpart. The linking number (Lk) describes how the two ssDNA strands of a DNA helix are linked together and is comprised of two components: twist (Tw) and writhe (Wr). The linking number of a general DNA molecule is given as

$$Lk = Tw + Wr$$

Tw corresponds to the number of times the two ssDNA strands twist round each other, whilst Wr is the number of times the dsDNA helix overlaps itself. For a relaxed DNA molecule, the linking number is simply the number of times the two strands crossover each other:

$$Lk° = \frac{N}{h}$$

Where N is the number of bases and h is the helical pitch. Therefore the degree of supercoiling for a given DNA molecule is known as the linking difference and given by:

$$\Delta Lk = Lk\ - Lk°$$

When $\Delta Lk < 0$ the DNA is negatively supercoiled (underwound) as the DNA molecule contains fewer twists than the relaxed case, whilst when $\Delta Lk > 0$ the DNA is positively supercoiled (overwound) as it contains more twists than the relaxed case. Topology is conserved as long as the individual DNA strands remain unbroken meaning that any change in the Tw must be accompanied by an equal and opposite change in the Wr, and vice versa. Typically for low linking differences it is usually more energetically favourable for the DNA to partition supercoiling into writhe over twist (Figure 5).

$$\Delta Wr = -\Delta Tw$$

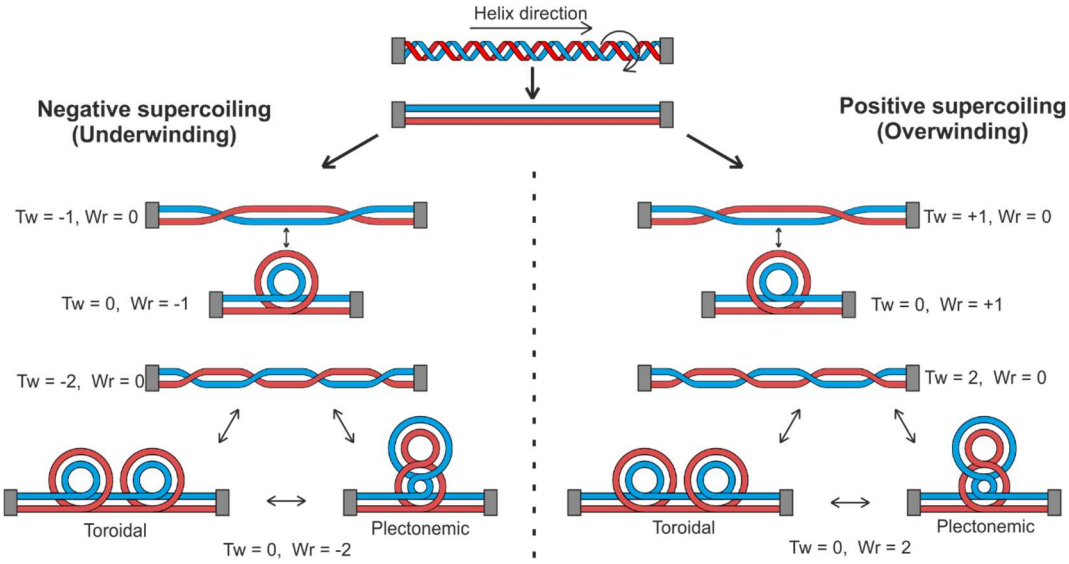

Figure 5: Effect of positive and negative supercoiling on a constrained linear DNA fragment. It can be seen that the contortions in positive and negatively wound DNA have opposing handedness. The red and blue strands depict the two ssDNA strands in a single dsDNA molecule.

In the case of a constrained strand, such as a segment of DNA between two proteins, local topological variations are allowed. One example is in the nucleus of cells, where DNA binds to histone proteins. As histones induce negative supercoiling of the DNA molecule, segments between the histones must under wind so as to maintain the linking number [43]. This also occurs when DNA is intercalated with a molecule such as ethidium bromide, EtBr. The induced underwinding results in twisting and writhing of the DNA

molecule. In order to change the supercoiling of a molecule, one or both of the ssDNA strands have to be broken and then ligated back together [44]. In vivo this is mediated by topoisomerases, which are able to break the sugar-phosphate backbone and re-orientate the strands before ligating them back together [45]. The physical consequence of DNA supercoiling results in contortions of the DNA molecule, known as plectonemes or toroids. A supercoiled DNA molecule will always adopt a conformation that is most energetically favourable. So, although a supercoiled DNA molecule is in a higher energy state that its relaxed counterpart (i.e. when $\Delta Lk=0$), provided that the linking difference remains constant, the supercoiled molecule will relax to the lowest energy conformation available to it. From this point of view, although the molecule is holding strain energy, we could say that a supercoiled DNA molecule is "relaxed" in its particular topological state. This idea has relevance to the work in this thesis when considering how curvature is generated in single-sheet origami.

2.7 **DNA damage**

Helical destabilisation can be caused by damage to the DNA molecule. This typically involves some form of a chemical reaction with various part of the DNA helix such that it deviates from the idealised form. There are various types of DNA damage that can occur, resulting in single-base and double-base modifications as well as single- and double-strand breaks, i.e. breakage of the phosphodiester backbone bonds [46]. Single-base modifications include oxidation, methylation and hydrolysis. These are typically caused by reactive oxygen species (ROS) and their non-specificity in how they target the DNA helix. Double-base modifications typically include crosslinking of bases, requiring high energy from sources such as UV radiation. A common crosslinking photoproduct is cyclobutane pyrimidine dimers (CPDs), which is the formation of a covalent linkage between adjacent pyrimidine bases [47]. Higher energy electromagnetic radiation, such as UVC and X-rays can result in single and double strand breaks. Another wide classification of DNA damage is the formation of adducts, which involves the reaction

with carcinogenic chemicals. An overview of the types and sources of DNA damage are given in figure 6.

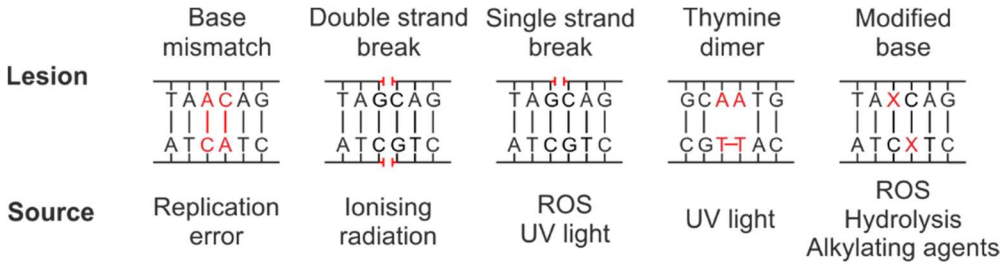

Figure 6: Examples of DNA damage and how it presents it self in a DNA molecule, with the red sections denoting the deviations from B-form DNA.

As the main purpose of DNA is to carry genetic information, organisms have developed processes that can be used to repair the DNA molecule. One of the most common is nucleotide excision repair (NER), where a segment of the ssDNA is removed either side of the damage. The remaining undamaged DNA helix is then used as a template to repair the damage. If the rate of damage exceeds the rate of repair however, DNA transcription and replication pathways are disrupted, leading to mutagenesis. DNA mutagenesis can also be caused by intercalators. Intercalators are planar hydrophobic molecules able to bind between the base pairs, disrupting the base stacking as well unwinding and deforming the helix. Although this does not result in direct damage of the DNA strand, it can lead to errors during the reading of the DNA strand, which can cause mutagenesis. Excessive mutations in the DNA sequence can lead to cell death as well as the formation of cancerous cells. As the majority of the genome is non-coding genes for protein expression, mutations of the DNA which are present do not necessarily give rise to deleterious effects in vivo straight away.

2.8 **DNA in biology**

The complete DNA sequence of an organism, known as the genome, encodes the necessary information required to produce the molecular machinery required for the normal operation of organism. It also acts as the method by which genetic information is transferred from mother to daughter cells. A core concept is the “Central Dogma of Molecular Biology” which describes the flow of genetic information [48]. DNA partakes in

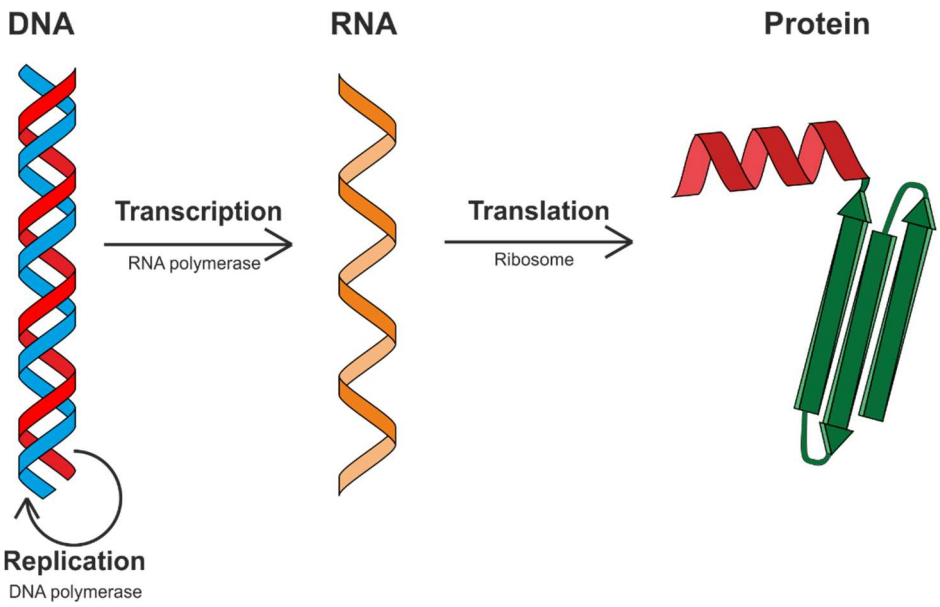

Figure 7: Central dogma of molecular biology, showing how genetic information is turned from DNA into proteins, highlighting the molecular machinery in each prcoess.

two processes: replication and transcription. Replication describes the process of how the DNA sequence is replicated, so that it can be transferred to daughter cells, whilst transcription is the process by which the DNA sequence is used to create RNA and eventually proteins. Once the DNA has been transcribed into RNA, the RNA sequence is then translated into proteins, which are the molecules which carry all the necessary task for an organism's survival.

As DNA is used to generate RNA and subsequently proteins, any change in the DNA sequence can result in changes downstream. This is why maintaining the correct DNA sequence is such an important factor. In vivo DNA is found in eukaryotic and prokaryotic cells. The main difference is how the DNA is stored. In eukaryotic cells, DNA is found in the nucleus of a cell, whilst in prokaryotic it is found in the nucleoid. The DNA in eukaryotic cells is stored in a compacted linear form, known as chromosomes. The chromosomes themselves are made from a chromatin fibre, which is made from DNA being wrapped around histone proteins. The DNA in prokaryotes is stored inside the nucleoid, in a supercoiled circular form. The need to compact DNA is to reduce the volume it occupies, due the relatively long lengths of its corresponding linear form. The sequence of the genome can be broken into sequences known as genes, which

correspond to production of certain proteins. These genes can be activated and deactivated, meaning that not all of the genome is used for the production of proteins. It also means that genes can be turned on and off, through the incorporation of certain epigenetic factors. In eukaryotic cells, DNA is also found in gametes. As chromosomes come in pairs, these are broken down in gametes. The normal process of cell division, mitosis, results in two identical cells. When a cell forms gametes however, it produces two cells which each contain half the number of chromosomes of the adult cell. It is also possible for sections of the chromosome to be exchanged with one another, in a process known as homologous recombination.

3 DNA nanotechnology

3.1 Introduction

There are two methods for the manufacture of devices at the nanoscale: top-down and bottom-up. Top-down techniques such as photolithography suffer from limitations such as the diffraction limit of light, whilst other techniques such as electron beam lithography suffer from poor parallelisation. Top-down methods are however, able to create nanometre sized features through etching of crystal planes in substrates. Bottom-up processes however focus on the exploitation of the self-assembly exhibited by molecules. One area of inspiration has been biopolymers, specifically DNA. The rules which govern DNA-DNA interactions are perhaps some of the most well understood in nature, leading to the innovation that is DNA nanotechnology. The chemical and physical properties that have evolved over time allowing for the encoding of genetic information, has led to DNA becoming the robust molecule that we know today. The specific Watson-Crick base pairing combined with the predictability of DNAs three-dimensional structure has allowed for the creation of fully addressable nanostructures.

3.2 Structural DNA nanotechnology

The most important aspect to designing nanostructures from DNA is the need for a non-1D, stable structural motif. In nature DNA typically exists as a linear molecule for replication and transcription purposes. Tertiary DNA structures limit the ability of molecular machines to traverse the DNA strand, which is why the few tertiary structures that do exist are typically short lived. One example is the Holliday junction, an intermediate 4-way junction that appears during genetic recombination**.** The Holliday junction is unstable due to the sequence symmetry in the DNA strands; ideal for nature, not so much for nanotechnologists. It was Nadrian Seeman who first theorised and reported the construction of an immobile Holliday junction by rationally designing the DNA sequences [1]. It took nearly a decade for the next breakthrough to occur, which once again came from Seeman. The immobile Holliday junction lacked structural rigidity

due to there being only one reciprocal strand exchange (the process whereby a strand starts on one helix and crosses over to the next). Through his process of reciprocal strand exchange, Seeman was able to design multiple structural motifs; the most well-known and used being the double-crossover (DX) [49]. The arrival of the DX motif lead to the creation of DNA “tiles”, which consisted of a DX motif with “sticky-ends”. These sticky-ends are ssDNA overhangs whose sequence are designed to complement that of another tile. This allowed for the creation of 2D DNA lattices, which relied only on the self-assembling nature of DNA [50]. DNA hairpin loops were also incorporated into these DX tiles, demonstrating how DNA could be used to create periodic structural and functional arrays. Other structural motifs were also created, further increasing the scope of the field. One limitation that persists still today is the ability to create micron sized arrays with full addressability. The relatively small size of the DX tile meant that many hundreds would be needed to create large-scale aperiodic arrays, increasing the complexity of design.

3.3 **DNA origami**

Named after the Japanese art of paper folding, DNA origami refers to the method of creating arbitrary 2D/3D shapes by “folding” or routing a long, viral strand of ssDNA (scaffold) with shorter ssDNA oligomers (staples) being generated to complement the routing pattern of the scaffold strand. In his inaugural paper, Rothemund demonstrates the process by designing several 2D shapes, perhaps most notably is the smiley face [3]. Rothemund also demonstrates the ability to functionalise the origami with hairpin loops, creating a map of the Americas and using DNA to write the word “DNA”.

Rothemund discusses the process of origami design in detail, with the routing pathway and crossover spacing being the two most important aspects. In the early days of DNA origami, most were designed using custom software. The rise in interest of origami however, has led to dedicated software packages to aid with the design process which when combined with additional tools for origami structure prediction make the whole process somewhat trivial. Despite this however, the details outlined by Rothemund still

remain relevant. The first important design aspect is the routing of the scaffold. Similar to the rules of Seemans DX tiles, each crossover subunit requires adjacent helices to be anti-parallel. This allows the staple strands to form a series of interconnecting DX junctions, adding stability and rigidity to the structure. Although it has been demonstrated to use a routing pathway that has parallel helices, the anti-parallel routing remains the most dominant method [51].

3.3.1 **Staple design**

A staple strand can be broken into three segments: head, body and tail. The point at which the staple strand switches between helices is a crossover point and is where the segments of the staple connect the scaffold together. Schematics of origami tile design usually show a gap at the crossover but structurally this is not the case. As there are no unpaired bases, it is only the phosphodiester bond between two segments which span the inter-helical gap. Crossovers are spaced along the helices such that the stretching of the bond at the crossover is minimised apart. This requires the bases either side to be in line with one another. This spacing is known as the single crossover (SX) spacing and

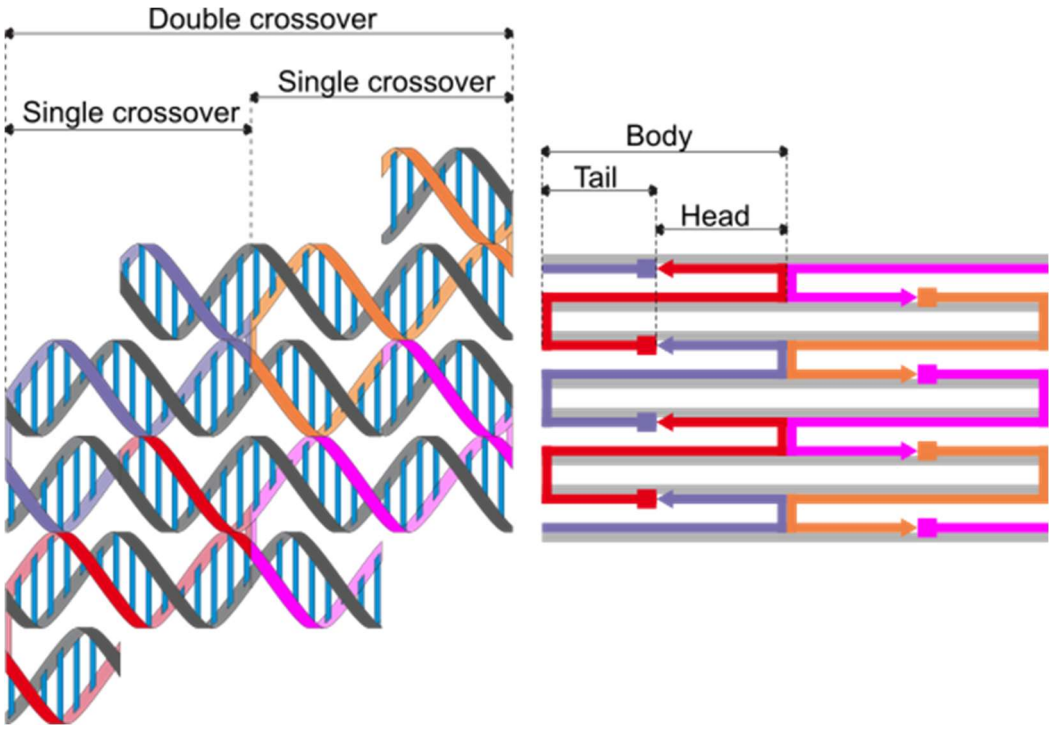

Figure 8: Left: Schematic of how the bases in the scaffold and staple strands bind together and the definition of the single and double crossover spacing. Right: Simplified schematic highlighting the sections of the staple strands.

refers to the distance between crossovers at either end of the body segment (Figure 8). SX spacings may also consist of the head and tail of two differing staples, leading to a nicked segment of DNA. The double-crossover (DX) spacing is the gap between crossovers occurring between pairs of adjacent helices; comprised of the two SX spacings. The DX spacing is always a number of full-turns, whilst the ideal SX spacing is dependent on the both the spatial offset between the helices and the native form of the DNA.

3.3.2 **Square based**

The first origami designed by Rothemund were single-layer origami (SL-O) built using the square-based (SQ) lattice. Here the offset between helices is 180° (½ turn), meaning that the ideal SX spacing is an odd-number of half-turns. The SQ lattice has also been

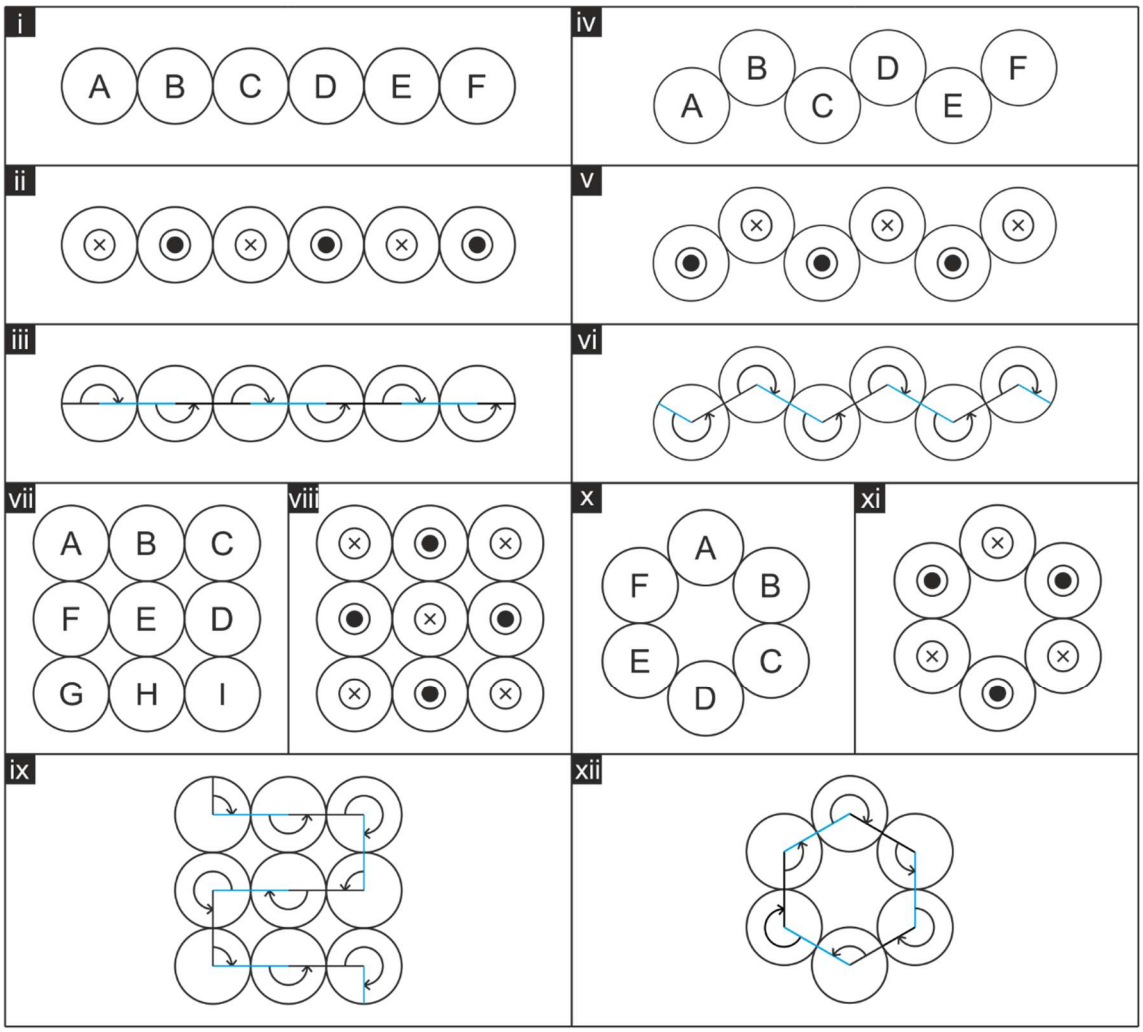

Figure 9: Schematics showing the offset between adjacent helices and the angle through which crossovers must rotate for i-iii) SL-O SQ, iv-vi) SL-O HC, vii-ix) ML-O SQ and x-xii) ML-O HC origami.

used to create multi-layered origami (ML-O), where the helices are offset by 90°. For SQ ML-O the staples have multiple adjacent helices to choose from when forming crossovers. Figure 9 gives an example of how the crossover may look, but there is a multitude of ways to connect the helices. In general, the ideal SX spacing is some multiple of a quarter helical turn.

The design of DNA origami assumes that the native form of DNA in solution is B-form, with a helical pitch of 10.50 bp. In the case of SQ SL-O, the ideal SX spacing is typically designed to be 1.5 turns, which correlates to 15.75 bp for B-form DNA. As it is not possible to have a non-integer number of bases, the native SX spacing is generally

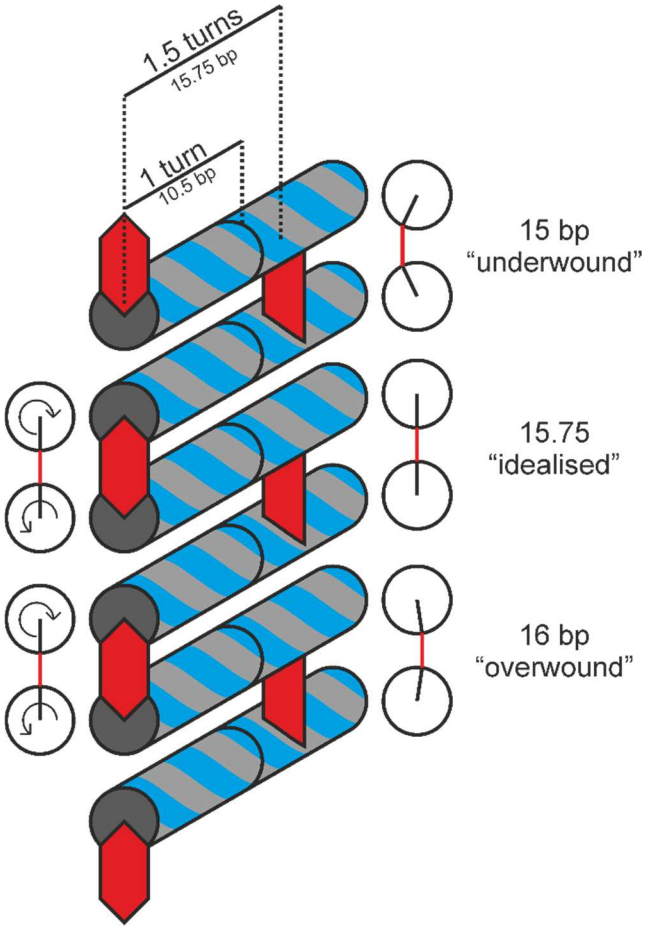

Figure 10: Schematic showing the offset between bases either side of the crossover that arises when the crossovers deviate from the idealised B-form spacing, denoting their relative supercoiling w.r.t twisted DNA.

designed such that it contains 16 bp. This leads to a mismatch between the ideal and native SX spacings; resulting in stress at the crossover points. This stress accumulates

along the length of the origami resulting in twisting or curvature of the origami tile. The mismatch is also present in ML-O origami due to a quarter turn containing 2.625 bp.

3.3.3 **Honey comb**

The other common lattice used for designing origami is the honey-comb (HC) lattice, where the offset between helices is 120°. With adjacent helices being anti-parallel, the direction through which the SX spacing must rotate is either clockwise or anticlockwise. This means that the ideal SX spacing is either 120° or 240°. A spacing of 120° corresponds to 3.5 bp for B-form, which is too small to ensure adequate binding between the DNA strands; it is also requires a non-integer number of bases. The solution is to increase the SX spacing by one full turn, meaning the ideal spacings are either 480° or 240°, which for B-form DNA is 14 bp and 7 bp respectively. As HC origami require an integer number of bases between crossovers, there is no issue of mismatch, meaning that they do not exhibit curvature, unless rationally implemented [52].

3.3.4 **Lattice free**

Both SQ and HC use tightly packed helices and crossovers at set intervals, limiting the complexity of origami design. One recent development to expand the range of potential 2D and 3D structures is the wireframe method [53]–[55]. Here the origami is routed in such a way that it creates a series of vertices and lines. Vertices are connected using similar methods to create multi-arm junctions with the addition that poly-T segments are introduced to increase the flexibility whilst the edges are represented as a series of crossover junctions, leading a variety of 2D shapes.

An extension of the wireframe method for creating nanoscale 3D shapes is to recreate them as polygon meshes. Here 3D shapes are represented as a series of triangles, with each edge being a single helix and each vertex designed such that the scaffold is non-crossing, resembling a simple DNA junction. This method is a series of interconnected multi-arm junctions, but unlike the wireframe, requires the junctions to remain rigid to retain their 3D structure. Bathe and colleagues have extended this further to design 3D shapes where the edges consist of DX motifs, increasing the rigidity. There is also no

limitation on the need to have a mesh of triangles. Other methods used custom routing of the scaffold to create 3D structures, such as those designed by Han et al. [56].

3.3.5 **CAD design**

During the early days of structural DNA nanotechnology, the design of immobile junctions required DNA sequences be heterologous to ensure that domains would bind properly. To this end, Seeman developed SEQUIN, a FORTRAN based program where the user would sketch a 2D line drawing [57]. SEQUIN would then generate a set of DNA sequences ensuring that they were sufficiently different so as to prevent incorrect domains from binding. This was later expanded to GIDEON in 2006, which featured an easy to use interface as well as a simple 3D representation of the molecule. It was at this time however Rothemund invented DNA origami; changing the landscape of structural DNA nanotechnology forever. Rothemund details the design method used in his original paper, using a program known as “multishapes.m” for the generation of DNA sequences; which was never released. The second demonstration of DNA origami came from a group in China, who created a custom PERL script for the design of the staple strands [58].

The first open access CAD program for DNA origami was SARSE. Originally developed by Anderson et al. in 2007 for analysing RNA alignments, it was later modified in 2008 to be used for DNA origami [59], [60], and the same year also saw the release of Tiamat and caDNAno, which have since gone on to be the most common software for origami design [61], [62]. Tiamat by Han et al. allows for designing lattice-free origami, replacing SEQUIN and GIDEON, whilst caDNAno is used for the design of square and honeycomb based origami.

As DNA origami has become more prominent and the routing methods complex, researchers have sought to create software that is more accessible. Both Tiamat and caDNAno require input from the user when designing the routing path, but include simple 3D models of the helices to keep track of the process. Recent developments in origami, such as the wireframe methods developed by Hogberg and Bathe have created

specialist software requiring minimal input from the user. Hogberg's group developed vHelix, where the user must first construct a 3D triangle mesh of the nanostructure they wish to create [54]. vHelix then automatically generates a scaffold route and the staples such that each edge is represented by a single double-helix. In DAEDALUS, developed by Bathe and colleagues, the input model can be any 3D shape [55]. Here each edge is comprised of a crossover motif and allows for shapes with faces which are not limited to triangles.

Once the origami had been designed and the staple sequences generated, there was no way to check if they would result in the desired structure unless they were visualised, with techniques such as AFM or EM. The development of modelling software has allowed for rapid error checking, reducing the financial costs associated with any potential sequence errors during the design process.

Before the invention of origami, scientists have tried to model small artificial DNA structures. As origami increased the size of DNA nanostructures, it also increased the computational requirements needed to model such structures. The first tool developed to model origami structure was CanDo [63]. Developed in 2011 by Dietz and Bathe, it took a finite-element approach to modelling origami. CanDo is an online web service that uses a mechanical model of the double-helix, assuming that it is homogenous rod with axial stretching, twisting and bending. When it was first developed it only allowed submissions from caDNAno but has since been updated to allow submissions form Tiamat and DAEDULUS.

Although imaging methods such as AFM and TEM are used to categorise DNA origami, they typically lack sufficient resolution for full structural details on the origami properties in solution. One of the problems with CanDo is that it does not consider the effect of electrostatic and solvent-mediated forces. In 2013 the first full-atomistic simulation of DNA origami was carried out using NAMD, allowing researchers to visualise structural fluctuations [64]. Due to the computational power required for full-atomistic simulations, NAMD still remains out of reach for the average user, although methods have been

developed to simplify the modelling process. In 2010 Doye and colleagues created OxDNA, a coarse-grain approach to modelling DNA nanostructures [65]. Unlike the two extremes of CanDo and NAMD, OxDNA lies in the middle offering detailed simulations without the need for large computing power. In 2015 it was revised to OxDNA2 to include differing widths for the major and minor grooves as well as a new electrostatic interactions to include modelling under varying salt concentrations [66].

3.4 DNA origami applications

3.4.1 Scaling up

The size of a single origami tile is limited by the length of the scaffold strand. Most origami are folded using M13mp18 as the scaffold strand, due it to being easily accessible through commercial sources. One of the earliest attempts to create large origami was by Zhang, who created a 26k nt ssDNA strand using molecular biology techniques [67]. This was later replicated by Marchi et al. who created the largest single origami tile, using a scaffold of 51k nts [68]. Increasing the size of the scaffold strand requires a larger staple set, which is one of the highest financial costs associated with DNA origami. Whilst Zhang purchased theirs commercially, Marchi et al. had created an “inkjet” based method for creating oligomers, using freely available plans. Other methods have also been developed such as that by Praetorius et al., who demonstrated that it is possible to use bacteriophages to create staple strands of arbitrary length and sequence [69]. The inkjet method used by Marchi et al. however still requires a high upfront cost, meaning that the average researcher is still reliant of commercially sourced staple strands.

An alternative approach to creating origami super-structures was demonstrated by Zhao et al. who used an additional ssDNA strand as a secondary scaffold [70]. The secondary scaffold strand was loosely folded into shape, with sticky-ends in the origami tiles themselves designed to bind to the secondary scaffold strand. A benefit of this approach is that the origami tiles can retain a core set of staples, with only the edge staples needing to be replaced. More recently Tikhomirov et al. demonstrated a multi-stage process for the hierarchal assembly of origami superstructures [5]. Similar to Zhao et al. a single

origami is used where a core set of staples are retained. Rather than using a secondary scaffold, rational design of sticky-ends were used to join origami tiles together. A multi-stage step approach was taken to increase the yield of super-structures, where certain tiles were mixed together, before being mixed with other groups. This resulted in the first micron-scale origami with full addressability, whilst maintaining a relatively small staple set. A limitation of this approach however is the need to have a suitable number of sticky-ends to ensure adequate and error-free binding between tiles, which is partially limited by the size of the original origami tile.

Base stacking interactions between origami tiles was first noted by Rothemund who incorporated poly-T overhangs into staple strand that are along the edge of the origami, where the scaffold strand crosses over, to disrupt the inter-tile interactions. Base stacking interactions can however be exploited to create arrays of origami tiles. Suzuki et al. deposited origami onto a lipid bilayer, allowing the origami to remain mobile. Base stacking interactions between origami tiles would then occur, creating large scale arrays [7]. This technique was also used by Woo et al. on a mica surface, using a buffer containing Na^+ ions to reduce the mica-DNA interaction, keeping the origami tiles mobile [71]. The greatest downside to base stacking between tiles is that they are non-specific meaning that there is no control over the ordering of tiles. The use of sticky-ends has however offered some control, but is still susceptible to unwanted interactions.

3.4.2 **Functionalisation**

One goal of nanotechnology and bottom-up fabrication techniques is the ability to position nanomaterials with nanometre precision, something that DNA origami is well placed to solve. The well-ordered and characterised structure as well biological importance has meant that DNA is one of the most well understood biomolecules. This has led to numerous chemical modifications of the DNA molecule enabling it to become functionalised with a wide range of nanoparticles.

The first step in creating functionalised DNA origami is to create DNA-nanoparticle conjugates. A chemically modified oligomer is incubated with the target nanoparticle,

which in the case of gold nanoparticles requires a thiol-modified oligomer. Conjugates containing a single oligomer are isolated using agarose gel electrophoresis (AGE), which also removes excess DNA. At the same time, staple strands in the origami are modified such that they contain a sticky-end that is complementary to that used in the conjugate. Both the modified origami and conjugates are incubated and subsequently filtered using AGE to isolate the desired structures. For larger, anisotropic particles such as gold nanorods, several binding sites in the origami are required to ensure accurate binding and orientation. The spacing and length of the sticky-ends is an important design aspect, as it affects the finer placement of nanoparticles.

Ding et al. were the first to demonstrate the placement of multiple gold nanoparticles into origami structures [72]. Since then a number of 1D, 2D and 3D DNA-gold architectures with unique properties have been created. One of the most interesting areas is the design of plasmonic structures, where the close proximity of gold nanoparticles can lead to increase plasmonic resonance. DNA origami offers a way to finely tune the position and orientation of DNA, as demonstrated by Pal et al. [73]. DNA origami has also been used to arrange quantum dots (QDs), semiconductor nanocrystals with unique electronic and optical properties. Controllable positioning of QDs will allow for novel materials, as QD have already shown great promise in a wide range of applications [74].

One of the greatest benefits of DNA origami is that it allows multiple functional groups to be attached to a single structure. This was recently demonstrated by Li et al. with the targeted delivery and release of an anti-cancer drug [75].

3.4.3 **Dynamic structures**

The most common method of creating dynamic DNA structures has been to take advantage of toe-hold strand displacement reactions. Commonly referred to as strand-displacement reactions; two ssDNA strands are bound together, with one of the strands containing additional unbound bases. A third ssDNA strand is design to complement the original ssDNA strand which contains the unpaired region. The third strand is then able

to bind to the unbound section, and then displace the strand that was originally bound, being longer the third strand has a higher energy of interaction with the template.

Dynamic DNA structures such as DNA walkers had already been developed before DNA origami, exploiting strand displacement reactions. Seeman was the first however to demonstrate how a DNA walker could be placed on an origami tile, making the complexity of dynamic systems possible [76]. The ability to program rules into DNA sequences has also led to some of the first DNA base computers, being able to perform logical operations. More recently though, Thubagere demonstrated the ability of DNA origami supported walkers for the transport and sorting of various cargo [77].

Anderson et al. were the first to demonstrate a dynamic DNA device using strand-displacement reactions [78]. Their use of a “lock and key” systems allowed for the opening and closing of a 3D DNA origami box. In the locked state, two extended strands along its edge were bound to those on the neighbouring face. In the presence of a “key” ssDNA strand, the extended strands became separated, opening the box. More complicated dynamic structures have since been developed, with Ke et al. demonstrating the ability to create multi-conformation DNA origami with the addition of ssDNA strands that would complement ssDNA strands bound between two regions of the origami [79]. Kuzuya et al. demonstrated how a target molecule could be used to alter the conformation of a pair of nanotweezers [80].

3.4.4 **Biophysical studies**

An important aspect of DNA storage in biology is the wrapping of DNA inside of the nucleus. DNA origami offered a way to study the small forces and dimensions involved, revealing details on the packing of DNA. Dietz et al. created a DNA origami hinge allowing for the sub nanometre placement of a nucleosome pair, to study how salt concentrations can affect their dissociation whereas Le et al. used a nanocaliper device to study their wrapping efficiency. Other methods have involved DNA origami to constrain dsDNA segments, allowing for the study of dynamic processes such as T7 RNA polymerase transcribing the constrained dsDNA using high speed AFM. Yamamoto et

al. use a DNA origami frame to study how DNA bending is required for the binding of certain proteins [81]. This frame technique has recently been expanded to study how RecA searches for homologous sequences [82].

DNA origami has also been used to study the forces involved in single molecules. Techniques typically involve attaching nanometre sized proteins to micron-sized beads, which are subsequently probed using optical and magnetic tweezers. DNA origami offers the ability to create more rigid structures, meaning that it is possible to measure lower forces. Kilchherr et al. used a DNA origami supported method for measuring the forces of base-stacking at single molecule level [83]. Nickels et al. developed an origami force clamp method, to probe the single molecules on a parallel scale using FRET [84].

One of Seeman's original goals for DNA origami was the ability to created 3D crystals for use in determining the crystal structure of proteins. The recent advent of cryo-EM has allowed for near-atomic resolution of variety of biological molecules. The recent work of Dietz group have managed to get cryo-EM of DNA origami to sub nanometre resolution [85]. The combination of cryo-EM and DNA origami may finally allow for the structural determination of small proteins due to the ability of DNA origami to place proteins in with nanometre precision, forming crystalline-like structures.

Membrane nanopores are important for controlling transport across cell membranes. It has been demonstrated that DNA origami nanopores can be inserted into lipid bilayers [86]. This can be extended up to large structures such as vesicles or microbubbles, allowing for transport across the membrane. DNA origami nanopores have also shown to be electrically conductive, which may lead to novel DNA sequencing techniques by acting as gatekeepers when combined with solid state nanopores [87].

4 Imaging DNA origami with AFM

4.1 Introduction

Atomic force microscopy (AFM) is a scanning probe microscopy (SPM) technique that is highly suited for imaging of biomolecules at the single molecule level. Its versatility allows for data collection in a wide range of environmental conditions ranging from vacuum to liquid, something that is matched only by optical based techniques. The advantage AFM has over optical techniques is the ability to image individual molecules, surpassing the limits of optical resolution without the need for additional agents, such as fluorescent dyes which can alter the native form of DNA. The other group of microscopy techniques are electron based, typically requiring the sample to be both conductive and imaged under vacuum, which too can lead to alterations of the DNA helix. Although recent advancements in electron microscopy, such as cryo-EM have shown to be able to achieve high-resolution imaging of DNA origami, AFM offers easier sample preparation methods as well as increased sample throughput.

The focus of this thesis is on the adsorption orientation of DNA origami nanotiles onto mica from bulk aqueous solution, studying how the structure of DNA affects the apparent curvature as well as physical properties of the tiles themselves. This requires imaging under physiological conditions to maintain the DNA in B-form. Imaging under aqueous solution removes unwanted surface adsorption and binding effects that may occur through drying of the sample. The recent advancement in AFM instrumentation allows for high-speed imaging, improving sample throughput. It has also allowed for easier imaging under aqueous conditions, something that has been taken advantage of in this thesis.

4.2 Scanning probe microscopy

SPM instruments utilise the interaction between the sample surface and a sharp nanometre sized probe to obtain data. The first atomic force microscope (AFM) was developed by Binnig and Rohrer, based on the scanning tunnelling microscope (STM)

which had earnt them the 1986 Nobel Prize for Physics [88], [89]. STM relies on the tunnelling of electrons between the probe and sample. This results in high resolution images in the Z-direction due to the exponential relationship between tunnelling current and tip-sample separation. STM however requires the sample be conductive, one of the key reasons that lead to the development of the AFM. Unlike STM, AFM collects data by measuring the deflection of a flexible cantilever as it interacts with the sample. The deflection is typically measured through the reflection of a laser spot on the back of the cantilever, which is why AFM can be used in a range of environments and on a range of samples [90]–[94]. With advancements in microfabrication techniques as well as AFM instrumentation, the size of the cantilever can be made smaller to be more sensitive to forces, leading to high resolution images of soft biological samples under aqueous conditions.

4.3 **AFM instrumentation**

In AFM a sharp tip attached to the end of a flexible cantilever is scanned across the sample, where the physical interaction between the tip and sample is used to generate high-resolution topographical micrographs. AFM has numerous modes of operation but the core component still remains: the AFM probe. The AFM probe is a micro fabricated device usually made of silicon or silicon nitride that consists of a flexible cantilever with an integrated sharp tip. It is the tip which interacts with the sample through both long and short-range forces. The choice of cantilever size and shape is dependent on the samples

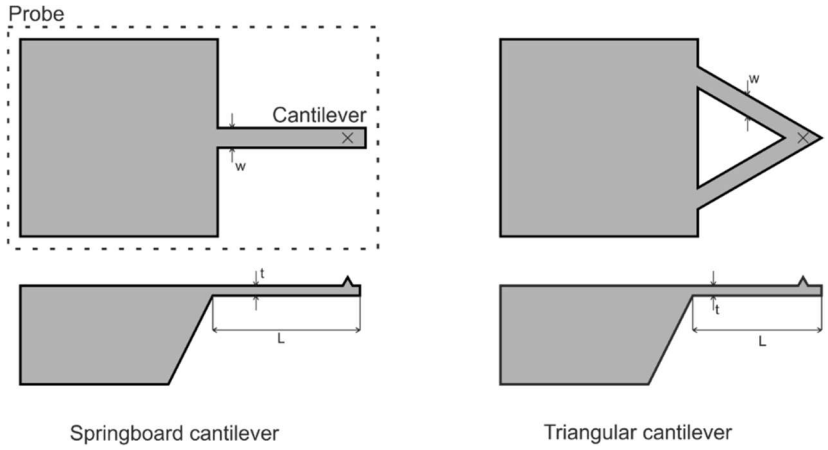

Figure 11. Common cantilever design demonstrating the spring board (left) and the triangular (right) cantilevers.

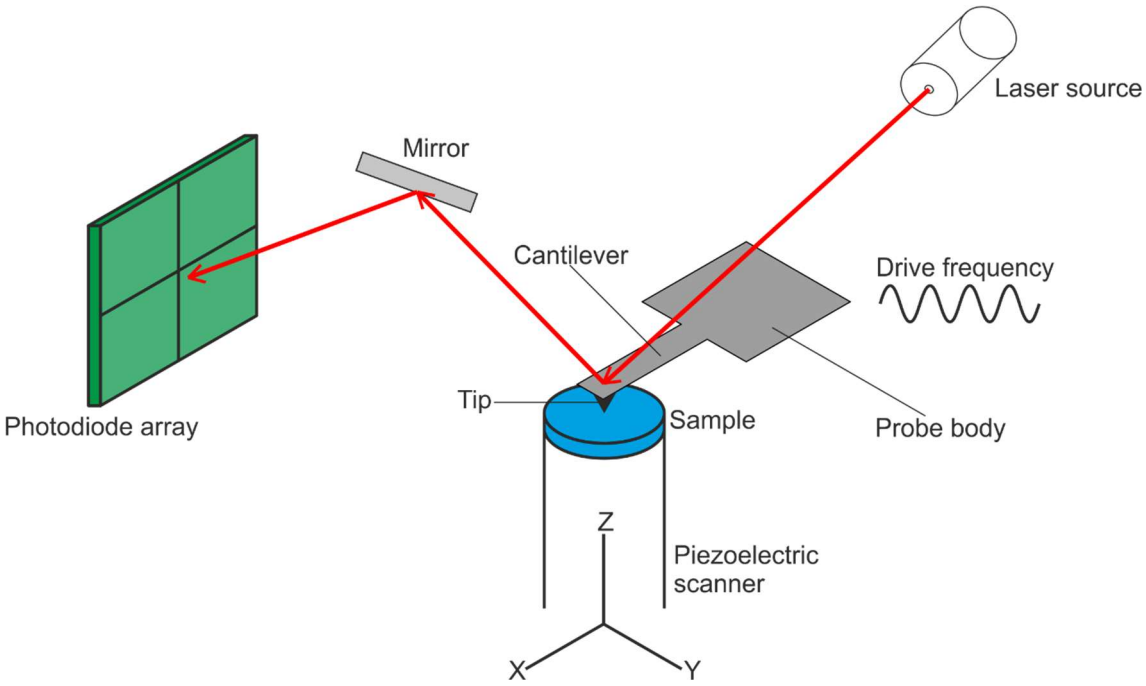

Figure 12: Schematic of a basic sample-scanning AFM mounted on a piezoelectric scanner. This setup is not representative of all AFM systems, but all utilise a similar method. The probe is mounted in a holder (not shown) which controls the drive frequency (if applicable).

mechanical properties as well as the imaging mode used. Cantilevers vary in spring stiffness from 0.01 to 400 Nm^{-1} with the tip sharpness being in the range of nanometres [95]. Careful probe selection is key for acquiring high-resolution topographical and quantitative data dependent on the sample measured and the application, e.g. imaging or force measurement. Figure 11 details the two most common probe cantilever design.

Tip-sample interactions are the main source of force on the cantilever. This force results in sub-nanometre deflections of the cantilever, requiring a sensitive deflection measurement system. The most common method for cantilever deflection is the optical lever method, where a laser spot is focused onto the top-side of the cantilever [96]. This laser spot is then reflected onto a photodiode, with one or more intermediate mirrors used to direct the laser. This set up allows for amplification of the deflection signal, providing a vertical or Z-direction sensitivity of 0.01 nm [97], [98]. Accurate resolution in the X-Y direction is maintained with scanners typically made from piezoelectric materials along with closed loop feedback systems. A piezo tube is also used to maintain accurate Z-positioning [99], [100]. Although the specifics of AFM systems vary by manufacturer, the general concepts remain the same (see figure 12). Some AFMs control the Z

direction by mounting the sample on the piezo tube, whilst others mount the probe onto the piezo tube.

4.4 Forces in the AFM

Images are collected in AFM by the forces that occur between the tip and the sample. The total force acting on the probe results in a deflection, which can be modelled using Hooke's law:

$$F = -kx$$

Where F is the total force acting on the cantilever, k is the spring constant and x is the deflection. As the spring constant is known, and the deflection measured, the force on the cantilever can be calculated. The force between the sample and the tip can be modelled by the Lennard-Jones potential (Figure 13). At extended ranges, the force on the cantilever arises from van der Waals forces, which are relatively weak and always attractive. At low separation, the idea of "physical" interaction is questioned, as the Pauli Exclusion Principle states that no two identical fermions can occupy the same state [101].

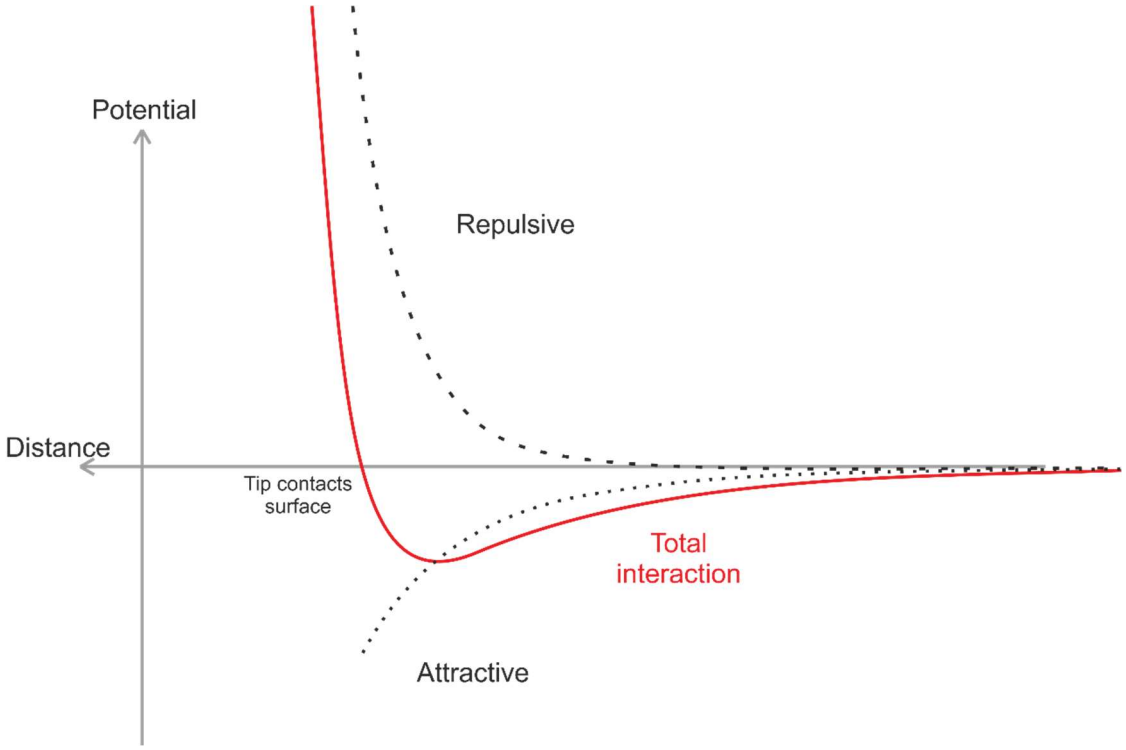

Figure 13: Graphical representation of the Lennard-Jones potential: The dashed lines represent the contributions from long-range van der Waals forces, with the repulsive forces coming from the electron cloud interaction between the tip and sample.

This results in a repulsive force, that is highly dependent on the separation and has been exploited for high-resolution imaging.

Other forces act on the probe and are a result of environmental conditions. In ambient conditions there exists a thin water layer on both the sample and the tip. When the two are brought into close proximity, the two water layers interact with each other, causing a capillary force on the tip [102]–[104]. This can cause the tip to snap onto the surface and is commonly seen in force-distance curves. This snapping action can result in sample and tip damage. The capillary force is not present under aqueous or vacuum conditions. The laser spot can cause heating of the cantilever, altering its relative stiffness. This has been mitigated to an extent with the design of smaller cantilevers and low-power laser spots. When imaging in aqueous conditions, hydrodynamic forces arise due to the relative motion of the probe and the sample which can perturb the sample. This too has been mitigated with the design of smaller cantilevers. It is also known that van der Waals forces are shielded in liquid due to the random orientation of the dipole moments. Imaging under vacuum eliminates these environmental interaction forces, with the cantilever deflection being dependent only on the interaction between the sample and the probe. This can lead to atomic or even sub-atomic resolution if the feedback control is optimised, with the cantilever being sufficiently stiff and the tip sufficiently sharp. The downside however is not all samples are suited for imaging in vacuum.

4.5 **Imaging modes**

AFM can be operated in various modes. The first mode that was developed was contact mode, which is still in use today and can be operated in either constant height or constant force mode. In constant height mode, the tip is maintained at a constant set point regardless of sample topography. As the tip is scanned across the surface, the forces cause the cantilever to deflect, which is then recorded. In constant force mode, the deflection of the cantilever is maintained at a constant set-point. As the tip is scanned across the surface, the change in topography and forces cause the deflection to change. The change in deflection is detected through the laser spot and is fed into feedback loop,

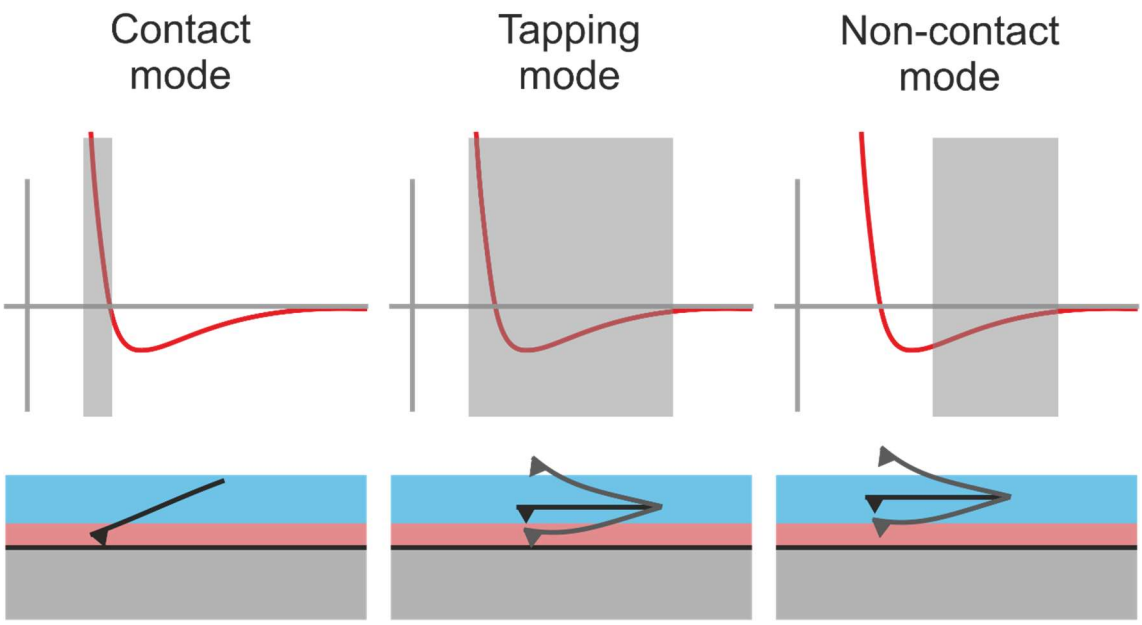

Figure 14: Simplified view of where the three main AFM modes operate. The blue denotes an attractive force, whilst the red repulsive. The sample is depicted as grey. In tapping mode the cantilever is driven such that it intermittently contacts the surface, whilst in non-contact mode the AFM is able to operate through interactions that are solely attractive forces.

which alters the z-piezo position so as to maintain the deflection set-point. The rate at which the z-piezo reacts to changes in the topography is controlled by a PID controller, and is limited in the response time of the z-piezo. Constant height mode is typically used for samples that are known to be flat, as movement of the z-piezo can introduce noise, which can be amplified by the feedback loop.

The most common mode of AFM is intermittent-contact (IC) mode. This is also referred to as TappingMode™ or AC-mode, depending on the AFM manufacturer [105]. For simplicity it is referred to as tapping mode throughout this thesis. In tapping mode, the cantilever is driven at a constant drive amplitude and frequency. The frequency chosen is at or close to the resonant frequency of the cantilever. There is an inherent phase-shift between the driving amplitude and the amplitude at the free-end of the cantilever. When the tip is brought into close proximity with the surface, sample-tip interactions reduce the free amplitude. The reduced amplitude of the free-end is maintained at a user defined set-point, and is used in the feedback loop to move the z-piezo during scanning. The interaction with the surface causes a retardation of the free-end oscillation, as the rate at which energy is dissipated is dependent on the properties of the sample [106], [107].

This changes the phase-shift between the driving frequency and the frequency of the free-end of the cantilever, allowing for phase imaging of the sample. Phase imaging can be used to image samples that would otherwise appear identical in the topographical image [108], [109]. Due to the intermittent contact, lateral forces are minimised in tapping mode due to the short-interaction time between the tip and the sample. Tapping mode can result in tip and sample damage if the amplitude set-point is too low, due to excess energy being dissipated into the sample.

The amplitude of oscillation in tapping mode means that the tip is continuously brought into and out of physical contact with the surface. It is possible to tune the system such that the tip does not physically contact the surface, but rather interacts with the attractive van der Waals forces as well as the repulsive forces [90], [110]–[112]. This allows for non-contact (NC) AFM imaging. NC-AFM typically operates in the attractive regime, feeling only effects of the van der Waals. It is also possible however to image close to the surface, such that the tip just feels repulsive forces. In this regime, the AFM is able to obtain higher resolution images due to the greater change in force over the same distance [113]. As both NC mode and tapping mode are forms of amplitude modulation (AM) imaging, it is important to distinguish between the two. NC mode can also operate in frequency modulation (FM) mode where the interaction with the surface causes a shift in the resonant frequency of the probe. The systems responds to this by changing the drive frequency of the cantilever, to maintain a constant amplitude of the free-end.

AFM can also be used to obtain force-distance curves, allowing for quantitative analysis on the physical properties of the sample. This has been extended into modes such as ForceVolume and quantitate nanomechanical mapping (QNM). Both of these modes are variations of tapping mode, with the exception that the deflection of the cantilever is continually monitored. The deflection response of the cantilever as it comes into contact with the surface can then be used to obtain information such as sample adhesion, energy dissipation and hardness etc.

4.6 **High speed AFM**

One of the issues with AFM is the rate at which samples can be scanned, due to the physical interaction required between the tip and sample. There are two limiting factors which have since been overcome, leading to the development of faster AFM systems [114]–[119]. These are the rate of which the tip is oscillated and the rate at which the sample is moved. In tapping mode, the AFM probe has to physically contact the surface during each cycle. To ensure adequate sample interaction at each pixel, the cantilever needs to be oscillated at higher frequencies. One of the ways to achieve this is with the design of stiffer cantilevers. This however limits the softness of the sample that can be imaged. This was overcome with the development of smaller cantilevers, which allows for both softer cantilevers and higher drive frequencies. This also required the development of more responsive and higher bandwidth electronic systems, due to the increased data output. This was solved by the development of an RMS-DC converter that was capable of using a half-wave to convert the signal, rather that 5-6 waves that were previously required[114], [120].

The issue of speeding up sample movement was first demonstrated by Ando et al. who created a stacked piezo system [120]. Previously piezo tubes consisted of four crystals that worked in tandem to give the x, y and z movement. The systems designed by Ando remedied this by having the X and Y piezo in one plane, and the z piezo in another. This decouples the X and Y from the Z, removing vibrations. The stacking of piezo means that the sample can be moved in both X and Y simultaneously. There are now a range of commercial high speed AFM systems, such as the Bruker Dimension FastScan used in this work. The rate at which AFM systems can now scan has also lead to manufactures differentiating between high speed and video rate. High speed AFM was used extensively in this thesis due the increased sample throughput, allowing for increased statistical sampling and analysis.

4.7 Imaging parameters

An AFM user has control over key parameters of the system. In contact mode, the user adjusts the deflection set-point. A higher set-point corresponds to greater force on the tip, increasing sample damage and tip wear. In tapping mode, the drive amplitude and frequency are kept constant throughout. Rather than a deflection set-point, tapping mode maintains the amplitude set-point, corresponding to the absolute value of the amplitude, rather than a change in the amplitude. If the amplitude set-point is too low, excess energy is dissipated into the sample, resulting in damage. Similarly if the drive amplitude is too high, the relative difference between the drive amplitude and the amplitude set-point can result in tip damage. In QNM mode, the maximum force on the oscillating cantilever is kept constant. This is similar to the amplitude set-point in tapping mode, but takes into account the physical properties of the sample.

The rate at which the system responds to changes in the deflection or amplitude is controlled by electronic feedback systems, known as PID controllers. An AFM user has control over the proportional (P) gain and the integral (I) gains. These gains affect the rate at which the z-piezo is adjusted, due to changes in the deflection or amplitude. Higher gains cause the system to respond quicker, sacrificing the signal-to-noise ratio as a result of high sensitivity which can arise due to thermal fluctuations. This can result in a noisy image. Conversely, low gains can cause the system to respond slowly, resulting in increased dwell times and can damage the tip. A key part of AFM is that the tip is scanned across the surface. This results in a fast and slow scan axis. The fast scan axis is typically set parallel to the long axis of the cantilever, whilst the slow axis is perpendicular.

Resolution in AFM images are dependent on all the above factors. One of the most important factors that is beyond the control of the user is the tip radius. Ideally the tip would be one atom, such that force acts only on one spot. As this is rarely the case, the tip interacts over a certain volume, known as the interaction volume. If the tip radius is larger, it interacts over a greater volume, reducing the ability to obtain high resolution

images. This is why preservation of tip sharpness is key in obtaining high resolution images.

Although the cantilever is often tuned to its resonant frequency so as to obtain the largest free amplitude, increasing Z-resolution, intermittent contact mode can operate at any frequency. As liquid is 600 time denser than air, a greater driving set-point amplitude is required to overcome dampening forces due to the liquid. This results in a wide, low resonant peak. The ratio of the height to the width of the peak is quoted as the Q factor. Vacuum has the greatest Q factor, as there are no damping effects present. Air has the second best, with Q value in the range of 10-500, whilst liquid has the worst in the range of 3 or even less.

4.8 AFM imaging of DNA molecules

4.8.1 Substrate choice

The wide range of length scales afforded by AFM means that it is not always possible to image samples directly. In the case of nanometre and micrometre samples, a substrate is required to mount the sample. There are two main criteria that must be fulfilled to allow for imaging of DNA and DNA origami. Firstly, the substrate must be flat so as to discern topographical difference between the DNA and the substrate. Secondly the substrate must form an adequate bond with the DNA so that it is not perturbed by motions of the tip. The most commonly used substrates for the study of DNA are HOPG, glass, silicon and mica. HOPG and silicon both require modification to ensure adequate binding whilst glass lacks long-range flatness. The mica surface however is both negatively charged and atomically flat, making it ideal for studying DNA in both liquid and ambient conditions [97], [121]–[123].

4.8.2 Imaging of DNA molecules

Mica is the collective name given to a set of silicate based layered materials. In AFM, the most common mica used is muscovite (ruby) mica. The muscovite mica layered structure can be easily cleaved with tape, to reveal a near-atomically flat surface. When

mica is cleaved, the interfacial K^+ ions are shared between the two surfaces [124]. Under aqueous conditions the K^+ ions dissociate from the surface into the liquid, leaving a negatively charged mica surface. As DNA in solution contains an excess of Mg^{2+} ions to neutralise the negative sugar-phosphate backbone, the Mg^{2+} ions are able to bind to the negative sites in the mica. This forms a layer of Mg^{2+} ions, which the DNA is then able to bind to. This mediated DNA-mica interaction with Mg^{2+} is known as a salt-bridge [125].

As the Mg-DNA interaction is non-specific and relatively weak, the DNA molecules are able to laterally diffuse across the surface, causing the DNA to adopt a surface equilibrated conformation [126]. This diffusion prevents individual DNA molecules from being imaged under aqueous conditions as they can be diffusing too quickly and/or perturbed by the AFM tip. In order to image DNA molecules under aqueous solution, the mica is typically pre-treated with Ni^{2+} [127]. Nickel forms a stronger bond with the mica surface, such that even when the DNA-buffer solution is deposited, the Mg^{2+} ions are unable to displace the Ni^{2+}. The Ni-DNA interaction is also stronger than the Mg-DNA interaction. This limits the diffusion of the DNA when adsorbed, causing them to become kinetically trapped, adopting a 2D conformation that is representative of the 3D solution structure [128], [129]. Nickel pre-treatment is also required for imaging ssDNA molecules under ambient conditions due to the weaker Mg-DNA interaction [130].

4.8.3 **Imaging of DNA origami**

As origami are higher dimensional structures than linear DNA molecules, their solution structure is believed to affect their adsorption orientation onto mica. The solution structure of origami is determined by the underlying crossover composition and arrangement. For square-based single-sheet origami the inability to have a non-integer number of base pairs between crossovers means that the origami exhibit a curvature reflecting the underlying crossovers. CanDo is a commonly used finite-element model whose results are taken as de facto during the analysis of DNA origami. This is discussed in chapter 6, along with the impact of crossover composition and arrangement in chapter 8.

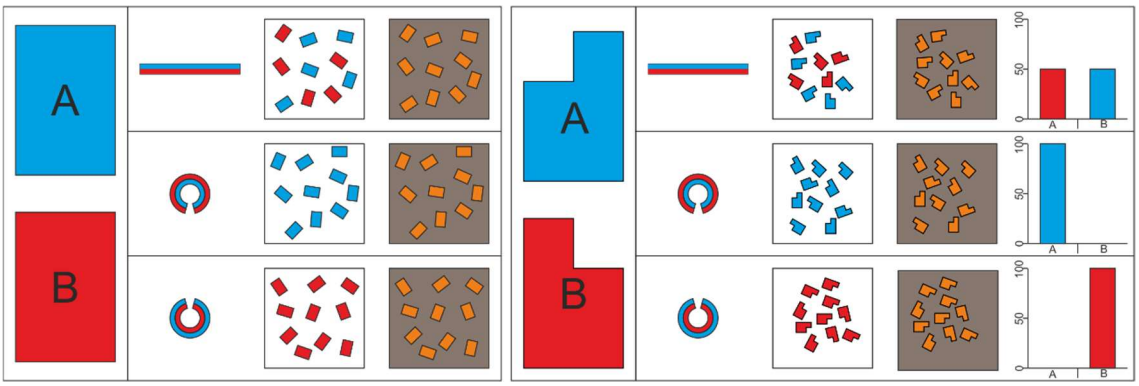

Figure 15: Fundamental notion explaining adsorption orientation of origami tiles. The asymmetrical tiles allow for differentiation of orientation, as demonstrated in the mock AFM images. Binding ratios are therefore reflective of the underlying curvature, highlighting the extreme cases.

As AFM is a surface-based technique, binding orientation information is lost when imaging symmetrical DNA origami due to the inability to distinguish between the origami "faces". This is shown in figure 15, which demonstrates the extreme case of a curved origami and how this would appear when imaged with AFM. This can be alleviated by using an asymmetric tile, such as that used in this work, and previously demonstrated by Marchi et al. [68]. Curvature of origami has also been investigated with SAXS and EM, by Baker et al. and Mallik et al. respectively [131], [132]. A downside with SAXS is that it is only able to distinguish the magnitude of curvature and not its orientation. This

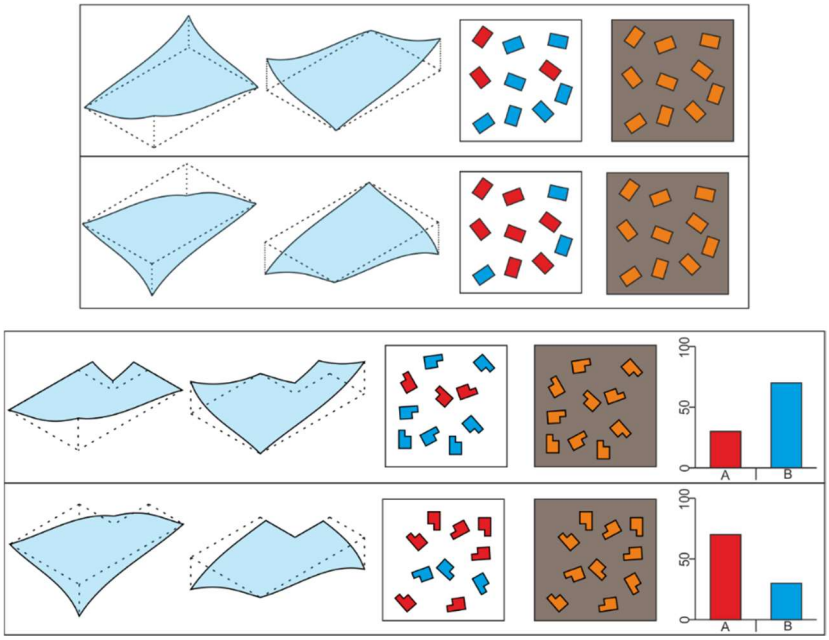

Figure 16: Top; curvature of a symmetrical origami based on realistic crossover spacing's. It is still not possible to infer solution curvature with AFM. Bottom; curvature of an asymmetric origami with realistic curvature. Although it is possible to infer orientation, the axis around which the origami curves cannot be measured.

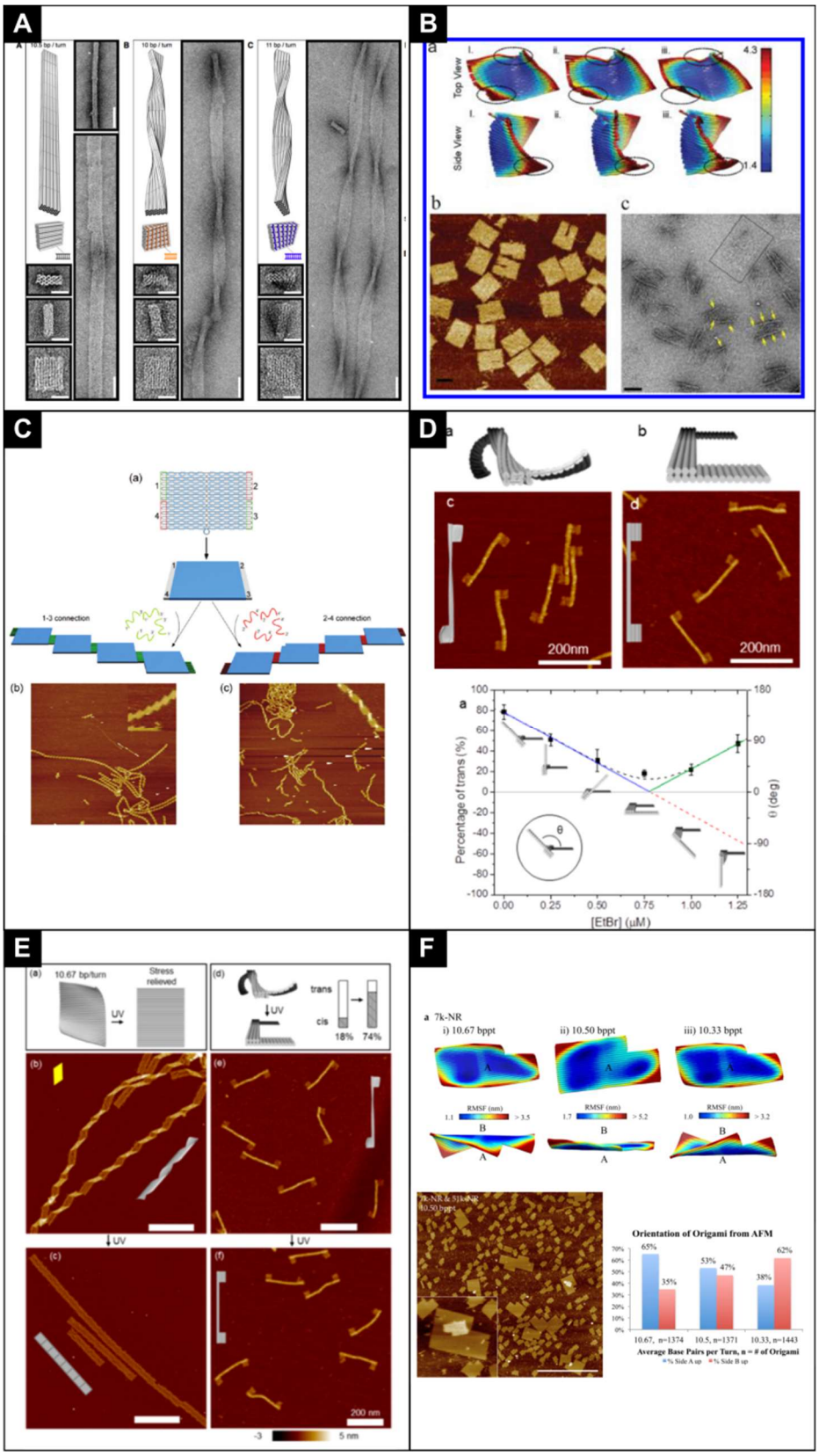

Figure 17: A) Helical bundles showing how base insertion/deletion causes twisting [52]. B) CanDo models, AFM and EM images of a rectangle with a crossover spacing of 16 bp [132]. C) Overview of formation of "nanoribbons" by joining diagonally opposed tiles [37]. D) Models, AFM images and observed binding of "flagpole" origami with increasing EtBr concentration by analysing *cis* and *trans* conformations [134]. E) Effect of UV radiation on the presence of "nanoribbons" as well on the flagpole origami [133]. F) CanDo models of smaller 7k nt origami, with AFM images showing size comparison between 51k nt and 7k nt origami. Binding statistics of larger 51k nt origami [68].

is demonstrated in figure 16, showing how a symmetrical origami can curve, based on CanDo models as well as results of this work. In the EM paper of Mallik et al. they were able to demonstrate how an origami with a 10.67 helical pitch curves, as seen in figure 17. The symmetrical nature of the tile means that it isn't possible to determine if the origami is curved like that in figure 15 or figure 16, since they would both appear the same. This inability to distinguish the orientation of the tile is also present in the work by Dietz et al. [52]. They designed a honeycomb based helical bundle, demonstrating that the insertion/deletion of bases can cause the origami to adopt a left or right-handed twist (figure 17). The same problem that is present with the inability to distinguish between a symmetrical single-sheet origami is prevalent in these twisted bundles, as there are two possibilities for the formation of a left or right-handed helix.

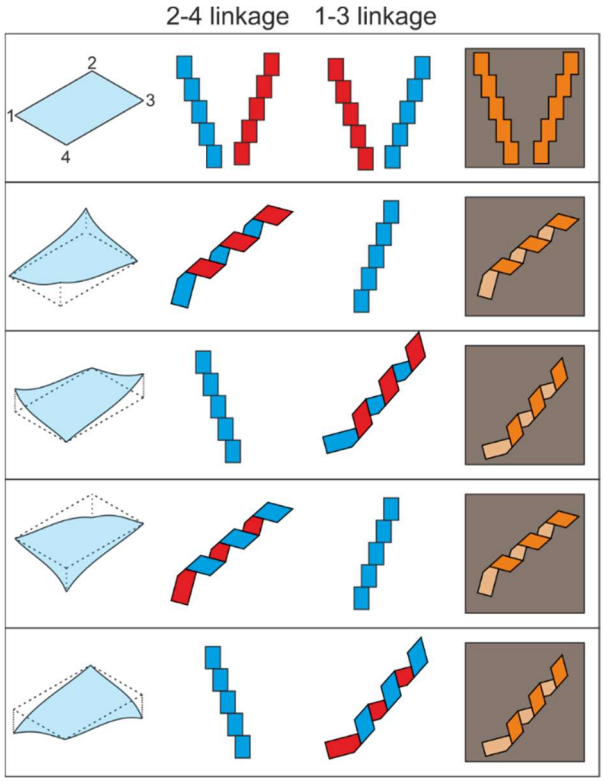

Figure 18: Potential structure and orientation of nanoribbons. The mock AFM images demonstrate how the two left- or right-handed ribbons would appear, showing that the axis around which the tile curves cannot be determined.

One of the methods to determine the magnitude and direction of origami curvature was demonstrated by Li et al. who formed "nanoribbons" of DNA origami by linking curved origami together [37]. As CanDo has shown that certain corners of origami are curved, linking these corners together will form a twisted structure, whilst linking the flat corners

would create a flat structure. In figure 18 it can be seen how curved origami can be linked together, and the resultant structure's that would form depending on the direction in which the tiles are linked. Similar to single symmetrical origami tiles, there are two cases which can result in either a left or right-handed nanoribbon. As they used a single tile design, basing their results on CanDo models, there is still an issue as to whether or not CanDo is correct since there are two potential causes for the formation of a right-handed nanoribbon. The main difference between the two right and left handed super-helices is the orientation of the starting origami. This information is lost in AFM images, with both cases appearing the same.

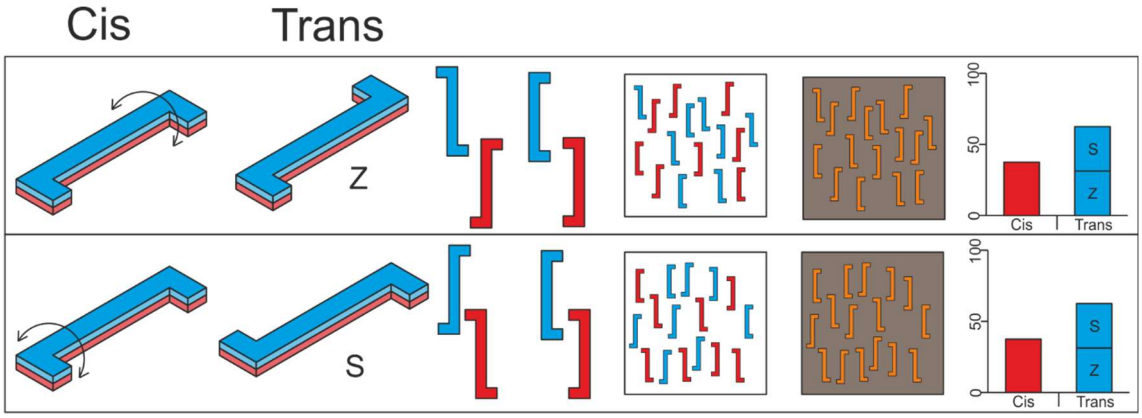

Figure 19: Schematic demonstrating the inability to determine under- and over-wound of flagpole origami due to symmetry of the design.

Another attempt to measure the effect of tile curvature using both UV irradiation as well as intercalators came from the Choi group [133], [134]. They first used intercalators, which induces unwinding of the helix. The use of a "flagpole" structure allowed for distinguishing between a *cis* and *trans* conformation, by the position of the two flags either side of the central pole. The degree of twist in the origami was analysed through the proportion of origami observed to be *cis* or *trans* in AFM images. The problem is that the under or over-winding of one end is identical to that of the other and as such it cannot be determined if the flagpole is under or over-wound. This is a similar argument to the single-sheet origami where alternative corners curve in or out of the plane. Although the *trans* version can be either S-shaped or Z-shaped, they can be superimposed onto each other when flipped (Figure 19). In theory however, detailed analysis on the tiles observed with the S- or Z-conformations would be able to determine the angular offset between

the two flags on either end, assuming the flags would be able to influence the binding orientation.

The origami tile designed by Marchi et al. solves this degeneracy issue by using an asymmetric tile, such that it is possible to distinguish binding orientation of origami with AFM. Figure 16 demonstrates the possible ways that this asymmetric origami can curve, by changing the supercoiling of origami. CanDo predicts that the under and over-wound origami will curve into opposing planes, causing origami to bind with opposing faces on top. This was the exact result shown by Marchi et al. suggesting that CanDo is in fact correct. The CanDo model generated by Marchi et al. was for a smaller DNA origami using the M13mp18 scaffold, whilst the binding statistics were of a larger origami which used a custom 51k-nt scaffold. There are no results published for the smaller origami, which was a source of frustration due to the results observed in this thesis conflicting with those of Marchi et al. This is discussed in chapter 6, explaining how the larger origami has a lower effective Mg^{2+} concentration, affecting the DNA's helical stability

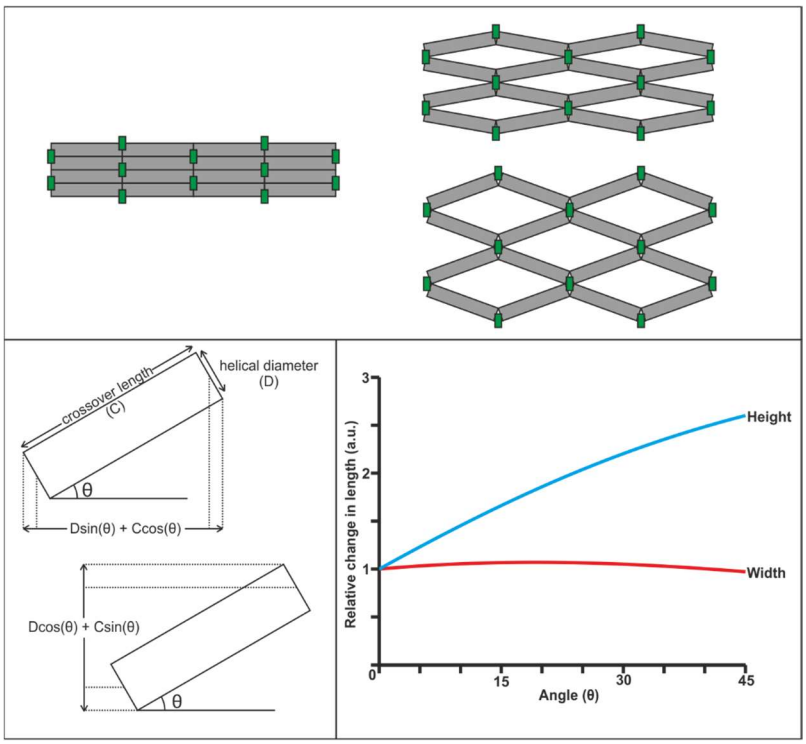

Figure 20: Schematic of the internal diamond lattice that is observed with DNA origami tiles. The rough geometric diagram demonstrates how the width of the origami would experience a greater change with increased electrostatic repulsions.

such that it is not strictly canonical B-form. Additionally, the OxDNA models in chapter 6 combined with the binding results further show how inaccurate the CanDo software is.

Once DNA origami is bound to mica, regardless of the effects of curvature, there a several factors which affect its apparent physical properties, such as width and length. The tightly packed helices of lattice-based origami means that the helices exert repulsive electrostatic forces on one another. This effect was first noted by Rothemund and it causes the DNA origami to appear wider than the idealised design, when imaged under liquid conditions [3]. This causes the appearance of an internal diamond lattice, where the corners are the crossovers and the edges are the DNA strands between the crossovers. In high resolution images of DNA origami there is an apparent asymmetry in the heights of the edges of these diamonds, as some of the DNA strands between crossovers are nicked. This allows the DNA to relax, causing them to deviate from the idealised B-form shape, as discussed in chapter 8, and is the source of the “major axis” hypothesis. This inter-helical gap is observed in both helical bundles as well as single sheet origami that have differing crossover lengths, with literature noting the structural and mechanical differences, as seen in figure 21. The effect is most noticeable along the axis perpendicular to that of the DNA helices. Figure 20 details how the width of the origami would theoretically change with an increase in electrostatic repulsion, noting that the effect is more noticeable along the axis perpendicular to the helices. This was the main reason width measurements were recorded and analysed in the results chapter, to measure the repulsion as well as helix stability. This internal diamond structure is only observed for hydrated DNA origami. Imaging origami under ambient conditions can result in a variety of observed structures due to various drying effects. The AFM work in this thesis was carried out under aqueous conditions, so as to remove any effect that may occur due to the sample drying affecting observed binding statistics. The inter-helical spacing is also dependent on the relative ionic concentration. The electrostatic repulsion between the helices as well as the DNA-Mica binding is dependent on the Mg^{2+} concentration, this is explored in chapter 6.

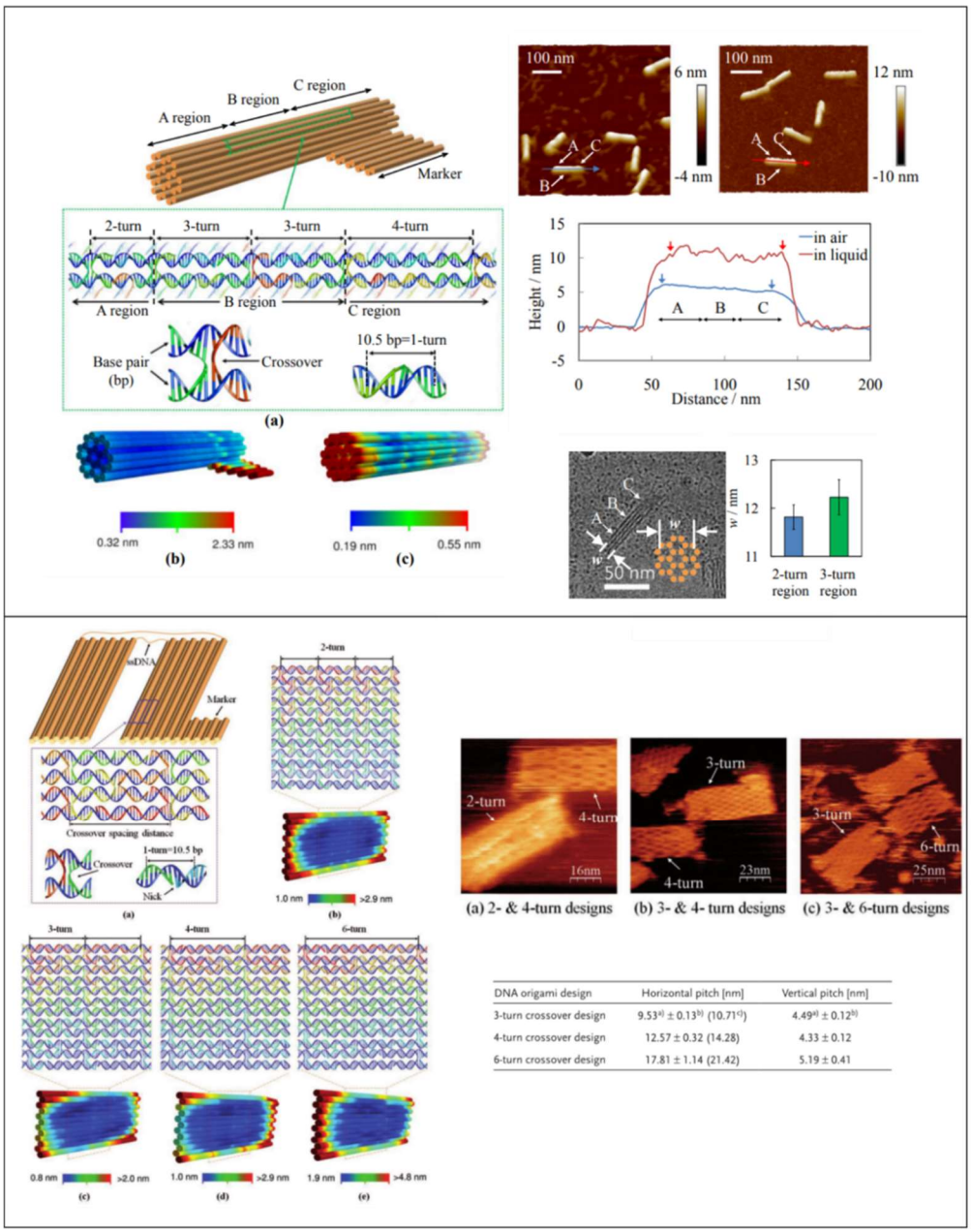

DNA origami design	Horizontal pitch [nm]	Vertical pitch [nm]
3-turn crossover design	9.53[a] ± 0.13[b] (10.71[c])	4.49[a] ± 0.12[b]
4-turn crossover design	12.57 ± 0.32 (14.28)	4.33 ± 0.12
6-turn crossover design	17.81 ± 1.14 (21.42)	5.19 ± 0.41

Figure 21: Top: Models of helical bundle showing placement of crossovers with varying spacing's. Height profiles detail the difference between imaging of origami in air and liquid, as well as the difference observed in the varying regions [148]. Bottom: Origami showing how a marker section is used, with the other section containing varying crossover spacing, along with simple schematics showing staple arrangement. AFM images highlight difference observed with differing crossover spacings [149].

DNA origami binding to mica under aqueous conditions is often taken for granted, since they bind and are immobile in conditions that individual smaller DNA molecules are sometimes not. This has allowed origami to be imaged under a wide variety of conditions. Most notable is the folding and depositing in the presence of Na^+ ions, which greatly affect the surface mobility as shown by Woo and Rothemund, as Na^+ is known to weaken

the DNA-mica interaction [71]. The hope was to make the origami mobile, such that blunt-end interactions would cause the formation of arrays. This was achieved, but the lack of control over the adsorption orientation means that this method is perhaps not ideal for creating large-scale structures. DNA origami have also been imaged on a supported lipid bilayer, with the aim of creating large-ordered arrays [7], [135]. This was demonstrated by Suzuki et al. who were able to deposit origami without the need of anchoring them to the bilayer [7]. This has led to some of the largest periodic arrays. As previously

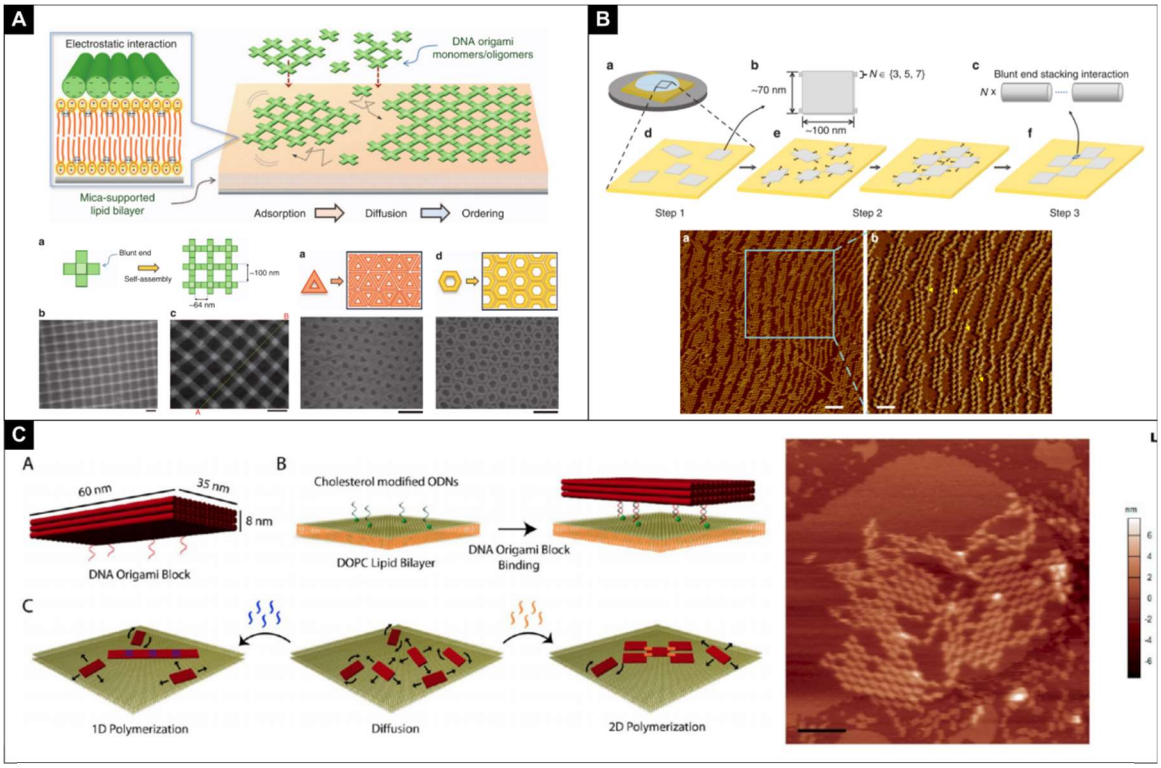

Figure 22: A) AFM images of adsorbed origami onto a lipid bilayer, showing how base stacking interactions, along with increased mobility, cause the formation of arrays [7]. B) Deposition of origami onto mica under Na^+. Increased mobility leads to origami forming arrays with base-stacking interactions [71]. C) Anchoring of origami to a lipid bilayer using cholesterol to anchor origami [135].

mentioned however, the lack of control over adsorption orientation as well as inter-tile binding leads a lot to be desired. One proposed method has been to generate lithographic templated substrates, which are designed to be hydrophilic such that the DNA binds in a specific place. This effect was taken further with the recent publication by Gopinath et al. who showed that by modifying one of the origami surfaces with ssDNA, it is possible to orientate them on the surface [136].

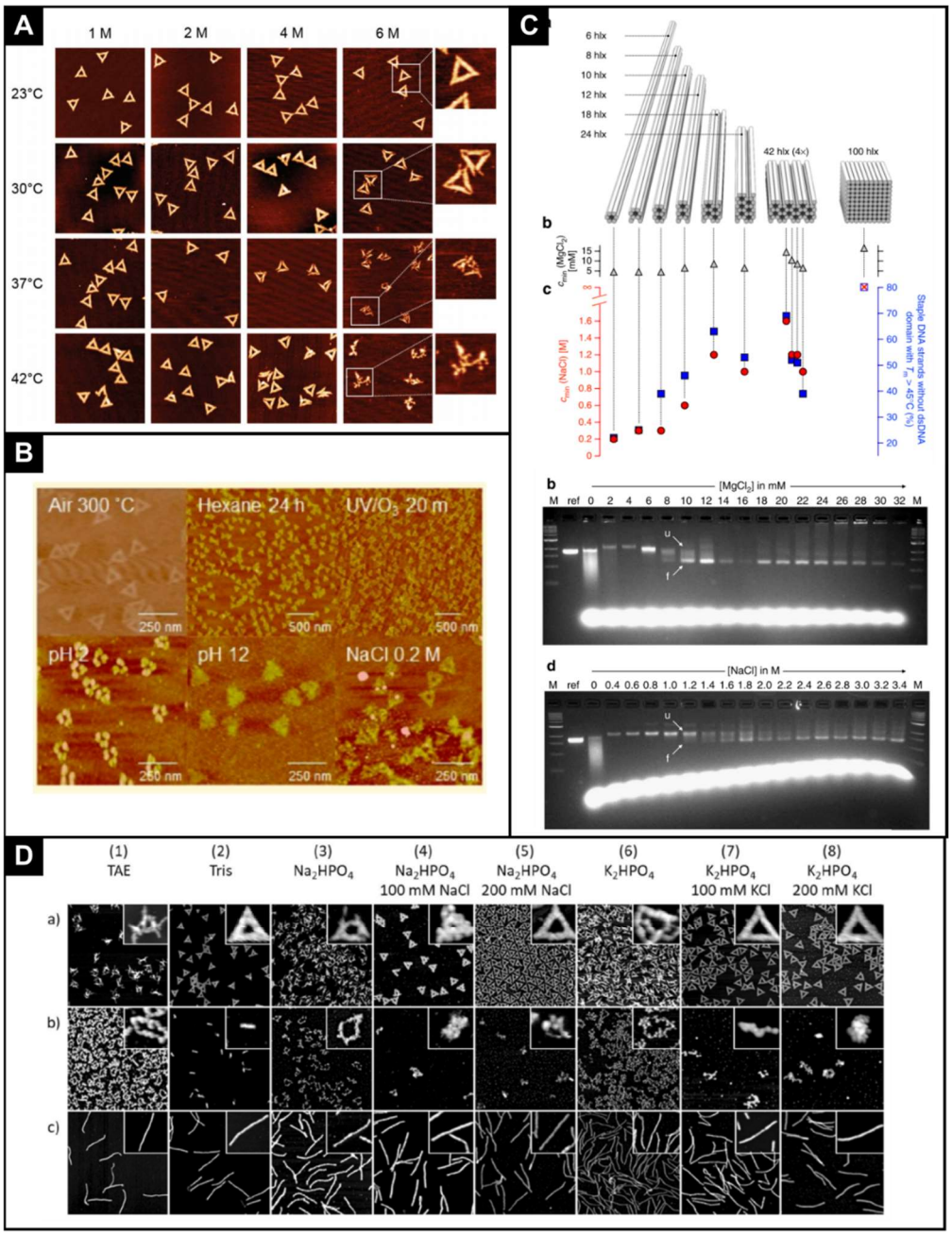

Figure 23: A) AFM images of triangular origami under solutions of urea and GdmCl [137]. B) AFM images of triangular origami under varying buffers (labelled) [138]. C) Overview of origami designs and their movement through AGE, highlighting yield of folding under Mg^{2+} and Na^{+} [139]. D) AFM images of triangular origami under varying buffers as well as varying conditions (UV exposure, high temperature) [140].

The recent review article by Ramakrishnan et al. details the various environments that DNA origami has been shown to be stable in, highlighting its usability in a variety of buffers [137]. Most of these are derived from biological environments, which is just one potential area of DNA origami. Of the works discussed in the review however, most methods to assess origami structure have focused on their appearance on substrates and their degree of yield during the folding, rather than measuring the structural effects

of these buffers. An overview of some of the buffers are shown in figure 23, where AFM as well as agarose gel electrophoresis (AGE) where the main methods used to assess the folding yield [138]–[141].

5 Methods

This section details the main experimental procedures used to fold and image the DNA origami constructs used in this work, with references to other methods that are used in literature, highlighting the broad spectrum of folding buffers as well as techniques.

5.1 Preparation of DNA origami

Original files of the origami used in this work were obtained from Thomas LaBean, the corresponding author of the paper from which the designs in this thesis were based on. A list of the staple strands used in this work are given in the appendix.

Lyophilised staple strands were purchased from Integrated DNA technologies, Inc. with standard desalting. These were re-suspended to a concentration of 100 μM. A 50 μL aliquot from each individual staple solution was taken and mixed with others in their corresponding column. This gave 20 columns for each origami design. A further 50 μL was taken from each column mixture and combined together. This gave a final staple solution of 1 mL with each staple at 384 nM.

A standard folding mixture contained:

4 μL M13mp18 @ 100 nM

10 μL staple stock @ 384 nM

10 μL 400 mM Tris, 10mM ethylenediaminetetraacetic acid (EDTA)

10 μL 125 mM Mg-acetate

53 μL ddH_2O

This gave a final Mg^{2+} concentration of 12.5 mM along with an m13mp18 concentration of 4 nM with a 40x staple excess. The folding mixture was then heated to a temperature of 95°C and held for 4 mins, then cooled to 20°C at a rate of 1°Cmin^{-1}. Once folded, the mixtures were left at 4°C for a minimum of 12 hrs before imaging.

The folded mixtures were used as a stock solution from which aliquots were taken and diluted such that the final origami solution was 1 nM with a 10x staple excess. It was at this stage that the ionic concentration was altered, by diluting samples into mixtures containing salts, TAE and water to obtain the desirable final Mg^{2+} or Ba^{2+} concentrations (or mixture of). Staples were left in solution as filtration methods can lead to potential contaminants in solution, as well as unknown salt:DNA concentrations.

5.2 **UV exposure**

UV exposure of tiles was carried using a Pen-Ray Mercury lamp (Ultra-Violet products Ltd, Cambridge, UK) product no. 90-0012-01 (11SC-1). Intensity of the UV lamp was measured using a compact power and energy meter console (Thorlabs, part no.: PM100D) using a S120VC UV-sensitive photodiode sensor. The recorded irradiance was 17 Wm^{-2}. Samples were exposed in 1 min intervals for fine UVC exposures, equating to a dosage of 1.02 $kJm^{-2}min^{-1}$. Lamp spectra from the manufacture noted a peak emission at 254 nm (UVC).

Samples were folded with a 10 nM m13mp18 excess. An 80 µL aliquot was taken, which was diluted to 800 uL into an Ultra-micro cuvette (Brandtech Scientific, INC, product no.: 759235). After each exposure, a 40 µL aliquot was taken for AFM imaging.

5.3 **AFM imaging**

Images of the origami were captured in liquid using the Bruker Dimension FastScan AFM using FastScan-D probes (Bruker, Billerica MA). To prepare samples for imaging, 10 µL of the folded mixtures was deposited onto freshly cleaved mica and left to incubate at room temperature for 3 mins. After incubation, 240 µL of imaging buffer was added. The sample was then placed onto the AFM platform and the AFM head slowly lowered until the mica surface was in focus. The AFM was used in Tapping mode (liquid) with the cantilevers tuned using the auto tune feature.

5.4 **Sample analysis**

To achieve adequate statistical analysis of the binding ratio of tiles, images were collected by scanning areas that are 9x9 μm in size, with a pixel resolution of 3072x3072. These images were manually processed using FIJI, counting the number of tiles with the A- or B-face on top. Tiles whose orientation could not be determined were used for calculating errors. For width measurements of the tiles, this was reduced to 3 μm whilst maintaining the pixel resolution. For width measurements, a single image was taken so as to not perturb the tiles to an excessive degree, affecting their observed widths. Captured images were then analysed using Gwyddion due to increased number of line profiled that can be extracted. These line profiles were then imported into OriginPro 9.1, where the second derivative of the line profiles were used to determine the width.

Due to the similarity and nature of analysis used for this work, most AFM images are similar in appearance. For improved reading, AFM images are omitted from the main text of this work as the author feels it detracts from the results. A series of example images are however given in the appendix, highlighting the tile design, buffer conditions and image resolution. The appendix also contains details on the analysis and significance of the scanning areas used. High resolution imaging of the DNA origami is however detailed in chapter 8.

6 Effect of Magnesium on origami curvature

DNA origami has shown to be a versatile tool for a wide range of applications. One area of interest is having the ability to control the adsorption orientation of origami onto substrates. Being able to control orientation will lead to increase yields in experimental procedures such as surface supported biosensors, DNA walkers or applications where the DNA is functionalised. Measuring the adsorption orientation also offers a method for determining the solution structure of origami, where certain buffers may lead to changes in the structure of the origami. This is important for applications where the origami are used in an “exotic” buffer, which may cause unwanted/unknown structural changes.

The crossover spacing of DNA origami has shown to cause twisting or curvature of the design, especially in square-based origami [37], [131], [134], [142]. This is particularly important for single-sheet origami, which are intrinsically more flexible than multi-layered origami. The benefit of using single-sheet origami is that they offer greater surface areas for surface-supported applications. The increased flexibility also means that it is easier to “tune” the curvature in a laboratory environment, and thereby bias the orientation of surface binding for controlling and creating hierarchical assemblies and devices based on single-sheet origami.

AFM is used for measuring the curvature of origami as it allows for imaging under liquid conditions, maintaining the physiological conditions that DNA requires. It also does not require the use of dyes as in high resolution optical microscopy, which are often intercalators, which may alter the structure. Finally, studying origami on a surface is reflective of applications whereby DNA is adsorbed onto substrates.

6.1 Cause of origami curvature

Supercoiling of DNA occurs to counteract the addition/removal of helical turns. The addition of helical twists results in DNA that is positively supercoiled (overwound), whilst the removal of helical twists results in negatively supercoiled DNA (underwound). DNA

wants to maintain the helical pitch imposed by the solution conditions, which is typically assumed to be B-form with a helical pitch of 10.50 bp [143]. The addition/removal of helical twists alters the helical pitch of the DNA. To counteract this, the DNA forms contortions known as toroids or plectonemes, when twist partitions into writhe. The handedness of the writhe is opposite to the direction of twist. This is seen in figure 5 (chapter 2), where the twisted state of overwound DNA is right-handed, whilst the supercoils are left-handed.

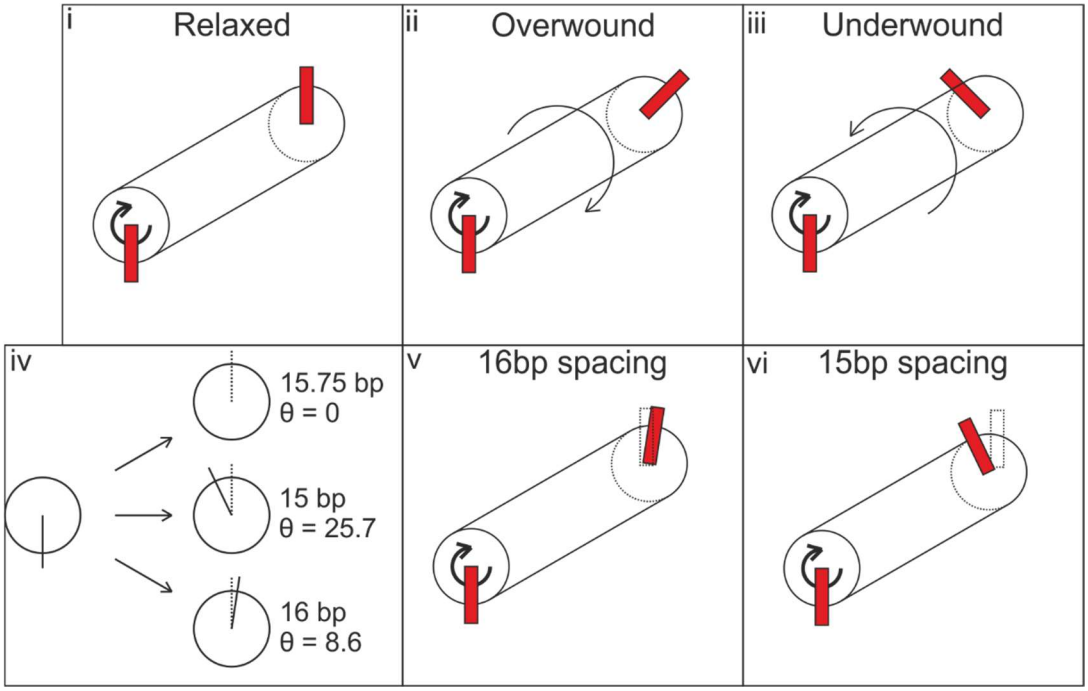

Figure 24: i) Orientation of bases seperated by 1.5 turns. Relative orientation of bases for ii) overwound and iii) underwound DNA. iv) angular mismatch of 16 bp and 15 bp crossovers, relative to the idealised 1.5turns of 15.75 bp. Orientation of bases for a v) 16 bp and vi) 15 bp crossover, highlight the mismatch to 15.75 bp.

For square-based single sheet-origami, the crossovers have to be spaced an odd number of half-turns apart. This is typically 1.5 turns, which for B-form DNA would require 15.75 bp. As it is not possible to have a non-integer number of bases, crossovers are typically spaced 16 bp or 15 bp apart. Figure 24i shows how the bases in relaxed DNA are orientated when it rotates 1.5 turns. Figures 24ii and 24iii show how over or under-winding the helix would alter the orientation of the bases from the relaxed case. Figures 24v and 24vi show how the bases are orientated in crossovers that are spaced 16 bp and 15 bp apart respectively. It can be seen that the orientation of the 16 bp is the same

as the orientation of overwound DNA (in its twisted state). In the literature, the supercoiling or rather curvature of origami is defined as the left or right-handed twist that is resultant of the writhe seen for supercoiled DNA [52]. The important distinction is that the crossovers are not supercoiled, but rather they mimic the over or under-winding that occurs in the twisted state of supercoiled DNA. This distinction is important as it states that the curvature is simply a result of the angle through which the crossovers rotate, rather than the supposed mismatch between the crossover spacing and the idealised spacing. This is seen in literature, where underwinding of the DNA helix induced by EtBr causes origami with 16 bp crossovers to appear planar [134].

6.2 **Design overview**

A general overview of the origami design used in this is given in figure 25. The design is 30 helical turns in length, which corresponds to 20 crossovers of 1.5 turns each along the long axis of the tile. Due to the inability to have a non-integer number of bases between crossovers, designs use spacings of 16 bp and 15 bp to alter the degree of supercoiling in DNA origami. Table 1 describes how the average helical pitch can be varied by changing the crossover composition.

No. 16 bp	20	19	18	17	16	15	14	13	12	11	10	9	8	7	6	5	4	3	2	1	0
No. 15 bp	0	1	2	3	4	5	6	7	8	9	10	11	12	13	14	15	16	17	18	19	20
Resultant width	320	319	318	317	316	315	314	313	312	311	310	309	308	307	306	305	304	303	302	301	300
Helical Pitch	10.67	10.63	10.60	10.57	10.53	10.50	10.47	10.43	10.40	10.37	10.33	10.30	10.27	10.23	10.20	10.17	10.13	10.10	10.07	10.03	10.00

Table 1: Potential crossover compositions and resultant helical pitches for origami that is 30 helical turns (20 crossovers) in length.

The first origami design used in this work uses crossovers that are all 16 bp in length. This would cause the origami to have an expected average helical pitch of 10.67 base pairs per turn (bppt), if it was fully constrained. The second design uses crossover spacing's such that the expected average helical pitch is 10.50 bppt. which requires fifteen 16bp crossovers and five 15bp crossovers (Table 1). The position of the 15 bp crossovers are outlined in figure 25. The third design has ten 16bp crossovers and ten 15 bp crossovers, creating a tile that has an expected average helical pitch of 10.33 bppt, whose average mismatch is equal and opposite to that of the 10.67, with respect to the 10.50 bppt tile, which is expected to be planar. Each design uses the entirety of the

scaffold strand so as to prevent binding effects that may arise from an ssDNA overhang. As each design slightly varies in length due to the crossover spacing, the length of the bottom two helices varies for each design. This is highlighted in figure 25, and is the only means of distinguishing the three designs in AFM images.

Based on the concept of supercoiling as previously discussed, the 10.67 tile can be considered to be overwound, whilst the 10.33 tile is underwound. The 10.50 tile should have no mismatch to B-form DNA. As the helical pitch of B-form is said to range from 10.4 to 10.6 bp, the three tiles used in this work serve as a means to study how the helical pitch of DNA varies with cationic concentration and species [144], [145]. The arrangement of the crossovers and the effect this has on computer models is discussed in chapter 8. Each of the tiles has the same overall shape, essentially a rectangle with a notch taken out of the same corner. This introduced asymmetry in the shape allows for

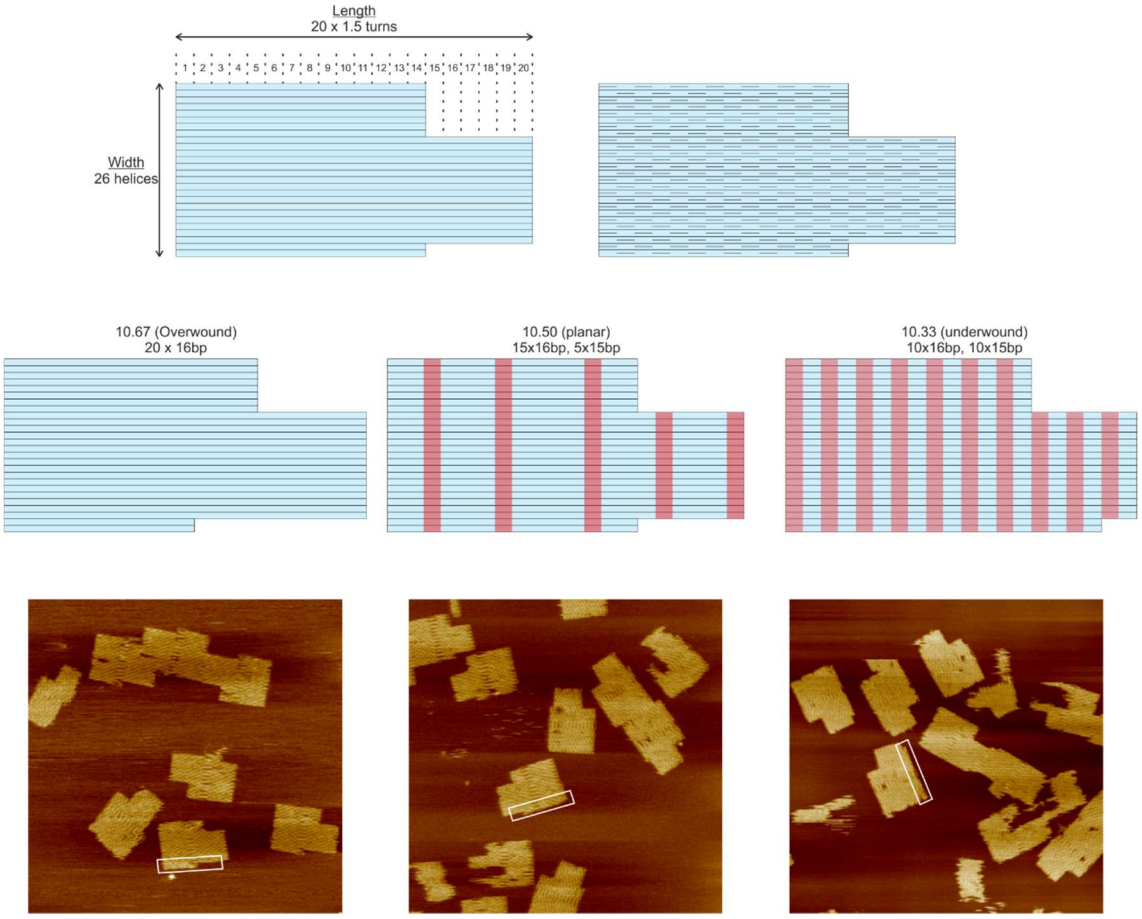

Figure 25: Plan views of the three similar origami designs used in this work. Top right highlights the position of nicked crossovers. Position of 16 bp (blue) and 15 bp (red) crossovers for the 10.67, 10.50 and 10.33 tiles. AFM images of the three origami under aqueous conditions (scale = 500 nm). White boxes highlight the overhanging double helical domains.

orientation discrimination when imaged with AFM. For simplicity, results and models are drawn with the A-face on-top.

6.3 Results and discussion

6.3.1 CanDo

CanDo is most commonly used CAD package for predicting origami structure, aiding error-checking during the origami design process. As most origami are designed with CaDNAno or Tiamat, CanDo has been modified over the years to accommodate for these file types. An in-depth implementation on the methodology used by CanDo is given in the papers by Castro et al. and Kim et al., showing the efficacy of CanDo [63], [146]. The models generated are of the average solution structures, highlighting the degree of flexibility of the helices. Blue corresponds to regions that are more strained and hence resistant to thermal fluctuations, whilst red refers to helices that are less strained. The CanDo models for the three origami designs are summarised in figure 26. The CanDo models agree with the models of Marchi et al., suggesting that the utilisation of the entire M13mp18 scaffold strand does not alter the predicted structure [68].

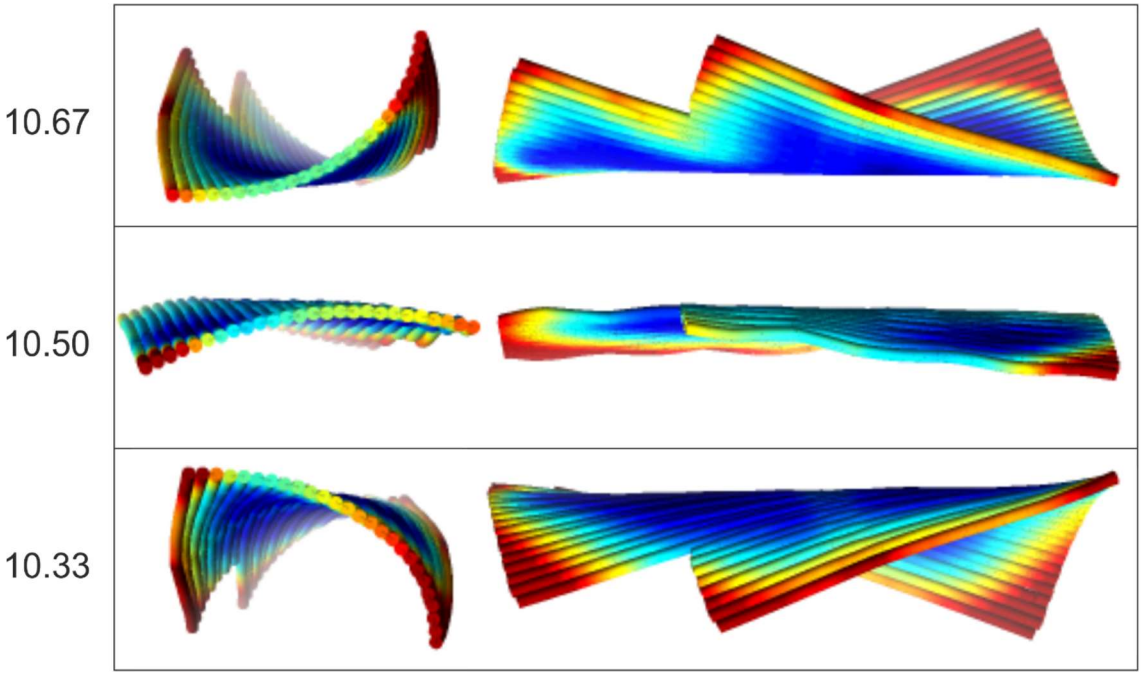

Figure 26: CanDo models for the 10.67, 10.50 and 10.33 origami used in this work. All tiles are orientated with the A-face on top. It can be seen that the 10.67 and 10.33 curve into opposing planes. There axis around which the origami curve can be seen to not lie parallel to the helices contained within the tiles.

The CanDo model for the 10.67 design shows a curved structure with a right-handed chirality, as predicted form the underlying crossover composition with respect to the ideas of supercoiling. The structure of the 10.33 tile shows that the curvature is left-handed, supporting with the idea of supercoiling in origami. The main difference is that the plane into which the origami curve is opposite for the two designs, suggesting that the origami will bind with opposing faces when imaged with AFM. This was the outcome of the results presented by Marchi et al. [68]. The 10.50 exhibits a slight degree of curvature, perhaps due to the arrangement of the crossovers not being evenly spread throughout the design, creating domains that are locally over or under-wound.

6.3.2 **OxDNA**

OxDNA is another CAD package that was developed to predict DNA nanostructures. The main difference between OxDNA and CanDo, is that OxDNA takes a coarse-grain approach to the modelling, offering increased resolution. The OxDNA models in this work were generated by Prof. Jonathan Doye (University of Oxford, UK) and Dr. John S. Schrek (Columbia University, NYC), two of the original designers of the OxDNA software. Implementation of the OxDNA software is summarised in papers by Doye et al. and Snodin et al., which highlights the recent advancements in the software, allowing for modelling under varying salt concentrations [66], [147]. An overview of the predicted origami structures are given in figure 27.

The OxDNA models of the 10.67 tile show that the tile curves into the same plane as the CanDo models. The degree of curvature appears to increase with the Na^+ concentration, suggesting that the DNA is better stabilised. Na^+ has already been shown to be an effective cation for the folding and neutralising of DNA origami, but was not used for this. The change in curvature of the origami can therefore only be used as a qualitative guide. The models of the 10.50 design show a slight curvature across the Na^+ series, opposite to the direction of bias for the CanDo models. For the 10.50 design, increasing the Na^+ concentration appears to have little effect on the degree of curvature. The OxDNA models for the 10.33 design show that the plane into which the origami curve is the same

as that of the 10.67, unlike CanDo which predicts an opposite direction of the curvature. The 10.33 OxDNA models also exhibits a left-handed twist, which is to say that it does not go against the idea of supercoiling. Figure 28 shows the main differences between the CanDo and OxDNA models for the DNA origami used in this work. The models are orientated in the same direction for clarity. The key point is that the 10.33 is curved in opposite directions depending on the model used.

The contradiction between the OxDNA and CanDo models for the 10.33 (underwound) tile were the basis for the analysis of current literature in chapter 4, as it demonstrates how interpretation of results can be influenced by a lack of incomplete data. The contradiction also shows why the papers by Li et al. and Dietz et al. are not enough to demonstrate the true direction of curvature or twist of origami [37], [52]. This contradiction is resolved in the next section, detailing which models are correct and how this applies to current literature.

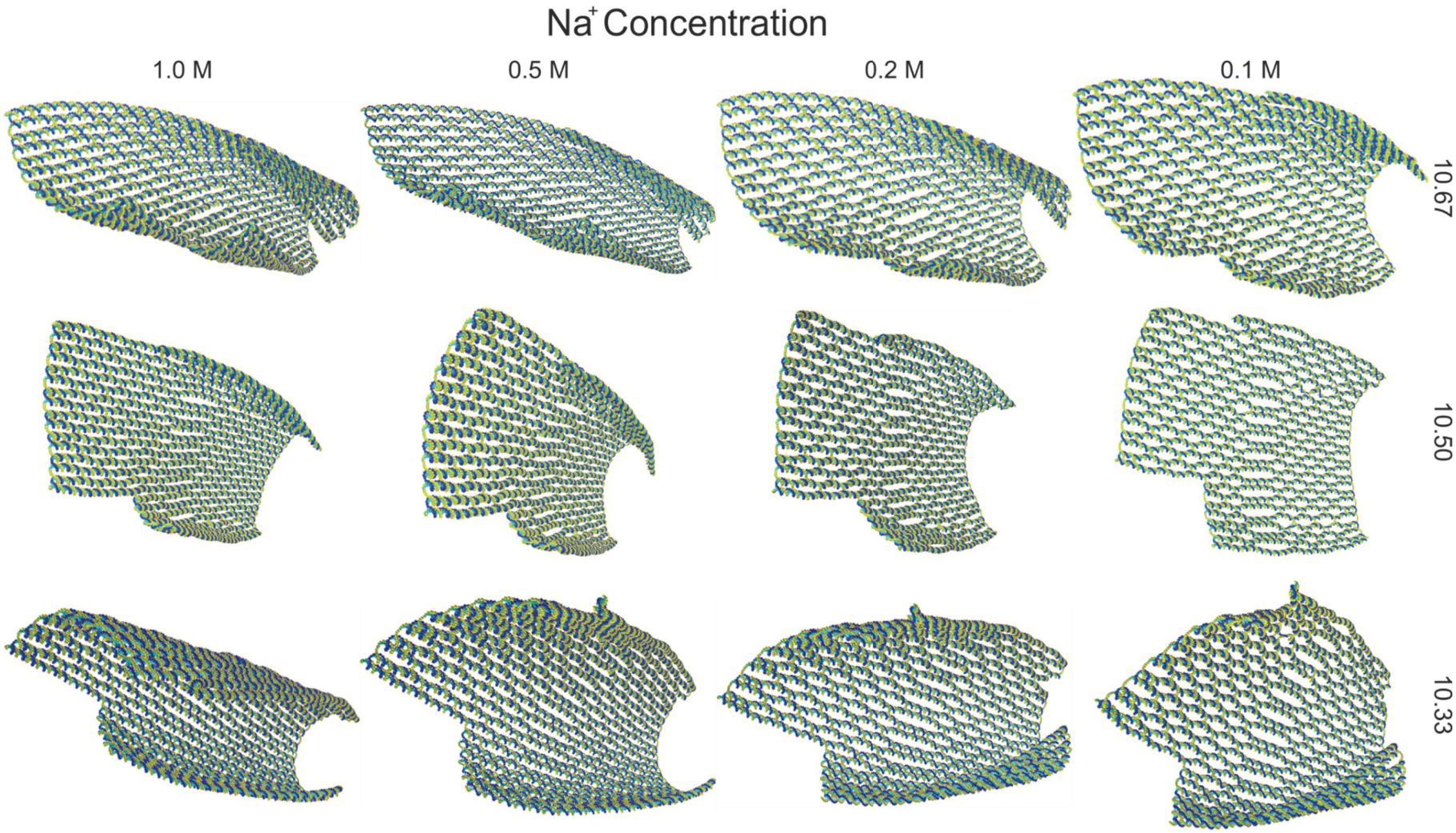

Figure 27: OxDNA models for the 10.67, 10.50 and 10.33 origami used in this work showing how the curvature varies with increasing Na^+ concentration. It can be seen that all tiles curve into the same plane, with the magnitude of curvature varying with Na^+ concentration.

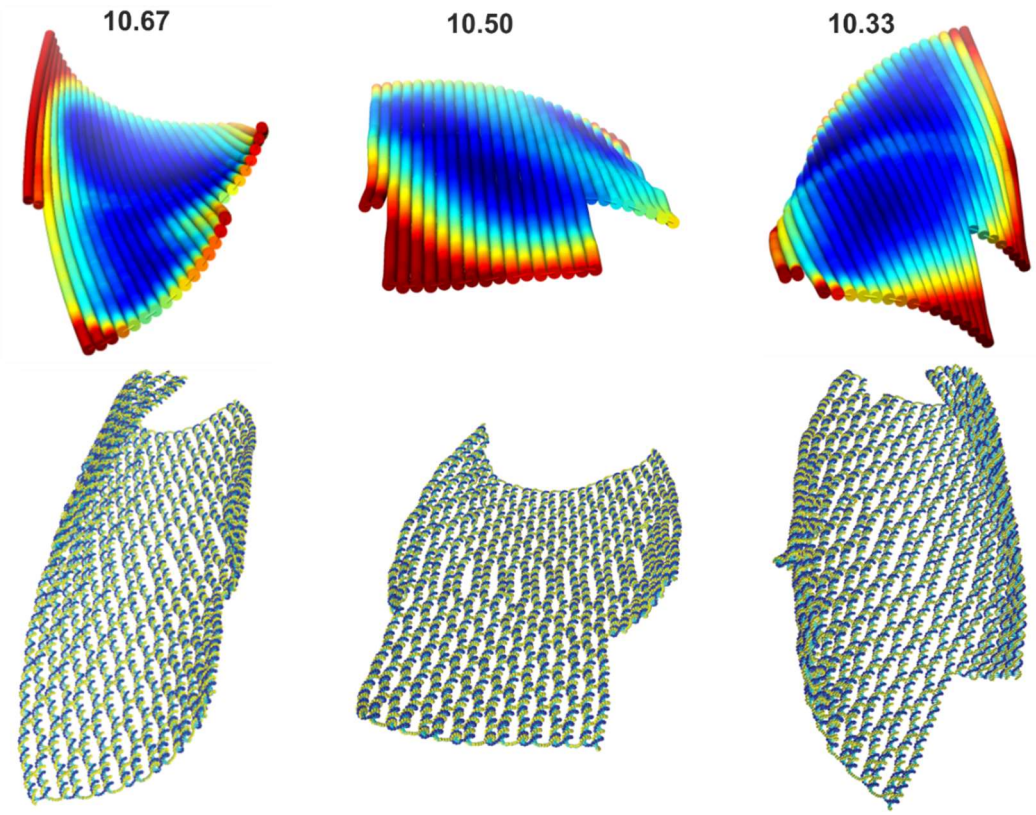

Figure 28: CanDo (top) and OxDNA (bottom) comparing the direction of curvature for the 10.67, 10.50 and 10.33 origami tiles. All tiles are orientated with the A-face up. It can be seen that the 10.50 and 10.33 have opposing curvatures between the two model sets.

6.3.3 **Binding of origami to mica by AFM**

To assess what effect Mg^{2+} has on the stabilisation of the DNA helix, each of the DNA origami were imaged under aqueous conditions with Mg^{2+} ranging from 3.125 to 25 mM. The proportion of the tiles observed to be A-face up was used to infer the orientation and magnitude of origami curvature. To maintain constant DNA concentrations, the tiles were folded with a scaffold concentration of 4nM with a 40x staple excess. Samples were then aliquoted out and diluted to origami concentration of 1nM with a 10x staple excess. Results are presented in figure 29.

Most DNA origami are folded with a Mg^{2+} concentration of 12.5 mM, sourced from either $MgCl_2$ or $Mg(CH_3COO)_2$ (Mg-ace) in the presence of TAE. As TAE contains EDTA, a known chelating agent, the Mg^{2+} is therefore chelated, which lowers its effective concentration. Preliminary results showed that at low Mg^{2+} concentrations with a 1xTAE concentration, a combination of excess monovalent (tris) ions as well as Mg^{2+} chelation prevented origami from binding. As a result, the ratio of Mg^{2+} to TAE was maintained constant. A summary of the Mg^{2+} and TAE concentrations are given in table 2, highlighting the effective Mg^{2+} concentration and number of Mg^{2+} ions per nucleotide in solution. It was assumed that each nucleotide in the staple strands as well as the EDTA in solution would sequester Mg^{2+} ions. For simplicity, the results refer to the assumed Mg^{2+} concentration, rather than the effective Mg^{2+} concentration.

Scaffold length (nt)	Scaffold concentration (nM)	Excess staple concentration (nM)	Nucleotide concentration (mM)	Mg^{2+} concentration (mM)	EDTA concentration (mM)	Effective Mg^{2+} concentration (mM)	Mg^{2+} per nt
7249	1	10	0.04	25	2	23	528.81
				21.875	1.75	20.125	462.71
				18.75	1.5	17.25	396.61
				15.625	1.25	14.375	330.51
				12.5	1	11.5	264.40
				9.375	0.75	8.625	198.30
				6.25	0.5	5.75	132.20
				3.125	0.25	2.875	66.10

Table 2: Number of excess Mg^{2+} ions per nucleotide for the three tile designs when imaged under varying Mg^{2+} TAE concentrations.

From figure 29 it can be seen that the 10.67 tile binds with a preference to the A-face on top in the typical concentration of 12.5mM Mg^{2+}. As the Mg^{2+} concentration is decreased

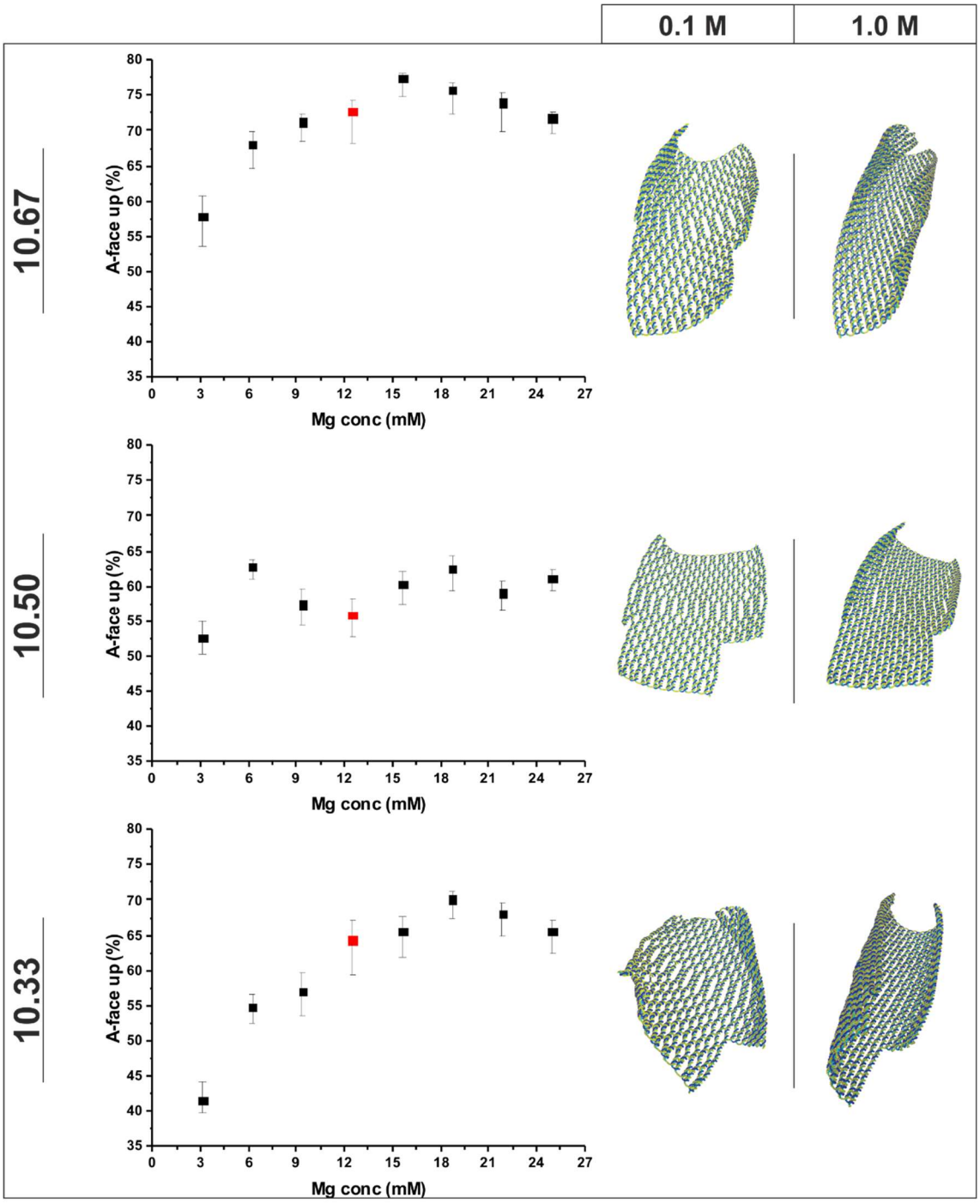

Figure 29: Proportion of tiles observed with the A-face up under varying Mg^{2+} concentrations. Red data points correspond to "standard" conditions of 12.5 mM Mg^{2+}, 1xTAE. OxDNA models are used as representatives to explain the trend of increasing curvature, with only those in 0.1M and 1.0 M Na^{+} concentrations shown.

to 3.125 mM the bias decreases, with a final bias observed of 57.8%. When the concentration of Mg^{2+} was increased above 12.5 mM, the origami exhibited greater curvature, reaching a maximum bias of 77.4% at 15.625 mM. After this the bias started to decrease, reaching a point of 71.7% at 25mM. Throughout the Mg^{2+} series, the bias remained consistent to the direction of A-face up. The binding of the 10.50 tile shows a

slight bias to the A-face up across the Mg^{2+} series, remaining fairly consistent throughout, with some fluctuation but a trend of slightly increasing bias with Mg^{2+} concentration. The overall trend indicates that the 10.50 remains planar, independent of Mg^{2+} concentration. Similar to the 10.67 tile, the 10.33 tile exhibits a bias to the A-face up under 12.5mM Mg^{2+}, strongly suggesting that the two tile designs are curved into the same plane (as in the OxDNA model). As the Mg^{2+} concentration is decreased, the 10.33 becomes planar until 3.125 mM, where the bias flips from A-face up to B-face up. At increased magnesium concentration, the 10.33 becomes more curved, as like the 10.67 tile, exhibiting a peak in curvature at 18.75 mM. The curvature then decreases as Mg^{2+} concentration further increases.

At “standard” conditions of 12.5 mM Mg^{2+}, both the 10.33 and 10.67 tiles exhibit bias to the A-face up, indicating that the two tiles are curved into the same plane. This is the result predicted by the OxDNA models and is highlighted alongside the binding results in figure 29 showing how the Na^{+} extremes of the OxDNA models are reflective of the observed binding. At elevated Mg^{2+} concentrations, the decrease in curvature for the 10.33 and 10.67 tiles is attributed to an increase in shielding of electrostatic repulsion between the tightly packed helices. This decrease in curvature attributed to an increase in Mg^{2+} concentration infers that the electrostatic repulsions acts as an additional source of curvature for the origami tiles. This is a limitation of the OxDNA models, where Na^{+} is used for the simulations and not during experimentation, such that a like-for-like comparison wasn’t obtained. The reason for the shift in the peak of maximum curvature of the two designs is attributed to the length of the underlying crossovers. At low Mg^{2+} concentrations, the electrostatic repulsion between the helices maintains a maximum deformation. As the 16 bp crossover is longer, it experiences a greater overall deformation. This means that an increase in shielding is experienced sooner, as the 15 bp crossovers would still be at maximum deformation. This change in the lengths of the crossovers means that the 10.67 tile starts to feel the effect of increased shielding sooner that the 10.33 tile and hence the observed shift in maximum curvature. Although this

would imply that the origami would become more biased to the A-face up at lower Mg^{2+} concentrations, the lower Mg^{2+} concentration alters the overall stability of the DNA helix. This means that the DNA is more flexible, making it resistant to the electrostatic repulsions. This also means that the angle through which the crossover rotates is lessened, causing the origami to flatten out.

Scaffold length (nt)	Scaffold concentration (nM)	Excess staple concentration (nM)	Nucleotide concentration (mM)	Mg^{2+} concentration (mM)	EDTA concentration (mM)	Effective Mg^{2+} concentration (mM)	Mg^{2+} per nt
51466	5	50	1.54	12.5	2	10.5	6.80
	4.5	45	1.39				7.56
	4	40	1.24				8.50
	3.5	35	1.08				9.72
	3	30	0.93				11.33
	2.5	25	0.77				13.60
	2	20	0.62				17.00
	1.5	15	0.46				22.67
	1	10	0.31				34.00
	0.5	5	0.15				68.01

Table 3: Number of excess Mg^{2+} ions per nucleotide for the three tile designs used by Marchi et al. Scaffold, staple, Mg^{2+} and EDTA concentrations are based on their published methods.

The combination of the OxDNA models and binding of the DNA to the mica is not enough to determine the axis around which the origami curve, as seen in the models. The results of Dietz et al. and Li et al. show that for an origami with a greater number of bases between crossovers, such as the 10.67 tile, there exists a right-handed helix, whilst for a lesser number of bases between crossovers, there exists a left-handed twist. This is necessary to assign the correct OxDNA models to the correct tile, as AFM alone cannot determine the axis around which the tile curves. The OxDNA and CanDo models were used as the basis for the figures in chapter 4, describing how information on the axis about which origami curve is lost in AFM images, whilst information on the plane into which they curve is preserved.

The results of Marchi et al. suggested that the oppositely twisted origami would bind with opposing faces to the mica. Table 3 shows the amount of Mg^{2+} ions per nucleotide in the origami used by Marchi et al., indicating that the maximum Mg^{2+} excess is approximately 68 ions per nucleotide. This is the similar case seen for the 10.33 tile used here under a Mg^{2+} concentration between 6.25 and 3.125 mM, where there is a flip in the bias of the origami. This highlights that the Marchi et al. tiles exist in a constant destabilised state,

due to the increased overall DNA concentration. This is important for comparisons of origami sizes, as the degree of helix stabilisation affects the overall curvature of the tile.

6.3.3.1 Width of adsorbed tiles

It has been noted in the literature that the electrostatic repulsion between the tightly packed helices of DNA origami results in the formation of an internal diamond lattice [3]. It is believed that the size of these diamond cavities is dependent on the length of the crossovers themselves, with 2.5 and 3.5 turns resulting in a smaller relative bending, as the repulsion is spread out over a larger length [148], [149]. The work in this thesis looked at how the Mg^{2+} concentration affects the apparent width of the origami themselves, as this can cause the origami to change size when on a surface. Results are shown in figures 30 and 31. This is important for the creation of large scale arrays, as the change in width will alter the relative position of functional groups.

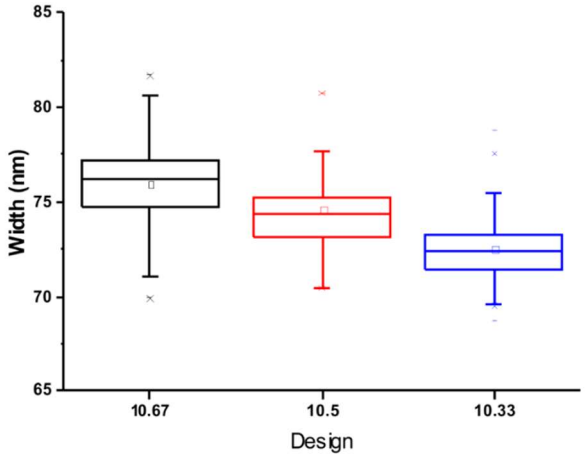

Figure 30: Widths of the three origami tiles under 12.5 mM Mg^{2+}, 1xTAE on mica under aqueous conditions. The decrease in width across the designs is reflective of their underlying crossover composition.

The results in Figure 30 show that under a Mg^{2+} concentration of 12.5 mM, the widths of the origami tiles are representative of their underlying crossover spacing, such that the 10.67 is the widest at 76 nm and the 10.33 the thinnest, at 72.5 nm. The widths of the origami were also measured under varying Mg^{2+} concentrations, to assess the effects of both electrostatic repulsion and degree of helix stability. At lower Mg^{2+} concentrations, the origami generally became wider due to decreased shielding of the electrostatic

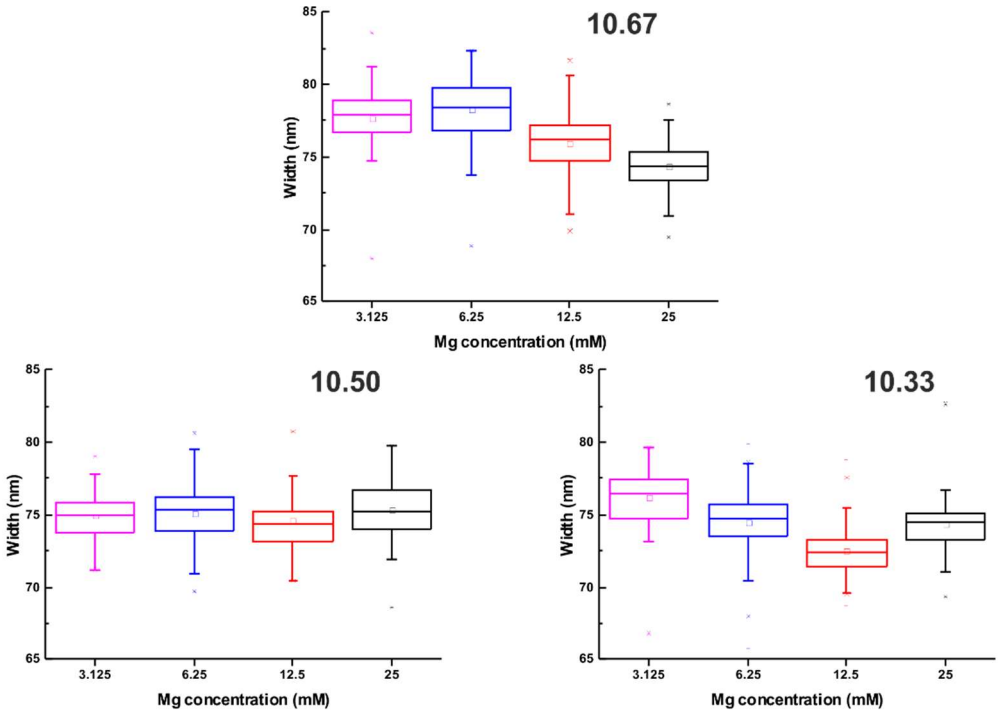

Figure 31: Widths for the 10.67, 10.50 and 10.33 tiles under varying Mg^{2+} concentrations adsorbed onto mica. Imaged under aqueous conditions. See table 2 for effective Mg^{2+} concentrations.

forces. It is also caused by an increase in DNA flexibility, allowing it to deform more. The Mica-DNA interaction is believed to remain constant throughout, due to the complete neutralisation of the mica surface. It also noted that for DNA molecules, the DNA-mica bond remains relatively weak, even under high Mg^{2+} concentrations, which is why the use of a stronger binding agent such as Ni^{2+} is typically used.

The main reasoning for measuring the widths of the origami, rather than the lengths, is that a change in the deformation results in a greater change of the origami widths, as seen in chapter 4. Although the length of the origami themselves differ in length by 10 bp across the designs, equating to ~3.4 nm, the change in length attributed to a change in the underlying diamond lattice results in minimal changes of the origami, as discussed previously in chapter 4.

6.4 Conclusions

The results of this work show that the underlying crossover composition of origami results in a change of axis about which the origami curve, rather than a change of the plane into

which the origami curve. This is evidenced in the OxDNA models only, as it is not possible to determine from AFM images. The underlying curvature of origami is a result of the total angle through which the crossovers rotate, as determined by their length and the helical pitch of the DNA in solution. The binding also highlights a contribution to the curvature from the inherent electrostatic repulsion between the tightly packed helices, which also shows the importance of the effective Mg^{2+} concentration, which has a two-fold effect of both altering the overall helical pitch and secondly the helix stability of the DNA contained within the tiles. These two effects complete to give a maximum in the effective curvature of the tile at a given Mg^{2+} concentration, except for the 10.50 tile which remains largely planar.

7 Controlling DNA origami curvature

7.1 Introduction

The results of the previous chapter demonstrate the effect that the inherent crossover spacing has on the curvature of origami tiles, highlighting that all designs curve into the same plane. The effect of Mg^{2+} concentration on the curvature of the tiles, along with the similarities observed for the 10.67 and 10.33 show how helix stabilisation can affect the curvature of single-sheet origami. These results act as a baseline for investigating methods of controlling origami curvature. The results from the previous chapter also demonstrate the intrinsic link between DNAs helical structure with the observed width of the tiles, which allow for finer placement of functional groups.

The main reason for altering the curvature of origami is to expand the available conformation, such that a single design can be used for a variety of applications. One such area of interest is the ability to bias adsorption orientation, increasing the efficacy of novel surface-supported materials. Other applications involve methods such as targeted drug delivery, which means interfacing with biologically relevant systems. These broad ranging applications places limitations on the methods developed for controlling curvature. There have been several methods for controlling the structure of folded origami; including intercalators such as EtBr, UV radiation and cationic concentration as well as species [133], [134], [139], [150]. In vivo applications limit the use of intercalators or chemical adducts, due to potential interference with biological processes. This also limits the use of cationic species, which will dissociate from the DNA once in vivo.

This chapter expands on the work of others, where UV radiation has been used to alter the structure of the DNA contained with origami, highlighting the impact UV radiation has on the crossover spacing. These results, combined with those of the previous chapter, act as the basis for determining how buffers containing Ba^{2+} as well as Ba^{2+} and Mg^{2+} impact the curvature of single-sheet origami.

7.2 **UV exposure**

The spectrum of UV light can be categorised into three main types: UVC (100-280 nm), UVB (280-315 nm) and UVA (315-400 nm). On Earth, UVC light generated by the sun is absorbed by the atmosphere, whilst UVB and UVA are able to penetrate to the surface. Long term exposure to UVB and UVA radiation can result in skin cancer of humans, as a result of direct and indirect damage to DNA [151]. UVA radiation is able to penetrate deeper into the skin, causing indirect damage by the formation of ROS, which subsequently damages DNA. The energy of UVB is high enough that it is able to directly damage DNA, resulting in photoproducts. The higher energy of UVC not only causes direct damage to DNA strands, resulting in photoproducts, but also creates single and double strand breaks [152].

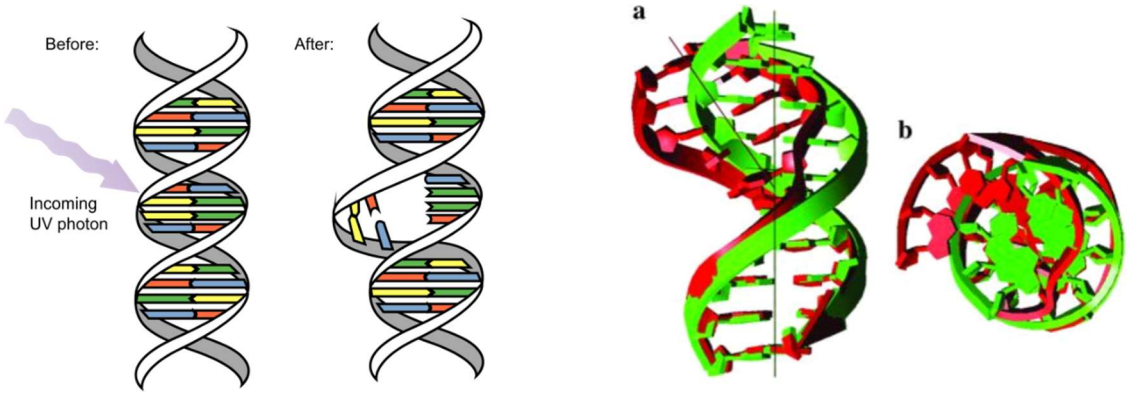

Figure 32: Left: Schematic showing how CPD results in binding of adjacent bases. Right: crystal structure of CPD (red) and how it deviates from the B-form of DNA (green) [47].

UVC radiation has been shown to induce structural changes of DNA origami as a result of the formation of these photoproducts [133]. The most common photoproduct associated with UV radiation is cyclobutane pyrimidine dimers (CPDs). The most common type of CPD results when there are two adjacent thymine bases on the same strand, with the high-energy photon creating a covalent link between the two [153]. This also disrupts the base pairing with the associated adenines on the complementary strand. Chen et al. demonstrated that both UVB and UVC are able to directly alter the conformation of origami, with UVA only being effective when combined with the use of

an intercalating agent [133]. It has been recently demonstrated that UVA can result in the formation of CPD in DNA origami through purposeful design of thymine overhangs between helical domains, resulting in the origami becoming rigid and resilient to harsh environments [154]. The results of Chen et al. suggest that CPD causes destabilisation of the DNA helices due to the disruption of the base pairing. The crystal structure of a thymine-thymine CPD however shows that the DNA backbone becomes distorted, resulting in an unwinding of the helix by 9°, as seen in Figure 32 [47]. The work in this section looks at how UVC radiation damages the DNA strand, emphasising how both CPD formation as well as single and double strand breaks alter curvature of single-sheet origami.

7.3 Cation introduction

Although intercalators have shown to be an effective means of altering origami structure, they prove difficult to eliminate once inserted between the bases. Chen et al. figured out that this could be achieved by using an excess of staple strands to displace the bound intercalators from origami [134], but this may be unpractical for many applications. Intercalators can also lead to local distortions of the DNA structure due to the stochastic nature of their binding [44], meaning each origami may contain differing amounts and locations of intercalated bases. Cations do not suffer from these downsides, allowing for global changes in the origami structure. It has already been demonstrated that Na^+ can be used to increase the mobility of origami once adsorbed onto mica [71]. It is hoped that cations can be used to bias the adsorption process but altering the solution structure of origami, with a subsequent buffer wash to control surface mobility as well as structure.

Magnesium is the most commonly found cation in vivo, which acts to shield the phosphate backbone from both inter and intra-strand electrostatic repulsions, stabilising the DNA helix. The previous results demonstrate that there is an interplay between the DNA and excess Mg^{2+} ions in solution, due to the relatively weak interaction between the Mg^{2+} and the negative phosphate backbone. The results in the previous chapter also demonstrate how small changes in the degree of helix stabilisation as well as

electrostatic repulsion between neighbouring double-strands affects the curvature of origami. This is evidenced by the changes in curvature between the designs and how the magnitude/rate of change is similar for those in varying Mg^{2+} concentrations.

There are two main modes of cations binding to the DNA helix, which are broadly categorised as binding to the bases or to the sugar phosphate backbone [22], [24], [155]. It has been demonstrated that all cations, to an extent, bind to both the bases and the backbone, with there being a spectrum from the two extremes [156]. It has already been demonstrated that Na^{+} can be used to fold multi layered structures, requiring higher concentrations due to a combination of the monovalent charge as well as decreased charge density of the sodium ion [139]. More recently however, Marras et al. demonstrated how origami is stable in the presence of Spd^{3+}, Ca^{2+}, K+, with the ions also stabilising ssDNA overhangs, allowing for control over a DNA origami hinge [150].

This work looks at how Ba^{2+} binds to the DNA helix, and the effect it has on the apparent curvature of DNA origami. This was expanded to include observations of the three tile designs in mixtures of both Ba^{2+} and Mg^{2+}, to investigate the potential of using cationic mixtures for controlling curvature, expanding the phase space for choosing solution conditions for folding DNA origami. The results of the three origami folded in Mg^{2+} as well as those exposed to UV allow determination of how Ba^{2+} binds to DNA, and what effect this has on origami curvature.

7.4 Results and discussion

7.4.1 UV exposure

Each origami design was folded with 10nM M13mp18 concentration. Once folded, the origami were diluted to a concentration of 1 nM with a final volume of 1 mL. The 1 nM tile solution was then placed into a disposable cuvette, which was subsequently exposed to UVC radiation. Aliquots were taken after each dosage, with the remaining solution used for continuous exposure. An aliquot of the unexposed solution was taken as a control, to ensure accurate folding of the origami. All origami were imaged under

aqueous conditions with a buffer containing 12.5 mM Mg-ace, 1xTAE. Binding results are presented in Figure 33, with width measurements in Figure 34.

In contrast to the results of the tiles in varying Mg^{2+} concentrations, where the curvature of both the 10.67 and 10.33 tiles followed similar trends, low UVC exposure doses cause the 10.67 to become less curved, whilst the 10.33 tiles becomes more curved (up to approximately 10kJ/m2 exposure). The difference observed for the 10.67 and 10.33 tiles exposed to UVC indicates that the DNA helix does not destabilise for doses under 10 kJm^{-2}. The change in curvature observed can be attributed to unwinding induced by CPD formation as well as single and double-strand breaks.

As discussed previously (chapter 6), the underlying crossover spacing determines the degree of twist for the crossovers, such that the 16 bp crossovers are overwound, whilst the 15 bp crossovers are underwound. Unwinding induced by CPD formation therefore reduces the degree of overwinding for 16 bp crossovers whilst emphasising the degree of unwinding for the 15 bp crossovers. As the 10.67 origami consists solely of 16 bp

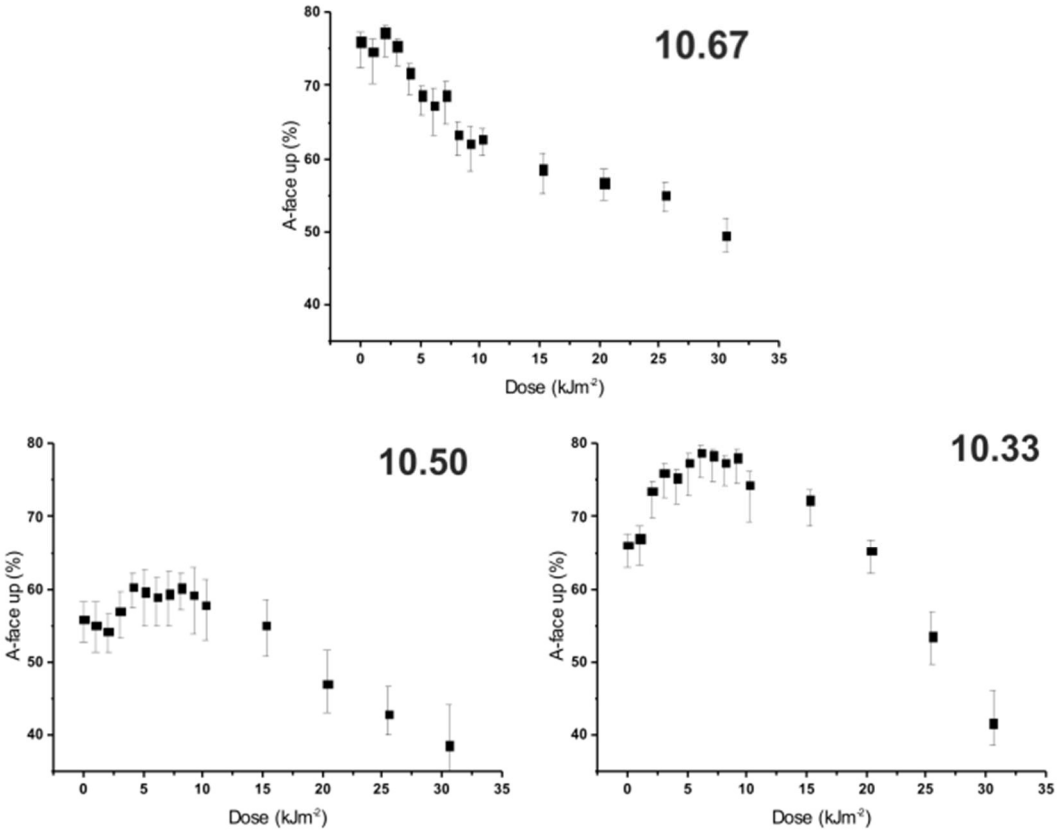

Figure 33: Binding of the 10.67, 10.50 and 10.33 tiles with increasing UVC dosages. Example AFM images as well as details on analysis are given in the appendix.

crossovers, the degree of twist across the tile is lessened as the number of CPDs present increases. This is apparent in figure 33, where the bias observed for the 10.67 tile decreases, indicating a reduction in the curvature. The increase in curvature observed for the 10.50 and 10.33 tiles is attributed to the composition of 16 and 15 bp crossovers contained within each respective design. As the 10.50 tile contains fifteen 16 bp and five 15 bp crossovers, the overall twist tends to that which is more underwound. As the 10.33 tile contains a higher proportion of 15 bp crossovers, CPD formation results in a relatively higher degree of unwinding, increasing the curvature of the tile. The increase in curvature for the UVC exposed 10.50 and 10.33 reflects the bias observed for the tiles in the Mg^{2+}, where tiles curve into the same plane, due to the mismatch of the spacings relative to the solution-induced helical pitch , and hence idealised spacing, .

At elevated UVC dosages (>10 kJm^{-2}) all three origami designs experience a decrease in curvature due to the formation of single and double-strand breaks. This is seen in the 10.67 tile as the rate at which the curvature decreases slows down. This effect is more

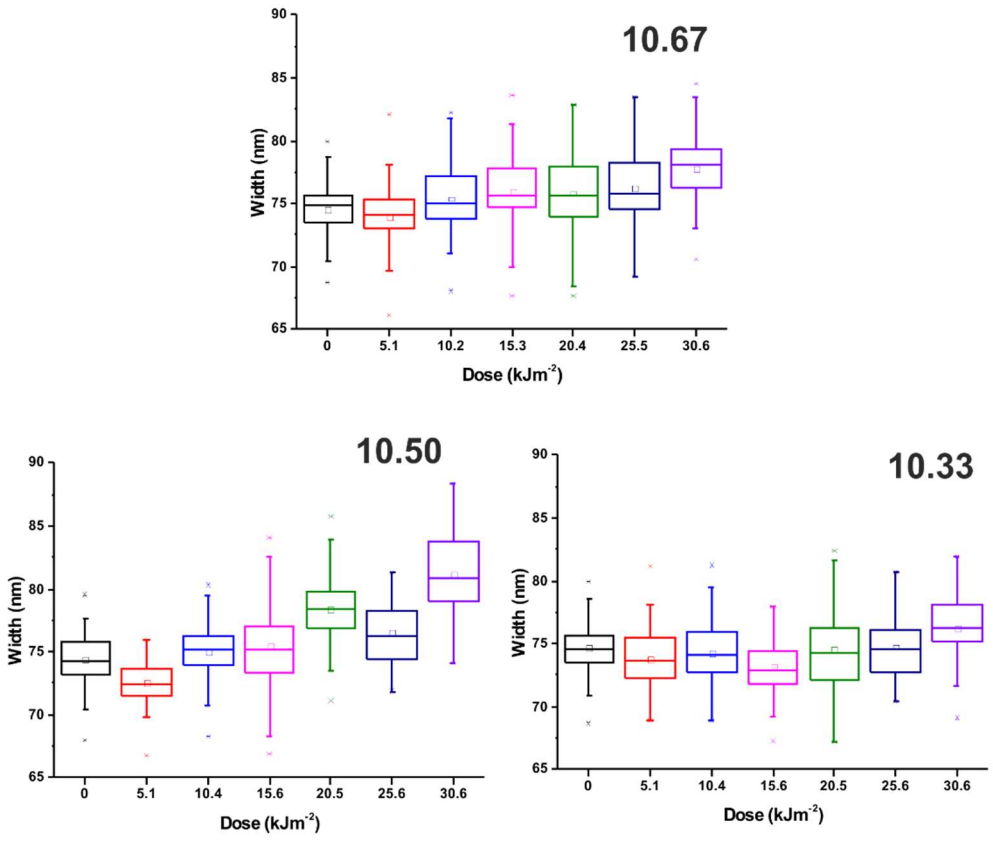

Figure 34: Widths of the 10.67, 10.50 and 10.33 tiles with increasing UVC exposure.

apparent for the 10.50 and 10.33 tiles due to the initial increase in curvature associated with CPD formation. This changeover between CPD formation and single and double strand break formation is also apparent in width measurements of UVC exposed tiles. All tiles experience a very slight decrease in width upon UV exposure, associated with CPD formation, as seen in figure 34. The widths then start to increase, highlighting the formation of single and double strand breaks. This is most apparent in the 10.67 tile, where the curvature continually decreases with UVC exposure, despite an initial small decrease and then continuous increase of width. The curvature and width results taken together imply that strand breakage is occurring with a fairly constant frequency due to UV exposure, but that the CPD photoproduct formation is a more dominant effect, which will saturate when all possible neighbouring thymine-thymine bases have created adducts.

The trend observed for the 10.67 tile in decreased Mg^{2+} and UVC-exposed are similar, leading one to assume that the decrease in curvature is attributed to helix destabilisation. The increase in curvature of the 10.50 and 10.33 tiles exposed to UVC radiation however demonstrate that CPD formation causes unwinding, rather than helix destabilisation. This shows how the results of Chen et al. incorrectly attribute the decrease in curvature to helix destabilisation, because they used origami lacking a range of crossover compositions [133].

7.4.2 **Pure Ba^{2+} solutions**

Similar to the tiles in varying Mg^{2+} concentrations, the tiles here were folded following the same protocol, with the exception that $BaCl_2$ was used instead of $Mg(C_2H_3O_2)_2$. Binding and width results of the tiles are shown in Figures 35, 36 and 37. The main result of the tiles folded in Ba^{2+} solutions deposited is that they are much flatter across the three tile designs compared to their Mg^{2+} counterparts, giving A/B ratios close to 50%. This indicates that the DNA helix is less stabilised in the presence of Ba^{2+}, such that the crossover angles cannot be transmitted into twisting (curvature) of the whole origami

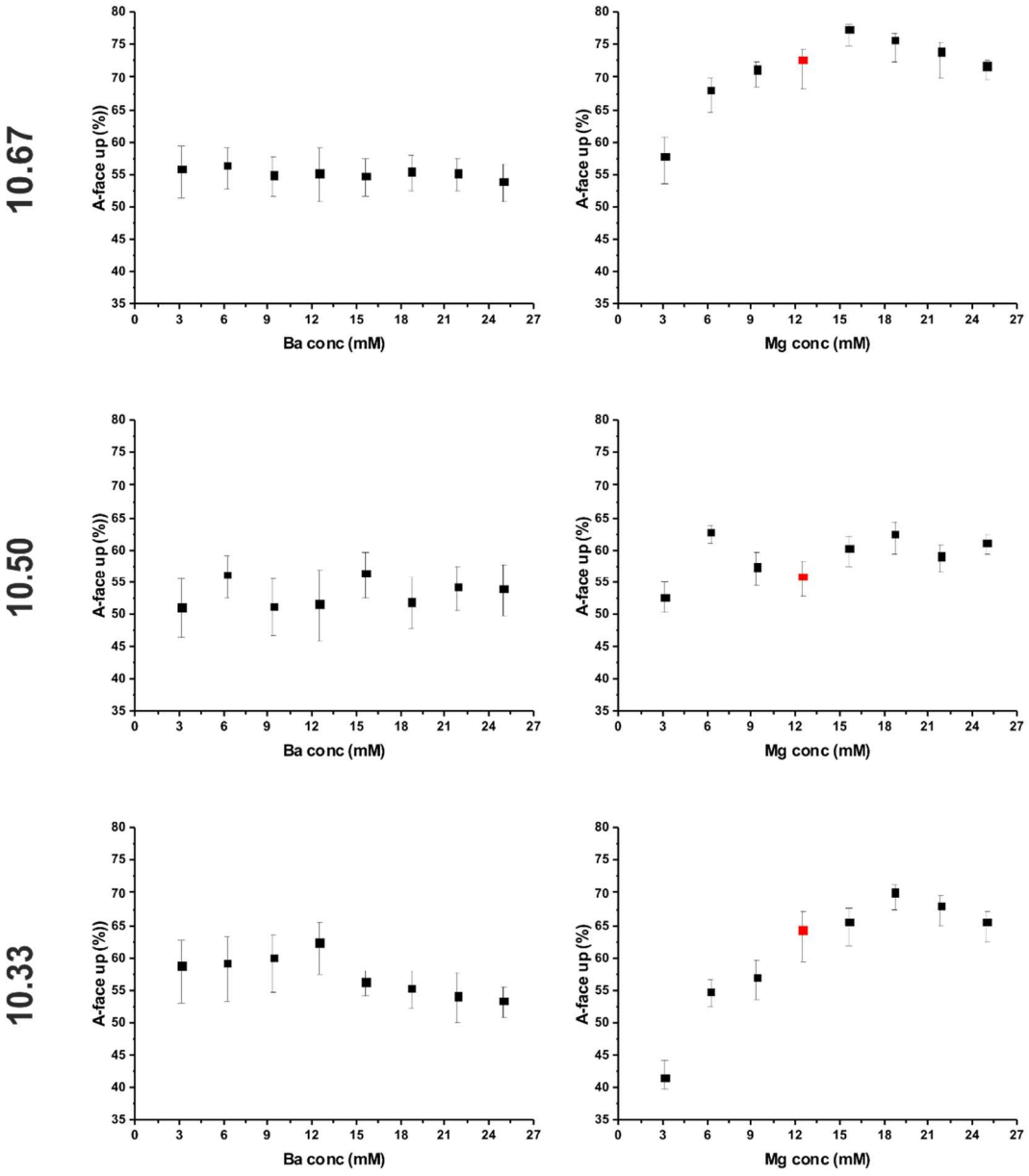

Figure 35: Left: binding of the tiles deposited in buffers containing various Ba^{2+} concentrations. Right: binding of the tiles deposited in buffers containing Mg^{2+}.

because the double-strands between crossovers are now not sufficiently rigid to transmit this geometrical strain.

The results of the tiles imaged under Mg^{2+} combined with the OxDNA models highlight how the magnitude of curvature exhibited by the varying crossover compositions of the tiles is dependent on the mismatch between the total origami length and that of the idealised case. This effect was observed in the UVC exposed tiles, where CPD induced unwinding increased the curvature of the 10.33 tile, due to the increase in the mismatch. A similar effect is observed for the tiles folded under Ba2+, where the increased bias of the 10.33 tile compared to that of the 10.67 and 10.50 tiles, demonstrate that the underlying helical pitch of the DNA in solution becomes slightly overwound (figure 36). This reduces the mismatch in the 10.67 and 10.50 whilst increasing it in the 10.33 tile, resulting in the observed changes in the curvature. Destabilisation of the DNA is observed in the widths of the tiles, which once again reflect the underlying crossover

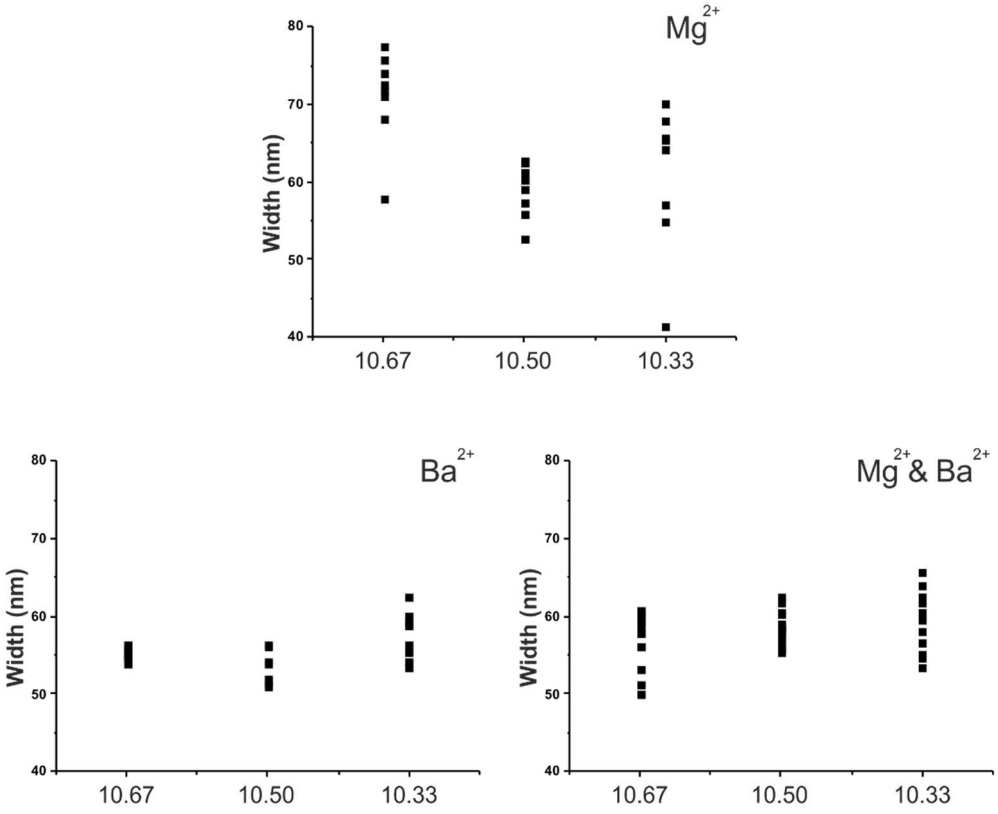

Figure 36: Total binding observed of the tile designs in buffers containing Mg^{2+}, Ba^{2+} and Mg^{2+} & Ba^{2+} mixtures across, demonstrating the range of curvatures observed across the differing buffer solutions.

spacing (figure 37). The widths are greater than those of the Mg^{2+} tiles due to the overall increase in flexibility of the DNA, allowing greater deformations from the electrostatic repulsions that arise from the tightly packed helices. The results highlight that the binding mode of Ba^{2+} is different from that of Mg^{2+}.

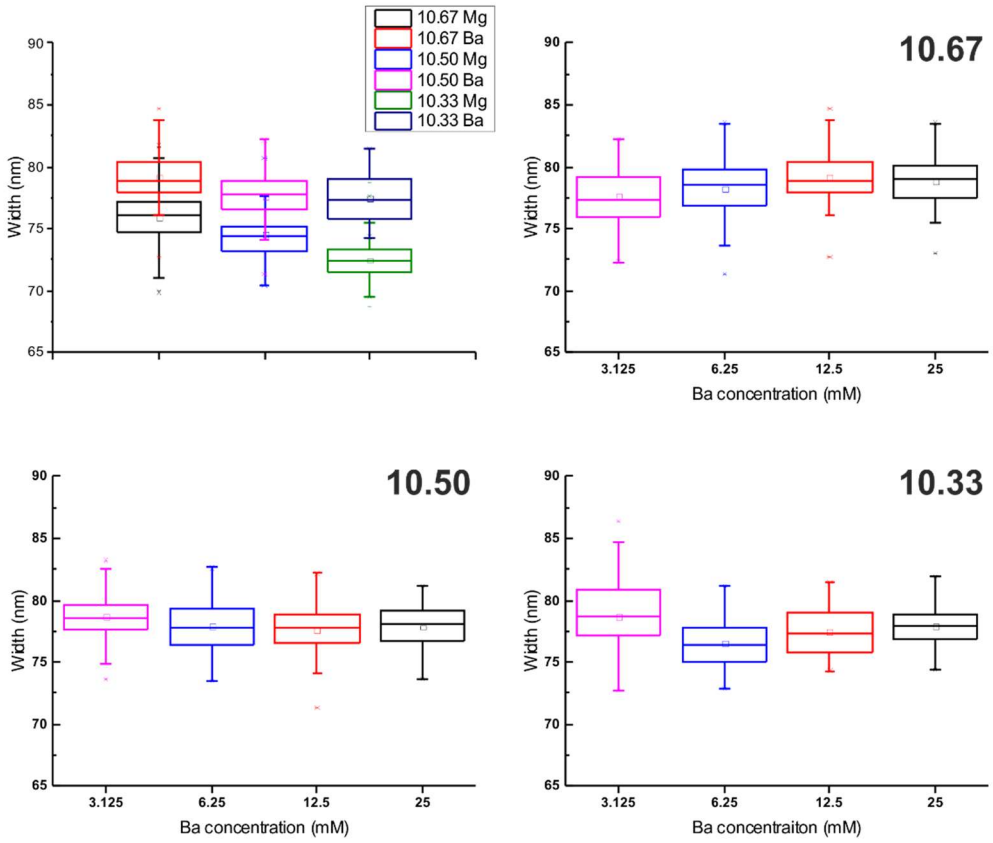

Figure 37: Top left: Comparison of widths of tiles in 12.5 mM Ba^{2+} and 12.5 mM Mg^{2}, showing how Ba^{2+} leads to wider tiles. The same trend is observed, highlighting how the underlying crossover spacing correlates to widths. Remaining figures show the widths of the three tiles (as labelled) under varying Ba^{2+} concentrations.

7.4.3 **Binding results of barium and magnesium mixtures**

To aid with the results of the tiles in buffers containing only Ba^{2+}, origami were imaged in buffers containing various concentrations of both Mg-ace and $BaCl_2$ to examine the difference in the binding modes between the cationic species, and how curvature may be controlled with “exotic” buffers. Tiles were folded in either 12.5 mM Mg-ace or $BaCl_2$ with 1xTAE with an M13mp18 concentration of 4 nM. These were then diluted to a 1 nM tile concentration, varying the concentration of both Mg^{2+} and Ba^{2+} to achieve the respective concentrations as seen in the results in Figure 38. The results of the tiles in mixtures of Ba^{2+} and Mg^{2+} show an increase in curvature for the 10.33 tile in solutions

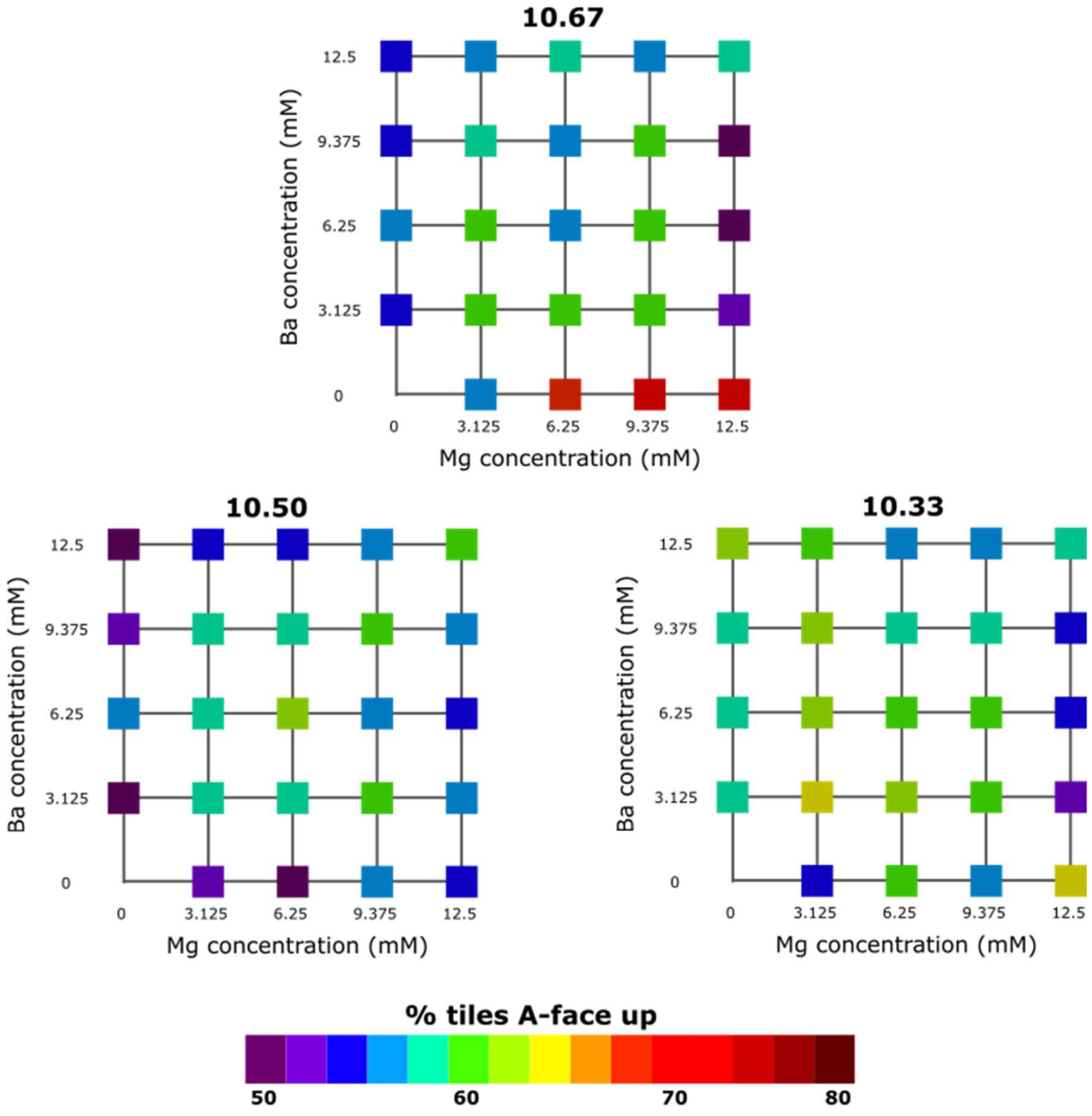

Figure 38: Plots showing how buffers containing mixtures of Mg^{2+} and Ba^{2+} affect the binding of the three tile designs.

where the total ionic concentration is less than that of the tiles in pure Mg^{2+} solutions. This is most apparent in a solution containing both 3.125 mM Ba^{2+} and Mg^{2+}, where the curvature is 65.6%, similar to that observed for 15.625 mM Mg. There is a similar peak observed in the 10.50 tile, in a solution containing 6.25 mM of both Ba^{2+} and Mg^{2+}. There appears to be no overall trend in the 10.67 tile**,** due to the overwinding of the DNA in solution, as seen for tiles in pure Ba^{2+}. The increase in curvature for the 10.50 and 10.33 tiles suggest that Ba^{2+} and Mg^{2+} are co-operatively binding to the DNA helix as a result of their differing binding modes, with the Ba^{2+} preferentially binding the bases and the Mg^{2+} binding to the sugar-phosphate backbone [21], [157]. Deviations from these "islands of stability" are attributed to both an increase in the overall ionic concentration, increasing the shielding between helices, as well as the competiveness between the two ionic species.

It was seen in the Mg^{2+} results that there is an ionic concentration at which the 10.33 tile obtains a maximum curvature. Although this was not observed for the 10.50 tile, it can be assumed that this is present in mixture of both Ba^{2+} and Mg^{2+} due to the shift in the native helical pitch of the DNA to an overwound state. When Ba^{2+} ions are added to solutions containing 12.5mM Mg, there is a sharp decrease in the curvature observed for both the 10.33 and 10.67 tiles. This is believed to be caused by the Ba^{2+} preferentially binding to the DNA helix, dominating the curvature. Figure 36 shows the curvature observed for the three tiles in solutions of mixtures containing both Mg^{2+} and Ba^{2+}. It can be seen that, on average, the 10.33 tiles exhibit an overall higher curvature than both the 10.50 and 10.67 tiles, indicating that the twist caused by the crossover composition is further from the "minimum" point. This is similar to the tiles in Mg^{2+} where the 10.67 and 10.33 both exhibit greater curvature than the 10.50, as they both deviate from the helical pitch of 10.50. The combination from the results suggest that Ba^{2+}, relative to Mg^{2+}, induces a slight overwinding of the DNA helix in DNA origami.

The binding of the tiles in mixtures containing both Ba^{2+} and Mg^{2+} act as a method for controlling curvature by further changing the inherent helical pitch and degree of

stabilisation of the DNA helix, demonstrating that it is possible to alter the curvature of tiles once folded, removing the need to design tiles with inherently different crossover spacings. The binding of the tiles to the mica under Ba^{2+} also demonstrate how the flexibility of tiles can be altered, which allow for the use of a buffer wash step to alter the inherent size of the origami once on a surface. The work demonstrated by Woo et al., where Na^{+} was used to alter the strength of binding to the surface, shows how DNA can become mobile once deposited. This allowed the origami to rearrange themselves, forming base stacking interactions between tiles and creating large-scale constructs [71].

7.5 Conclusion

The results of this section further highlight the effect of the underlying twist of the crossover and how this correlates to the overall global twist/curvature of the origami. The increase in bias to the A-face up for the 10.50 and 10.33 under UV exposure shows how the bias for tiles remains in the same plane, regardless of the underlying crossover spacing. This is important for applications where one decides how to functionalise the surface of origami to ensure that the functional groups are accessible to the user. The formation of single and double strand breaks however demonstrate that extreme damage to the DNA can result in the curvature being reduced, but leads to disintegration of tiles, making them ineffective for in vivo applications. The recent work of Gerling et al. however demonstrates that it is possible to design methods for UV exposure that do not cause long-term damage to DNA origami structures [154].

The results of the tiles in Ba^{2+}, demonstrate the resilience of DNA in “exotic” buffers, and how there is more to learn about the robustness of origami. Literature has already demonstrated that once folded, the origami can remain intact up to high temperatures as well as survive in low ionic strength buffers [138]–[140]. This work furthers this, by demonstrating how non-biologically relevant cations can be used for the folding of DNA origami. It is hoped that these results will lead to increased study of cations and they effect they have on DNA origami. The results of binding for tiles in mixtures highlights how combinations of cations can also be used to alter the structure of origami, but also

demonstrates the sensitivity of origami to foreign cations, which could lead to unwanted consequences.

8 High resolution AFM imaging of DNA origami

8.1 Introduction

The definition of high-resolution imaging is dependent on both the sample and microscopy technique. Optical based methods are typically limited by the diffraction and wavelength of light, although methods such as STORM can help reduce this. Despite this however, there are few methods that allow imaging of the DNA helix under aqueous conditions, such that the DNA remains in B-form. In this particular work, high-resolution refers to obtaining images of the internal structure of DNA origami tiles, such that the individual DNA strands can be imaged, along with secondary structure of the DNA itself.

This chapter looks at how DNA origami tiles appear when imaged with AFM under aqueous conditions, highlighting how the underlying stapling design affects the various regions of the DNA origami, such as the presence of the internal diamond lattice as well as the seam. It focuses on the difference observed when the tiles are adsorbed onto mica, as well as nickel modified mica, leading the development of methods to alter the structure of DNA origami. High resolution imaging also allows for the possibility to measure how staples strands bind to the scaffold strand, highlighting how the regions of the staple affect the images obtained.

8.2 Results and discussion

8.2.1 General imaging

Analysis of the adsorption orientation of the tiles used in thesis were taken from images that were 9x9 μm in the XY direction with a resolution of 3072x3072 pixels. This places a resolution limit of 3 nm for each pixel, such that the internal structure of origami tiles cannot be resolved. Even at decreased scan sizes, internal resolution of the tiles is only achievable with relatively sharp probes, due to tip convolution effects that arise. One issue that is present in imaging origami tiles at increased magnifications is that of sample

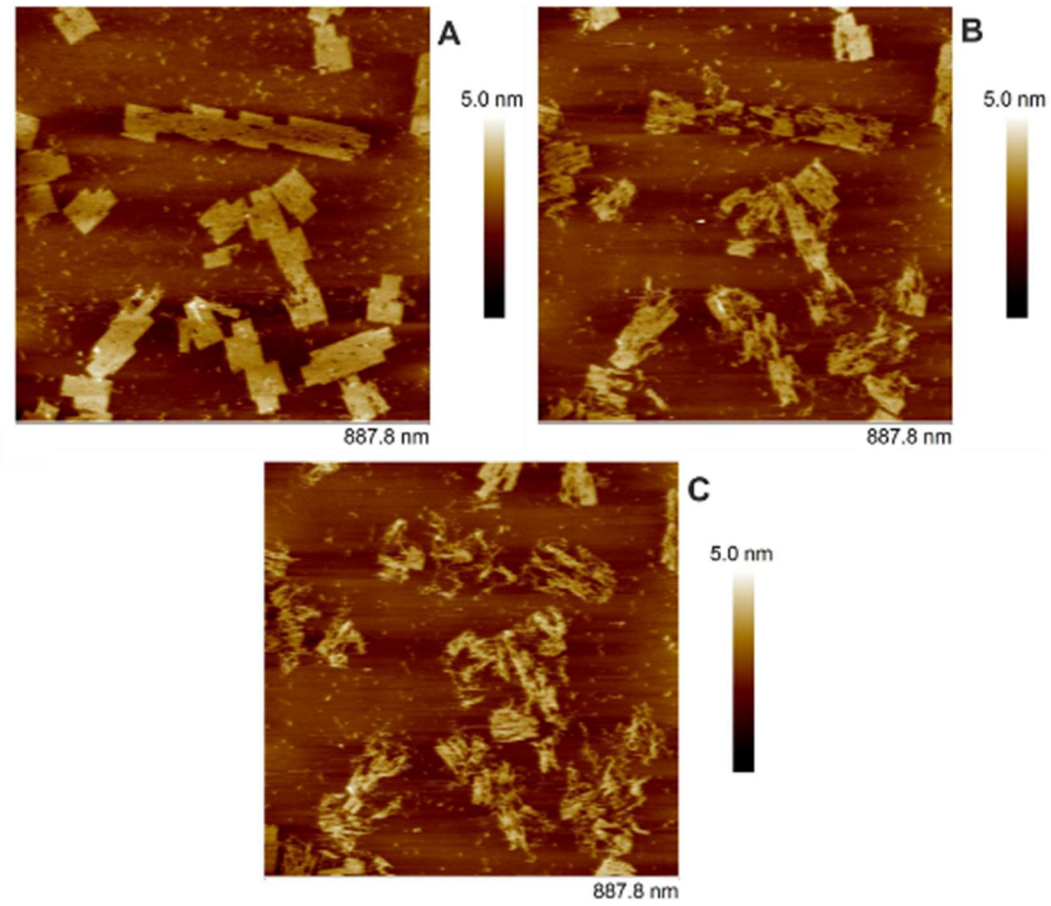

Figure 39: AFM images of the 10.67 tile demonstrating how sustained high imaging forces lead to tile degradation. A) 0s, B) 4m32s, C) 9m5s.

perturbation, due to high imaging forces, which can be seen in figure 39, where continuous high imaging forces can lead to tile degradation. This was a problem for obtaining width of tiles, as perturbing the sample can skew the measurement by distorting the tile on the surface. As a result, samples were imaged only once during width measurements, so as to minimise any bias that may occur from tip movement. This issue of sample perturbation was also apparent in samples of UV exposed tiles, where the decreased DNA rigidity makes them more susceptible to being degraded due to physical interaction with the tip when compared to their un-exposed counter parts.

From the results of chapter 6 it can be seen that the effective Mg^{2+} concentration plays a pivotal role in the adsorption orientation of tiles. One other important factor is the concentration of tiles in solution, such that the concentration is high enough to obtain statistically relevant results, but low enough such that the tiles do not interfere with each other during adsorption from solution. Figure 40 shows the difference in surface

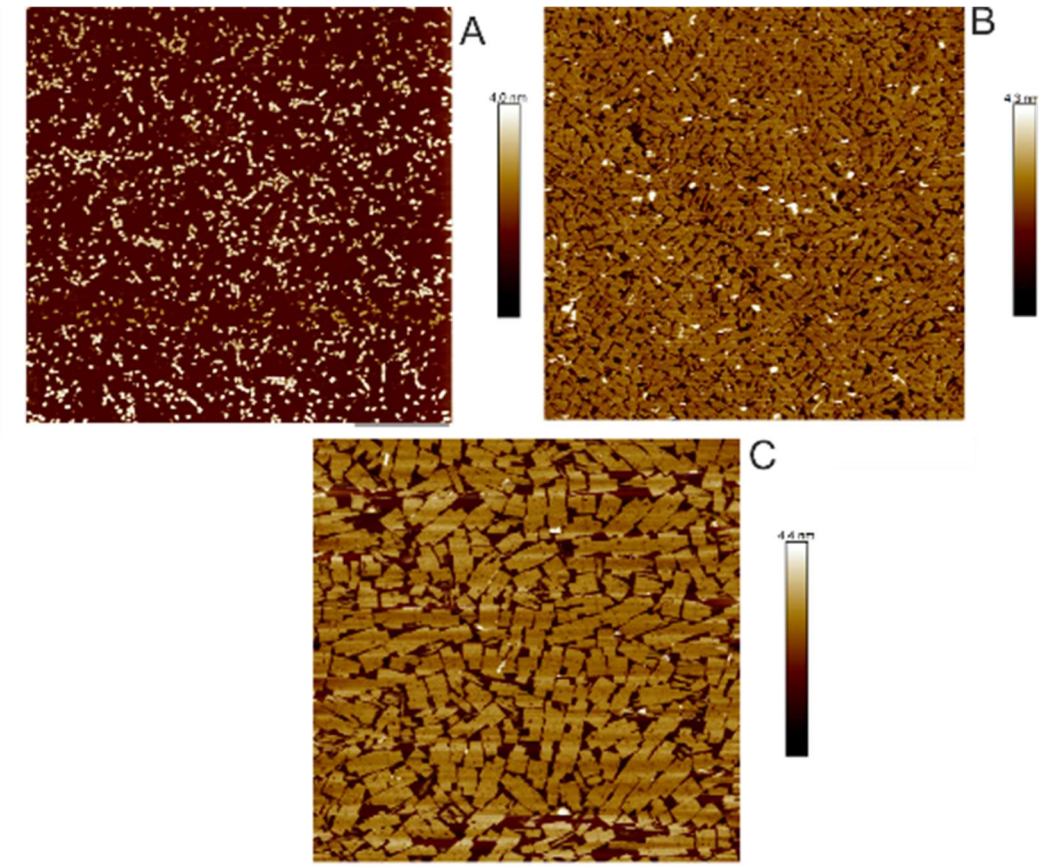

Figure 40: AFM images showing the density of tiles at A) 1 nM, 9 µm scan, B) 4 nM 3 µm scan and C) 6 nM, 1 µm scan.

coverage of a tile solution at 1 nM, 4 nM and 6 nM. The lack of a DNA multi-layer in both the 4 nM and 6 nM solutions, suggests that the origami tiles retain some mobility on a layer of DNA origami with DNA-DNA interactions being weaker than that of DNA-mica interactions. In addition to this, the relatively high number of adsorbed tiles makes it difficult to distinguish orientation of individual tiles.

One of the common features observed when imaging origami tiles is the presence of concatemers, whereby multiple tiles appear to form a single larger structure. The formation of concatemers in this work is not fully understood but is believed to be caused by base stacking interactions between origami tiles in solution. It is also possible that staple strands along the edges bind between origami tiles, although this has not been explored. One of the aims in literature is to create large scale origami designs through the purposeful design of staple strands and sticky-end overhangs. Although the origami used in this work contained poly-T overhangs along the edge of the design, to try and disrupt base stacking interactions, preventing the formation of concatemers, the

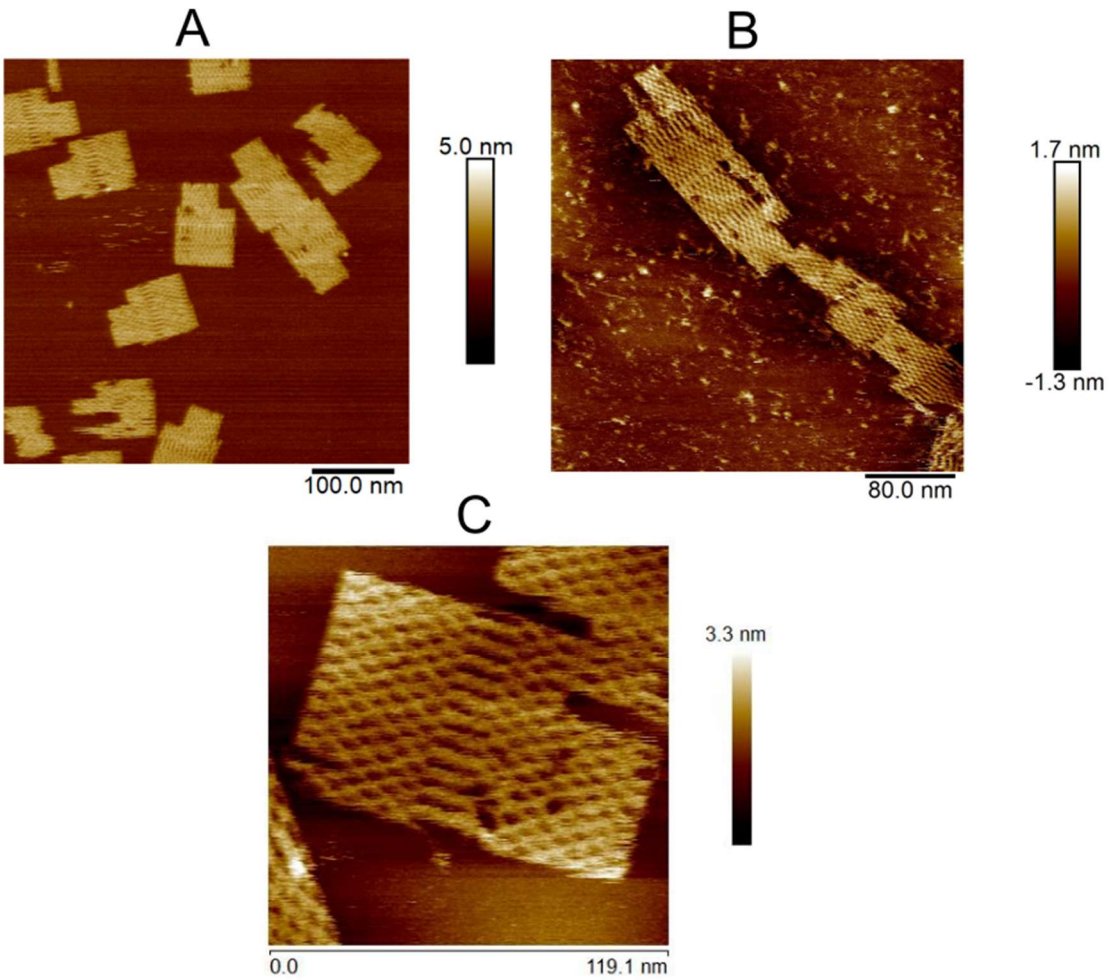

Figure 41: Example AFM images of the tiles under aqueous conditions at varying lengthscales. The seam is noticable in all, with the diamond alttice visible in both B and C.

appearance of short-length concatemers would suggest that base stacking interactions between tiles can still occur. This is believed to occur due to the poly-T overhangs not remaining rigidly in place. This can be seen in AFM images, where the ends of two adjoining tiles line up. These concatemers were not used during the analysis of tile adsorption orientation as it was felt they would not accurately reflect the magnitude and direction of curvature in individual tiles.

In higher magnification images of origami tiles, the appearance of an internal diamond-shaped lattice, which is caused by the electrostatic repulsion between the tightly packed helices as well as the crossover positioning. This diamond lattice has been discussed previously, and was the underlying reason for the increased in widths observed under different solution conditions. In addition to the diamond lattice, there is also the seam of the origami, where the scaffold strand switches direction. The use of a seam was

originally implemented by Rothemund, as it was noted that AFM images of tiles without a seam, caused stretching of the tiles, resulting in a so-called hour-glass effect. The change in appearance observed for the seam compared to the diamond lattice is due to the presence of three crossovers between the adjacent helices, such that the lengths of the two DNA helices between the crossovers are unable to deform to create a diamond lattice. The presence of the seam is used by a commercial company (Gattaquant GMBH, Hiltpoltstein) which utilised it as a method for nanorulers as a means of calibration in AFM images. In addition to the diamond lattice, holes in the tiles appear to be an occurrence in high magnification images, which are believed to be caused by a lack of staple strand bound to the scaffold strand. It is not known however if these holes are cause by the tip distorting the sample and dislodging the staples, or if it is a consequence of a mis-fold during the formation of the origami.

8.2.2 **Sub-nm resolution**

Sub nanometre resolution of the DNA helix under aqueous solution using AFM is a difficult challenge to overcome due to a variety of factors that can affect image quality. One of the major limiting factors is tip sharpness, which remains out of control of the AFM user. Although recent advancements in probe manufacture have led to increased tip sharpness, preservation of the tip sharpness is the greatest limiting factor. Another limiting factor is relative motion between the sample and the tip, whether it is caused by drift of the piezo systems themselves at small scan sizes or perturbations between the tip and sample. These factors are ever present during attempts of high-resolution imaging and are the main reasons for the methodologies used for attempting high resolution imaging.

The primary approach taken to obtain high resolution images was to preserve tip sharpness, by imaging the origami with a high amplitude set-point in tapping mode, so as to minimise energy dissipation into the sample. This can be seen in some of the low magnification images, where there is a lack of observable internal structure. Attempts at

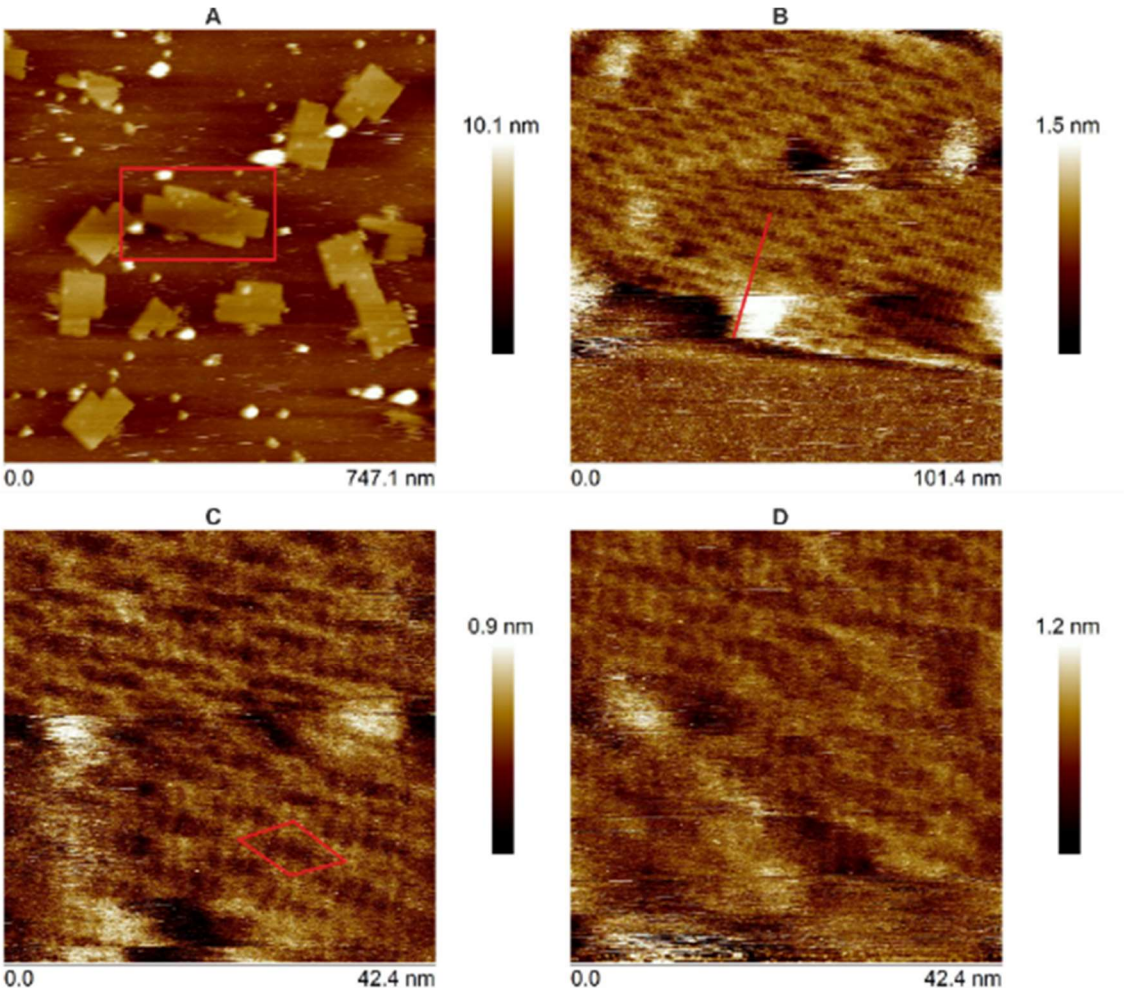

Figure 42: Montage of a 10.67 dimer concatemer under aqueous conditions. A) Red box highlights zoom of subsequent images. B) Red line hihglights join between the two tiles. C) Red rhombus highlights one of the internal dimaond structures. D) Subsequent image following on from C where the tile appears to have moved.

high resolution imaging are summarised in figures 42 to 45, highlighting the subsequent scans and increase in magnification used throughout.

Figure 42 was one of the earliest attempts at high resolution imaging of the tiles. The tiles were deposited in standard Mg^{2+} buffer with no surface pre-treatment. In this attempt, a dimer was imaged as it was believed that this would be less mobile due to the increase surface area binding the origami to the mica. In figure 42B the red line highlights the join between the two tiles, which shows how base stacking interactions between tiles causes the appearance of a seamless linkage. Unlike previous low magnification images, the diamond lattice appears to be interlaced with bumps, which are the grooves of the DNA helix. There is also the presence of the seam in figure 42B, which can be seen along the right-hand side of the image. Similar to the rest of the origami, there is also the

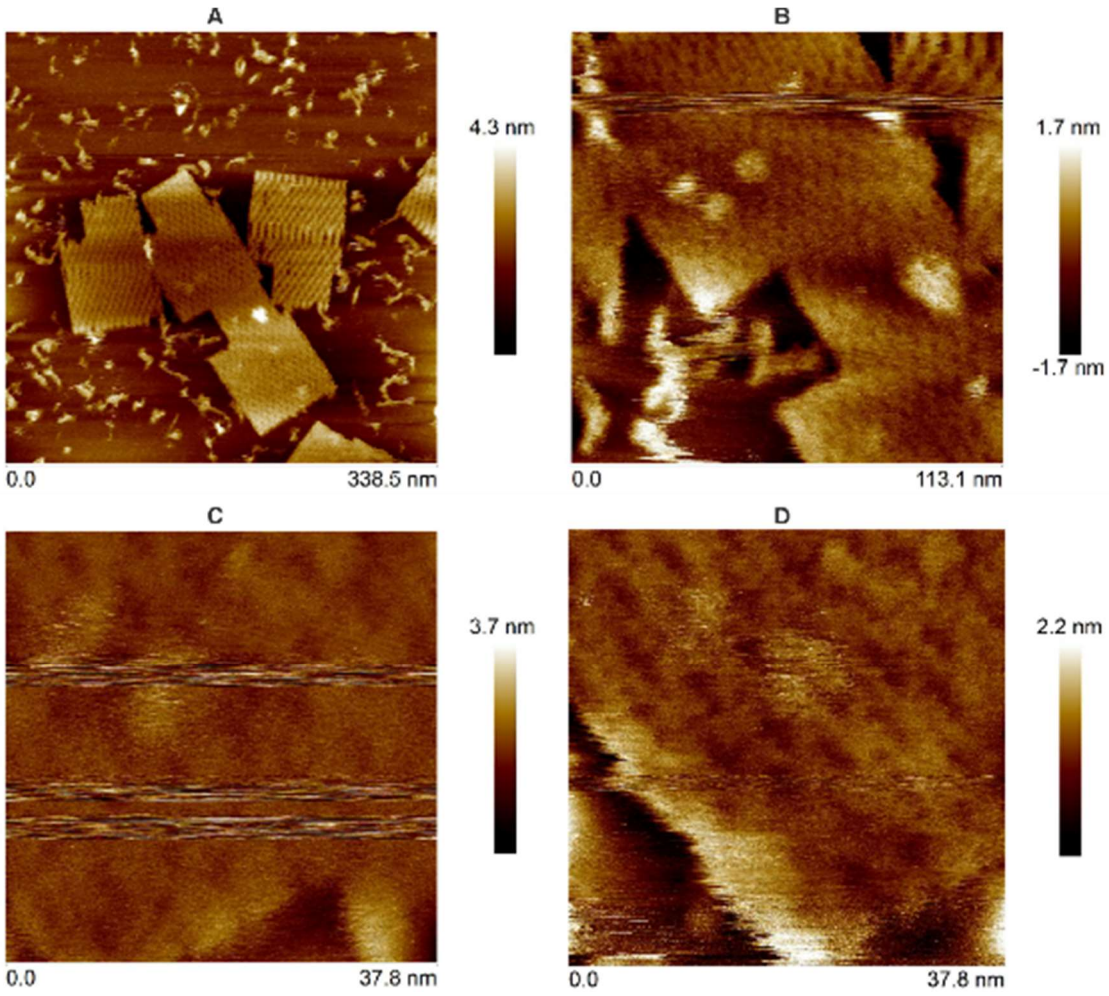

Figure 43: Montage of a 10.50 dimer imaged under aqueous conditions on a Ni2+ treated mica surface. A and B show the subsequent increase in magnification after finding an initial candidate to scan. C and D are scan of the same area, having altered the scanning parameters. The diamond lattice and bumps are visible in D.

presence of topographical periodicity along the DNA contained within the seam. An example of one of the diamonds is highlighted in figure 42C. The position of the repeating period along the DNA strands, when combined with the diamond lattice, highlights that there is a single groove between the crossovers, with the crossover themselves consisting of four bumps. This is consistent with the underlying stapling pattern, with the crossover spacing's being 1.5 turns in length corresponding to three grooves.

Another attempt looked at reducing the mobility of the tiles, by depositing them onto a nickel pre-treated mica surface with a solution containing 5 mM $NiCl_2$. The images of this attempt are summarised in figure 43. The main difference between this attempt and that previous, is the mica surface itself, which appears to be covered in a layer of staple strands, due to the increased strength of binding, as is observed with singular linear and

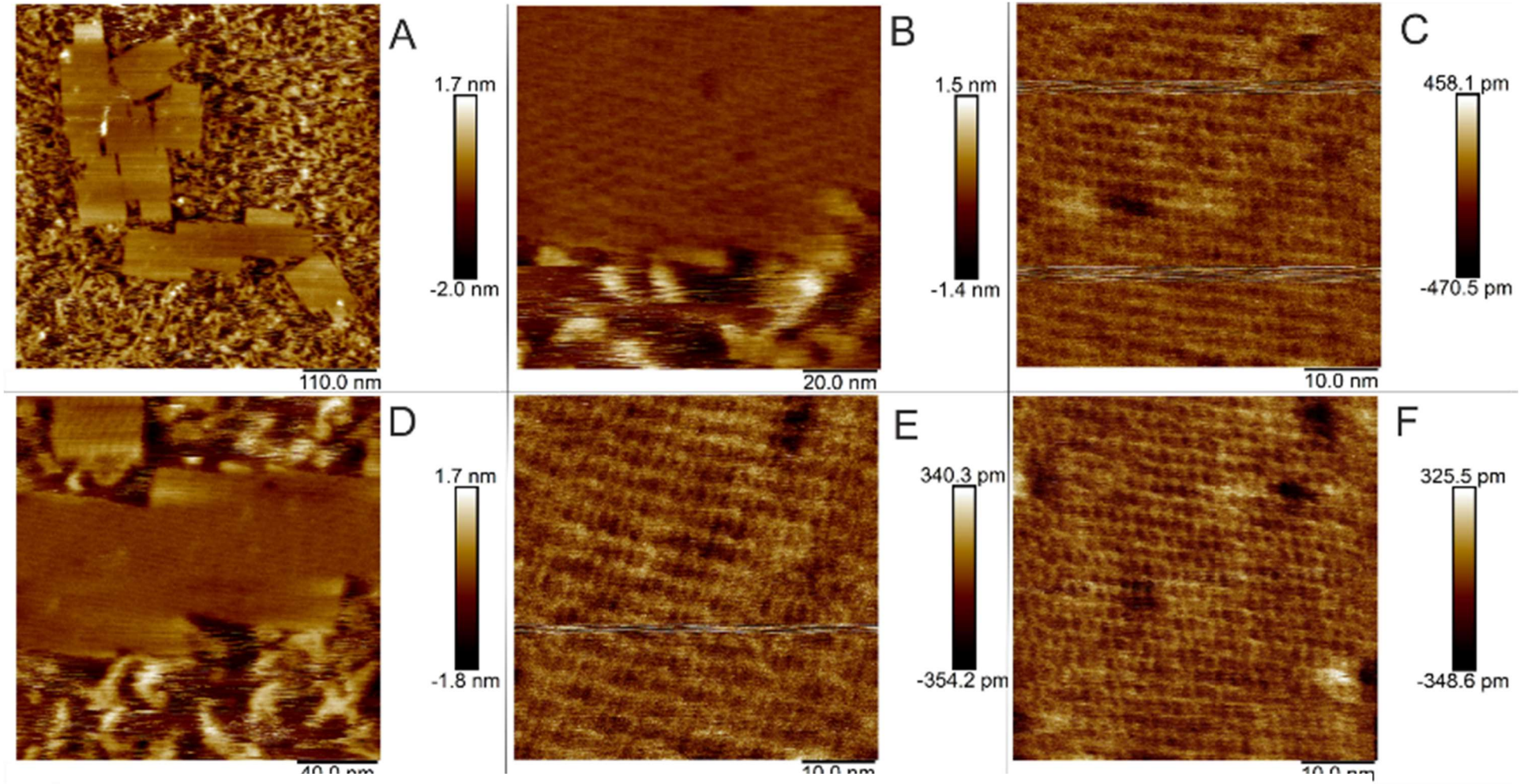

Figure 44: Montage of scans on a 10.67 tile whose helices are parallel to the fast-scan axis of the AFM. Unlike previous attempts, there is no apparent internal diamond lattice, or seam.

circular DNA molecules in literature. The presence of the internal structure, such as the seam and diamond lattice is observable in figure 43A. Subsequent scans of increasing magnification reveal a similar occurrence to that in figure 42, with the grooves of the DNA strands presenting themselves as bumps along the DNA strands. Unlike before however,

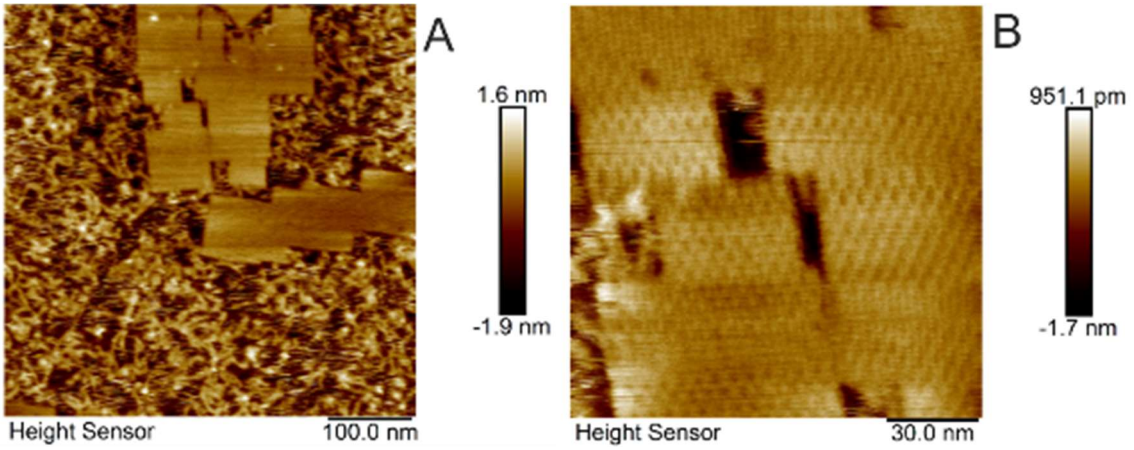

Figure 45: Attempt at high resolution imaging of tiles whose helices are perpendicular to the fast–scan axis. Same sample as in figure 44.

the appearance of the bumps is different, which may suggest an increased attraction to the mica surface. Other causes of this may arise from tip geometry, which can influence how the force from the DNA is “felt”, affecting how the DNA appears.

A final attempt at high resolution imaging is shown in figures 44 and 45. Similar to the second attempt, the samples were deposited on a nickel treated mica surface, except this time the mica was pre-treated with a 50 mM solution. Unlike the previous two attempts, this allowed imaging of two different tiles with varying orientations. It is believed that the relative orientations of the helices with respect to the scanning direction of the tip affects the interaction between the tip and the DNA, and be used to explain the disparity between the two origami orientations. The high resolution images themselves however show a very different internal structure of those previous. The difference in the appearance is believed to not be caused by the relative orientation of the helices, but the increases strength of binding to the mica surface, preventing an apparent formation of diamonds for the origami whose helices are parallel to the fast scan axis. This effect has

been highlighted in literature, where it was shown that the mica-DNA binding can influence the structure of the DNA.

8.2.3 **2.5 turn**

One of the challenges with obtaining helical resolution of DNA contained within DNA origami tiles is the “coherence” length of the DNA strands. DNA origami can be considered as a series of short 1.5 turn DNA segments, connected through crossovers. The coherence length is in effect the crossover spacing, and is used to describe the distance over which the DNA remains a single un-nicked strand. In an attempt to increase the coherence length, the stapling pattern of the origami was altered such that a region contained a series of 2.5 turn crossovers. A schematic of this modification is given in figure 46, along with AFM images.

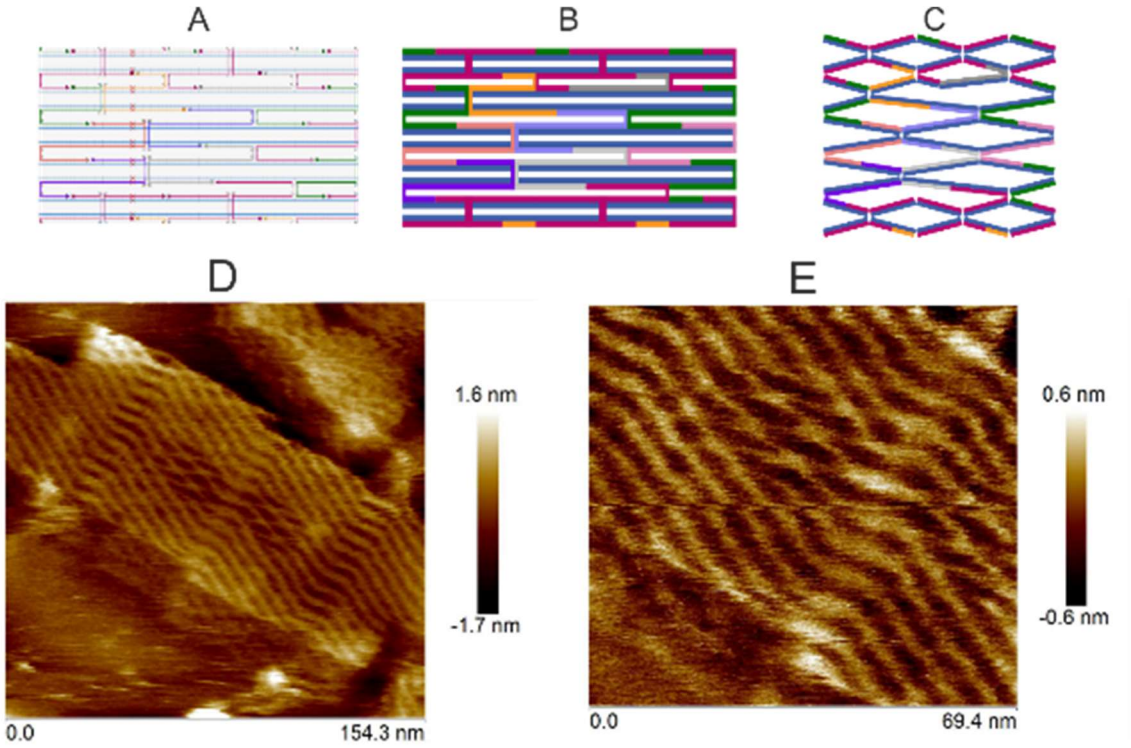

Figure 46: A) caDNAno image of the staple pattern for the inclusion of staples with 2.5 turns. B) Schematic, showing the routing of the staple strands. C) Schematic showing how electrostatic repulsions would result in internal diamond lattice. D-e) Subsequent scan of a dimer concatemer, showing the internal structure as a result of the modification.

Similar to the original attempts at high resolution imaging, increasing the staple length seemed to offer little help in obtaining measurements on the helical structure of the DNA contained with origami tiles. Despite a change in appearance on the internal diamond

lattice, other attempts resulted in similar quality images, highlighting the difficulty of high-resolution imaging. The results however demonstrate the effect that a longer crossover length has on the structure of the diamond lattice, demonstrating that the initial diamond lattice is in fact a result of the underlying stapling pattern. The increase in size of the diamond lattice highlights how internal modifications can be implemented as a means to alter the structure of origami, allowing for placement of larger groups in the plane of DNA itself, as well as a potential alternative method to create nanopores or nanofilters from DNA origami.

8.2.4 **Major axis hypothesis**

Under certain imaging conditions, a modified internal structure becomes apparent; which is termed here as the “major axis”. This major axis is caused by the position of nicks and staple strands of the DNA origami which when combined with electrostatic repulsions, causes the two opposing sides of each diamond to be topographically higher. The sides of all the diamonds join up forming an apparent solid diagonal strand present. A schematic on how this arises is given in figure 47, along with example AFM images. The major axis is therefore believed to arise due to the position of the ligated strands aligning, making it appear that there is a solid DNA strand running through the design. This has given rise to the idea that the crossover arrangement affects the curvature of the origami tiles, which can be used to describe the curvature of the tiles under conditions of 12.5 mM Mg-ace, 1xTAE.

To test this hypothesis, several variations of the 10.33 tiles were designed with caDNAno and modelled using CanDo. Although the work in this thesis has already shown how CanDo can be inaccurate for certain origami, the results can act as a qualitative method for comparing crossover arrangements. Examples are summarised in figure 48, where each origami design has the same average crossover composition across each helix, such that they all have an average helical pitch of 10.33. The most striking result however is that in the top two models, where the resultant CanDo model predicts opposing curvature despite the same overall composition. In addition to the major axis, there is

also the minor axis, which is the composition of the nicked crossover strands. The difference in crossover arrangement for these two theoretical designs in figure 48 causes the major and minor axes to vary in their composition. This causes the first to have a major axis that is solely 16 bp, which is also the case for the 10.67 tile, whilst the arrangement of crossovers in the opposing design has a major axis that is wholly

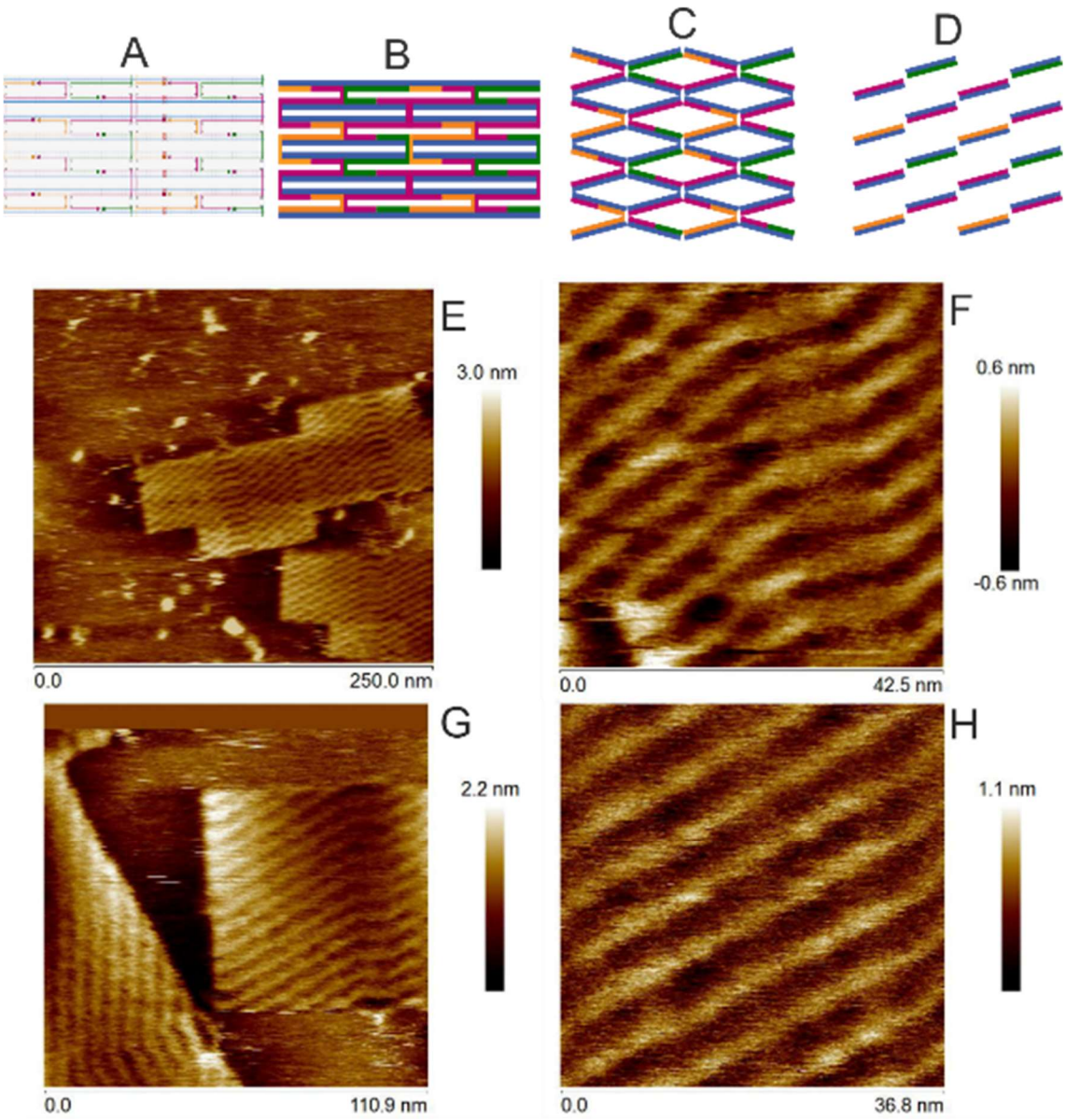

Figure 47: A) caDNAno image showing the position and routing of the staple strands. B) Simple schematic showing the staple pattern. C) Schematic showing how the electrostatic repulsions result in the internal diamond lattice. D) Position of crossover spacings which are made of ligated DNA segments. E-H) Montage of AFM of decreasing scan sizes on a 10.50 tile. The presence of the major axis is clearly visible, reflecting the ligated crossover spacings.

composed of 15 bp. The composition of the major and minor axis between the two causes the axis about which the origami tiles curve to rotate about the face. The

theoretical design of the 10.33 tile which has a major axis of all 15 bp and a minor of all 16 bp causes the CanDo model to exhibit a left-handed twist, whilst the 16 bp major and 15 bp minor has a right-handed twist.

The composition of the major and minor axis therefore serve as an additional means for the direction of curvature present in the tiles. Despite the overall helical pitch being that

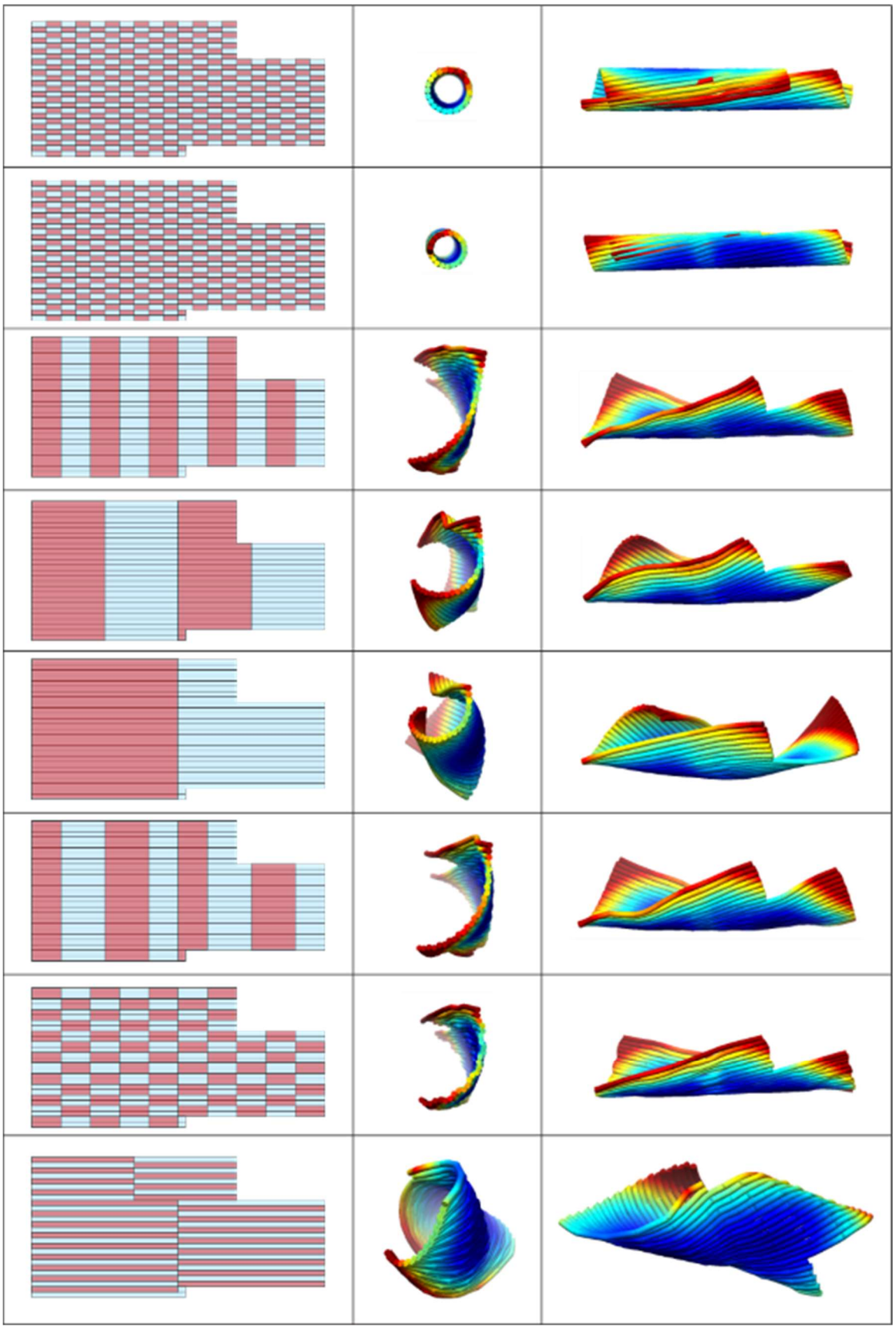

Figure 48: Series of schematic and CanDo models of the 10.33 tile with varying crossover arrangements. In the schematics, red corresponds to 15 bp crossover with blue corresponding to 16 bp.

of an underwound origami, with a presumed left-handed curvature (based on previous observations and theories), the arrangement of the crossovers within the tiles act as an additional method to quantify origami curvature. Although these two represent an extreme case, it nonetheless demonstrates the possibility of altering origami curvature simply by altering the arrangement of crossovers. One of the main reasons for this analysis was the recent work of SAXS paper who created an origami design of 10.44 and an unusual crossover arrangement. CanDo models of how the crossover arrangement affects the curvature of a tile, which is constructed of 1:2 15:16 bp crossovers is given in figure 48. Similar to the theoretical models seen for the 10.33 tile, CanDo models demonstrate that by changing arrangement of the crossovers, the major and minor axis can be altered. These are all purely theoretical, but the widespread usage of CanDo and its inaccuracy (as demonstrated in chapter 6) means that further investigation is required, and that comparison between models simply based on averages does not serve well.

8.2.5 **Increasing staple length**

To investigate if the major axis is a result of the ligated strands aligning in the origami tile, another modification was made to the staples strands. Six staples were chosen and replaced with 3 longer staples, so as to create a region where the parts of the minor axis would appear solid, i.e. no nicks between crossovers, such that two rhombuses were formed with no nicks. A schematic of the modification is given in figure 49, along with the corresponding AFM images. The solid lines in Figure 49D correspond to the strands of DNA which do not contained nicked strands. As seen in Figure 47, these un-nicked strands appear to be solid in the AFM images, whilst the nicked strands are less prominent. It was hoped that the modified strands, as outlined in Figure 49, would appear solid. Similar to the previous attempts at high resolution imaging however, measuring the change in appearance of three crossover segments proved to be a difficult task in that it was not possible to differentiate between nicked and un-nicked strands. The attempts did however demonstrate again the ability to image the grooves of the DNA, through the

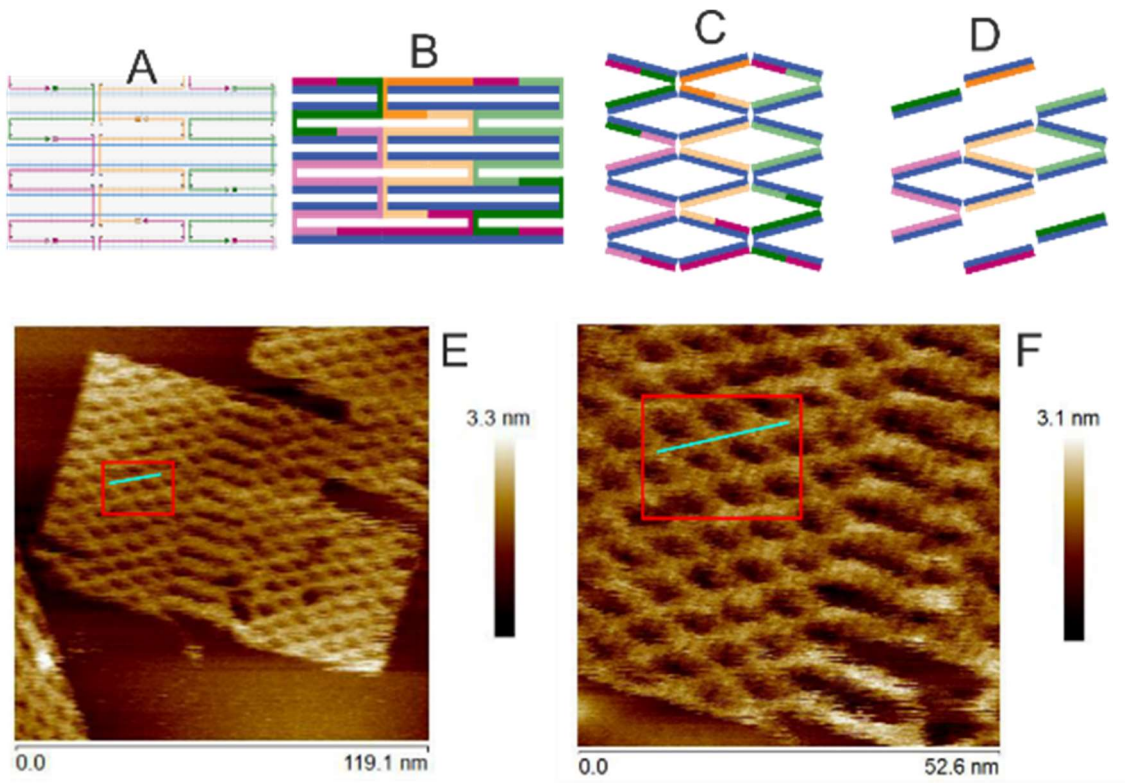

Figure 49: caDNAno image of the staple pattern for the inclusion of staples that traverse 5 helices, rather than the standard 3. B) Schematic, showing the routing of the staple strands. C) Schematic showing how electrostatic repulsions would result in internal diamond lattice. D) Schematic showing where the minor axis would appear to be solid. E-F) AFM image of the modified tile. The red box highlights the area. The modified staples are below the blue line.

appearance of bumps along the strands, but the small coherence length once again proves how difficult it is to obtain sub-molecular imaging of the DNA helix.

8.3 **Conclusion**

High resolution imaging of the origami tiles was not the main focus of this thesis, as it was known from the start that imaging the DNA helix under aqueous conditions is a challenging task. The results however demonstrate that the ability to modify the origami with longer crossovers act as an additional method for functionalisation. The use of double-length staples, spanning five adjacent helices, also demonstrates that this origami can still fold, at least for this limited staple substitution. They also reveal an asymmetry in the internal structure of the origami themselves, the major and minor axis, which combined with CanDo models, appears to be a method to alter the curvature of origami by changing the underlying arrangement of crossovers. This outcome is, however, hypothetical at the moment, because it is clear that CanDo models cannot

always reliably predict the degree of curvature and even the direction of curvature. Current methods to functionalise origami include the incorporation of hairpin loops, which are placed at the crossover junction or along the spacing between two crossovers. Single strand overhangs or modifications to the 3’ and 5’ ends can also be placed at the head and tail of the staple strand. It is currently unknown how the methods of functionalisation will impact the underlying crossover spacing, and hence structure of DNA origami. This leads to the question if all staples can truly be used as a functional site, requiring modification of the underlying stapling pattern to retain structural rigidity.

9 Final Conclusions

Curvature of origami arises from the mismatch between the angle through which the DNA helix contained in crossovers rotates compared to that of idealised case. For single-sheet square-based origami, the idealised angle is an odd-number of half-turns whilst the angle through which the DNA helix rotates is dependent on the helical pitch, stability and number of DNA bases between crossovers. The handedness of the curvature is related to the concepts of supercoiled DNA, whilst the plane into which the origami curves appears to be independent of mismatch. It is the authors opinion that a misnomer exists in literature on the cause of origami due to the mislabelling of supercoiling and misunderstanding on the stability of DNA contained within origami, such that curvature simply reflects the mismatch as the DNA exists in B-form, or slight variation as determined by the relative salt concentration.

With the exception of the 10.33 tile in a solution containing 3.125 mM Mg^{2+}, all tiles exhibit the same bias to the A-face up, demonstrating that all tiles curve into the same plane. This result is consistent with the OxDNA models, highlighting how CanDo can be inaccurate and misleading for certain origami designs. The change in magnitude of curvature observed for the tiles is a result of the underlying degree of stabilisation of the DNA helix, due to the effective Mg^{2+} concentration as well as the electrostatic repulsion between the helices due to them being tightly packed. In both the 10.67 and 10.33 tiles, decreasing the Mg^{2+} concentration from 15.625 mM corresponds to a decrease in the observed curvature, demonstrating how the DNA becomes less stable. When the Mg^{2+} is increased, there is a peak in curvature observed for both the 10.67 and 10.33 tiles. The subsequent drop in curvature is caused by a fully stable helix along with an increase in shielding between the tightly packed helices. The difference in the position of the peaks for the 10.67 and 10.33 tile is attributed to the underlying crossover spacing, where an increase in shielding is experienced sooner for the 10.67 tile, due to a longer crossover spacing which results in a drop in the deformation of the DNA sooner. Although

this deformation is present at lower Mg^{2+} concentrations, it remains at a constant level due to the crossover spacing's being of consistent length in each design.

Despite previous observations that the helical pitch of DNA is 10.50, the slight bias for surface binding seen for the 10.50 tile would suggest that the helical pitch varies slightly. The bias may also be a result of the crossovers having dimension to them, such that they influence the twist of adjacent crossover spacings. The decrease in magnitude of the 10.33 tile compared to that of the 10.67 tile, with respect to the 10.50 tile however, suggests that the crossovers tend to a slightly underwound state, and as such the relative mismatch for the 10.33 tile is less than expected. This effect is also apparent in the tiles folded in Ba^{2+}, where despite a large apparent decrease in helix stability, the tiles still exhibit some bias when adsorbed onto mica. Generally, the mismatches of the 10.67 and 10.33 tiles compared to the 10.50 represents a change in helical pitch of only ±1.6%, highlighting the sensitivity of the origami. The AFM binding results of the tiles in varying Mg^{2+} therefore corresponds to minimal changes in the DNA helix, which may go unnoticed by molecular machinery in vivo, or in molecular biological applications.

As the origami flatten out once bound to the mica surface, there is no direct way to measure along which axis the origami is curved. Although both OxDNA and CanDo show how the axis of curvature for the 10.67 and 10.33 tiles is not parallel to the DNA helices contained within the origami, there is no way for this to be experimentally verified with the techniques used in this thesis. Fortunately, the results of Mallik et al., Li et al. and Dietz et al. can be used to explain the axis of curvature. The results of Mallik et al. highlight that there are two curved corners of the origami, as seen in the EM images. This is the same result seen by Li et al., who joined diagonally opposed corners of overwound origami, highlighting the appearance of a right-handed chirality in the nanoribbons. The results of Dietz et al. show that an underwound origami (10.33 tile) exhibits a left-hand chirality. These three papers however all lack the use of an asymmetrical tile design, such the plane into which the origami curves cannot be determined. When the results of this thesis are combined with the work in literature

however, the true direction of curvature can be deduced, which highlights that the OxDNA models are in fact representative of the underlying crossover spacing.

The results of Marchi et al., on which the origami used in this work was based, demonstrated that tiles with opposing degrees of supercoiling, as determined by the crossover spacing, causes an opposing bias in AFM images. The results presented by Marchi et al. however discuss the binding of a larger origami folded with a 51k nt scaffold, which has been calculated in this thesis to have a lower effective Mg^{2+} concentration. This correlates to the tiles in thesis, folded under Mg^{2+} concentrations between 3.125 and 6.25 mM Mg^{2+}. This notion of effective Mg^{2+} can therefore be used to describe the observed binding of the three large tiles in work by Marchi et al., highlighting the importance of effective Mg^{2+} concentration on the structure of origami in general.

When the tiles in this thesis were exposed to UVC radiation, the changes in curvature can be attributed to both unwinding induced by CPD formation along with the formation of single and double strand breaks. Under doses of 10 kJm^{-2}, the decrease in curvature for the 10.67 tile is attributed to unwinding of the overwound helices, whilst the increase in curvature of the 10.50 and 10.33 tile is attributed to an increase in unwinding of the underwound helices. This not only highlights how the curvature of origami is in fact a result of the twist of crossovers, but that the magnitude of curvature is a result of the underlying mismatch. At UVC exposures above 10 kJm^{-2} all tiles experience a decrease in curvature that is attributed to the formation of single and double strand breaks. This causes the structure of the DNA to degrade, as seen in both the width measurements as well as AFM images of the tiles. The formation of backbone breaks along the strand are detrimental to the underlying integrity of the origami tiles, which is assumed to be present even at low UVC does. The decrease in curvature attributed to ~10 kJm^{-2} is a result of the three origami designs having the same composition. The decrease however cannot be strictly attributed to the CPD formation becoming saturated, such that they no longer form, or that the build-up the single and double strand breaks start to dominate.

The binding of the tiles under Mg^{2+} as well as the tiles exposed to UV radiation act as a baseline for the tiles folded in Ba^{2+}, to help determine the difference between helix stabilisation and changes in mismatch. When folded in pure Ba^{2+}, the overall trend across the three tiles is indicative of an under stabilised helix. When comparing the trend across the tiles for all Ba^{2+} solutions however, the average curvature for the 10.33 tile, compared to both the 10.67 and 10.50 is greater. This indicate that the mismatch is greater, such that the helical pitch of DNA solution has become slightly overwound in the presence of Ba^{2+}. This increase in the overwinding of the DNA therefore decreases the mismatch for the 10.67 and 10.50 tiles, causing them to have a relatively lower bias than that of the 10.33. This effect is also observed in solutions containing both Ba^{2+} and Mg^{2+}, where the ions co-operatively bind to the DNA helices in all three tiles. This effect is most apparent in the 10.33 tile, where the stabilised overwound DNA causes the mismatch to become greater, resulting in a larger curvature. The relatively small magnitude of curvature for the 10.67 and 10.50 tiles is therefore attributed to the mismatch being less. These results show not only how various cations bind to the helix, i.e. bases or phosphate backbone, but that the correct assignment of twist is important for determining the effect of cations on the DNA helix itself. In essence, the sensitivity of origami can be used a tool for measuring the effect of cations on the helical pitch of DNA, without the need to crystallise DNA strands, making the process easier.

The appearance of the tiles under AFM, when imaged at high magnification and with high resolution highlights the appearance of a major axis, which is due to the composition of the crossover spacing containing both nick and ligated DNA strands. This leads to the concept of crossover arrangement having an effect on the origami curvature, as evidence by the work of Benn et al. whose crossovers were offset so as to increase the overall curvature of the origami [158]. This result also highlights how the underlying arrangement of crossover themselves can affect the curvature, as seen qualitatively with the CanDo models. This also indicates that the average pitch of the tiles is not necessarily a good indicator of the tile curvature. The modification of the tile to include 2.5 turns between

crossovers not only demonstrates that the diamond lattice is in fact due to the length of the crossovers and electrostatic repulsion between the helices, but that they act as a potential method for creating nanopores, as well as augmenting methods to functionalise origami and/or surfaces. This allows groups to be placed in the plane of the origami, such that groups could bind directly to the mica, rather than on a particular face of the origami, making the possibility of removing the DNA easier for future applications such as solid state devices, where aqueous conditions and the presence of organic material may prove detrimental.

9.1 Future work

With DNA origami, form follows function. Understanding the factors which affect origami structure is therefore important, as it will help lead to new design methods. The results of this thesis have demonstrated how the underlying crossover composition causes single-sheet origami to curve into the same plane, whose magnitude is determined by the mismatch relative to the helical pitch of DNA as determined by the solution conditions.

The associated cost with producing varying origami designs is one of the limiting factors for experimental validation. To this end, techniques such as cryo-EM as well as OxDNA modelling should be utilised to create a robust data set exploring how the underlying crossover composition affects origami structure, aiding the AFM results of this thesis. This will allow for greater exploration of how the crossover arrangement affects origami structure. The origami used in this contained crossovers which were spaced 1.5 turns apart, using crossover spacings of 16 bp and 15 bp to alter the mismatch across the length of the origami. This concept should be expanded further to crossovers with varying lengths, such as 0.5 turns and 2.5 turns, to help understand how the rigidity and hence curvature of tiles, is affected. The use of smaller staples will offer a greater number of sites for modification, but may limit the ability of the origami to fold. Longer staples may also affect the origami curvature and rigidity, but this has yet to be fully explored. The UV irradiation results have already demonstrated how an origami with crossover

spacing's such that the average helical pitch is less than that of the 10.33 tile binds to mica. This would require further verification, such as the purposeful design of an origami with all 15 bp crossover. This is important for functionalisation of origami, where hairpin loops may allow relaxation of the crossover spacing, such that it twists similar to a 16bp staple, altering the inherent structure of the origami tile.

Creating large scale arrays relies on joining smaller origami tiles together. This has been demonstrated both in solution as well as on a substrate in the literature. Creating origami arrays in solution has employed the method of both sticky ends as well as staples which are integrated into both tiles. The difference between these two methods however is the rigidity of the bond, such that the curvature of the two tiles may influence one another. This may lead to super-structures with unexpected consequences. This was demonstrated in the Li et al., with a similar effect assumed to occur with other origami designs. Ribbons would be undesirable in origami super-structures as they cause opposing faces of the super-structure to bind to the mica surface. As such control over the curvature of the tile is an important factor to consider, something which this thesis has explored. The results within this thesis, demonstrate that the curvature such as Marchi et al. could be changed, by folding the origami under increased Mg^{2+} concentrations. Surface based methods for assembling 2D arrays at present lack a degree of control of how tiles bind, due to the non-specific nature of base stacking interactions. Surface orientation as well as mobility can be modulated with cationic concentration species, allowing for increased yield over functional groups on origami.

The issue of origami functionalisation has not been explored into too much detail in the literature to date. Of interest is the effect that functional groups have on the underlying twist of the crossover spacings, such that they may not be truly representative of the designed spacing. The work of Li et al. theorised that hairpin loops exert electrostatic repulsions across the surface of origami, causing it to curve. It did not however consider the potential changes in strain that may be associated at the point where the DNA protrudes from the surface. This also raises the question of the effect on the structure of

origami if all staples are used as a means for surface modification, independent of whether or not the protrusions are nucleic acid based or not.

The recent review by Ramakrishnan et al. discusses the main areas of origami applications, which include biophysical and biochemical, biomedical and material science applications [137]. This review details the various types of buffers used to study how the origami structure is affected, highlighting how one of the aims is to develop method to preserve the origami structure under in vivo environments. To this end, the application of material sciences represents the best case scenario for DNA origami, due to its ability to place functional groups with nanometre precision. The results of the Ba^{2+} work in this thesis add to this plethora of studied environments, expanding the potential buffers that lead allow origami to fold. One of the main objectives of this work however, was the results on the effect that Ba^{2+} has on the origami structure itself, rather than other methods which have focused on a more general view of assessing origami structure. This highlights the need for increased detailed analysis on the effects of buffers on DNA origami, especially where the structure of origami is of up most importance. The need for better analytical methods when examining the structure of DNA origami is important for its survival in the future, to prevent it from remaining a curiosity.

10 Appendix

10.1 **10.33 staples**

11[152]13[151]	AGCTATATTTAGCAAAATTAAGCAGATTCAAA
7[120]9[119]	ATAGTAAGTCCCCCTCAAATGCTTAGATTAAG
10[199]9[215]	TACCTTTTCCAACAGGTCAGGATCATTAAA
5[184]7[183]	AGATGGTTTTATGCGATTTTAAGAAAATAGCG
15[280]17[279]	ACGCGCCTATTGAGAATCGCCATACGAGAAAA
4[263]2[264]	TATTCTGGGGTTGATATAAGTAAGGTTTAG
1[184]3[183]	GTCGCTGAGGGATCGTCACCCTCATTGTATCA
19[280]21[279]	ACCTGAGCAAAGAAATTGCGTAGACGTTATTA
23[120]25[119]	CCGTAAAGCGCGCTTAATGCGCCGAAGGGATT
8[263]6[264]	CGCCACCTCAGACGATTGGCCTGCCAGAAT
14[199]13[215]	ATAAATTATGATATTCAACCGTCTTGCGGG
17[280]19[279]	CTTTTTCAGATTAAGACGCTGAGATTTCAATT
11[184]13[183]	AAGGTGGCATCCAATAAATCATACTCAAATCA
25[248]24[264]	CATCACTTGCCTGAGTAGAAGAAGTAATAAA
9[248]11[247]	TTTGGGAAACATTCAACCGATTGATACCGAAG
6[231]4[232]	GTAAGCGCTGGTAATAAGTTTTAGAGGCTG
9[216]10[200]	GGTGAATTTATTGACGGAAATTATTTAGAGAG
16[327]14[328]	CTTACCAAAAAATAATATCCCAAGAACAAG
16[295]14[296]	GGGCTTAGTTTATCAACAATAGAGGAATCA
23[152]25[151]	AGCCCCCGCGGTCACGCTGCGCGTATCCTGAG
20[71]18[72]	TTTGCGTTTTTCAAGCTTGCATGCCTAACGACGG
14[135]12[136]	CCTGAGAGTAATGTGTAGGTAAAATAAAGCC
21[280]23[279]	ATTTTAAATTGAGGAAGGTTATCTAAACATCG
13[216]14[200]	AGGTTTTGTTAGCGAACCTCCCGATCTAGCTG
20[199]19[215]	CCTGGGGAGCCGGAAGCATAAAAACGGATT
18[231]16[232]	GACTACCACTATATGTAAATGCGGCATTTT
12[199]11[215]	CATTAACATCAATTCTACTAATGCAAGAAA
15[216]16[200]	ACAAAAGGGTAATAAGAGAATATAATCAAAAA
8[231]6[232]	ACCACCCGCCGCCAGCATTGACCCGTTCCA
21[152]23[151]	AGCAAGCGGATAGGGTTGAGTGTTCTAAAGGG
4[231]2[232]	AGACTCCCTCAGTACCAGGCGGCCCTCAGA
13[312]15[311]	GAGCCTAATTTTTATTTTCATCGTATAAGTCC
22[71]20[72]	ATCAGGGTTTTATTGGGCGCCAGGGTAGAGGCGG
19[312]21[311]	TCAAGAAATATCAAAATTATTTGCATCATTTT
10[359]8[360]	CAACATAGCGACAGAATCAAGTATCGGCAT
22[231]20[232]	CCGTCAAGACTTTACAAACAATTAACAGTA
22[295]20[296]	AAAGGAAAGTTTGAGTAACATTACGTAAAA
23[312]25[311]	AAGATAAATCTGAAATGGATTATTGAACAATA
19[216]20[200]	CGCCTGATCATCGGGAGAAACAATGTGTAAAG
15[312]17[311]	TGAACAAGGTATAAAGCCAACGCTATTTCATC
10[263]8[264]	AAGGGCGTTAGAGCCAGCAAAACTCAGAGC
25[280]24[296]	ATCGGCCTTGCTGGTAATATCCATACATTGG
13[344]15[343]	CCATATTAAGTACCGCACTCATCGTCCTAATT
16[231]14[232]	CGAGCCATAAAGTAATTCTGTCAGAACGCG
21[184]23[183]	GGCGAAAAAAATCCCTTATAAATCGGGAAAGC
5[248]7[247]	CAGTGCCTGCAGTCTCTGAATTTAAGGAGGTT
1[248]3[247]	TACCGTAAACCCTCAGAACCGCCAATAAGTGC
13[280]15[279]	AATCTTACGCCCAATAGCAAGCAAAATGCAGA
23[88]25[87]	CACCCAAATATGGTTGCTTTGACGAATCAGAGCG
17[184]19[183]	GCGCCATTGGCGATCGGTGCGGGCTTCCACAC

11[248]13[247] CCCTTTTTTATCAGAGAGATAACCATTAGTTG
13[152]15[151] AGGGTGAGTCTACAAAGGCTATCATTTGTTAA
14[71]12[72] CATATGTTTTTTTTATTTCAACGCAATTTGCGGG
0[199]1[183] TCTGTATGGGATTTTGCTAAACATATATTCG
7[88]9[87] AGATACATACGAGAATGACCATAAATAGTCAG
14[295]12[296] TTACCGCCAACGCTAACGAGCGATTAACTG
2[71]0[62] GTAATGCTTTTCTTTAATTGTATCGGGGCTCCAAAAGGAGCTT
4[135]2[136] CCAACTTGACCCCCAGCGATTACAACGGCT
15[152]17[151] AATTCGCAACATTAAATGTGAGCGGCTTTCCG
0[167]1[151] CAGTTTCAGCGGAGTGAGAATAGATGACAAC
21[344]23[343] ATTATCATACCTCAAATATCAAACTCAGTATT
14[167]12[168] TGAGAGAAAAGGCCGGAGACAGAGGCAAGG
17[152]19[151] GCACCGCTCCAGCTGGCGAAAGGGTTTCCTGT
1[216]2[200] TCAGGGATCCCTCAGAGCCACCACAAAGGCCG
5[216]6[200] GGAGTGTATCATACATGGCTTTTGTCATTGTG
6[103]4[104] CATTATTCCAAATCAACGTAACAACGGTGT
24[263]22[264] AGGGACAGAACTGATAGCCCTAAAAATATC
15[184]17[183] ATTTTTTACGTCTGGCCTTCCTGTCAGGCAAA
25[62]24[72] TTCTTTCCTCGTTAGAGCACGTA
2[199]1[215] CTTTTGCGGCTTGCAGGGAGTTCCTCATTT
24[135]22[136] CACCCGCCACTAAATCGGAACCGTTCCAGT
2[103]0[104] TGAGGAACGAGGTGAATTTCTTATTTTTTC
1[88]3[87] CTTGCTTTGTTTCCATTAAACGGGAACCTAAA
22[359]20[360] TTGCTGACATATTCCTGATTATTTGTTTGG
2[231]0[232] ACCGCCAAGCAAGCCCAATAGGAAAGTTTT
9[120]11[119] AGGAAGCCATGCTGTAGCTCAACAACCATTAG
14[103]12[104] TGAACGGAACCCTCATATATTTTGTACCAA
8[103]6[104] TCAGAAAAACGCCAAAAGGAATCGGAACAA
11[344]13[343] ATGATTAATTACAGAGAGAATAACATAAACAG
16[199]15[215] TAATTCGACCAATAGGAACGCCAAGTACCG
6[167]4[168] ATTATACGAACGAGTAGTAAATACGAGGCG
25[120]24[136] TTAGACAGGAACGGTACGCCAGAAACCACCA
4[103]2[104] ACAGACCGGCAAAAGAATACACCTTTTTCA
13[120]15[119] ATGCCTGAGTCTGGAGCAAACAAGAAGCAAAT
17[312]19[311] TTCTGACCTTAGAATCCTTGAAAAAACAAACA
6[199]5[215] AATTACCTAATTTCAACTTTAAATGATACA
24[231]22[232] TTCTGACATTTTTGAATGGCTAGATTAGAG
12[263]10[264] GCGCTAAAAGAAAAGTAAGCAGAAAGACAA
3[120]5[119] TCATCTTTTGAAAGAGGACAGATGAAAGCTGC
10[295]8[288] AATTCATTACCATTAGCAAGGCCGGAACCAGAGCCAC
2[263]0[264] TACCGCCCACTGAGTTTCGTCACAGACAGC
18[359]16[360] CTTGCTTGATAAATAAGGCGTTAGAAAAAG
18[263]16[264] TAGTGAAGCAAGACAAAGAACGTTTAACAA
8[71]6[72] TCAGGTCTTTTGGAATACCACATTCAATCAGTTG
5[152]7[151] AAACACCACAGTCAGGACGTTGGGACCCTCGT
9[184]11[183] AAGCAAACAATTGCTCCTTTTGATGAGCTGAA
11[216]12[200] CAATGAAAAAGCCCAATAATAAGAAGTAGTAG
1[152]3[151] AACCATCGATCGGAACGAGGGTAGTACCAAGC
24[103]22[104] CGCGTACTCAAGTTTTTTGGGGAGAACGTG
24[327]22[328] TCAATCGACAGAGGTGAGGCGGCCTCAATC
25[216]24[232] GTTGTAGCAATACTTCTTTGATTTAGAACCC
3[280]5[279] AATAGGTGTTTTCCCCCTGCCTATTTCGGTATAAAC
21[248]23[247] TCGTATTAGCACTAACAACTAATATTAGTCTT
19[152]21[151] GTGAAATTGCGTTGCGCTCACTGCAGAGTTGC
7[152]9[151] TTACCAGATACTGCGGAATCGTCAATCGCGTT
8[327]9[311] CATCTTTTCATAATCAAAATCACCGGAAACG

12[231]10[232] TTGAGTTTAGCAATAGCTATCTGGGAGGGA
3[152]5[151] GCGAAACATCAATCATAAGGGAACCTGACGAG
21[120]23[119] GCCCTTCAAAGAGTCCACTATTAATCGAGGTG
22[103]20[104] GACTCCAAGTGAGACGGGCAACGCTGCATT
16[71]14[72] GTAGATGTTTTACCCCGGTTGATAATATGTCAAT
11[280]13[279] ACAAAGTTTGAACAAAGTCAGAGGTTATCCTG
19[184]21[183] AACATACGTGCCTAATGAGTGAGCCCCCAGCA
22[263]20[264] TTTAGGAAATCCTTTGCCCGAATTTTCAGG
18[71]16[72] CCAGTGCTTTTGGCGCATCGTAACCGACGTTGGT
1[280]3[279] AACTACAATTTTTATCACCGTACTCAGGTAGCCCGG
14[231]12[232] AGGCGTTAAGCCTTAAATCAAGCACAAGAA
6[71]4[72] AGATTTATTTTGTAATCTTGACAAGATGACCTTC
18[199]17[215] TGGGAAGCGCCATTCAGGCTGCTAGGTTGG
4[167]2[168] CAGACGGAAGTACAACGGAGATGCAGCGAA
19[88]21[87] ACTCTAGACGGCCAACGCGCGGGGGGTTTTTC
0[263]1[247] CCTCATAGTTAGCGTAACGATCTAACCCATG
18[103]16[104] TTTTCCCAGGGGACGACGACAGAAACGGCG
5[280]7[279] AGTTAATGTTTTATAAATCCTCATTAAATGATATTC
3[184]5[183] TCGCCTGAATGTTACTTAGCCGGATGGGCTTG
1[120]3[119] TGATACCGCTTTGAGGACTAAAGATAAAACAC
0[135]1[119] AACTAAAGGAATTGCGAATAATAAAACAGCT
17[216]18[200] GTTATATATTTTTAACCTCCGGCTGCAACTGT
0[231]0[200] GTCGTCTTTCCAGACGTTAGTAAATGAATTT
4[71]2[72] ATCAAGATTTTCACTACGAAGGCACCTAAAATAC
20[263]18[264] TTTAACGGAGGCGAATTATTCAAGAGTCAA
17[248]19[247] ATCCAATCTTTATCAAAATCATAGGTTACAAA
7[280]9[279] ACAAACAACACCGGAACCGCCTCCTCACCAGT
16[359]14[360] CCTGTTTTGTAGAAACCAATCAACGGGTAT
5[88]7[87] TTCATTACACAGGTAGAAAGATTCACTAATGC
24[199]23[215] AGCGAAAGTGGCGAGAAAGGAAACGTGGCA
9[152]11[151] TTAATTCGCGGATGGCTTAGAGCTACCTGTTT
8[385]9[375] TTACTGTAGCGCGTTTTCTTGCCTTT
8[135]6[136] CATTGAAAGCAACACTATCATAAAGAAAAA
20[135]18[136] CAGTCGGTCATGGTCATAGCTGGGATGTGC
3[216]4[200] GGGTTTTGTCAAGAGAAGGATTAGTCCGCGAC
16[103]14[104] GATTGACACAGGAAGATTGTATAGAATCGA
13[376]15[375] CGATTTTTTTTTCCTTATCATTCCAAGAATAATCGG
2[135]0[136] ACAGAGGATAGTTGCGCCGACAAAAGGAAC
22[135]20[136] TTGGAACCCGCCTGGCCCTGAGCCGCTTTC
9[344]11[343] AATCAGTATAAAAGAAACGCAAAGGAACTGGC
15[376]17[375] CTGTCTTTTTTTCGGAATCATAATTACTAAATAAGA
3[248]5[247] CGTCGAGAAAACATGAAAGTATTAAACGGGGT
15[120]17[119] ATTTAAATGATTCTCCGTGGGAACTATCGGCC
14[263]12[264] TAGAAGGCACCCAGCTACAATTGTAATTGA
17[344]19[343] GACCGTGTCTGTAAATCGTCGCTATTTAACAA
22[199]21[215] ATCGGCATCCTGTTTGATGGTGGGATTTAG
13[88]15[87] ATTTTTAGTAATCGTAAAACTAGCCAGAAAAG
8[359]9[343] TTTCGGTCATAGCCCCCTTATTAAGCACCGT
12[359]10[360] GCAGCCTGACTCCTTATTACGCAAAGGTGG
15[88]17[87] CCCCAAAACGTAATGGGATAGGTCTGCATCTG
16[263]14[264] CGCCAACACAACATGTTCAGCTATCAGATA
14[359]12[360] TAAACCATTTATCCCAATCCAATGAAAATA
19[344]21[343] TTTCATTTTTCTGAATAATGGAAGGGAGCGGA
20[295]18[296] CAGAAATAAAAGAAGATGATGACATAGCGA
21[216]22[200] AAGTATTATAGATAATACATTTGAGTTCCGAA
24[71]22[72] TAACGTGTTTTCGATGGCCCACTACACCGTCT

9[88]11[87] AAGCAAAGACTAAAGTACGGTGTCCCCAATTC
25[312]24[328] TTACCGCCAGCCATTGCAACAGGTTTGACGC
9[376]11[375] AGCGTCAGTTTTTAGAAAATACATACATAGTATGTT
25[152]24[168] AAGTGTTTTTATAATCAGTGAGGCGCTGGCA
6[263]4[264] GGAAAGCTGAGTAACAGTGCCCGAACCTAT
18[135]16[136] TGCAAGGATCGCACTCCAGCCAAGTAACAA
23[344]22[360] AACACCGCCTGCAACAGTGCCACGCATCACC
10[71]8[72] TCATTCCTTTTTTTACCCTGACTATTATCAAAAA
21[88]23[87] TTTTCACCACGTCAAAGGGCGAAAAGTGAACCAT
20[231]18[232] CCTTTTATGCTTTGAATACCAAGTCTGAGA
11[376]13[375] AGCAAACGTTTTTGTTTAACGTCAAAAAATAAGAAA
17[376]19[375] ATAAACACTTTTAATCAATATATGTGAGATGGAAAC
20[359]18[360] ATTATACGAATTACCTTTTTTATGAATAAC
11[120]13[119] ATACATTTATAAAGCTAAATCGGTTAAATGCA
15[248]17[247] GACAATAAATGTAATTTAGGCAGATGATGCAA
23[280]25[279] CCATTAAAACCAGTCACACGACCACTCAAACT
23[184]25[183] CGGCGAACGGAGCGGGCGCTAGGGCCACCGAG
8[167]6[168] CGTCCAACGACGATAAAAACCAACTGGCTC
23[216]24[200] CAGACAATCTGAAAGCGTAAGAATGGGAAGAA
3[88]5[87] ACGAAAGAAGGCGCATAGGCTGGCACCGGATA
10[167]8[168] ATTTTTGAGCTTCAAAGCGAACCTGGATAG
20[103]18[104] AATGAATGGATCCCCGGGTACCCGCCAGGG
7[184]9[183] AGAGGCTTTAGTAAAATGTTTAGACAGACCGG
25[88]24[104] GGAGCTAAACAGGAGGCCGATTACTACAGGG
21[312]23[311] GCGGAACAGGTCAGTTGGCAAATCACCAGCAG
25[184]25[215] TAAAAGAGTCTGTCCATCACGCAAATTAACC
10[231]8[232] AGGTAAAATCACCGTCACCGACTCAGAGCC
17[88]19[87] CCAGTTTGAGTCACGACGTTGTAAGCAGGTCG
18[295]16[296] TAGCTTAAATATATTTTAGTTACAACAGTA
12[71]10[72] AGAAGCCTTTTATATAACAGTTGATTTGGAAGTT
11[312]13[311] CAATAATACGCATTAGACGGGAGATCTTTCCA
2[167]0[168] AGACAGCCCCACGCATAACCGAACTTTCAA
9[312]11[311] TCACCAATTTTATTTTGTCACAATAGGAAACG
8[199]7[215] GGGGTAATTGCAAAAGAAGTTTAACCACCA
20[167]18[168] ATTAATTGTTATCCGCTCACAACTCTTCGC
5[120]7[119] TCATTCAGTAATAAAACGAACTAATACGAGGC
10[103]8[104] ATATGCACGGATTGCATCAAAATAAACAGT
18[167]16[168] TATTACGTCTGGTGCCGGAAACAGCCAGCT
12[327]10[328] AGGGAAGACGGAATACCCAAAAACACCACG
10[327]8[328] GAATAAGGAAACCATCGATAGCGCGTTTGC
24[350]25[350] TTGAAATACCTACATAAAAACGCTCATGTT
7[216]8[200] CCAGAGCCTCAGAGCCGCCACCAGTGCCAGAG
22[167]20[168] AGCCCGAGTCCACGCTGGTTTGTAACTCAC
6[135]4[136] TCTACGTTGAATAAGGCTTGCCCGAACTGA
12[295]10[296] AACACCCACCAGAAGGAAACCGCAATAGAA
10[135]8[136] GAATATACGAAAGACTTCAAATTAAATATT
23[248]25[247] TAATGCGCTTCTGGCCAACAGAGAAGTAATAA
13[248]15[247] CTATTTTGCTTATCCGGTATTCTACAGACGAC
0[289]1[279] TTCGCCTGTAGCATTCCACCAGTACA
11[88]13[87] TGCGAACGATGACCCTGTAATACTGGATAAAA
19[248]21[247] ATCGCGCATCAGATGAATATACAGTCGACAAC
0[103]1[87] ACGTTGAAAATCTCCAAAAAAAATTTATCAG
12[103]10[104] AAACATTAGTAGATTTAGTTTGTGTTTTAA
19[120]21[119] ATTCGTAAGAAACCTGTCGTGCCAAGCTGATT
16[167]14[168] TTCATCATTAAATTTTTGTTAAGCTATTTT
22[327]20[328] AATATCTAAGAAACCACCAGAAGGTTAGAA

16[135]14[136]	CCCGTCGTGTAAACGTTAATATGGTCATTG
13[184]15[183]	CCATCAATAATGCCGGAGAGGGTAATCAGCTC
4[199]3[215]	CTGCTCCTAAATTGTGTCGAAAGATTAGCG
18[327]16[328]	TTTTCCCTAAATTTAATGGTTTTACAAATT
19[376]21[375]	AGTACATATTTTATCAATATAATCCTGACAGATGAT
17[120]19[119]	TCAGGAAGCGATTAAGTTGGGTAAGAGCTCGA
12[135]10[136]	TCAGAGCCGCAAATGGTCAATATAATTGCT
24[167]22[168]	AGTGTAGATTTAGAGCTTGACGAAAAGAAT
20[327]18[328]	CCTACCAACAAAATTAATTACATTAATTAA
15[344]17[343]	TACGAGCAAGTATCATATGCGTTAGAAATACC
14[327]12[328]	CAAGCCGTTTGCCAGTTACAAAATAAAAAC
24[295]22[296]	CAGATTCAATACCGAACGAACCAACAGTTG
9[280]11[279]	AGCACCATATGGTTTACCAGCGCCATAGCCGA
12[167]10[168]	CAAAGAATTTCATTTGGGGCGCAAGAGGTC
21[376]23[385]	GGCAATTCTTTTAAATGAAAAATCTAAAGCTGAGAGCCAGCAGCTT
7[248]9[247]	GAGGCAGGCTCAGAACCGCCACCCTTGAGCCA

10.2 **10.50 staples**

7[248]9[247]	CACCCTCAGTTTGCCATCTTTTCACATTCA
21[376]23[385]	CGTTATTATTTTATCGCCATTAAAAATTGATAGCCCTAAAACTT
4[71]2[72]	AAAGAGGATTTTGAGGACTAAAGACTTTCGGCTACA
17[312]19[311]	GGTTATATTTTGAATTACCTTTTCAATAAC
22[327]20[328]	CGGTCAGTGAAGTATTAGACTTTAACCAGAAG
9[344]11[343]	AGCAAAATAAAGAACTGGCATGATTTTTAAGA
2[199]1[215]	ACCATCGCATAGTTGCGCCGACAAACTCAGGA
21[152]23[151]	TGCAGCAAAGATAGGGTTGAGTGTAAGGGAGC
2[103]0[104]	CAGCATCAAAATCTCCAAAAAAACAACTTT
20[359]18[360]	ATCATTTTCGCAGAGGCGAATTATATGAAACA
18[263]16[264]	AACCTTGCATTTATCAAAATCATAGAAAAAGC
24[71]22[72]	GCTTTCCTTTTTGATGGCCCACTACGTACCGTCT
20[295]18[296]	AGATGATGTTTACATCGGGAGAAATTAATGGA
13[120]15[119]	TTAGAACCAGGCTATCAGGTCATTCCCAAAAA
20[167]18[168]	AACTCACTGTGAAATTGTTATCGATCGGTG
19[152]21[151]	GTTTCCTGATTAATTGCGTTGCGCGAGAGAGT
21[88]23[87]	TTTCTTTTACGTCAAAGGGCGAAAAGAACCATCA
1[216]2[200]	GGTTTAGTATAGGTGTATCACCGTTGACAACA
17[152]19[151]	CCAGCCAGCTTCGCTATTACGCCATCATAGCT
14[71]12[72]	TAATCGTATTTTACCCTGTAATACTTTTTACCAAAA
11[152]13[151]	GATACATTTCCAATAAATCATACAGCAATGCC
3[280]5[279]	GATTAGCGTTTTCAGGAGTGTACTGGTAATGGCTTT
19[376]21[375]	AATTACCTTTTTATTTTAAAAGTTTGAGCCCGAA
25[62]24[72]	TTCGTTAGAATCAGAGCATAACGT
18[327]16[328]	CAATTTCAAACTATATGTAAATGCAAATACCG
10[135]8[136]	AGGTCATTAAGCAAAGCGGATTGCAAATGTTT
14[263]12[264]	CAAGTACCGGTATTCTAAGAACGCCAGCCTTT
15[344]17[343]	ATAAACAATAAATTTAATGGTTTGTGATGCAA
22[71]20[72]	ATCAGGGCTTTTTGCGTATTGGGCGCCAGCGGGGAG
21[120]23[119]	GATTGCCCAAGAGTCCACTATTAAGAGGTGCC
18[167]16[168]	CGGGCCTCTTTCCGGCACCGCTTCGCGTCT
20[263]18[264]	TGTTTGGATAACGTCAGATGAATAGAGTGAAT
20[199]19[215]	GTGTAAAGCAACATACGAGCCGGAATTTGCAC
19[248]21[247]	TTCAGGTTTTATACTTCTGAATAAGGTTAT

17[376]19[375] CTTTTTCATTTTGAGCAAAAGAAGATGTCATTTC
19[280]21[279] CAGTACCTGCAATTCATCAATATACAACTAAT
10[231]8[232] TTGTCACACAAAGACAAAAGGGCGATAATCAA
25[120]24[136] GAACGGTACGCCAGAATCCTGAGACCACACCC
23[88]25[87] CCCAAATCTGCTTTGACGAGCACGTGGGAGCTAA
10[359]8[360] AATACCCACACCAGTAGCACCATTGAAACCAT
20[135]18[136] CGCTTTCCGAATTCGTAATCATGGGCTGGCGA
4[231]2[232] CGTATAAATTATTCTGAAACATGAATAAGTAT
1[248]3[247] CCTCAGAAGTCGAGAGGGTTGATAAGTATT
12[71]10[72] ACATTATGTTTTGCAACTAAAGTACGGTAACATGTT
20[103]18[104] TGCATTACGACTCTAGAGGATCTAAGTTGG
3[152]5[151] GAGGCAAATGTCGAAATCCGCGACTTACCCAA
7[280]9[279] CCAGAACCTCGGCATTTTCGGTCATATTGACG
15[88]17[87] CCCCGGTTAACAAACGGCGGATTGGGGCGCAT
24[231]22[232] CCTACATTCATTGGCAGATTCACCAAATATCA
13[280]15[279] TTAGCGAATCATTCCAAGAACGGGATTTTCGA
0[167]1[151] TTTTGTCGTCTTTCCAGACGTTATTTATCAG
2[167]0[168] CGCTGAGCGAGGTGAATTTCTTATCTAAAG
6[167]4[168] CAACTTTAACAAAGCTGCTCATTCGCCTGA
9[184]11[183] TCGCGTTTGCAAACTCCAACAGGTAACCTGTT
13[184]15[183] TGAGAAAGATTCAACCGTTCTAGCTTCGCATT
8[359]9[343] CGATAGCAGCACCGTAATCAGTAGTTAGAGCC
6[231]4[232] CCTTGATAAATGGAAAGCGCAGTCACAGTGCC
10[263]8[264] AAACGCAAAGGGAGGGAAGGTAAATAGCCCCC
21[248]23[247] CTAAAATAACCTTGCTGAACCTCAGTCACA
6[103]4[104] ACGTTGGCTGGCTGACCTTCATAGACGGTC
5[216]6[200] AAAGCCAGTTCACAAACAAATAAACCAGAACG
12[199]11[215] AAGGTGGCTTTTCATTTGGGGCGCCACCCTGA
25[216]24[232] TACTTCTTTGATTAGTAATAACATTGGAAATA
15[312]17[311] AAAGGTAAATAAATAAGGCGTTATAGGTTG
15[216]16[200] GCTTAATTATAAAGCCAACGCTCATTTTAACC
17[280]19[279] AGACTACCATAAATCAATATATGTTACAGTAA
11[312]13[311] CAATAGCTATCCAAATAAGAAACAGGTTTT
22[295]20[296] CACGCTGAGCCGTCAATAGATAATTGATTATC
8[103]6[104] CATAAATTCAGTTGAGATTTAGCAGTCAGG
18[295]16[296] AACAGTACTTTTTAACCTCCGGCTAATAAGAA
2[263]0[264] TAAGTGCCCCGCCACCCTCAGAGCATAGGAAC
23[248]25[247] CGACCAGTCAGGAAAAACGCTCACACTTGC
0[135]1[119] ATTTTCTGTATGGGATTTTGCTAAAAGGCTCC
17[120]19[119] GACGACAGTGTGCTGCAAGGCGATCCCGGGTA
16[231]14[232] TTACCAGTGAGAATCGCCATATTTAAGCAAGC
22[167]20[168] TAGCCCGGCGGTCCACGCTGGTAGTGAGCT
16[295]14[296] TAAACACCTAAGAGAATATAAAGTCGGCTGTC
7[88]9[87] AAGATTCAATTCATTGAATCCCCCTGACCATA
22[103]20[104] GACTCCACACCAGTGAGACGGGGTGCCAGC
4[199]3[215] AAAGTACACAGCGATTATACCAAGCCTATTTC
16[263]14[264] CTGTTTAGTAATTTAGGCAGAGGCTATTAAAC
23[280]22[296] AGAGATAGAACCCTTCTGACCTGAAACAGTGC
1[120]3[119] AAAAGGAGATCGTCACCCTCAGCAATACGTAA
3[216]4[200] GGAACCTACAGTTAATGCCCCCTGCGCGAAAC
24[263]22[264] CATTGCAAAATAAAAGGGACATTCAAAAATCT
16[327]14[328] ACCGTGTGAGTAATTCTGTCCAGAATTTACGA
18[231]16[232] TAATTTTCAGATTAAGACGCTGAGACAAATTC
5[248]7[247] TTACCGTTGTTGAGGCAGGTCAGGAACCGC
23[152]25[151] CCCCGATTACGCTGCGCGTAACCAAGTGTTTT
24[103]22[104] CTATGGTAAGTTTTTTGGGGTCAGAACGTG

16[135]14[136] AAATGTGATTGTATAAGCAAATATTTTGAGAG
6[71]4[72] CGAACTAATTTTCAGATGAACGGTGTACCAACTTTG
16[167]14[168] GGCCTTCAATATTTTGTTAAAATGATAAAT
17[248]19[247] AATAGTGATTCTGTAAATCGTCGGTAGATT
8[135]6[136] AGACTGGATAATGCAGATACATAACTTATGCG
8[263]6[264] TTATTAGCGAGCCACCACCCTCAGCCAGCATT
19[312]21[311] GGATTCGCTTATCATCATATTCCACATTTG
3[184]5[183] TTGACCCCACGGAGATTTGTATCATCAGTGAA
16[103]14[104] CCGTGGGGATAATCAGAAAAGCGCCTGAGA
15[248]17[247] CCAACATGTATCATATGCGTTATAAGAGTC
4[167]2[168] TAAATTGAGAATACACTAAAACTATTCGGT
8[231]6[232] AATCACCGAGAGCCGCCACCCTCAACGATTGG
9[376]11[375] GCAAGGCCTTTTCCGAGGAAACGCAATGTTACCA
10[167]8[168] GAGAGTAGGAAGCCCGAAAGACAAAAGAAG
15[280]17[279] GCCAGTAAGGAATCATAATTACTAGGTCTGAG
17[216]18[200] GATAGCTTCCTTAGAATCCTTGAAGCCATTCA
19[344]21[343] CAAAATCGGCGGAACAAAGAAACCCAAACAAT
25[152]24[168] TATAATCAGTGAGGCCACCGAGTGCAAGTGT
8[385]9[375] TTGGAAACGTCACCAATACCATTA
18[135]16[136] AAGGGGGATATCGGCCTCAGGAAGTCAACATT
0[289]1[279] TTAGGGATAGCAAGCCCACACCACCC
25[88]24[104] ACAGGAGGCCGATTAAAGGGATTGGCGCGTA
11[344]13[343] AAAGTAAGTTACAAAATAAACAGCCTATTTTG
15[184]17[183] AAATTTTTCGCCATCAAAAATAATTCTGGTGC
23[312]22[328] AGAATACGTGGCACAGACAATATTAGGTGAGG
23[184]25[183] CGAACGTGGGGCGCTAGGGCGCTGAAAAGAGT
23[120]25[119] GTAAAGCATAATGCGCCGCTACAGTTAGACAG
21[312]23[311] AGGATTTAATTAACACCGCCTGCAAGCGTA
9[312]11[311] TCACCGACGCAGTATGTTAGCAAGAAATAG
6[263]4[264] GACAGGAGCCAGTAAGCGTCATACATAAGTTT
11[248]13[247] CAGAGAGAAATAACATAAAAACAATAGAAG
24[167]22[168] AGCGGTCTAGAGCTTGACGGGGCAAAAGAA
10[199]9[215] GACCGGAATAATTCGAGCTTCAAATATGGTTT
13[248]15[247] GCTTATCCGCACTCATCGAGAACAACAACG
14[359]12[360] CAAGAAAATACAATTTTATCCTGAGAGCCTAA
10[327]8[328] CTTATTACTTGAGCCATTTGGGAACGACAGAA
21[280]23[279] AGATTAGAGAGCCAGCAGCAAATGTGGCCAAC
15[152]17[151] TAAACGTTCTGTAGCCAGCTTTCAATCGCACT
10[295]8[288] AATACATATCATTAAAGGTGAATTCTGTAGCGCGTTTTCA
5[120]7[119] ATCTTGACAACTGGCTCATTATACGAATACCA
20[231]18[232] GTTAGAACGAAATAAAGAAATTGCCTATTAAT
17[184]19[183] CGGAAACCAACTGTTGGGAAGGGCCGCTCACA
19[88]21[87] CTGCAGGTATGAATCGGCCAACGCGGGTGGTT
9[216]10[200] ACCAGCGCATCAATAGAAAATTCAGCGAACCA
11[376]13[375] GAAGGAAATTTTACGAGCGTCTTTCCAATCTTAC
14[167]12[168] TAATGCCGTGTAGGTAAAGATTGTAGTAGC
16[359]14[360] TTCTGACCCATGTTCAGCTAATGCGTCCTGAA
22[199]21[215] AAATCGGCAAATCCTGTTTGATGGTTGGCAAA
22[263]20[264] AAAGCATCTCTTTAGGAGCACTAAATCCTGAT
11[216]12[200] ACAAAGTCGGGAGAATTAACTGAAGAGCTGAA
22[135]20[136] TTTGGAACTTCACCGCCTGGCCCTTCACTGCC
14[231]12[232] CGTTTTTAAGCAAGCAAATCAGATGGGAAGCG
19[184]21[183] ATTCCACACCTGGGGTGCCTAATGTTGCCCCA
21[216]22[200] TCAACAGTATCAATATCTGGTCAGTGGTTCCG
8[167]6[168] TTTTGCCGAGGCATAGTAAGAGTTTAATTT
1[280]3[279] TCATTTTCTTTTGGGTTTTGCTCAGTACAGGATTAG

12[295]10[296] GTTTAACGAAGAGCAAGAAACAATACGTAGAA
3[248]5[247] AAGAGGCTTCAGTGCCTTGAGTATCTGAAT
11[88]13[87] GTTTCATTAAAGCTAAATCGGTTGGCGGGAGA
15[376]17[375] GCCTGTTTTTTTAATATATTTTAGTTAGAGAAAA
20[327]18[328] GAGCGGAACTGATTGCTTTGAATAACATTTAA
4[103]2[104] AATCATACATTAAACGGGTAAAGCGAAAGA
7[184]9[183] TCATAACCAGCGAGAGGCTTTTGCTTCAAATA
25[184]25[215] CTGTCCATCACGCAAATTAACCGTTGTAGCAA
24[135]22[136] GCCGCGCTCTAAATCGGAACCCTATGTTCCAG
20[71]18[72] AGGCGGTTTTTTACGGCCAGTGCCAAGCACGACGTT
8[327]9[311] TCAAGTTTGCCTTTAGCGTCAGAATCACCG
9[120]11[119] ATAGTCAGTTTGCGGATGGCTTAGTTCCCAAT
14[199]13[215] AATATGATGCCGGAGACAGTCAAACATTACCG
9[248]11[247] ACCGATTGAGACACCACGGAATACTAATAT
11[184]13[183] TAGCTATAATCAATTCTACTAATACAAAAGGG
21[184]23[183] GCAGGCGAAAAATCCCTTATAAATAAAGCCGG
1[88]3[87] TCACGTTGGGAACGAGGGTAGCAATTCATGAG
13[216]14[200] CGCCCAATTTTTCATCGTAGGAATTCACCATC
11[280]13[279] CCAATAATTCAAAAATGAAAATAGGAGGCGTT
4[263]2[264] TAACGGGGGAGACTCCTCAAGAGACAGGCGGA
14[135]12[136] ATCTACAACTCATATATTTTAAATGGCAAGGC
2[71]0[62] GAGGCTTTTTTTAAGGAATTGCGAATAATAGAAAGGAACAACTATT
8[71]6[72] TTTAAACATTTTCGGAACAACATTATTATAATAAAA
18[359]16[360] AACATCAAGCAAGACAAAGAACGCATTTCATC
5[184]7[183] TAAGGCTTATTGGGCTTGAGATGGCAACACTA
13[88]15[87] AGCCTTTAGCAAACAAGAGAATCGCATATGTA
8[199]7[215] ACCAAAATCTCGTTTACCAGACGACGGAACCG
19[120]21[119] CCGAGCTCAGTCGGGAAACCTGTCCAACAGCT
12[359]10[360] TTTGCCAGCAGATAGCCGAACAAAAATAACGG
0[103]1[87] CAACAGTTTCAGCGGAGTGAGAATAATTTTT
12[327]10[328] TTATCCCAATCTTACCGAAGCCCTTAAGACTC
18[103]16[104] GTAACGCTGCATCTGCCAGTTTCGGATTCT
13[312]15[311] GAAGCCTTAAACCAATCAATAATACCGACA
14[295]12[296] TTTCCTTACCTCCCGACTTGCGGGGATTTTTT
3[88]5[87] GAAGTTTCAGGGAACCGAACTGACAGACCAGG
4[135]2[136] TGTTACTTCGAAGGCACCAACCTAAGGCCGCT
9[88]11[87] AATCAAAATATAATGCTGTAGCTCGTCTGGAA
3[120]5[119] TGCCACTAAGCCGGAACGAGGCGCCAAGAGTA
6[135]4[136] ATTTTAAGAAGAACCGGATATTCACTGCTCCA
13[152]15[151] TGAGTAATGGAGAGGGTAGCTATTTTAAATTG
14[103]12[104] GTCTGGATTTCAACGCAAGGATAAAGCCTC
5[152]7[151] ATCAACGTAATCATTGTGAATTACCGCCAAAA
22[359]20[360] AACCACCATCGTATTAAATCCTTTGTAACATT
7[120]9[119] CATTCAACTAGCGTCCAATACTGCTGACTATT
19[216]20[200] GTAAAACACTACCATATCAAAATTAGCATAAA
10[103]8[104] TGCTGAAATCAGGTCTTTACCCGGAATCGT
1[152]3[151] CTTGCTTTGCTTGCAGGGAGTTAAAAACGAAA
16[71]14[72] GGGATAGGTTTTAAACTAGCATGTCAATATGAACGG
16[199]15[215] AATAGGAAGTTAAATCAGCTCATTACAGTAGG
1[184]3[183] TGATACCGCCACGCATAACCGATAACTCATCT
18[71]16[72] GTAAAACGTTTTTCACGTTGGTGTAGATACCGTAAT
24[286]25[287] TCCAGAACAATATTAGGCCTTGCTGGTAATA
23[344]22[360] GCTATTAGTCTTTAATGCGCGAACACCGAACG
12[263]10[264] ACAGAGAGTAACCCACAAGAATTGTATAAAAG
6[199]5[215] AGTAGTAAGCCCTGACGAGAAACATCCTCATT
17[88]19[87] CGTAACCGCAGGGTTTTCCCAGTCTTGCATGC

18[199]17[215]	GGCTGCGCAGGCAAAGCGCCATTCAACATAGC
14[327]12[328]	GCATGTAGAAATCAAGATTAGTTGCATATTAT
11[120]13[119]	TCTGCGAAAGCAAAATTAAGCAATAAAAATTT
15[120]17[119]	CAGGAAGAGCGAGTAACAACCCGTGAGGGGAC
0[263]1[247]	CCATGTACCGTAACACTGAGTTTCCGCCAC
7[216]8[200]	CCTCCCTCGAACCAGAGCCACCACCGATAAAA
22[231]20[232]	AACCCTCATGAAAGGAATTGAGGAATGGAAGG
5[280]7[279]	TGATGATATTTTACCACCAGAGCCGCCGAGCCGCCA
0[199]1[183]	ACAGCCCTCATAGTTAGCGTAACGAAACAGCT
21[344]23[343]	TCGACAACGCAGAAGATAAAACAGTTTGAATG
12[167]10[168]	ATTAACATCGCAAATGGTCAATCAGGATTA
12[135]10[136]	AAAGAATTCGAGTAGATTTAGTTTTTGATAAG
0[231]0[200]	GTACAAACTACAACGCCTGTAGCATTCCACAG
24[199]23[215]	AAAGGAGCGCGAGAAAGGAAGGGATGAAATGG
13[344]15[343]	CACCCAGCATAATATCCCATCCTACGACGACA
12[231]10[232]	CATTAGACAGAGGGTAATTGAGCGAGTTTATT
25[248]24[264]	CTGAGTAGAAGAACTCAAACTATCCCGCCAGC
2[231]0[232]	AGCCCGGAACCGCCACCCTCAGAACGTCACCA
12[103]10[104]	AGAGCATCCATATAACAGTTGAAGCTTAAT
17[344]19[343]	ATCCAATCGAAAACAAAATTAATTCCAAGTTA
7[152]9[151]	GGAATTACAGAGGGGGTAATAGTAATCAAAAA
10[71]8[72]	TTAAATATTTTTGTTCAGAAAACGAGAATCAAATGC
23[216]24[200]	ATTATTTATTGACGCTCAATCGTCAGAAAGCG
2[135]0[136]	TTTGCGGGCCTTTAATTGTATCGGGTAAATGA
13[376]15[375]	CAACGCTATTTTATCAACAATAGATAAAGAACGC
9[152]11[151]	GATTAAGACCTTTAATTGCTCCTTGACCATTA
9[280]11[279]	GAAATTATCATAAAGGTGGCAACAAGTTAAGC
5[88]7[87]	CGCATAGGGAAGAAAAATCTACGTCAGGTAGA

10.3 **10.67 staples**

11[248]13[247]	GCGCATTATCCCAATCCAAATAAGATCGAGAA
10[231]8[232]	TACATACAACACCACGGAATAAGTCGTTTTCA
10[135]8[136]	TACCTTTAAGGTCTTTACCCTGACAAAGAAGT
13[344]15[343]	GAGGCGTTCGACAATAAACAACATATTTAGGC
21[248]23[247]	CTAAAGCACCAGCAGAAGATAAAACAATATTA
5[248]7[247]	ACAAACAACCTCAGAGCCGCCACCATCACCGG
23[88]25[87]	ACCCAAATTTTGACGAGCACGTATGCTAAACA
7[216]8[200]	GTTTGCCATTCGGTCATAGCCCCCAACACTAT
13[152]15[151]	TATATTTTAGCTGATAAATTAATGTTGTATAA
14[71]12[72]	AGAGAATCTTTTGGTTGTACCAAAAACAAGCATAAA
19[280]21[279]	AACCTACCTTTAAAAGTTTGAGTACAAATATC
8[359]9[343]	AATCACCAGTAGCACCATTACCATGACGGAAA
15[312]17[311]	CATATTTACGCGAGAAAACTTTTTAGCTTAGA
14[135]12[136]	GGTAGCTAGGATAAAAATTTTTAGTTAACATC
20[327]18[328]	CGACAACTAAAGAAATTGCGTAGAACAAAATC
22[295]20[296]	TAGCCCTAAATCAATATCTGGTCACCCGAACG
11[88]13[87]	TGCAACTAAGCAATAAAGCCTCAGTTATGACC
21[280]23[279]	AAACCCTCAAACATCGCCATTAAAACGCTCAT
12[135]10[136]	CAATAAATACAGTTGATTCCCAATTTAGAGAG
24[234]22[232]	TTCATCACTTGCTGGTAATATCCAGAACAGAGGTG
10[167]8[168]	GAAGCAAAAAAGCGGATTGCATCAGATAAAAA
22[263]20[264]	ACGAACCATCACCTTGCTGAACCTACATTATC

9[216]10[200] ACGCAAAGTAAAGGTGGCAACATAATATCGCG
24[103]22[104] ATGGTTGCCAAGTTTTTTGGGGTCAAAGAACG
17[312]19[311] TTAAGACGGCGAATTATTCATTTCCACGTAAA
21[88]23[87] TGGTTTTTAACGTCAAAGGGCGAAGAACCATC
10[327]8[328] GAAGGAAAAGGGAAGGTAAATATTTAGCAAGG
19[312]21[311] ACAGAAATCGTATTAAATCCTTTGGTTGGCAA
14[231]12[232] ATCGGCTGACCAAGTACCGCACTCAAACGATT
2[103]0[104] AAAGGCCGAAAGGAACAACTAAAGCTTTCCAG
12[263]10[264] ATTATTTAGACGGGAGAATTAACTAAGACTCC
13[376]15[375] AGGTTTTGTTTTCGACAAAAGGTAAAGTAGAGAATA
12[359]10[360] TATTTTGCATAAGAGCAAGAAACATTTTTAAG
15[88]17[87] CATGTCAAGATTCTCCGTGGGAACCGTTGGTG
21[184]23[183] CCAGCAGGGGCAAAATCCCTTATAAAGCCGGC
18[295]16[296] GAGCAAAATTGAAAACATAGCGATCAAATATA
24[167]22[168] GCGGTCACTAGAGCTTGACGGGGAAATCAAAA
25[88]24[104] GGAGGCCGATTAAAGGGATTTTAGCGCGTACT
11[120]13[119] TCCATATACATACAGGCAAGGCAACTTTATTT
13[216]14[200] GGTATTAATCTTTCCTTATCATTCAAGGCCGG
12[167]10[168] TCAATTCTTTTAGTTTGACCATTACCAGACCG
14[359]12[360] CCAGACGATTAGCGAACCTCCCGATTAGTTGC
11[376]13[375] GCAATAGCTTTTAAGCCTTAAATCAAGACTTGCGGG
16[327]14[328] ACAAAGAAACAACGCCAACATGTAGTTCAGCT
20[199]19[215] GCATAAAGTTCCACACAACATACGTATCAGAT
23[248]22[264] CCGCCAGCCATTGCAACAGGAAAAAATACCGA
8[231]6[232] TCGGCATTTCTTTTCATAATCAAAAGAACCAC
23[280]22[296] GGAAATACCTACATTTTGACGCTCCGAACTGA
0[103]1[87] ACGTTAGTAAATGAATTTTCTGTAAGCGGAGT
16[359]14[360] TATGTAAATTTCGAGCCAGTAATAAATTCTGT
22[167]20[168] GAATAGCCGCAAGCGGTCCACGCTCCTAATGA
2[231]0[232] TGCTCAGTTATAAGTATAGCCCGGAGGGATAG
21[120]23[119] AGCTGATTACAAGAGTCCACTATTGAGGTGCC
11[344]13[343] GCCCAATAACCCAGCTACAATTTTAAGAACGC
5[184]7[183] CCAAATCACTTGCCCTGACGAGAACGCCAAAA
16[295]14[296] TTTTAGTTCAGTAGGGCTTAATTGACAATAGA
18[231]16[232] TTGAATTAATATGTGAGTGAATAAGATAAATA
19[216]20[200] GATGGCAATCATCATATTCCTGATAGCCGGAA
11[152]13[151] CGAGTAGAACTAATAGTAGTAGCAAACCCTCA
7[120]9[119] AAAGATTCAGGGGGTAATAGTAAACCATAAAT
10[359]8[360] AAAAGTAATAAAGGTGAATTATCAGCCAGCAA
17[216]18[200] AAATCAATCCTTTTTTAATGGAAAAAGCGCCA
0[263]1[247] CTCAGAGCCACCACCCTCATTTTCAATAGGTG
1[152]3[151] AAAAAAGGACAACCATCGCCCACGCGGGTAAA
20[263]18[264] ATTTTGCGACTTCTGAATAATGGAACATCAAG
22[231]20[232] AGGCGGTCGAGAGCCAGCAGCAAAAGAAGGAG
6[135]4[136] TTTCAACTATAGGCTGGCTGACCTTGTATCAT
21[344]23[343] CTAAAATAATACGTGGCACAGACAATTCACCA
6[103]4[104] CGATTTTAGAGGACAGATGAACGGCGCGACCT
3[152]5[151] ATACGTAAAAGTACAACGGAGATTTCATCAAG
8[135]6[136] TTTGCCAGATCAGTTGAGATTTAGTGGTTTAA
11[184]13[183] TCGCAAATGGGGCGCGAGCTGAAATAATGTGT
11[280]13[279] TGAACAAAGCCAGTTACAAAATAACGTAGGAA
22[327]20[328] GAATGGCTTTGAAAGGAATTGAGGAAACAATT
14[327]12[328] AATGCAGAGCTTATCCGGTATTCTATCCTGAA
19[152]21[151] TCATAGCTACTCACATTAATTGCGCCCTGAGA
19[376]21[375] CTTTTACATTTTGCCGTCAATAGATAATCAACTAAT
13[184]15[183] AGGTAAAGAAATCACCATCAATATAATATTTT

20[231]18[232] CGGAATTATTCATCAATATAATCCAATTTCAT
23[184]25[183] GAACGTGGGGCGCTAGGGCGCTGGAGTCTGTC
14[167]12[168] ACCGTTCTAAATGCAATGCCTGAGAGGTGGCA
22[359]20[360] GCGTAAGATCTTTAGGAGCACTAAACATTTGA
4[199]3[215] CTCATCTTGAGGCAAAAGAATACAGGGGTCAG
4[135]2[136] CGCCTGATGGAAGTTTCCATTAAACATAACCG
25[62]24[72] TTTAGAATCAGAGCGGGAAACGTGCT
3[120]5[119] TTTCATGAAAATTGTGTCGAAATCTGTACAGA
8[167]6[168] CCAAAATATAATGCAGATACATAAACACCAGA
16[167]14[168] AAATAATTTTAAATTGTAAACGTTGATATTCA
19[344]21[343] TTTAACGTAAGTATTAGACTTTACAAGGTTAT
22[199]21[215] CCGAAATCCGAAAATCCTGTTTGAGCAACAGT
18[199]17[215] TTCGCCATTGCCGGAAACCAGGCACAGTACAT
21[312]23[311] ATCAACAGATTAGTCTTTAATGCGAATCGTCT
17[248]19[247] CTGTAAATATTAATTACATTTAACTGATTGTT
13[120]15[119] CAACGCAATTTTTGAGAGATCTACTGATAATC
11[312]13[311] ATCAGAGAACGCTAACGAGCGTCTAAATCAGA
5[88]7[87] CTTTGAAAAGAACTGGCTCATTATTTAATAAA
0[289]1[279] TTACCGCCACCCTCAGAATACCGCCA
12[295]10[296] CCTAATTTGTCAGAGGGTAATTGAATAACGGA
6[199]5[215] GAATAAGGACGTAACAAAGCTGCTCAGGAGGT
10[263]8[264] TTATTACGAATAGAAAATTCATATATCAAGTT
0[231]0[200] CAAGCCCAATAGGAACCCATGTACCGTAACAC
6[71]4[72] GGACGTTGTTTTTCATAAGGGAACCGAAAGGCGCAG
7[88]9[87] ACGAACTAGCGTCCAATACTGCGGAATGCTTT
14[103]12[104] TCAGGTCACTTTTGCGGGAGAAGCAGAATTAG
3[184]5[183] AAACGAAATGACCCCCAGCGATTATTCATTAC
9[344]11[343] TTATTCATGCAGATAGCCGAACAATGAGTTAA
19[120]21[119] CCCGGGTACTTTCCAGTCGGGAAACGGGCAAC
13[280]15[279] TCATTACCGAACAAGAAAAATAATTAAAGCCA
22[135]20[136] AGTTTGGAGCCCTTCACCGCCTGGTTGCGCTC
15[152]17[151] GCAAATATCGCGTCTGGCCTTCCTGGCCTCAG
4[167]2[168] GCGAAACATGCCACTACGAAGGCATGCGCCGA
16[199]15[215] GCTCATTTTCGCATTAAATTTTTGGGAATCAT
22[71]20[72] TATCAGGGTTTTCGGTTTGCGTATTGGGAACGCGCG
20[103]18[104] GCCAGCTGCCTGCAGGTCGACTCTGCAAGGCG
6[263]4[264] GCCACCACATAAATCCTCATTAAACGTTCCAG
22[103]20[104] TGGACTCCCTTTTCACCAGTGAGACCTGTCGT
1[280]3[279] CCCTCAGATTTTTGAAAGTATTAAGAGGCTATTATT
10[199]9[215] TTTTAATTGCCCGAAAGACTTCAATAAAAGAA
14[295]12[296] TAAGTCCTGCGCCCAATAGCAAGCTTCCAGAG
7[184]9[183] GGAATTACTCGTTTACCAGACGACAAAAGATT
16[103]14[104] ACCCGTCGTCATATGTACCCCGGTAAAGGCTA
6[231]4[232] CACCAGAGGTCAGACGATTGGCCTGATACAGG
9[312]11[311] ATTGAGGGCCGAGGAAACGCAATAGCGCTAAT
15[376]17[375] TAAAGTACTTTTGGCTTAGGTTGGGTTATACCTTTT
19[88]21[87] CTTGCATGCATTAATGAATCGGCCCGCCAGGG
18[359]16[360] CCTGATTGCATAGGTCTGAGAGACTATAACTA
3[88]5[87] ACGGCTACTTACTTAGCCGGAACGCTGACCAA
8[71]6[72] TAAATATTTTTTGGAAGAAAAATCTACGACCAGTCA
5[120]7[119] CCAGGCGCTTAATCATTGTGAATTACAGGTAG
4[231]2[232] AGTGTACTGTAACAGTGCCCGTATCGGGGTTT
4[263]2[264] TAAGCGTCCTGCCTATTTCGGAACCTGAGACT
15[120]17[119] AGAAAAGCAACATTAAATGTGAGCATCTGCCA
14[263]12[264] CTAATTTACCGTTTTTATTTTCATACAGCCAT
13[88]15[87] CTGTAATATTGCCTGAGAGTCTGGAAAACTAG

12[71]10[72] GCTAAATCTTTTCTGTAGCTCAACATGTATTGCTGA
8[199]7[215] CATAACCCGAGGCATAGTAAGAGCTTATTAGC
24[199]23[215] AAGGAGCGCGAGAAAGGAAGGGAACAAACTAT
16[71]14[72] GATTGACCTTTTGATGAACGGTAATCGTAGCAAACA
9[280]11[279] AGCGCCAAAAGAACTGGCATGATTGAACACCC
4[71]2[72] ACGGTCAATTTTGACAGCATCGGAACGAACCCTCAG
10[295]8[288] ATACCCAAAGACAAAAGGGCGACATCGATAGCAGCACCGT
24[135]22[136] CGCGCTTACTAAATCGGAACCCTAGTTGTTCC
13[248]15[247] CAAGCAAGCGAGCATGTAGAAACCTATCATAT
25[152]24[168] ATCAGTGAGGCCACCGAGTAAAAGCAAGTGTA
25[120]24[136] GGTACGCCAGAATCCTGAGAAGTGACACCCGC
23[120]25[119] GTAAAGCAATGCGCCGCTACAGGGACAGGAAC
12[327]10[328] TCTTACCAGATAACCCACAAGAATAGTTACCA
20[167]18[168] GTGAGCTAGTTTCCTGTGTGAAATTTGGGAAG
20[295]18[296] TTATTAATATATCAAAATTATTTGAATTACCT
0[135]1[119] CGTAACGATCTAAAGTTTTGTCGTGAATTGCG
7[280]9[279] GAGCCGCCAATCAGTAGCGACAGAGGTTTACC
25[184]25[215] CATCACGCAAATTAACCGTTGTAGCAATACTT
18[71]16[72] CACGACGTTTTTGTAATGGGATAGGTCAAAACGGCG
18[135]16[136] CAGCTGGCGGACGACGACAGTATCGTAGCCAG
23[152]25[151] CCCCGATTGCTGCGCGTAACCACCTTTTTATA
1[248]3[247] TATCACCGGAAGGATTAGGATTAGAAACAGTT
3[280]5[279] CTGAAACATTTTCAGTCTCTGAATTTACGCCAGAAT
23[344]22[360] GTCACACGACCAGTAATAAAAGGGACCTGAAA
16[263]14[264] AATGGTTTCAAATTCTTACCAGTAATCCCATC
17[184]19[183] GCTTCTGGTCAGGCTGCGCAACTGTGTTATCC
3[216]4[200] TGCCTTGAGGTAATAAGTTTTAACCTAAAACA
8[327]9[311] CCGGAAACGTCACCAATGAAACCATTCAACCG
18[103]16[104] ATTAAGTTCGCATCGTAACCGTGCGAGTAACA
9[120]11[119] CAAAAATCATTGCTCCTTTTGATAAGTTTCAT
11[216]12[200] CTTTACAGAACGTCAAAAATGAAAAGCTATAT
8[385]9[375] TTCCATTTGGGAATTAGACCGTCACC
9[152]11[151] TCAGAAGCCTCCAACAGGTCAGGATCTGCGAA
15[248]17[247] GCGTTATAGAAATACCGACCGTGTCCTTGCTT
15[184]17[183] GTTAAAATTTTAACCAATAGGAACCCGGCACC
17[88]19[87] TAGATGGGGGGTAACGCCAGGGTTGTGCCAAG
20[71]18[72] GGGAGAGGTTTTTGTAAAACGACGGCCATTCCCAGT
23[312]22[328] GAAATGGATTATTTACATTGGCAGATATTTTT
20[359]18[360] GGATTTAGCAGATGAATATACAGTCGGATTCG
21[152]23[151] GAGTTGCACGAGATAGGGTTGAGTAAGGGAGC
14[199]13[215] AGACAGTCATTCAAAAGGGTGAGACAAGAACG
23[216]24[200] CGGCCTTGCCTGAGTAGAAGAACTGAAAGCGA
12[199]11[215] TTTCATTTGGTCAATAACCTGTTTATAGCAGC
15[280]17[279] ACGCTCAAAATTTCATCTTCTGACTTTTCCCT
1[120]3[119] AATAATAAGGTCGCTGAGGCTTGCAAAGACTT
16[135]14[136] CTTTCATCCCCAAAAACAGGAAGACCGGAGAG
4[103]2[104] GCTCCATGAGAGGCTTTGAGGACTAGGGAGTT
12[231]10[232] TTTTGTTTAGAGAATAACATAAAAGTAGAAAA
18[327]16[328] GCGCAGAGCTGAGAAGAGTCAATAATCGCAAG
17[344]19[343] ATCAAAATCTTTGAATACCAAGTTTTTTCAGG
24[71]22[72] TTCCTCGTTTTTCGATGGCCCACTACGTAAACCGTC
15[216]16[200] AATTACTAAATAAGAATAAACACCTTAAATCA
20[135]18[136] ACTGCCCGCCGAGCTCGAATTCGTTATTACGC
2[71]0[62] CAGCGAAATTTTAACTTTCAACAGTTTCTGGGATTTTGCTAAACTT
8[263]6[264] TGCCTTTACCACCACCGGAACCGCCCCTCAGA
2[199]1[215] CTTAAACATCAGCTTGCTTTCGAGCCGTCGAG

3[248]5[247]	AATGCCCCATACATGGCTTTTGATTGATATTC
2[135]0[136]	ATATATTCTTTTTTCACGTTGAAAATAGTTAG
15[344]17[343]	AGAGGCATTGCTGATGCAAATCCAGTGAATTT
16[231]14[232]	AGGCGTTAGAAAAAGCCTGTTTAGAATCAATA
19[248]21[247]	TGGATTATGAACAAAGAAACCACCTGAAAAAT
6[167]4[168]	ACGAGTAGTGACAAGAACCGGATATACCAAGC
17[280]19[279]	TAGAATCCGAAGATGATGAAACAAAGGGTTAG
9[88]11[87]	AAACAGTTGATGGCTTAGAGCTTATTTAAATA
21[216]22[200]	GCCACGCTAGTATTAACACCGCCTTGGTGGTT
17[120]19[119]	GTTTGAGGGAAAGGGGGATGTGCTAGAGGATC
17[152]19[151]	GAAGATCGGTGCGGGCCTCTTCGCAATCATGG
7[152]9[151]	CATTCAACGCGAGAGGCTTTTGCATATTATAG
17[376]19[375]	TAACCTCCTTTTTCGGGAGAAACAATAAAACAGTAC
5[216]6[200]	TGAGGCAGCCGCCGCCAGCATTGACATTCAGT
5[152]7[151]	AGTAATCTTAAATTGGGCTTGAGAGAATACCA
2[167]0[168]	CAATGACACTCCAAAAGGAGCCTTACAACGCC
18[167]16[168]	GGCGATCGCACTCCAGCCAGCTTTGCCATCAA
9[376]11[375]	GACTTGAGTTTTTATCTTACCGAAGCCCATGAAATA
5[280]7[279]	GGAAAGCGTTTTACCCTCAGAACCGCCACTCCCTCA
18[263]16[264]	AAAACAAACGTCGCTATTAATTAACTAAATTT
19[184]21[183]	GCTCACAATGTAAAGCCTGGGGTGGGTTTGCC
10[71]8[72]	ATATAATGTTTTCATTGAATCCCCCTCAAATCGTCA
1[89]3[87]	AGAATAGCTTTTGCGGGATCGTCGGGTAGCA
8[103]6[104]	ACTGGATAACGGAACAACATTATTACCTTATG
25[216]25[234]	CTTTGATTAGTAATAATTT
1[216]2[200]	AGGGTTGAACCAGGCGGATAAGTGGTGAATTT
10[103]8[104]	TTTTTGCGCAGAAAACGAGAATGAATGTTTAG
9[248]11[247]	TCACAATCCAGTATGTTAGCAAACACAGGGAA
9[184]11[183]	AAGAGGAACGAGCTTCAAAGCGAAGATACATT
21[376]23[385]	AGATTAGATTTTAGATAGAACCCTTCTGACATTCTGGCCAACAGTT
0[199]1[183]	TGAGTTTCGTCACCAGTACAAACTTAATTGTA
12[103]10[104]	CAAAATTAAAGTACGGTGTCTGGAAGAGGTCA
13[312]15[311]	TATAGAAGACGCGCCTGTTTATCAAGAATCGC
7[248]9[247]	AACCAGAGGCGTCAGACTGTAGCGTTATTTTG
1[184]3[183]	TCGGTTTAGCTTGATACCGATAGTCCAACCTA
2[263]0[264]	CCTCAAGATACTCAGGAGGTTTAGCCGCCACC
0[167]1[151]	TGTAGCATTCCACAGACAGCCCTCATCTCCAA

10.4 **Modification staples**

10.4.1 **Double-length**

14[135]10[136]	GATCTACACCTCATATATTTTAAAAGGCAAGGCAAAGAATACG
	AGTAGATTTAGTTTTTGATAA
11[120]15[119]	TTCTGCGATAGCAAAATTAAGCAATAAAAATTTTTAGAACAAGG
	CTATCAGGTCATCCCCAAAA
9[152]13[151]	AGATTAAGACCTTTAATTGCTCCTTGACCATTAGATACATATCC
	AATAAATCATACTGCAATGC

10.4.2 **2.5-turn staples**

10[116]8[104]	GCTTAGAGCTTAATTGCTGAAATCAGGTCTTTACCCGGAATCG
13[93]15[87]	TTTATTTCAACGCGAGAGTCTGGAGCAAACAAGAGAATCTCAT ATGT
9[120]8[136]	TATAGTCAGAAGCAAAGCGGATTGAAAATGTT
9[152]11[146]	AGATTAAGACCTTTAATTGCTCCTTTTGATAAGAAGATTTAGTTT GA
13[149]15[151]	TGCCTGAGTAACGGAGAGGGTAGCTATTTTAAATT
14[123]12[121]	CTATCAGGTCATTGCCTAAGGATAAAAATTTTTAGAACCCTCATA AGAATTAGCAAA
9[88]11[92]	AAATCAAAATATAATGCTGTAGCTTGTCTGGAAGTTT
12[120]10[117]	ATTAAGCAATAAAGAGTTGATTCCCAATTCTGCGAACGAGTGGT CATTTTTGCGGATG
11[147]13[148]	CCATTAGATACATATCCAATAAATCATACAGGCAAGGCAATATTTTAAAT GCAA
11[93]13[92]	CATTCCATATAACCCTCAGAGCATAAAGCTAAATCGGTTTGCGGGAGAA GCC
16[135]14[124]	TAAATGTGATTGTATAAGCAAATATTTTGAGAGATCTACAAAGG
15[112]17[119]	CCCCAAAAACAGGAAGAGCGAGTAACAACCCGTGAGGGGA
16[103]15[111]	TCCGTGGTGATAATCAGAAAAG

10.5 **Example AFM images**

The next section shows a selection of the AFM images captured and used for the analysis of the adsorption orientation as well as width measurements used in this thesis. A brief description on the tile design such as scan size, m13mp18 and other miscellaneous details are given

10.5.1 **“Standard” conditions**

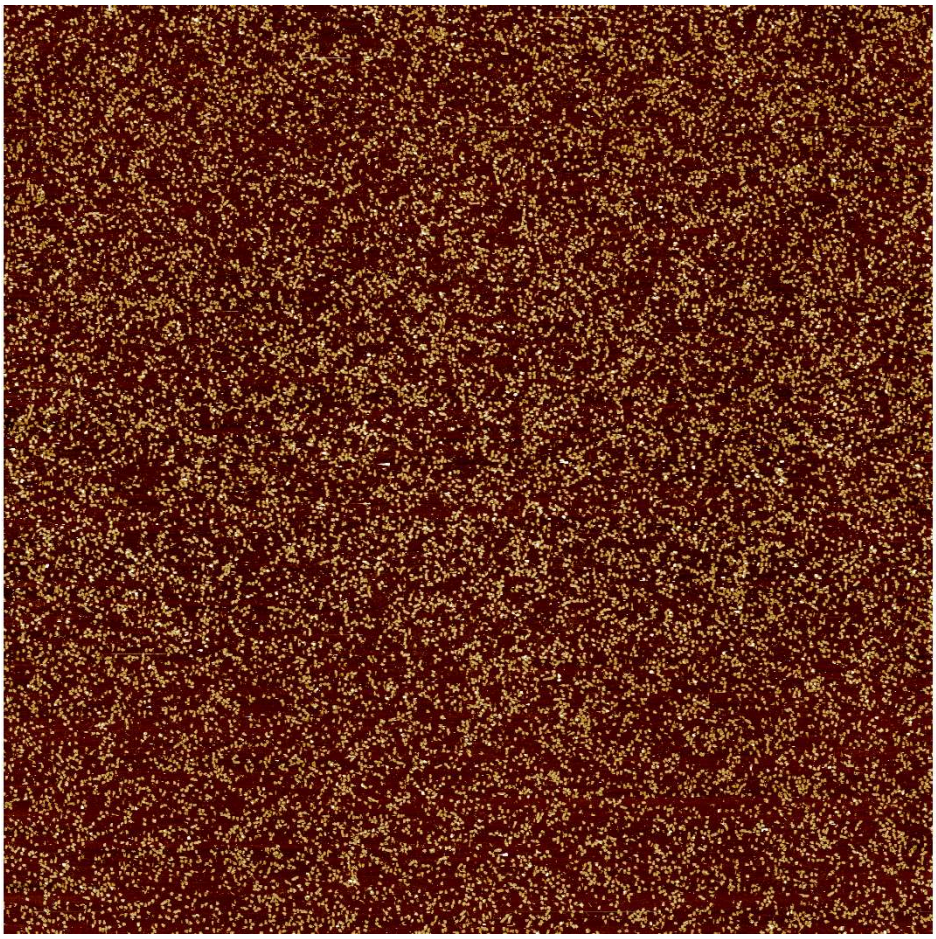

Figure 50: 10.33, 24 µm, 1 nM m13mp18, mica, 12.5 mM Mg-ace

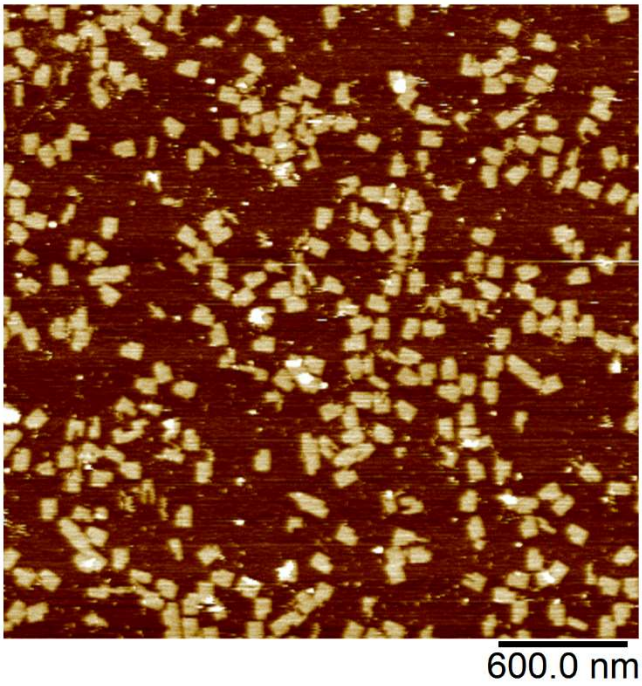

Figure 51: 10.33, 3 µm, 1 nM m13mp18, mica, 12.5 mM Mg-ace

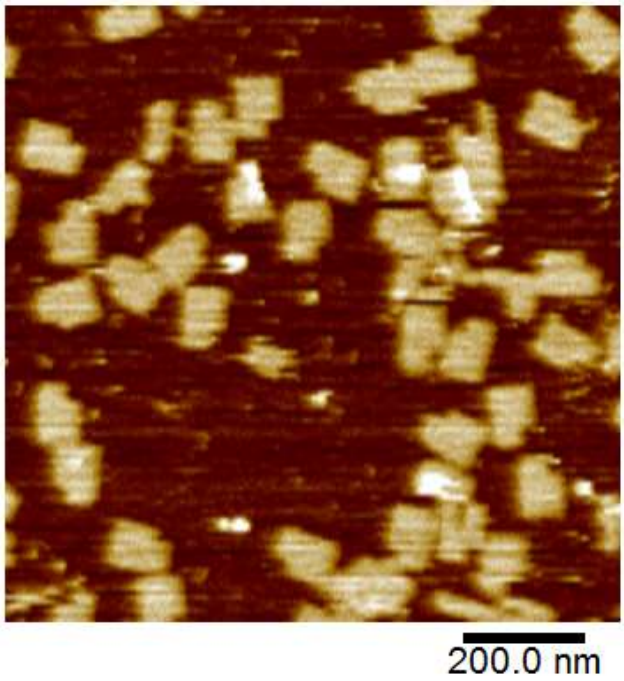

Figure 52: 10.33, 1 µm, 1 nM m13mp18, mica, 12.5 mM Mg-ace

10.5.2 Nickel Treated

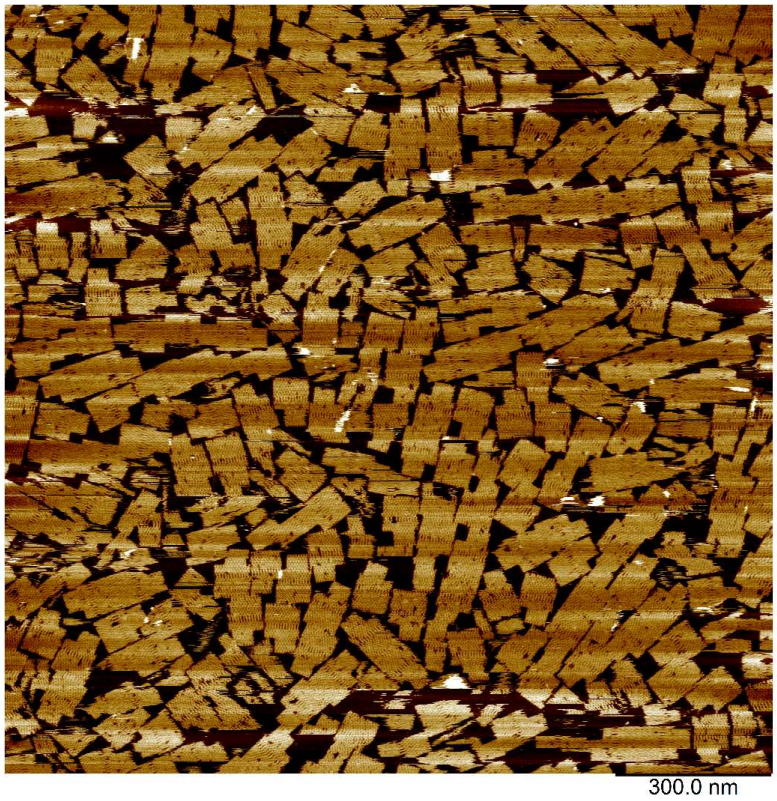

Figure 53: 10.67, 1.5 µm, 6 nM m13mp18, 10 mM nickel treated mica, 12.5 mM Mg-ace

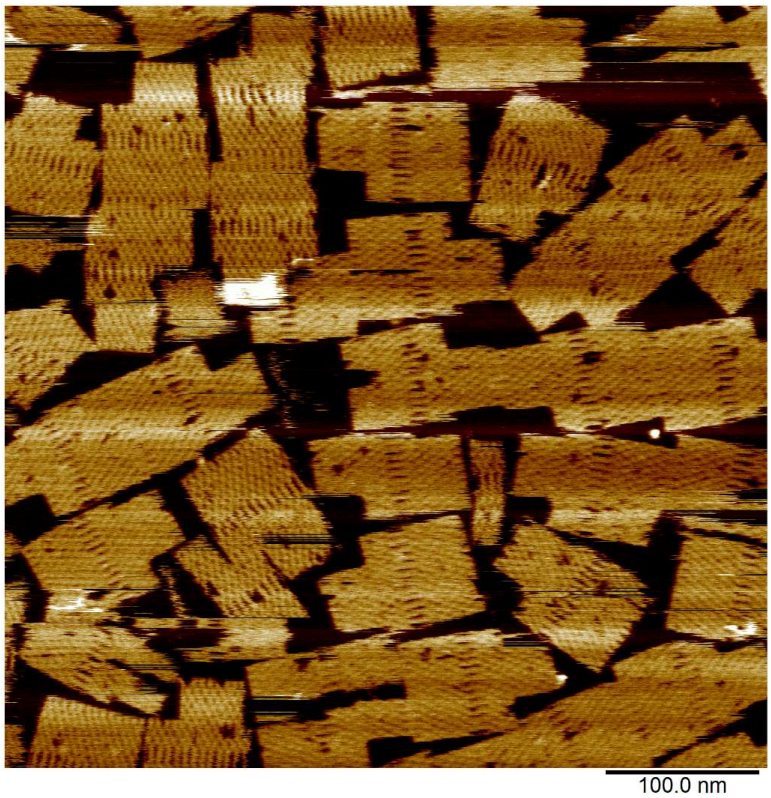

Figure 54: 10.67, 0.5 µm, 6 nM M13mp18, 10 mM nickel treated mica, 12.5 mM Mg-ace

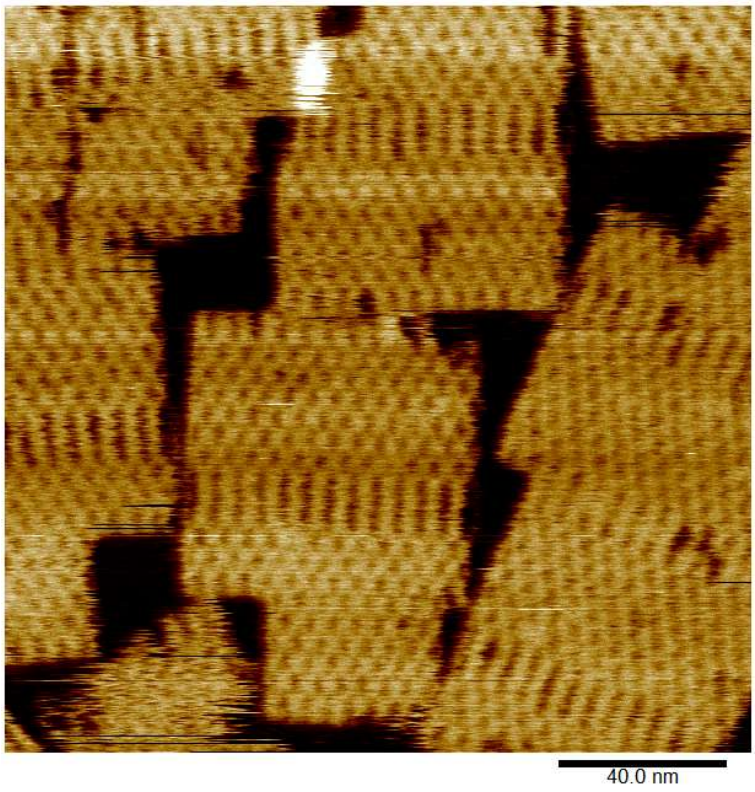

Figure 55: 10.67, 200 nm, 6 nM m13mp18, 10 mM nickel treated mica, 12.5 mM Mg-ace

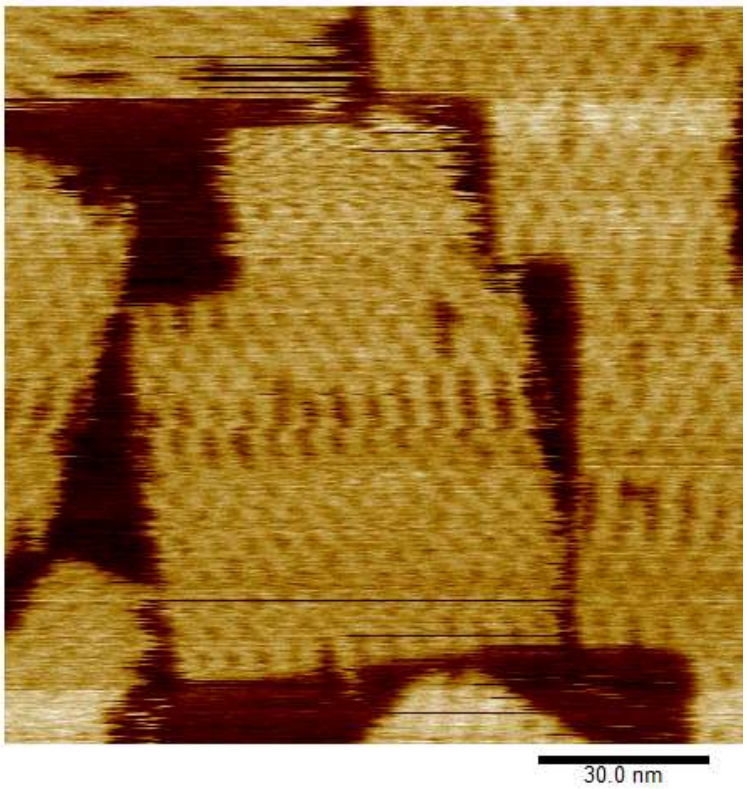

Figure 56: 10.67, 150 nm, 6 nM m13mp18, 10 mM nickel treated mica, 12.5 mM Mg-ace

10.5.3 UV exposed

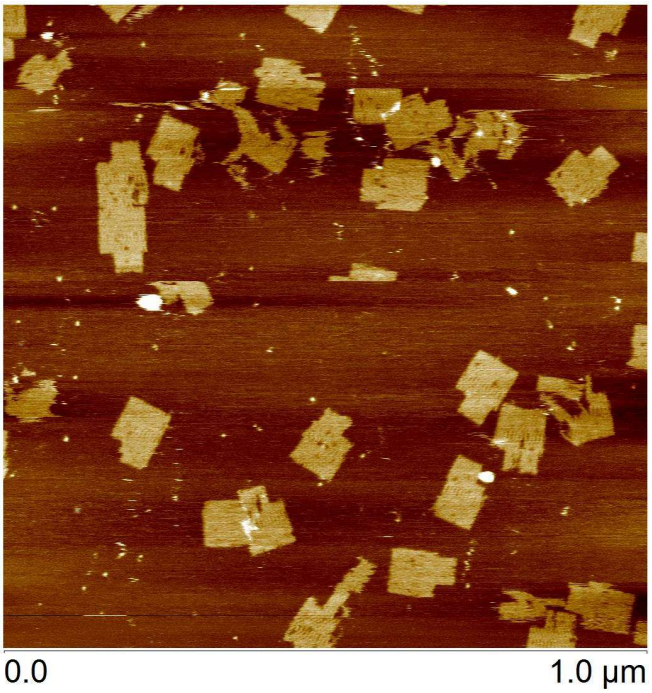

Figure 57: 10.67, 3 µm, 1 nM m13mp18, mica, 12.5 mM Mg-ace, 5 min UVC exposure

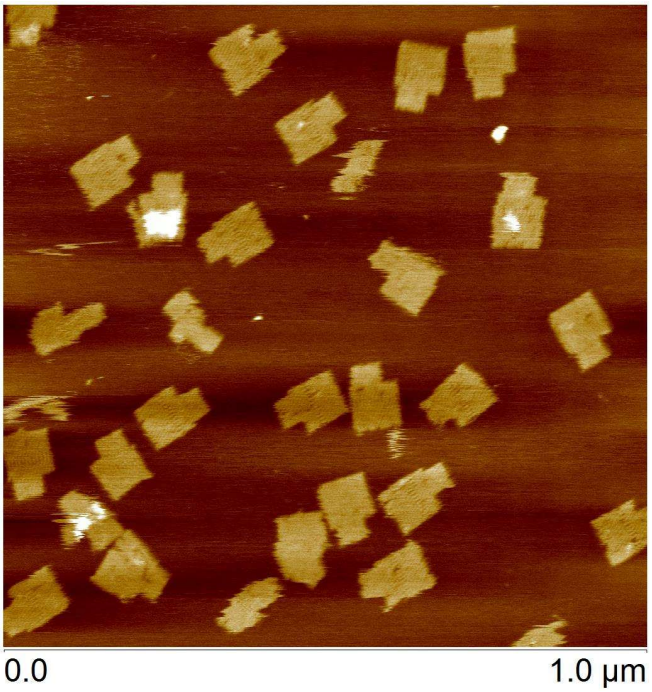

Figure 58: 10.67, 3 µm, 1 nM m13mp18, mica, 12.5 mM Mg-ace, 10 min UVC exposure

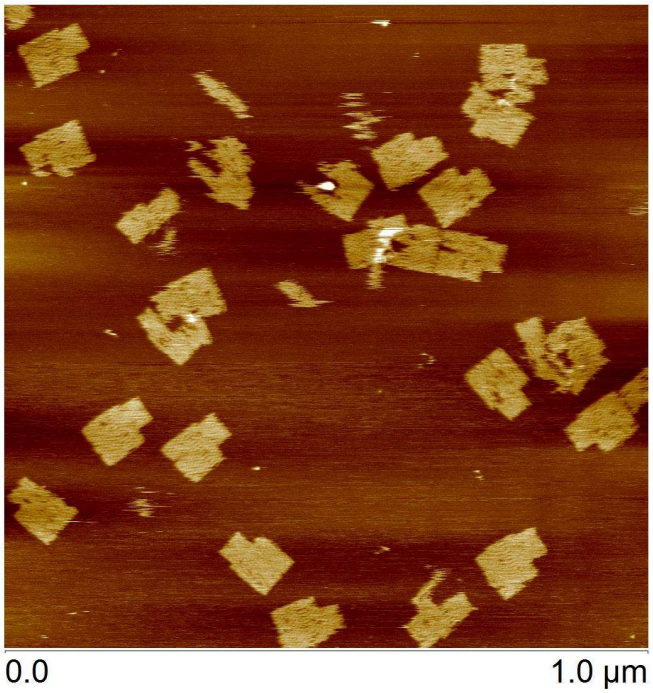

Figure 59: 10.67, 3 µm, 1 nM m13mp18, mica, 12.5 mM Mg-ace, 15 min UVC exposure

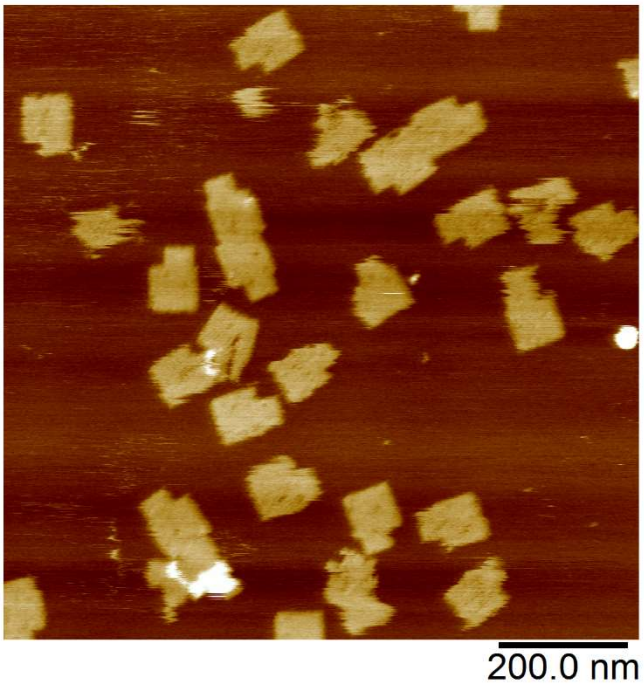

Figure 60: 10.67, 3 µm, 1 nM m13mp18, mica, 12.5 mM Mg-ace, 20 min UVC exposure

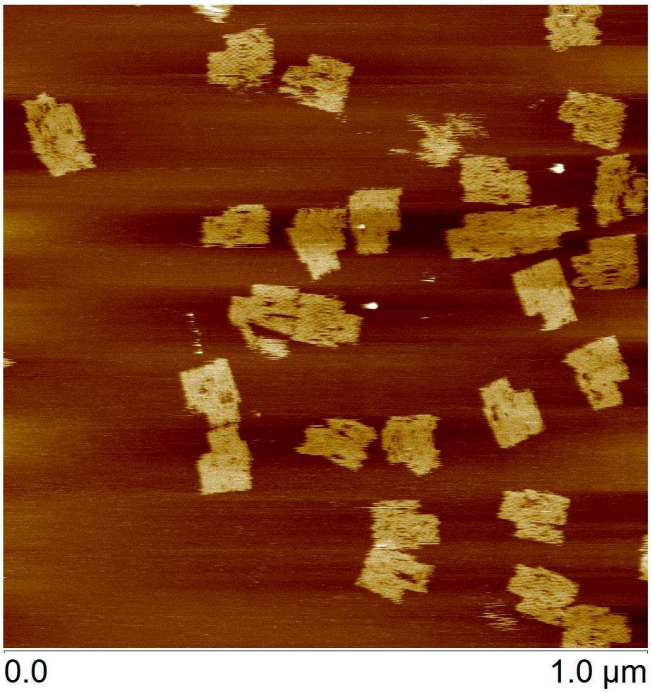

Figure 61: 10.67, 3 µm, 1 nM m13mp18, mica, 12.5 mM Mg-ace, 25 min UVC exposure

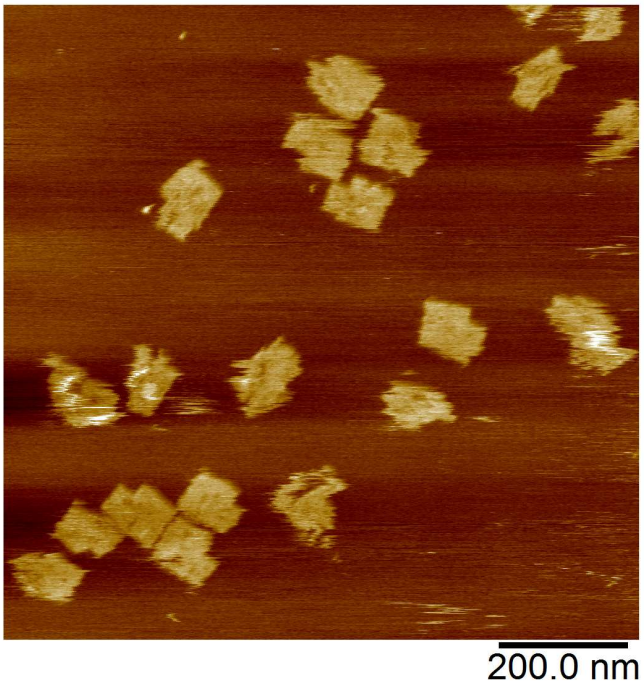

Figure 62: 10.67, 3 µm, 1 nM m13mp18, mica, 12.5 mM Mg-ace, 30 min UVC exposure

10.5.4 **Barium**

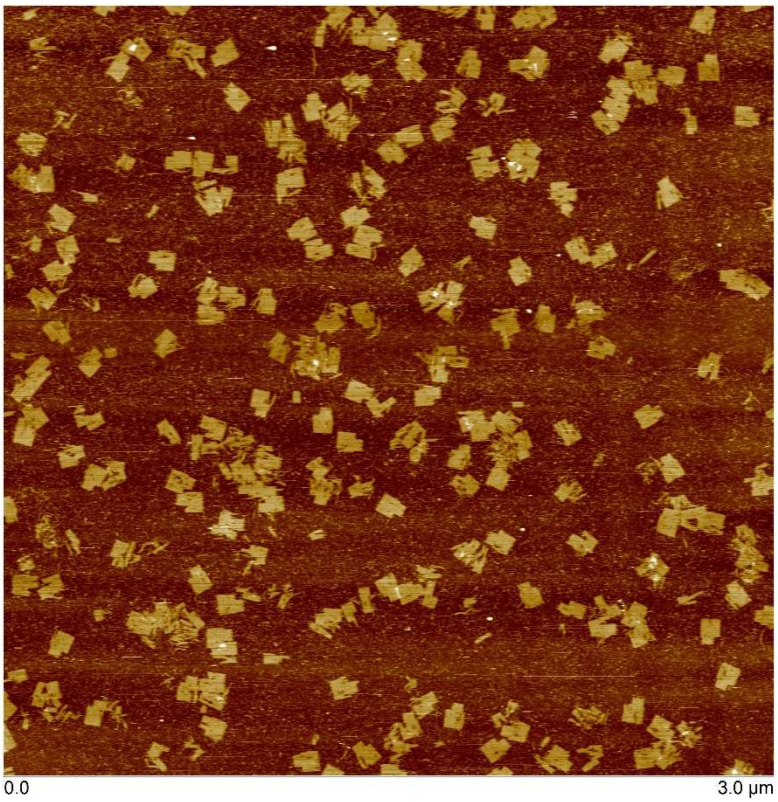

Figure 63: 10.33, 3 µm, 1 nM m13mp18, mica, 3.125 mM $BaCl_2$

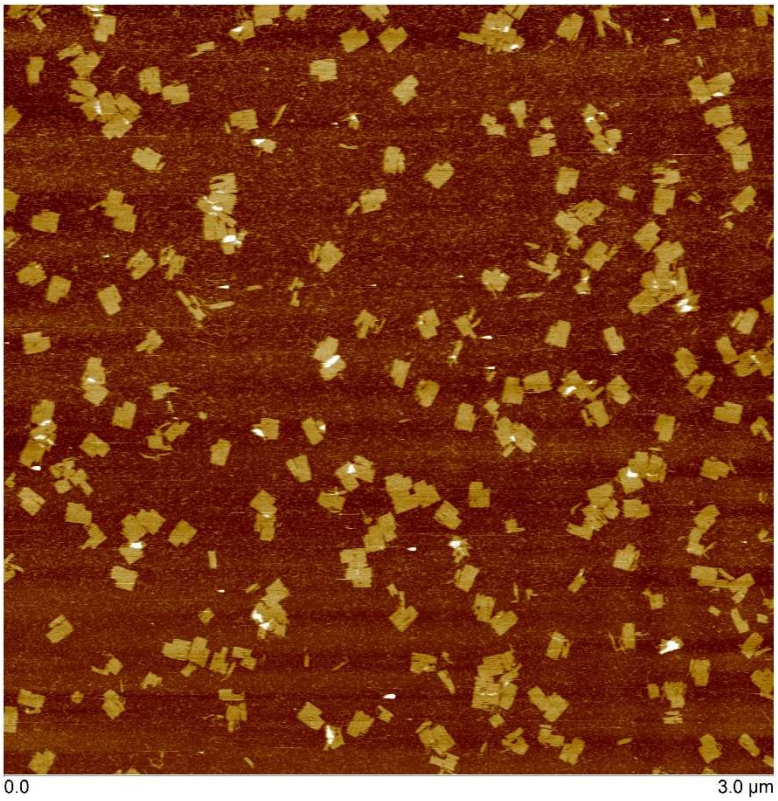

Figure 64: 10.33, 3 µm, 1 nM m13mp18, mica, 6.25 mM $BaCl_2$

Figure 65: 10.33, 3 µm, 1 nM m13mp18, mica, 12.5 mM $BaCl_2$

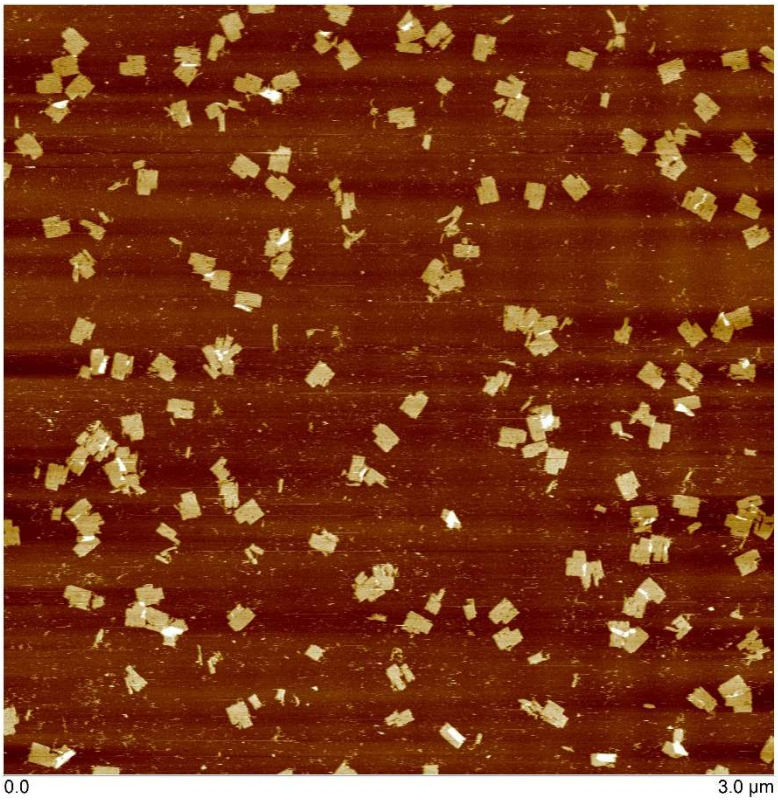

Figure 66: 10.33, 3 µm, 1 nM m13mp18, mica, 25 mM $BaCl_2$

10.5.5 Barium and Magnesium

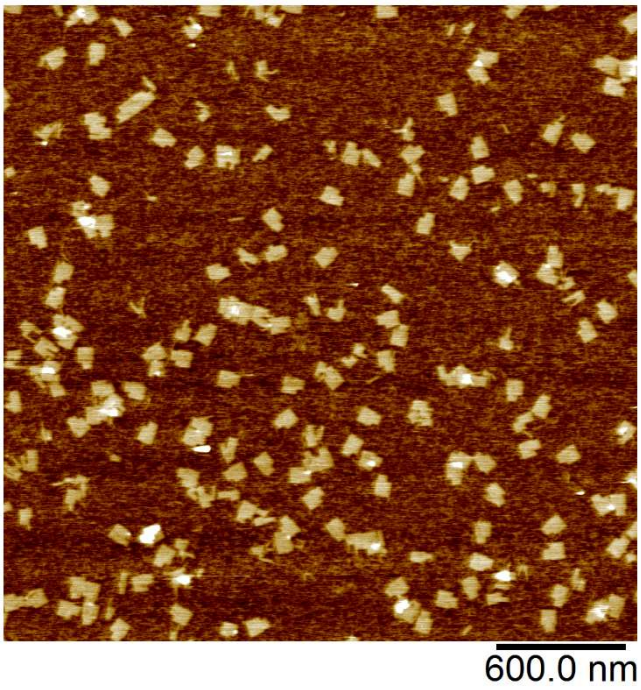

Figure 67: 10.50, 3 µm, 1 nM m13mp18, mica, 3.125 mM $BaCl_2$, 3.125 mM Mg-ace

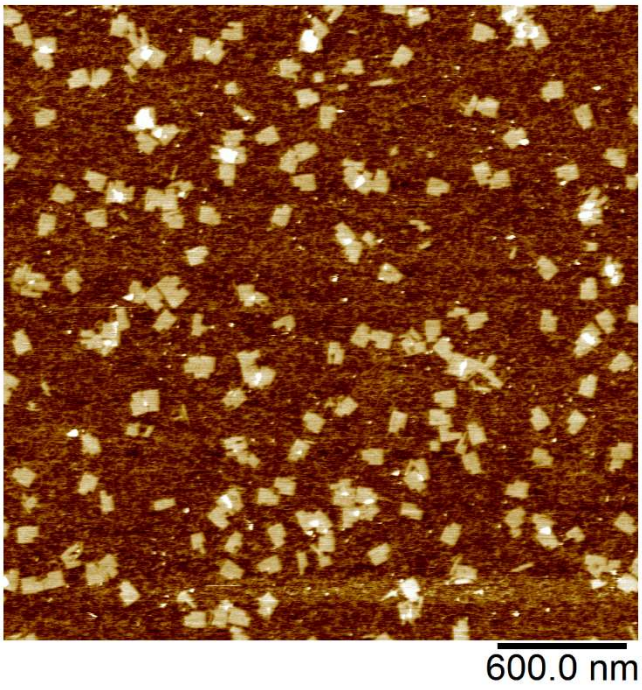

Figure 68: 10.50, 3 µm, 1 nM m13mp18, mica, 6.25 mM $BaCl_2$, 3.125 mM Mg-ace

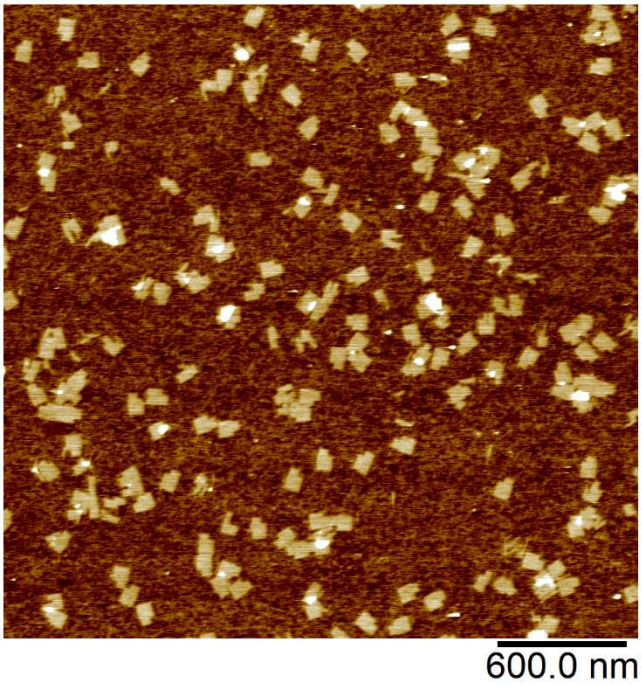

Figure 69: 10.50, 3 µm, 1 nM m13mp18, mica, 3.125 mM $BaCl_2$, 6.25 mM Mg-ace

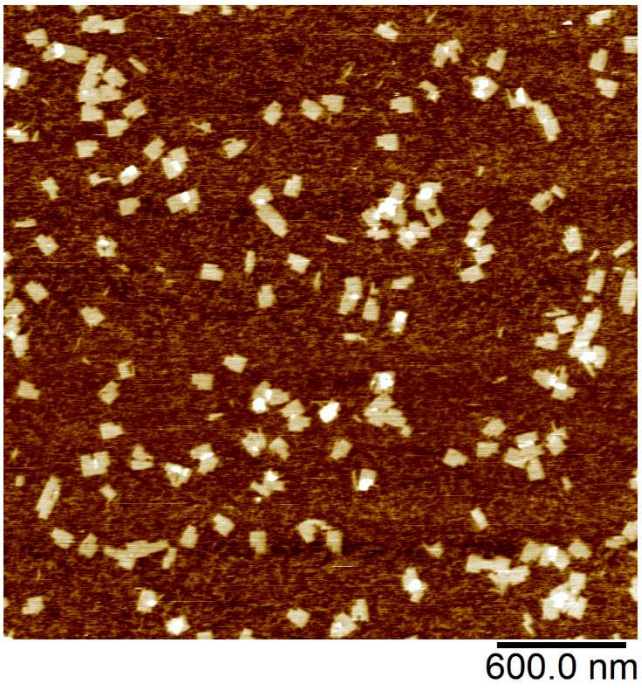

Figure 70: 10.50, 3 µm, 1 nM m13mp18, mica, 6.25 mM $BaCl_2$, 9.375 mM Mg-ace

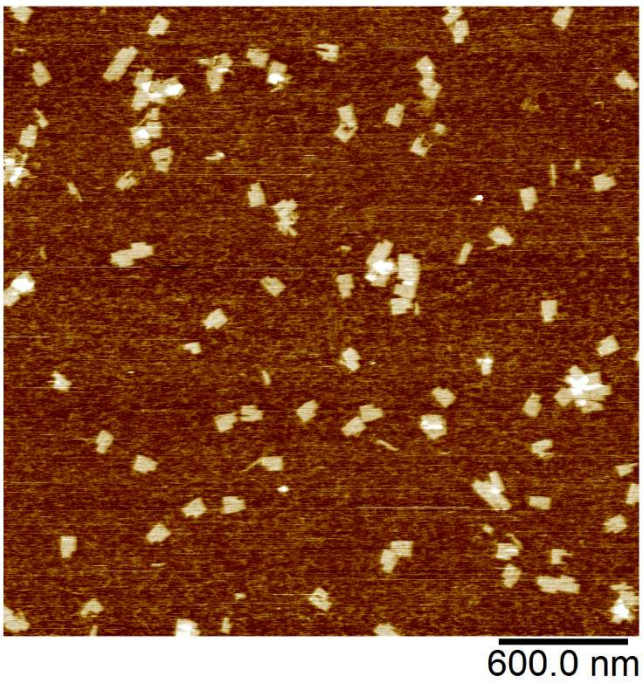

Figure 71: 10.50, 3 µm, 1 nM m13mp18, mica, 9.375 mM $BaCl_2$, 9.375 mM Mg-ace

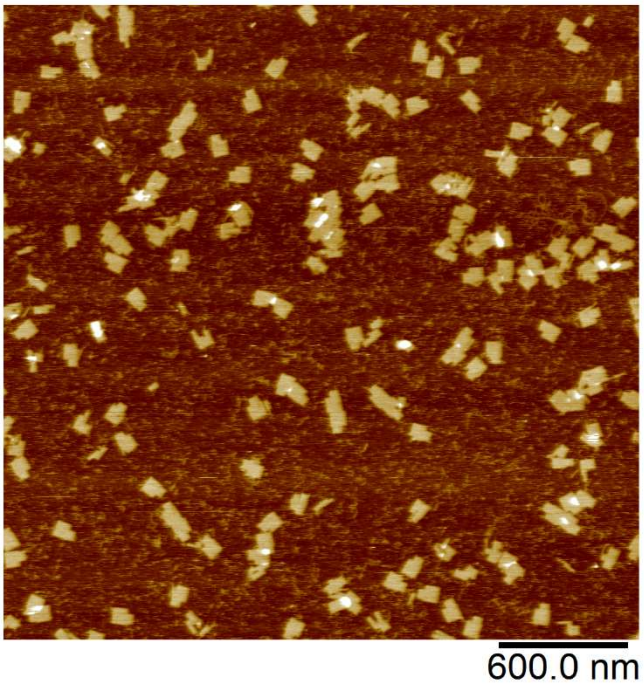

Figure 72: 10.50, 3 µm, 1 nM m13mp18, mica, 12.5 mM $BaCl_2$, 12.5 mM Mg-ace

10.5.6 **2.5 turn**

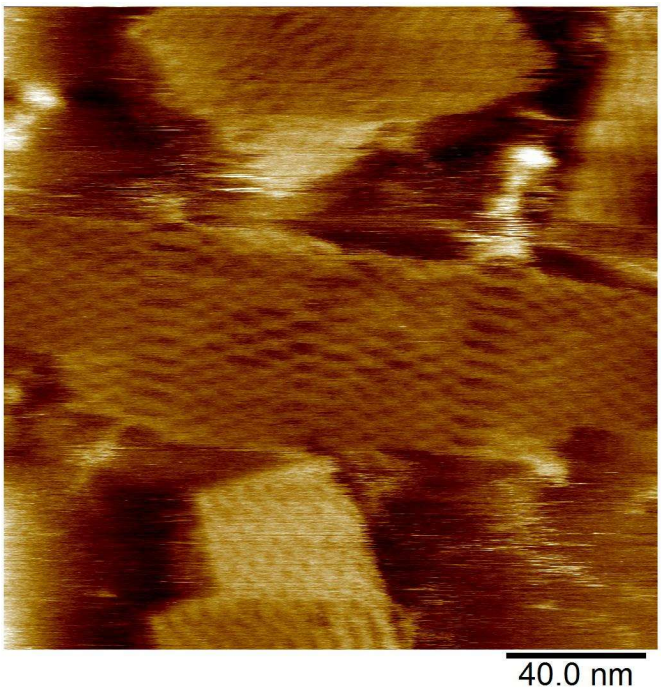

Figure 73: 10.67, 200 nm, 1 nM m13mp18, mica, 12.5 mM Mg-ace, 2.5 turn crossovers

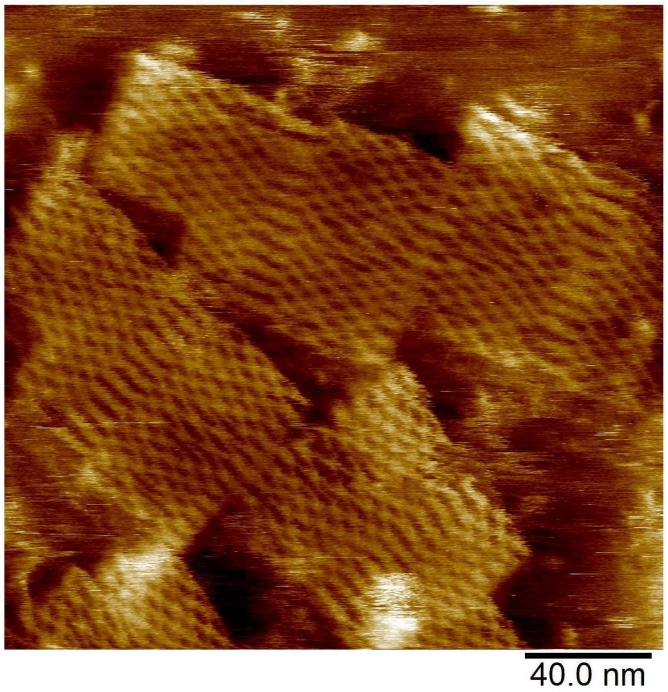

Figure 74: 10.67, 200 nm, 1 nM m13mp18, mica, 12.5 mM Mg-ace, 2.5 turn crossovers

10.6 **Image analysis**

The size of DNA origami, achievable scan areas of AFM and number of origami folded in solution all present issues for achieving accurate adsorption orientation data. This section introduces the methodology and reasoning for the image capture and analysis used throughout this work, addressing some of the issues.

10.6.1 **Adsorption analysis**

The adsorption orientation of samples was determined by analysis of AFM images. For each sample, two 9x9 μm AFM images with a digital resolution of 3072x3072 pixels were captured. The number of tiles observed to be A-face up (NA), B-face up (NB) and indistinguishable tiles (NNA) were manually recorded for one of these images. All results in this thesis are quoted as the proportion of tiles measured to be A-face up. Upper and lower limits are calculated based on the assumption that the indistinguishable tiles are wholly A-face up or B-face up, respectively.

Proportion tiles A-face up: $\frac{N_A}{N_A+N_B}$

Upper limit: $\frac{N_A+N_{NA}}{N_A+N_{B+}N_{NA}}$

Lower limit: $\frac{N_A}{N_A+N_{B+}N_{NA}}$

10.6.2 **Width measurements**

The width of origami tiles was determined by capturing images that were 1x1 μm in size at a digital resolution of 1024x1024 pixels. A total area of 3x3 μm was scanned, resulting in a total of 9 1x1 μm images. The images were analysed using the programme Gwyddion, as it allows for a greater number of line profiles to be extracted. A line profile with a width of 10 pixels was used for each origami, measuring the width adjacent to the seam. Tiles which were appeared to be degraded or not fully folded where not used for analysis. The data for the line profiles were then saved and imported into Origin. The width of the tile was determined to be the FWHM of the line profiles, which was calculated using built-in Origin functions. This was done to remove bias that may occur from the

author. The widths were then plotted using the box-plot function of origin. The total number of tiles for each data set ranged from 60-80.

10.6.3 Statistical analysis

The choice for imaging areas that are 9x9 µm in size is based on the work of a previous PhD student. The increase in scan rate offered by the newer AFM system meant that a single 9x9 µm image could be captured with a resolution of 3072x3072, rather than nine 3x3 µm images with resolutions of 512x512 pixels, as was previously done. This greatly reduced the time required to image samples. Although the newer system offers increased data output, the manual counting of tiles was a limiting factor during data analysis. This section looks at how the adsorption orientation of tiles is dependent on area size.

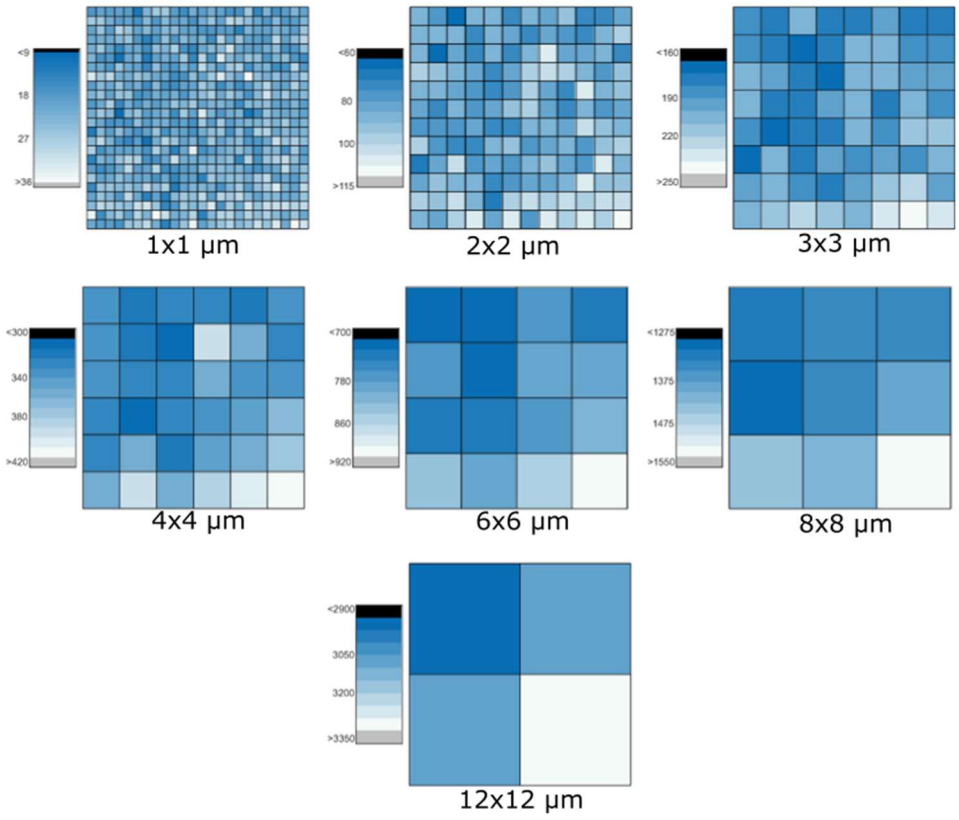

Figure 75: Number of countable tiles in each area of the larger 24x24 µm image, divided into smaller areas to explore the surface coverage

The binding of origami to mica is assumed to be uniform across the whole surface. As AFM images areas on the order of microns, there is a possibility to image non-uniform areas. Here, a 24x24 µm area of the sample was scanned (figure 50). The number of

countable tiles can be seen in figure 75, showing how this varies with the size of area scanned. This image was then divided into a set of 576 1x1 μm images, counting the N_A, N_B and N_{NA} tiles. A set of faux images were then generated, consisting of a random selection of these 576 images, to replicate an image that is nxn μm in size. This also assumes that each 1x1 μm area is independent of each other. For each set of faux images, a total of 1000 images were generated.

Figure 76 shows the proportion of tiles with the A-face observed for faux images that are nxn μm in size. For smaller faux images, there is a greater chance that the observed orientation is outside that of the larger 24x24 μm image, such that it does not accurately

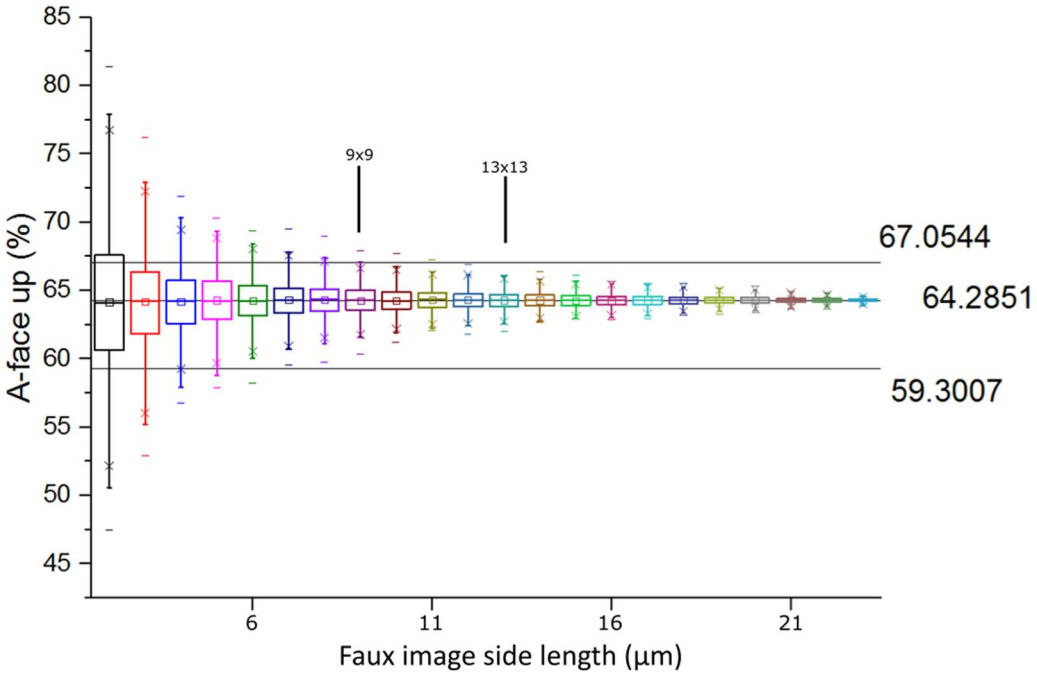

Figure 76: Binding orientations of tiles constructed from faux images using the set of images of the 24x24 μm image.

reflect the whole population. This illustrates how imaging an area that is too small is subject to fluctuations due to non-uniformity that is present at small length scales. As mentioned, two 9x9 μm images were captured for each sample although only one was analysed. In figure 76, the data sets for the 9x9 μm and 13x13 μm faux images are highlighted (n.b (2x92)½ = 12.73). As these data sets exclude the number of indistinguishable tiles (i.e. error bars) it is in the authors opinion that single 9x9 μm is sufficient for measuring the samples adsorption orientation and hence origami curvature

of the sample. This spread in the data sets of the faux images also demonstrate how small changes in observed binding, such as those in chapter 6 at elevated Mg^{2+} are not necessarily indicative of a change in curvature.

10.6.4 Conclusion

Although a large image would give better confidence in the adsorption orientation for samples, the current method of manual origami counting means that time is a limiting factor during data analysis. Although the size of images used is arbitrary, the results from the larger 24x24 μm image indicate that an image of 9x9 μm is sufficient for this work. Measuring widths of origami tiles still presents a challenge, with data required on ideal image forces to ensure a lack of tile perturbation as well as degradation.

11 Bibliography

[1] N. C. Seeman, “Nucleic acid junctions and lattices,” *J. Theor. Biol.*, vol. 99, no. 2, pp. 237–247, 1982.

[2] N. R. Kallenbach, R.-I. Ma, and N. C. Seeman, “An immobile nucleic acid junction constructed from oligonucleotides,” *Nature*, vol. 305, no. 5937, pp. 829–831, Oct. 1983.

[3] P. W. K. Rothemund, “Folding DNA to create nanoscale shapes and patterns.,” *Nature*, vol. 440, no. 7082, pp. 297–302, Mar. 2006.

[4] A. R. Chandrasekaran, N. Anderson, M. Kizer, K. Halvorsen, and X. Wang, “Beyond the Fold: Emerging Biological Applications of DNA Origami,” *ChemBioChem*, pp. 1081–1089, 2016.

[5] G. Tikhomirov, P. Petersen, and L. Qian, “Fractal assembly of micrometre-scale DNA origami arrays with arbitrary patterns,” *Nature*, vol. 552, no. 7683, pp. 67–71, Dec. 2017.

[6] A. Aghebat Rafat, T. Pirzer, M. B. Scheible, A. Kostina, and F. C. Simmel, “Surface-assisted large-scale ordering of DNA origami tiles.,” *Angew. Chem. Int. Ed. Engl.*, vol. 53, no. 29, pp. 7665–8, Jul. 2014.

[7] Y. Suzuki, M. Endo, and H. Sugiyama, “Lipid-bilayer-assisted two-dimensional self-assembly of DNA origami nanostructures,” *Nat. Commun.*, vol. 6, p. 8052, 2015.

[8] J. D. Watson and F. H. C. Crick, “Molecular structure of nucleic acids,” *Nature*, vol. 171, no. 4356, pp. 737–738, Apr. 1953.

[9] R. E. FRANKLIN and R. G. GOSLING, “Molecular Configuration in Sodium Thymonucleate,” *Nature*, vol. 171, no. 4356, pp. 740–741, Apr. 1953.

[10] R. M. Myers, S. G. Fischer, T. Maniatis, and L. S. Lerman, “Modification of the melting properties of duplex DNA by attachment of a GC-rich DNA sequence as

determined by denaturing gradient gel electrophoresis," *Nucleic Acids Res.*, vol. 13, no. 9, pp. 3111–3129, May 1985.

[11] E. Chargaff, "Human desoxypentose nucleic acid," *Nature*, vol. 165, no. 4202, p. 756, May 1950.

[12] P. L. Privalov, A. I. Dragan, C. Crane-Robinson, K. J. Breslauer, D. P. Remeta, and C. A. S. A. Minetti, "What Drives Proteins into the Major or Minor Grooves of DNA?," *Journal of Molecular Biology*, vol. 365, no. 1. pp. 1–9, 05-Jan-2007.

[13] R. A. Friedman and B. Honig, "The electrostatic contribution to DNA base-stacking interactions," *Biopolymers*, vol. 32, no. 2, pp. 145–159, Feb. 1992.

[14] P. Yakovchuk, E. Protozanova, and M. D. Frank-Kamenetskii, "Base-stacking and base-pairing contributions into thermal stability of the DNA double helix," *Nucleic Acids Res.*, vol. 34, no. 2, pp. 564–574, Jan. 2006.

[15] Z. J. Tan and S. J. Chen, "Nucleic acid helix stability: Effects of salt concentration, cation valence and size, and chain length," *Biophys. J.*, vol. 90, no. 4, pp. 1175–1190, Feb. 2006.

[16] O. D. Broekmans, G. A. King, G. J. Stephens, and G. J. L. Wuite, "DNA Twist Stability Changes with Magnesium(2+) Concentration," *Phys. Rev. Lett.*, vol. 116, no. 25, 2016.

[17] W. Fuller, T. Forsyth, and A. Mahendrasingam, "Water-DNA interactions as studied by X-ray and neutron fibre diffraction.," *Philos. Trans. R. Soc. Lond. B. Biol. Sci.*, vol. 359, no. 1448, pp. 1237-47; discussion 1247–8, Aug. 2004.

[18] R. Owczarzy, B. G. Moreira, Y. You, M. A. Behlke, and J. A. Wälder, "Predicting stability of DNA duplexes in solutions containing magnesium and monovalent cations," *Biochemistry*, vol. 47, no. 19, pp. 5336–5353, 2008.

[19] M. T. Record, "Effects of Na+ and Mg++ ions on the helix–coil transition of DNA," *Biopolymers*, vol. 14, no. 10, pp. 2137–2158, 1975.

[20] H. Deng and V. a Bloomfield, “Structural effects of cobalt-amine compounds on DNA condensation.,” *Biophys. J.*, vol. 77, no. 3, pp. 1556–1561, 1999.

[21] J. Duguid, V. a Bloomfield, J. Benevides, and G. J. Thomas, “Raman spectroscopy of DNA-metal complexes. I. Interactions and conformational effects of the divalent cations: Mg, Ca, Sr, Ba, Mn, Co, Ni, Cu, Pd, and Cd.,” *Biophys. J.*, vol. 65, no. 5, pp. 1916–1928, 1993.

[22] J. Anastassopoulou, “Metal-DNA interactions,” in *Journal of Molecular Structure*, 2003, vol. 651–653, pp. 19–26.

[23] C. Zimmer, G. Luck, and H. Triebel, “Conformation and Reactivity of DNA. 4. Base Binding Ability of Transition-Metal Ions to Native DNA and Effect on Helix Conformation with Special Reference to DNA-Zn(II) Complex,” *Biopolymers*, vol. 13, no. 3, pp. 425–453, 1974.

[24] G. H. Clever, C. Kaul, and T. Carell, “DNA-Metal Base Pairs,” *Angew. Chemie Int. Ed.*, vol. 46, no. 33, pp. 6226–6236, 2007.

[25] M. Ageno, E. Dore, and C. Frontali, “The alkaline denaturation of DNA.,” *Biophys. J.*, vol. 9, no. 11, pp. 1281–1311, 1969.

[26] M. C. Williams, J. R. Wenner, I. Rouzina, and V. a Bloomfield, “Effect of pH on the overstretching transition of double-stranded DNA: evidence of force-induced DNA melting.,” *Biophys. J.*, vol. 80, no. 2, pp. 874–81, 2001.

[27] K. S. Gates, “An overview of chemical processes that damage cellular DNA: spontaneous hydrolysis, alkylation, and reactions with radicals.,” *Chem. Res. Toxicol.*, vol. 22, no. 11, pp. 1747–60, Nov. 2009.

[28] T. R. Cech, “RNA as an Enzyme,” *Sci. Am.*, vol. 255, no. 5, pp. 64–75, Nov. 1986.

[29] P. Forterre, “The two ages of the RNA world, and the transition to the DNA world: a story of viruses and cells,” *Biochimie*, vol. 87, no. 9–10, pp. 793–803, Sep. 2005.

[30] W. Saenger, W. N. Hunter, and O. Kennard, “DNA conformation is determined by

economics in the hydration of phosphate groups," *Nature*, vol. 324, no. 6095, pp. 385–388, Nov. 1986.

[31] F. DiMaio, X. Yu, E. Rensen, M. Krupovic, D. Prangishvili, and E. H. Egelman, "A virus that infects a hyperthermophile encapsidates A-form DNA," *Science (80-.).*, vol. 348, no. 6237, pp. 914–917, May 2015.

[32] F. M. Pohl and T. M. Jovin, "Salt-induced co-operative conformational change of a synthetic DNA: Equilibrium and kinetic studies with poly(dG-dC)," *J. Mol. Biol.*, vol. 67, no. 3, pp. 375–396, Jun. 1972.

[33] H. Drew, T. Takano, S. Tanaka, K. Itakura, and R. E. Dickerson, "High-salt d(CpGpCpG), a left-handed Z′ DNA double helix," *Nature*, vol. 286, no. 5773, pp. 567–573, Aug. 1980.

[34] K. Hoogsteen, "The crystal and molecular structure of a hydrogen-bonded complex between 1-methylthymine and 9-methyladenine," *Acta Crystallogr.*, vol. 16, no. 9, pp. 907–916, Sep. 1963.

[35] J. Choi and T. Majima, "Conformational changes of non-B DNA," *Chem. Soc. Rev.*, vol. 40, no. 12, p. 5893, 2011.

[36] A. Bacolla and R. D. Wells, "Non-B DNA conformations, genomic rearrangements, and human disease," *Journal of Biological Chemistry*, vol. 279, no. 46. American Society for Biochemistry and Molecular Biology, pp. 47411–47414, 12-Nov-2004.

[37] Z. Li, L. Wang, H. Yan, and Y. Liu, "Effect of DNA hairpin loops on the twist of planar DNA origami tiles," *Langmuir*, vol. 28, no. 4, pp. 1959–1965, 2012.

[38] G. P. Schroth and P. S. Ho, "Occurrence of potential cruciform and H-DNA forming sequences in genomic DNA," *Nucleic Acids Res.*, vol. 23, no. 11, pp. 1977–1983, Jun. 1995.

[39] R. R. Sinden, M. J. Pytlos-Sinden, and V. N. Potaman, "Slipped strand DNA structures.," *Front. Biosci.*, vol. 12, pp. 4788–99, Sep. 2007.

[40] J. Zhao, A. Bacolla, G. Wang, and K. M. Vasquez, “Non-B DNA structure-induced genetic instability and evolution.,” *Cell. Mol. Life Sci.*, vol. 67, no. 1, pp. 43–62, Jan. 2010.

[41] M. L. Bochman, K. Paeschke, and V. A. Zakian, “DNA secondary structures: stability and function of G-quadruplex structures,” *Nat. Rev. Genet.*, vol. 13, no. 11, pp. 770–780, Nov. 2012.

[42] C. Chen *et al.*, “Study of pH-Induced Folding and Unfolding Kinetics of the DNA i-Motif by Stopped-Flow Circular Dichroism,” *Langmuir*, vol. 28, no. 51, pp. 17743–17748, Dec. 2012.

[43] A. Worcel, S. Strogatz, and D. Riley, “Structure of chromatin and the linking number of DNA.,” *Proc. Natl. Acad. Sci. U. S. A.*, vol. 78, no. 3, pp. 1461–1465, Mar. 1981.

[44] J. M. Benevides and G. J. Thomas, “Local conformational changes induced in B-DNA by ethidium intercalation,” *Biochemistry*, vol. 44, no. 8, pp. 2993–2999, 2005.

[45] E. L. Zechiedrich *et al.*, “Roles of topoisomerases in maintaining steady-state DNA supercoiling in Escherichia coli,” *J. Biol. Chem.*, vol. 275, no. 11, pp. 8103–8113, Mar. 2000.

[46] B.-B. S. Zhou and S. J. Elledge, “The DNA damage response: putting checkpoints in perspective,” *Nature*, vol. 408, no. 6811, pp. 433–439, Nov. 2000.

[47] H. Park *et al.*, “Crystal structure of a DNA decamer containing a cis-syn thymine dimer.,” *Proc. Natl. Acad. Sci. U. S. A.*, vol. 99, no. 25, pp. 15965–70, Dec. 2002.

[48] F. Crick, “Central dogma of molecular biology.,” *Nature*, vol. 227, no. 5258, pp. 561–3, Aug. 1970.

[49] F. Tsu-Ju, N. C. Seeman, T. J. Fu, and N. C. Seeman, “DNA double-crossover molecules.,” *Biochemistry*, vol. 32, no. 13, pp. 3211–3220, Apr. 1993.

[50] E. Winfree, F. Liu, L. A. Wenzler, and N. C. Seeman, “Design and self-assembly

of two-dimensional DNA crystals.," *Nature*, vol. 394, no. 6693, pp. 539–544, Aug. 1998.

[51] D. Han, S. Jiang, A. Samanta, Y. Liu, and H. Yan, "Unidirectional Scaffold-Strand Arrangement in DNA Origami," *Angew. Chemie*, vol. 125, no. 34, pp. 9201–9204, Aug. 2013.

[52] H. Dietz, S. M. Douglas, and W. M. Shih, "Folding DNA into twisted and curved nanoscale shapes.," *Science*, vol. 325, no. 5941, pp. 725–730, 2009.

[53] F. Zhang *et al.*, "Complex wireframe DNA origami nanostructures with multi-arm junction vertices.," *Nat. Nanotechnol.*, vol. advance on, no. 9, pp. 779–784, Sep. 2015.

[54] E. Benson *et al.*, "DNA rendering of polyhedral meshes at the nanoscale," *Nature*, vol. 523, no. 7561, pp. 441–444, 2015.

[55] R. Veneziano *et al.*, "Designer nanoscale DNA assemblies programmed from the top down," *Science (80-.).*, vol. 352, no. 6293, pp. 1534–1534, 2016.

[56] D. Han, S. Pal, J. Nangreave, Z. Deng, Y. Liu, and H. Yan, "DNA origami with complex curvatures in three-dimensional space.," *Science*, vol. 332, no. 6027, pp. 342–346, Apr. 2011.

[57] N. C. Seeman, "De novo design of sequences for nucleic acid structural engineering," *J. Biomol. Struct. Dyn.*, vol. 8, no. 3, pp. 573–581, Dec. 1990.

[58] L. Qian *et al.*, "Analogic China map constructed by DNA," *Chinese Sci. Bull.*, vol. 51, no. 24, pp. 2973–2976, 2006.

[59] E. S. Andersen *et al.*, "Semiautomated improvement of RNA alignments," *Rna*, vol. 13, no. 11, pp. 1850–1859, 2007.

[60] E. S. Andersen *et al.*, "DNA Origami Design of Dolphin-Shaped Structures with Flexible Tails," *ACS Nano*, vol. 2, no. 6, pp. 1213–1218, Jun. 2008.

[61] S. Williams, K. Lund, C. Lin, P. Wonka, S. Lindsay, and H. Yan, "Tiamat: A Three-

Dimensional Editing Tool for Complex DNA Structures," in *DNA Computing*, 2009, pp. 90–101.

[62] S. M. Douglas, A. H. Marblestone, S. Teerapittayanon, A. Vazquez, G. M. Church, and W. M. Shih, "Rapid prototyping of 3D DNA-origami shapes with caDNAno," *Nucleic Acids Res.*, vol. 37, no. 15, pp. 5001–5006, Aug. 2009.

[63] C. E. Castro *et al.*, "A primer to scaffolded DNA origami.," *Nat. Methods*, vol. 8, no. 3, pp. 221–229, 2011.

[64] J. Yoo and A. Aksimentiev, "In situ structure and dynamics of DNA origami determined through molecular dynamics simulations.," *Proc. Natl. Acad. Sci. U. S. A.*, vol. 110, no. 50, pp. 20099–104, Dec. 2013.

[65] T. E. Ouldridge, A. A. Louis, and J. P. K. Doye, "DNA nanotweezers studied with a coarse-grained model of DNA," *Phys. Rev. Lett.*, vol. 104, no. 17, pp. 1–4, 2010.

[66] B. E. K. Snodin *et al.*, "Introducing improved structural properties and salt dependence into a coarse-grained model of DNA," *J. Chem. Phys.*, vol. 142, no. 23, p. 234901, Jun. 2015.

[67] H. Zhang, J. Chao, D. Pan, H. Liu, Q. Huang, and C. Fan, "Folding super-sized DNA origami with scaffold strands from long-range PCR," *Chem. Commun.*, vol. 48, no. 51, pp. 6405–6407, 2012.

[68] A. N. Marchi, I. Saaem, B. N. Vogen, S. Brown, and T. H. LaBean, "Toward larger DNA origami.," *Nano Lett.*, vol. 14, no. 10, pp. 5740–7, Oct. 2014.

[69] F. Praetorius, B. Kick, K. L. Behler, M. N. Honemann, D. Weuster-Botz, and H. Dietz, "Biotechnological mass production of DNA origami," *Nature*, vol. 552, no. 7683, pp. 84–87, Dec. 2017.

[70] Z. Zhao, Y. Liu, and H. Yan, "Organizing DNA origami tiles into larger structures using preformed scaffold frames," *Nano Lett.*, vol. 11, no. 7, pp. 2997–3002, Jul. 2011.

[71] S. Woo and P. W. K. Rothemund, “Self-assembly of two-dimensional DNA origami lattices using cation-controlled surface diffusion.,” *Nat. Commun.*, vol. 5, p. 4889, Jan. 2014.

[72] B. Ding, Z. Deng, H. Yan, S. Cabrini, R. N. Zuckermann, and J. Bokor, “Gold nanoparticle self-similar chain structure organized by DNA origami,” *J. Am. Chem. Soc.*, vol. 132, no. 10, pp. 3248–3249, Mar. 2010.

[73] S. Pal, Z. Deng, H. Wang, S. Zou, Y. Liu, and H. Yan, “DNA directed self-assembly of anisotropic plasmonic nanostructures,” *J. Am. Chem. Soc.*, vol. 133, no. 44, pp. 17606–17609, Nov. 2011.

[74] H. Bui *et al.*, “Programmable periodicity of quantum dot arrays with DNA origami nanotubes.,” *Nano Lett.*, vol. 10, no. 9, pp. 3367–72, Sep. 2010.

[75] S. Li *et al.*, “A DNA nanorobot functions as a cancer therapeutic in response to a molecular trigger in vivo,” *Nat. Biotechnol.*, vol. 36, no. 3, pp. 258–264, Feb. 2018.

[76] H. Gu, J. Chao, S.-J. Xiao, and N. C. Seeman, “A proximity-based programmable DNA nanoscale assembly line,” *Nature*, vol. 465, no. 7295, pp. 202–205, May 2010.

[77] A. J. Thubagere *et al.*, “A cargo-sorting DNA robot,” *Science (80-.).*, vol. 357, no. 6356, p. eaan6558, Sep. 2017.

[78] E. S. Andersen *et al.*, “Self-assembly of a nanoscale DNA box with a controllable lid,” *Nature*, vol. 459, no. 7243, pp. 73–76, 2009.

[79] Y. Ke, T. Meyer, W. M. Shih, and G. Bellot, “Regulation at a distance of biomolecular interactions using a DNA origami nanoactuator,” *Nat. Commun.*, vol. 7, p. 10935, Mar. 2016.

[80] A. Kuzuya, Y. Sakai, T. Yamazaki, Y. Xu, and M. Komiyama, “Nanomechanical DNA origami ‘single-molecule beacons’ directly imaged by atomic force microscopy,” *Nat. Commun.*, vol. 2, no. 1, p. 449, Sep. 2011.

[81] S. Yamamoto, D. De, K. Hidaka, K. K. Kim, M. Endo, and H. Sugiyama, “Single molecule visualization and characterization of Sox2-Pax6 complex formation on a regulatory DNA element using a DNA origami frame,” *Nano Lett.*, vol. 14, no. 5, pp. 2286–2292, 2014.

[82] A. J. Lee, M. Endo, J. K. Hobbs, and C. Wälti, “Direct Single-Molecule Observation of Mode and Geometry of RecA-Mediated Homology Search,” *ACS Nano*, vol. 12, no. 1, pp. 272–278, Jan. 2018.

[83] F. Kilchherr, C. Wachauf, B. Pelz, M. Rief, M. Zacharias, and H. Dietz, “Single-molecule dissection of stacking forces in DNA,” *Science (80-.).*, vol. 353, no. 6304, pp. aaf5508-aaf5508, Sep. 2016.

[84] P. C. Nickels *et al.*, “Molecular force spectroscopy with a DNA origami-based nanoscopic force clamp,” *Science (80-.).*, vol. 354, no. 6310, pp. 305–307, Oct. 2016.

[85] X. -c. Bai, T. G. Martin, S. H. W. Scheres, and H. Dietz, “Cryo-EM structure of a 3D DNA-origami object,” *Proc. Natl. Acad. Sci.*, vol. 109, no. 49, pp. 20012–20017, Dec. 2012.

[86] J. R. Burns, E. Stulz, and S. Howorka, “Self-assembled DNA nanopores that span lipid bilayers,” *Nano Lett.*, vol. 13, no. 6, pp. 2351–2356, Jun. 2013.

[87] N. A. W. Bell *et al.*, “DNA origami nanopores.,” *Nano Lett.*, vol. 12, no. 1, pp. 512–7, Jan. 2012.

[88] G. Binnig and H. Rohrer, “Scanning tunneling microscopy,” *Surf. Sci.*, vol. 126, no. 1–3, pp. 236–244, Mar. 1983.

[89] G. Binnig and C. F. Quate, “Atomic Force Microscope,” *Phys. Rev. Lett.*, vol. 56, no. 9, pp. 930–933, Mar. 1986.

[90] A. San Paulo and R. García, “High-resolution imaging of antibodies by tapping-mode atomic force microscopy: Attractive and repulsive tip-sample interaction regimes,” *Biophys. J.*, vol. 78, no. 3, pp. 1599–1605, Mar. 2000.

[91] D. M. Czajkowsky and Z. Shao, “Submolecular resolution of single macromolecules with atomic force microscopy,” in *FEBS Letters*, 1998, vol. 430, no. 1–2, pp. 51–54.

[92] Y. Gan, “Atomic and subnanometer resolution in ambient conditions by atomic force microscopy,” *Surface Science Reports*, vol. 64, no. 3. North-Holland, pp. 99–121, 01-Mar-2009.

[93] C. A. J. Putman, K. O. Van Der Werf, B. G. De Grooth, N. F. Van Hulst, and J. Greve, “Tapping mode atomic force microscopy in liquid,” *Appl. Phys. Lett.*, vol. 64, no. 18, pp. 2454–2456, May 1994.

[94] P. K. Hansma *et al.*, “Tapping mode atomic force microscopy in liquids,” *Appl. Phys. Lett.*, vol. 64, no. 13, pp. 1738–1740, Mar. 1994.

[95] A. Alessandrini and P. Facci, “AFM: A versatile tool in biophysics,” *Measurement Science and Technology*, vol. 16, no. 6. IOP Publishing, pp. R65–R92, 01-Jun-2005.

[96] G. Meyer and N. M. Amer, “Novel optical approach to atomic force microscopy,” *Appl. Phys. Lett.*, vol. 53, no. 12, pp. 1045–1047, Sep. 1988.

[97] C. Bustamante and C. Rivetti, “Visualizing protein-nucleic acid interactions on a large scale with the scanning force microscope.,” *Annu. Rev. Biophys. Biomol. Struct.*, vol. 25, no. 1, pp. 395–429, Jun. 1996.

[98] D. Rugar and P. Hansma, “Atomic Force Microscopy,” *Phys. Today*, vol. 43, no. 10, pp. 23–30, Oct. 1990.

[99] G. Binnig and D. P. E. Smith, “Single-tube three-dimensional scanner for scanning tunneling microscopy,” *Rev. Sci. Instrum.*, vol. 57, no. 8, pp. 1688–1689, Aug. 1986.

[100] D. W. Pohl, “Dynamic piezoelectric translation devices,” *Rev. Sci. Instrum.*, vol. 58, no. 1, pp. 54–57, Jan. 1987.

[101] W. Pauli, “On the connexion between the completion of electron groups in an atom with the complex structure of spectra.,” *Zeitschrift für Phys.*, vol. 31, no. 1, pp. 765–783, Feb. 1925.

[102] G. S. Blackman, C. M. Mate, and M. R. Philpott, “Interaction forces of a sharp tungsten tip with molecular films on silicon surfaces,” *Phys. Rev. Lett.*, vol. 65, no. 18, pp. 2270–2273, Oct. 1990.

[103] L. Xu, A. Lio, J. Hu, D. F. Ogletree, and M. Salmeron, “Wetting and Capillary Phenomena of Water on Mica,” *J. Phys. Chem. B*, vol. 102, no. 3, pp. 540–548, 1998.

[104] J. Colchero, A. Storch, M. Luna, J. Gomez-Herrero, and A. M. Baro, “Observation of liquid neck formation with scanning force microscopy techniques,” *Langmuir*, vol. 14, no. 9, pp. 2230–2234, 1998.

[105] Q. Zhong, D. Inniss, K. Kjoller, and V. B. Elings, “Fractured polymer/silica fiber surface studied by tapping mode atomic force microscopy,” *Surf. Sci. Lett.*, vol. 290, no. 1–2, pp. L688–L692, Jun. 1993.

[106] J. P. Cleveland, B. Anczykowski, A. E. Schmid, and V. B. Elings, “Energy dissipation in tapping-mode atomic force microscopy,” *Appl. Phys. Lett.*, vol. 72, no. 20, pp. 2613–2615, May 1998.

[107] J. Tamayo and R. García, “Relationship between phase shift and energy dissipation in tapping-mode scanning force microscopy,” *Appl. Phys. Lett.*, vol. 73, no. 20, pp. 2926–2928, Nov. 1998.

[108] I. Schmitz, M. Schreiner, G. Friedbacher, and M. Grasserbauer, “Phase imaging as an extension to tapping mode AFM for the identification of material properties on humidity-sensitive surfaces,” *Appl. Surf. Sci.*, vol. 115, no. 2, pp. 190–198, Jun. 1997.

[109] S. N. Magonov, V. Elings, and M. H. Whangbo, “Phase imaging and stiffness in tapping-mode atomic force microscopy,” *Surf. Sci.*, vol. 375, no. 2–3, pp. L385–

L391, Apr. 1997.

[110] R. García and A. San Paulo, “Attractive and repulsive tip-sample interaction regimes in tapping-mode atomic force microscopy,” *Physical Review B*, vol. 60, no. 7. pp. 4961–4967, 1999.

[111] A. N. Round and M. J. Miles, “Exploring the consequences of attractive and repulsive interaction regimes in tapping mode atomic force microscopy of DNA,” in *Nanotechnology*, 2004, vol. 15, no. 4, pp. S176–S183.

[112] S. Santos, V. Barcons, J. Font, and N. H. Thomson, “Bi-stability of amplitude modulation AFM in air: Deterministic and stochastic outcomes for imaging biomolecular systems,” *Nanotechnology*, vol. 21, no. 22, p. 225710, Jun. 2010.

[113] S. Santos *et al.*, “Stability, resolution, and ultra-low wear amplitude modulation atomic force microscopy of DNA: Small amplitude small set-point imaging,” *Appl. Phys. Lett.*, vol. 103, no. 6, p. 063702, Aug. 2013.

[114] T. Ando, N. Kodera, E. Takai, D. Maruyama, K. Saito, and A. Toda, “A high-speed atomic force microscope for studying biological macromolecules,” *Proc. Natl. Acad. Sci.*, vol. 98, no. 22, pp. 12468–12472, Oct. 2001.

[115] M. B. Viani *et al.*, “Probing protein–protein interactions in real time,” *Nat. Struct. Biol.*, vol. 7, no. 8, pp. 644–647, Aug. 2000.

[116] G. E. Fantner, P. Hegarty, J. H. Kindt, G. Schitter, G. A. G. Cidade, and P. K. Hansma, “Data acquisition system for high speed atomic force microscopy,” *Rev. Sci. Instrum.*, vol. 76, no. 2, p. 026118, Feb. 2005.

[117] L. M. Picco *et al.*, “Breaking the speed limit with atomic force microscopy,” *Nanotechnology*, vol. 18, no. 4, p. 044030, Jan. 2007.

[118] A. D. L. Humphris, J. K. Hobbs, and M. J. Miles, “Ultrahigh-speed scanning near-field optical microscopy capable of over 100 frames per second,” *Appl. Phys. Lett.*, vol. 83, no. 1, pp. 6–8, Jul. 2003.

[119] A. D. L. Humphris, M. J. Miles, and J. K. Hobbs, “A mechanical microscope: High-speed atomic force microscopy,” *Appl. Phys. Lett.*, vol. 86, no. 3, p. 034106, Jan. 2005.

[120] T. Ando, N. Kodera, D. Maruyama, E. Takai, K. Saito, and A. Toda, “A High-Speed Atomic Force Microscope for Studying Biological Macromolecules in Action,” *Jpn. J. Appl. Phys.*, vol. 41, no. Part 1, No. 7B, pp. 4851–4856, Jul. 2002.

[121] Y. Yang, “Quantitative characterization of biomolecular assemblies and interactions using atomic force microscopy,” *Methods*, vol. 29, no. 2, pp. 175–187, Feb. 2003.

[122] L. S. Shlyakhtenko, a a Gall, J. J. Weimer, D. D. Hawn, and Y. L. Lyubchenko, “Atomic force microscopy imaging of DNA covalently immobilized on a functionalized mica substrate.,” *Biophys. J.*, vol. 77, no. 1, pp. 568–576, Jul. 1999.

[123] J. Zheng, Z. Li, A. Wu, and H. Zhou, “AFM studies of DNA structures on mica in the presence of alkaline earth metal ions,” *Biophys. Chem.*, vol. 104, no. 1, pp. 37–43, 2003.

[124] D. Pastré *et al.*, “Anionic Polyelectrolyte Adsorption on Mica Mediated by Multivalent Cations: A Solution to DNA Imaging by Atomic Force Microscopy under High Ionic Strengths,” *Langmuir*, vol. 22, no. 15, pp. 6651–6660, Jul. 2006.

[125] D. Pastré *et al.*, “Adsorption of DNA to mica mediated by divalent counterions: a theoretical and experimental study.,” *Biophys. J.*, vol. 85, no. 4, pp. 2507–2518, Oct. 2003.

[126] H. G. Hansma and D. E. Laney, “DNA binding to mica correlates with cationic radius: assay by atomic force microscopy.,” *Biophys. J.*, vol. 70, no. 4, pp. 1933–1939, Apr. 1996.

[127] D. J. Billingsley *et al.*, “Patchiness of ion-exchanged mica revealed by DNA binding dynamics at short length scales.,” *Nanotechnology*, vol. 25, no. 2, p. 025704, Jan. 2014.

[128] C. Rivetti, M. Guthold, and C. Bustamante, “Scanning force microscopy of DNA deposited onto mica: Equilibration versus kinetic trapping studied by statistical polymer chain analysis,” *J. Mol. Biol.*, vol. 264, no. 5, pp. 919–932, Dec. 1996.

[129] N. H. Thomson, S. Kasas, Smith, H. G. Hansma, and P. K. Hansma, “Reversible Binding of DNA to Mica for AFM Imaging,” *Chem. Rev.*, vol. 12, no. 24, pp. 5905–5908, 1996.

[130] J. Adamcik, D. V. Klinov, G. Witz, S. K. Sekatskii, and G. Dietler, “Observation of single-stranded DNA on mica and highly oriented pyrolytic graphite by atomic force microscopy,” *FEBS Lett.*, vol. 580, no. 24, pp. 5671–5675, Oct. 2006.

[131] M. A. B. B. Baker *et al.*, “Dimensions and Global Twist of Single-Layer DNA Origami Measured by Small-Angle X-ray Scattering,” *ACS Nano*, vol. 12, no. 6, p. acsnano.8b01669, Jun. 2018.

[132] L. Mallik *et al.*, “Electron Microscopic Visualization of Protein Assemblies on Flattened DNA Origami.,” *ACS Nano*, pp. 7133–7141, 2015.

[133] H. Chen *et al.*, “Conformational Effects of UV Light on DNA Origami,” *J. Am. Chem. Soc.*, vol. 139, no. 4, p. jacs.6b10821, Feb. 2017.

[134] H. Chen *et al.*, “Dynamic and Progressive Control of DNA Origami Conformation by Modulating DNA Helicity with Chemical Adducts,” *ACS Nano*, vol. 10, no. 5, pp. 4989–4996, 2016.

[135] S. Kocabey *et al.*, “Membrane-Assisted Growth of DNA Origami Nanostructure Arrays,” *ACS Nano*, vol. 9, no. 4, pp. 3530–3539, Apr. 2015.

[136] A. Gopinath, C. Thachuk, A. Mitskovites, H. Atwater, D. Kirkpatrick, and P. W. K. Rothemund, “Absolute and arbitrary orientation of single molecule shapes,” *Science (80-.).*, Aug. 2018.

[137] S. Ramakrishnan, H. Ijäs, V. Linko, and A. Keller, “Structural stability of DNA origami nanostructures under application-specific conditions,” *Comput. Struct. Biotechnol. J.*, Sep. 2018.

[138] S. Ramakrishnan, G. Krainer, G. Grundmeier, M. Schlierf, and A. Keller, “Structural stability of DNA origami nanostructures in the presence of chaotropic agents,” *Nanoscale*, vol. 8, no. 19, pp. 10398–10405, May 2016.

[139] T. G. Martin and H. Dietz, “Magnesium-free self-assembly of multi-layer DNA objects,” *Nat. Commun.*, vol. 3, 2012.

[140] C. Kielar *et al.*, “On the Stability of DNA Origami Nanostructures in Low-Magnesium Buffers,” *Angew. Chemie - Int. Ed.*, vol. 57, no. 30, pp. 9470–9474, Jul. 2018.

[141] H. Kim, S. Surwade, A. Powell, C. O’Donnell, and H. Liu, “Stability of DNA Origami Nanostructure under Diverse Chemical Environments,” *Chem. Mater.*, p. 140825004633002, 2014.

[142] J. H. Choi, “Understanding the Mechanical Properties of DNA Origami Tiles and Controlling the Kinetics of Their Folding and Unfolding Recon fi guration,” 2014.

[143] R. S. Mathew-Fenn, R. Das, and P. A. B. Harbury, “Remeasuring the Double Helix,” *Science (80-.).*, vol. 322, no. 5900, pp. 446–449, Oct. 2008.

[144] J. C. Wang, “Helical repeat of DNA in solution.,” *Proc. Natl. Acad. Sci. U. S. A.*, vol. 76, no. 1, pp. 200–203, 1979.

[145] D. Rhodes and A. Klug, “Helical periodicity of DNA determined by enzyme digestion,” *Nature*, vol. 286, no. 5773, pp. 573–578, Aug. 1980.

[146] D. N. Kim, F. Kilchherr, H. Dietz, and M. Bathe, “Quantitative prediction of 3D solution shape and flexibility of nucleic acid nanostructures,” *Nucleic Acids Res.*, vol. 40, no. 7, pp. 2862–2868, 2012.

[147] J. P. K. Doye *et al.*, “Coarse-graining DNA for simulations of DNA nanotechnology,” *Phys. Chem. Chem. Phys.*, vol. 15, no. 47, pp. 20395–20414, 2013.

[148] Z. Ma, K. Kawai, Y. Hirai, T. Tsuchiya, and O. Tabata, “Tuning porosity and radial

mechanical properties of DNA origami nanotubes via crossover design," *Jpn. J. Appl. Phys.*, vol. 56, no. 6S1, p. 06GJ02, Jun. 2017.

[149] Z. Ma *et al.*, "Rhombic-Shaped Nanostructures and Mechanical Properties of 2D DNA Origami Constructed with Different Crossover/Nick Designs," *Small*, vol. 14, no. 1, p. 1702028, Jan. 2018.

[150] A. E. Marras *et al.*, "Cation-Activated Avidity for Rapid Reconfiguration of DNA Nanodevices," *ACS Nano*, p. acsnano.8b04817, Sep. 2018.

[151] M. J. Peak, J. G. Peak, and B. A. Carnes, "INDUCTION OF DIRECT AND INDIRECT SINGLE-STRAND BREAKS IN HUMAN CELL DNA BY FAR- AND NEAR-ULTRAVIOLET RADIATIONS: ACTION SPECTRUM AND MECHANISMS," *Photochem. Photobiol.*, vol. 45, no. 3, pp. 381–387, Mar. 1987.

[152] J. Liu, X. Yao, P. Cloutier, Y. Zheng, and L. Sanche, "DNA Strand Breaks Induced by 0-1.5 eV UV Photoelectrons under Atmospheric Pressure," *J. Phys. Chem. C*, vol. 120, no. 1, pp. 487–495, Jan. 2016.

[153] S. Mouret, C. Baudouin, M. Charveron, A. Favier, J. Cadet, and T. Douki, "Cyclobutane pyrimidine dimers are predominant DNA lesions in whole human skin exposed to UVA radiation," *Proc. Natl. Acad. Sci.*, vol. 103, no. 37, pp. 13765–13770, Sep. 2006.

[154] T. Gerling, M. Kube, B. Kick, and H. Dietz, "Sequence-programmable covalent bonding of designed DNA assemblies," *Sci. Adv.*, vol. 4, no. 8, p. eaau1157, Aug. 2018.

[155] L. Čoga, "Interactions of metal ions with DNA," 2012.

[156] J. V. Burda, J. Šponer, J. Leszczynski, and P. Hobza, "Interaction of DNA Base Pairs with Various Metal Cations (Mg 2+ , Ca 2+ , Sr 2+ , Ba 2+ , Cu + , Ag + , Au + , Zn 2+ , Cd 2+ , and Hg 2+): Nonempirical ab Initio Calculations on Structures, Energies, and Nonadditivity of the Interaction," *J. Phys. Chem. B*, vol. 101, no. 46, pp. 9670–9677, 1997.

[157] E. Ennifar, P. Walter, and P. Dumas, “A crystallographic study of the binding of 13 metal ions of two related RNA duplexes,” *Nucleic Acids Res.*, vol. 31, no. 10, pp. 2671–2682, May 2003.

[158] F. Benn *et al.*, “Chiral DNA Origami Nanotubes with Well-Defined and Addressable Inside and Outside Surfaces,” *Angew. Chemie - Int. Ed.*, vol. 57, no. 26, pp. 7687–7690, Apr. 2018.

[159] R. D. Wells, “Non-B DNA conformations, mutagenesis and disease,” *Trends in Biochemical Sciences*, vol. 32, no. 6. Elsevier, pp. 271–278, 01-Jun-2007.